UNIVERSITÉ DE NANTES
UFR SCIENCES ET TECHNIQUES
(thèse en cotutelle avec UNIVERSITE « DUNĂREA DE JOS », GALAŢI, ROUMANIE)

___

École Doctorale SPIGA
Sciences Pour l'Ingénieur, Géosciences, Architecture

Année 2012

N° attribue par la bibliothèque
|__|__|__|__|__|__|__|__|__|__|

Commande de procédés d'intérêt environnemental (traitement biologique des eaux usées et production de microalgues en photobioréacteur)

_____

THÈSE DE DOCTORAT
Discipline : Sciences pour l'Ingénieur
Spécialité : Génie des Procédés

Présentée
et soutenue publiquement par

George Adrian IFRIM

Le 29 mars 2012, devant le jury ci-dessous

Président : Virel Mînzu, Professeur, Université « Dunărea de jos », Galaţi, Roumanie
Rapporteurs : Jean-Philippe STEYER, Directeur de Recherche au LBE, Narbonne, France
Radu-Emil PRECUP, Professeur, Université « Dunărea de jos », Galaţi, Roumanie
Examinateurs : Lionel BOILLEREAUX, Professeur, ONIRIS, Nantes, France
Sergiu CARAMAN, Professeur, Université « Dunărea de jos », Galaţi, Roumanie
Mariana TITICA, Maitre de Conférences, Université de Nantes (IUT St-Nazaire)

Directeurs de thèse *:* Lionel BOILLEREAUX, Professeur, ONIRIS, Nantes, France
Sergiu CARAMAN, Professeur, Université « Dunărea de jos », Galaţi, Roumanie
Co-encadrante : Mariana Titica, Maitre de Conférences, Université de Nantes (IUT St-Nazaire)

ED : ……

To my guardian angels:

my mother and my grandmother

ACKNOWLEDGEMENTS

In my opinion the three years path for achieving my maturity as a scientist were, so far, the most beautiful and yet the most difficult years of my professional life. Now, reaching the end, I look back and realize that it was quite a bumpy road, with many challenges that I managed to overcome thanks to the wonderful people that I met and that stood beside me along the way and that gave me the possibility to grow both as a researcher but also as an individual.

I will take this opportunity to give thanks to all the people without whom this thesis would not have been possible.

First of all I would like to express my gratitude for my extraordinary supervisors: Prof. Sergiu Caraman, Prof. Lionel Boillereaux and Assoc. Prof. Mariana Titica. They were my best advisors and my fair and exigent critics. I bow my head in front of their professionalism and I would like them to know that they are my role models both as scientists and individuals.

I also would like to give thanks to Prof. Viorel Mînzu, Prof. Radu Precup and Rsrch. Dir. Jean-Philippe Steyer for honoring me with their presence at my PhD thesis defense. Also, I would like to thank to Prof. Radu Precup and Rsrch. Dir. Jean-Philippe Steyer for their positive reports regarding my thesis.

In fulfilling the scientific work I had beneficiated of precious advises offered by Assoc. Prof. Guillaume Cogne and Asst. Prof. Marian Barbu and words cannot express my gratitude for their real support.

I would have not follow this path in life if it was not for the great Prof. Gabriela Bahrim that practically believed and supported me since my early steps in the academic world.

I can never forget Prof. Emil Ceangă to whom I thank for his vision and kind and warm advices.

I was fortunate enough to beneficiate of an international co-tutelage between “Dunărea de Jos” University, Galaţi, Romania and “Université de Nantes”, France that gave me the extraordinary opportunity to work with wonderful teams. Therefore, I would like to thank to GEPEA Laboratory collective, in France, and to all my Romanian colleagues, for their true help, support and team work.

Last, but not least, I would like to thank my wife and my family for their infinite patience and for their constant support. Thank you all for bearing me!

INTRODUCTION

The present thesis is the result of an international co-tutelage and of a very fructuous collaboration between Nantes University, France and "Dunărea de Jos" University, Galaţi, Romania. In the elaboration of the thesis, the main objectives kept in mind were the control of specific state variables of two bioprocesses with impact over the environment – the production of microalgae in photobioreactor and the aerobic wastewater treatment – and their coupling perspectives. Both bioprocesses were studied from a systemic viewpoint aiming to derive accurate nonlinear dynamic models on which basis reliable control algorithms can be synthesized.

The interest in studying the coupling perspectives of the two bioprocesses mentioned above derives from their potential to obtain a cost effective installation that aside from its role of treating wastewaters leads also to the production of microalgal biomass that represents a potential source of biofuels (biodiesel and biohydrogen). Furthermore, microalgae are able to treat air as a result of their capacity to bio-mitigate the CO_2 from flue gases. The microalgal biomass represents also a potential source for the production of therapeutic and industrial metabolites such as the long chain polyunsaturated fatty acids, pigments, polycarbohydrates, vitamins or various biological active compounds.

The laboratory researches regarding the two bioprocesses were performed as follows: the studies on photobioreactor were conducted in GEPEA Laboratory, Saint-Nazaire, France while the experiments on the wastewater treatment pilot plant were accomplished in a laboratory of "Dunărea de Jos" University, Galati, Romania.

The main contributions brought forth through this thesis are the development of a global model for the photoautotrophic growth of *Chlamydomonas reinhardtii*, a reduced model for control purposes, a dynamic nonlinear equation for the concentration of hydrogen ions (negative antilogarithm of pH), reliable nonlinear controllers for biomass, pH and specific light uptake validated with experimental data, a simple and reliable model for the aerobic wastewater treatment plants and an efficient linear robust controller for the dissolved oxygen in the aerobic tank.

The theoretical result, that is the thesis per se, of the researches is structured in three parts; the first two are treating each process separately, but based on a common approach, while in the third part there are evaluated the coupling perspectives.

The thesis is however preceded by an introductive part that motivates the necessity of studying the two processes, discussing the main natural bioprocesses which are involved in the treatment of wastewaters and their interrelations along with a brief presentation of the state of the art of phycoremediation evaluating the two research directions which are the direct usage of microalgae in wastewater treatment and the coupling of separate processes.

The *first part*, which refers to the modeling and control of the photoautotrophic growth process of microalgae in photobioreactor, consists of five chapters:

- The first chapter furnishes the basic concepts and the state of the art regarding the modeling and control of photobioreactors. A general approach of modeling the bioprocesses is also proposed, laying the basis for a common approach in modeling the two antagonistic bioprocesses;
- The second chapter details the materials and the methods used to fulfill the objectives regarding the validation of the proposed model and the practical implementation of the derived control algorithms;
- The third chapter presents in detail a global model for the photoautotrophic growth process of *Chlamydomonas reinhardtii* which delineates the main variables of the bioprocess which conduct to a precise prediction of the culture pH. The global photoautotrophic growth model associates three models, namely a radiative model, a biological model and a thermodynamic model. The nonlinear model was validated on experimental data furnished by GEPEA Laboratory.
- The forth chapter aims the design of nonlinear multivariable control algorithms based on the exact feedback linearizing control theory. The nonlinear multivariable control of photobioreactor is presented for both continuous and discontinuous cultures targeting the manipulation of measurable or estimable output variables such as biomass, pH, specific light uptake rate and lighted volume fraction. Because the proposed model is too complex to allow the synthesis of proper algorithms, it was reduced by differentiating the states with slow dynamics from the ones with fast dynamics which were converted into algebraic expressions. A nonlinear dynamic expression was also proposed for the concentration of hydrogen ions as an explicit function of biomass, total inorganic nitrogen and carbon. The degree of interaction between I/O signals was determined for continuous cultures in order to establish if the system allows the implementation of decentralized SISO controllers or requires a centralized MIMO controller.

- The fifth chapter presents the practical results obtained at the implementation of the control algorithms on the experimental bench. The experiments aimed the validation of specific controllers for biomass, pH and specific light uptake rate.

The *second part* assigned to the modeling and control of the aerobic wastewater treatment process has a similar organization, thus:

- The first chapter presents the state of the art regarding the modeling and control of the wastewater treatment plants;
- The second chapter reveals the materials and the methods utilized to accomplish the identification of the model parameters and to validate the proposed control algorithms on experimental data;
- The third chapter proposes a simple and reliable nonlinear model to describe the dynamics of a conventional aerobic wastewater treatment pilot with sludge recycling. An empirical model for secondary clarifiers is also proposed in this chapter. The model parameters were identified on experimental data acquired from the wastewater treatment pilot.
- The forth chapter presents the basic control strategies for the aerobic wastewater treatment plants. Two nonlinear multivariable control strategies were studied in simulation, evaluating the interactions between I/O channels in order to determine the necessity of using decentralized SISO or centralized MIMO controllers. The nonlinear controllers target the manipulation of output variables such as substrate concentration, dissolved oxygen concentration and F/M ratio. Due to the lack of reliable sensors for certain states variables and to the parametric uncertainties which significantly influence the system, a linear robust controller based on the quantitative feedback theory was developed for the monovariable control of the dissolved oxygen in the aerobic tank.
- The fifth chapter renders the good results obtained at the implementation of the robust QFT controller for the dissolved oxygen in the aerobic tank.

The *third part* is dedicated to the perspectives of coupling the photoautotrophic growth process of microalgae in photobioreactor with the aerobic wastewater treatment process and consists in two chapters regarding the modeling and control.

For the specialized reader, the thesis also comprises five appendixes that are practically an extension of the basic concepts regarding the photobioreactor studies in the actual context of the increasing implication of microalgae in biotechnological and environmental applications.

CONTENT

PART 0

MOTIVATION OF STUDYING THE TWO BIOPROCESSES: PHOTOSYNTHETIC GROWTH OF MICROALGAE IN PHOTOBIOREACTOR AND THE WASTEWATER TREATMENT

0.1. NATURAL BIOPROCESSES WITH APPLICATIONS IN WASTEWATER TREATMENT

***Abstract*:** This introductory section motivates the idea of coupling the two processes – the photoautotrophic growth of microalgae in photobioreactor and the wastewater treatment – through the existent interconnections between the natural bioprocesses that take place in an aquatic ecosystem.

Environmental processes require solid knowledge regarding the physical, chemical and biological nature of the aquatic environment in order to furnish reliable solutions for the design and operation of effective technologies for the protection of the environment and public health. The pollutants which contaminate the wastewater streams are as different as their sources. However, the constituents of interest for the biological treatment of wastewaters are the carbon, nitrogen and phosphorus concentrations. Apart from containing carbonaceous substrates and growth nutrients the wastewaters contain a huge variety of microorganisms and by providing a controlled environment for optimum microbial activity in a treatment plant, almost all present organics can be degraded. The microorganisms have a number of vital functions in the pollution control, responding to contamination by increasing their growth and metabolism. In the aquatic ecosystems contaminated with organics the microbial component provides the self-purification capacity of natural waters participating to a series of reactions such as aerobiosis, anaerobiosis, photosynthesis, nitrification, denitrification and anaerobic oxidation of ammonium (ANAMMOX) or methane (AOM). All these processes are interconnected as it is depicted in Fig.0.1.1.

The composition of any microbial cell consists in macroelements such as carbon, oxygen, nitrogen, hydrogen, phosphorus and sulfur. For their growth other nutrients are required such as cations (*e.g.* Mg^{2+}, Ca^{2+}, Na^{+}, K^{+}, Fe^{2+}), anions (*e.g.* $C\ell^{-}$, SO_4^{2-}), trace elements (*e.g.* Co, Cu, Mn, Mo, Zn, Ni, Se), which serve as components or cofactors of several enzymes, and growth factors such as vitamins (*e.g.* riboflavin, thiamin, niacin, vitamin B_{12}, folic acid, biotin, vitamins B_6) (Bitton, 2005). The microorganisms can be classified based on their metabolism considering two criteria: carbon source (CO_2 or organic carbon) and energy source (light or energy derived from the oxidation of inorganic or organic chemicals). Based on these the microorganisms can be photoautotrophs, photoheterotrophs, chemoautotrophs and chemoheterotrophs. Certain microorganisms are able to combine the metabolic pathways being known as mixotrophs.

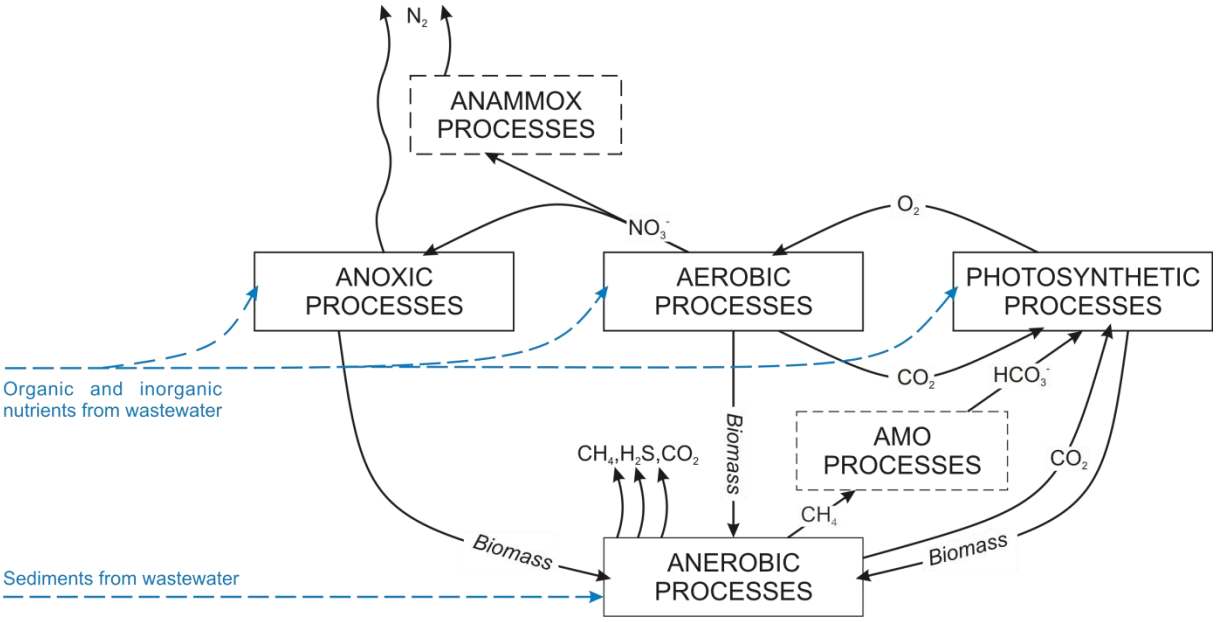

Fig.0.1.1. Biological processes within aquatic environments

The microorganisms can be divided further into three groups according to their response to molecular oxygen: strict aerobes, facultative anaerobes and anaerobes (which can be also divided in oxygen-tolerant and oxygen-intolerant).

When organic pollutants are discharged in natural receptors a complex population of microorganisms, formed by all classes presented above, is developing and competes for food.

Strict aerobes are present in a large number in the aquatic environment and perform significant roles in the degradation of wastes using free dissolved oxygen to completely mineralize the organic compounds to CO_2, H_2O, NH_4^+, HPO_4^{2-}, SO_4^{2-} and new microbial cell or sludge (Eq.0.1.1)

$$\text{organic compounds} + O_2 \xrightarrow{\text{respiration}} CO_2 + H_2O + NH_4^+ + HPO_4^{2-} + SO_4^{2-} + \text{new cells} \quad (0.1.1)$$

The nitrification processes occur also in aerobic conditions where strict aerobic, nitrifying bacteria such as *Nitrosomonas* and *Nitrobacter* are oxidizing NH_4^+ to NO_3^- in two steps (Eq.0.1.2 and Eq.0.1.3).

$$NH_4^+ + 1.5O_2 \xrightarrow{Nitrosomonas} NO_2^- + 2H^+ + H_2O + \text{energy} \quad (0.1.2)$$

$$NO_2^- + 0.5O_2 \xrightarrow{Nitrobacter} NO_3^- + \text{energy} \quad (0.1.3)$$

When the molecular oxygen is consumed from the aquatic environment or exists in extremely small concentrations (anoxic regime) the nitrate NO_3^- is used as oxygen source by the facultative anaerobes in denitrification processes. The process is performed mainly by chemoheterotrophic bacteria such as *Paracoccus denitrificans* and various *Pseudomonas*. They are involved in the complete reduction of nitrates to molecular nitrogen according to Eq. (0.1.4).

$$2NO_3^- + 10e^- + 12H^+ \rightarrow N_2 + 6H_2O \quad (0.1.4)$$

The photosynthetic processes work in synergy with the aerobic processes. Even though they might compete for organic substrates many microalgae are able to sustain both photoheterotrophic and photoautotrophic metabolism (Eq.0.1.5). Thus, the carbon dioxide which results from the aerobic respiration process can represent the carbonaceous substrate for microalgae. On the other hand the microalgae produce oxygen as a residue in the water photolysis reaction which will be further consumed by the aerobes.

$$CO_2 + H_2O + \text{light} \rightarrow O_2 + \text{microalgal cells} \quad (0.1.5)$$

When the free molecular oxygen or nitrates are depleted, nitrification stops and facultative anaerobes and aerotolerant anaerobes are degrading the organic compounds. In this case the organics are degraded through fermentative reactions to CO_2, H_2O, new bacterial cells, inorganic compounds and a variety of smaller compounds such as organic acids and alcohols (Eq.0.1.6).

$$\text{organic compounds} \xrightarrow{\text{fermentation}} CO_2 + H_2O + NH_4^+ + HPO_4^{2-} + H_2S + \textit{new cells} + \text{organic acids and alcohols} \quad (0.1.6)$$

These fermentative reactions result in incomplete oxidation of the organic compounds due to the fact that a part of the carbon is not incorporated into CO_2 and new bacterial cells. The rest of carbon is incorporated into fermentative products such as organic acids and alcohols which still contain energy and can be used as substrate for the photoheterotrophic organisms.

Anaerobiosis takes place at the bottom of lakes and rivers where the oxygen level is usually null. The substrate for anaerobiosis consists in the organic settleable solids from wastewaters and in the dead biomass from the aerobic, anoxic and photosynthetic processes. When strict anaerobes do not find appropriate conditions for growth the sediments will be incompletely degraded to organic acids and alcohols which are further involved in aerobic or photosynthetic processes. On the other hand, if strict aerobes are active the sediments will be digested to methane (CH_4), hydrogen sulfide (H_2S) and carbon dioxide (CO_2). A complete anaerobic process consists in three stages realized by different groups of bacteria: hydrolysis stage, acid-forming stage and methanogenesis stage. An overall reaction of the process can be written as follows:

$$organic\ compounds \xrightarrow{\substack{hydrolysis,acido\ and\ acetogenesis,\\ methanogenesis}} CO_2 + CH_4 \qquad (0.1.7)$$

Two other processes recently discovered are the anaerobic oxidation of ammonium (Eq.0.1.8) and methane (Eq.0.1.9) which are the most unexploited parts of the carbon and nitrogen cycles.

$$NH_4^+ + NO_2^- \rightarrow N_2 + 2H_2O \qquad (0.1.8)$$

$$CH_4 + SO_4^{2-} + H^+ \rightarrow CO_2 + HS^- + 2H_2O \qquad (0.1.9)$$

With regard to the roles of the two processes, the current information is that AMO and ANAMMOX are responsible for more than 75% of marine methane oxidation and 30–50% of marine ammonium oxidation. The AMO process furnishes CO_2 which can be used in photosynthetic processes.

Therefore the nature is extremely effective in what regards the waste management and, generally spiking, the biological wastewater treatment processes involve the intensification of the above described processes in controlled installations. All the processes presented above (except AMO) found technological applications in the biological wastewater treatment, giving good results.

In this context the huge potential of microalgae, resumed mainly to their capacity to use sunlight as energy source and their high requirement of nutrients, led to challenging researches regarding their use in the wastewater treatment processes.

0.2. PHYCOREMEDIATION – STATE OF THE ART

***Abstract*:** This chapter introduces a brief state of the art regarding the phycoremediation process highlighting the advantages and the disadvantages of using the microalgae in the treatment of wastewaters. There are emphasised the two research directions, the direct use of microalgae into wastewater streams and the coupling between individual processes.

The use of macroalgae and microalgae for the removal or biotransformation of pollutants, including nutrients and xenobiotics from wastewaters and CO_2 from waste air is known as *phycoremediation* (Olguin, 2003).

The researches were oriented in two main directions, either the microalgae are directly inoculated into wastewaters making use of their photoheterotrophic metabolism, high nutrient requirements and capacity to bioaccumulate heavy metals, or cultivated into separate photobioreactors (or open ponds) coupled with specific wastewater treatment units.

0.2.1. Wastewater treatment with microalgae

There are certain features of microalgae which encourage their use in wastewater treatment techniques such as their capacity to remove carbonaceous organic matter, their high requirements of nutrients (*i.e.* N and P) and their good ability to bioaccumulate heavy metals. In addition, many species of microalgae are able to sustain photoautotrophic or mixotrophic metabolism which qualify them for the bio-mitigation of CO_2, and hence for the waste air treatment. Certain species of microalgae (*e.g. Monoraphidium minutum*) are also able to tolerate moderate levels of NO_x and SO_x from flue gasses (Brown, 1996; Nagase *et al.*, 1998, 2001).

The microalgae are known to perform an important role in the purification of natural waters, feature which inspired numerous researches regarding their direct inoculation into various effluents (Dilek *et al.*, 1999; Wei *et al.*, 2008). It does not necessary mean that the conventional wastewater treatment processes are inefficient, but the phycoremediation may be a desired solution for the reduction of costs. The aerobic treatment for example requires free dissolved oxygen to be furnished through mechanical means, a procedure which is responsible for more than 50% of total electrical consumption of plants (Tchobanoglous *et al.*, 2003).

Another attractive characteristic of microalgae is the requirement of higher concentration of nutrients in comparison with the activated sludge. A conventional aerobic process with

activated sludge is able to reach good removal efficiencies at C:N:P ratios of maximum 100:5:1. Higher amounts of nitrogen require separate removal stages (and often separate tanks also) such as denitrification or ANAMMOX processes. The microalgal biomass, on the other hand, is able to incorporate a double quantity of nitrogen, their C:N:P ratio being 100:11:1.3 (Roels, 1983). The microalgae capacity of removing high concentrations of nutrients led to researches on various types of wastewaters (Voltolina *et al.*, 2005).

Besides their attractive advantages there are also certain limitations such as:

- The algal pounds require large areas for sunlight harvest while the conventional wastewater tanks (aerobic and anaerobic) are more compact;
- The separation between the treated water and algal cells is difficult to be realized, further filtration or centrifugation stages being required. Such processes will raise the exploitation costs of the plant;
- Phycoremediation may fail on certain types of wastewater (*i.e.* toxic compounds) due to the lack of specific enzymes. On the contrary, the sludge which contains a high number of bacterial, fungal and protozoal which live in synergy is better equipped to resist to various substrates;
- The microalgae (as well as the aerobes) are not able to treat highly loaded wastewaters, the anaerobic treatment being recommended to this end;
- The algal ponds are highly subjected to contamination by bacteria which may release algaecide compromising the culture.

The separation of microalgae from the treated water was approached by Shi *et al.*, (2007) who investigated the capacity of two green microalgae (*i.e. Chlorella vulgaris* and *Scenedesmus rubescens*) to remove the nitrogen and the phosphorus from wastewater. They immobilized the cells in a twin layer system based on self-adhesion on a wet, microporous, ultrathin substrate, reporting good removal efficiencies on municipal and synthetic wastewaters. Mallick (2002) also reviewed the immobilization techniques of microalgae available at that time.

Another challenging approach is the use of algal – bacterial consortiums to treat wastewater (Fig.0.2.1). In such cases the microalgae improve the removal efficiency of nutrients and provide O_2 to heterotrophic aerobic bacteria able to mineralize the organic matter, consuming in turn the CO_2 released form bacterial respiration. Obviously, this technique can be applied exclusively to the aerobically treatable effluents. Muñoz and Guieysse, (2006) reviewed the main results obtained at that time regarding algal – bacterial processes focusing on hazardous contaminants.

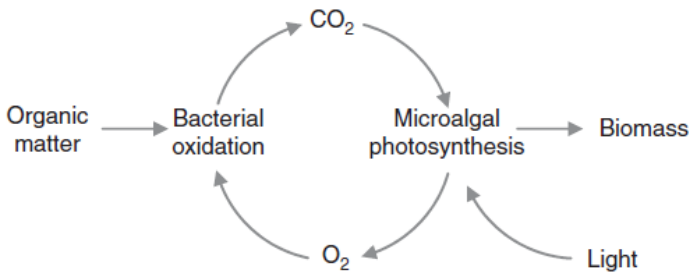

Fig.0.2.1. Principle of photosynthetic oxygenation in algal – bacterial processes (Muñoz and Guieysse, 2006)

This technique faces certain limitations related to the difficulty of harvesting the biomass from the treated effluent, to the large surface requirements for open systems and to unequal growth rates of microalgae and bacteria. In addition the interactions between microalgae and bacteria go often beyond a simple gas exchange, the bacteria excreting algaecides and the microalgae secreting antibiotics. Even though efficient separation techniques (*e.g.* filtration, centrifugation, flocculation) are used there is no guaranty that the microalga – bacterial biomass will meet the public acceptance to be commercialized. However, in the anticipation of developing reliable self-aggregation algal – bacterial processes (Gutzeit *et al.*, 2005) this technique remains a good candidate in lowering the costs of aerobic wastewater treatment plants.

0.2.2. Coupling between a biological WWTP and a PBR

In order to avoid compromising the effluent quality, the microalgal culturing techniques can be rather applied on the tertiary treatment of wastewaters, that represents the coupling between a conventional wastewater treatment plant with a photobioreactor. The coupling approach can be made in two directions, anaerobic plant – PBR (Fig.0.2.2) or aerobic plant – PBR (Fig.0.2.3), which represent only concepts for further researches.

The anaerobic digestion is practically the single wastewater treatment technique which is able to furnish a directly valuable product, the methane gas. In addition, an anaerobic digester is able to treat highly loaded wastewaters and to work with solid wastes. Despite these resolute advantages there are certain disadvantages such as the inability to remove nutrients which divert the attention to aerobic plants which are efficient in removing nutrients. A solution to encourage the use of anaerobic digesters is to treat their effluents into photobioreactors. The carbonaceous substrate used for microalgae can be the CO_2 generated at the combustion of

methane. Growing in a separate reactor under photoautotrophic conditions the microalgae are in this way kept safe from massive contamination. The microalgal biomass can be also harnessed in added value compounds while the waste biomass can be recycled back to the anaerobic digester.

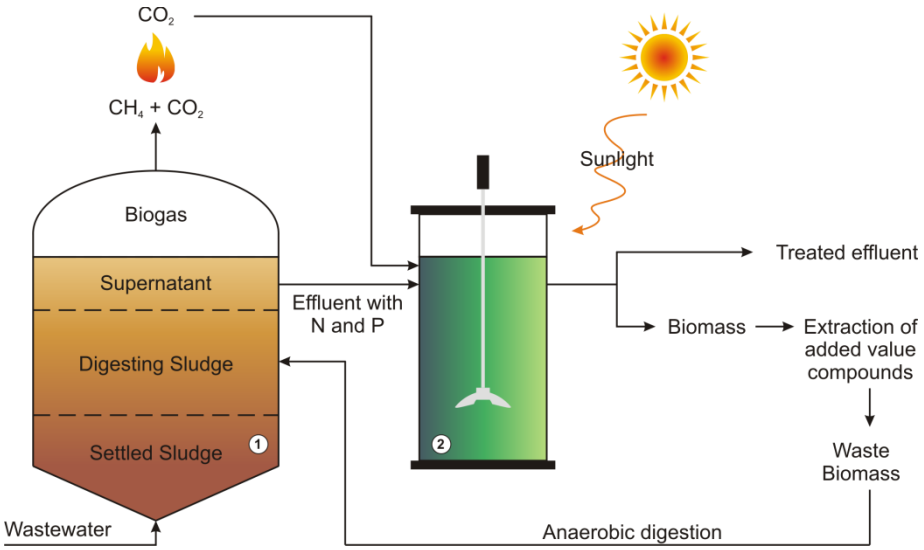

Fig.0.2.2. Coupling between a conventional anaerobic treatment plant and a photobioreactor (1 – up flow anaerobic digester, 2 - photobioreactor)

The aerobic plants are able to remove a certain quantity of nutrients (*i.e.* C:N:P – 100:5:1) and are efficient from many points of view, but expensive. When the nitrogen, for example, exceeds the ration mentioned above, additional denitrification stages are required.

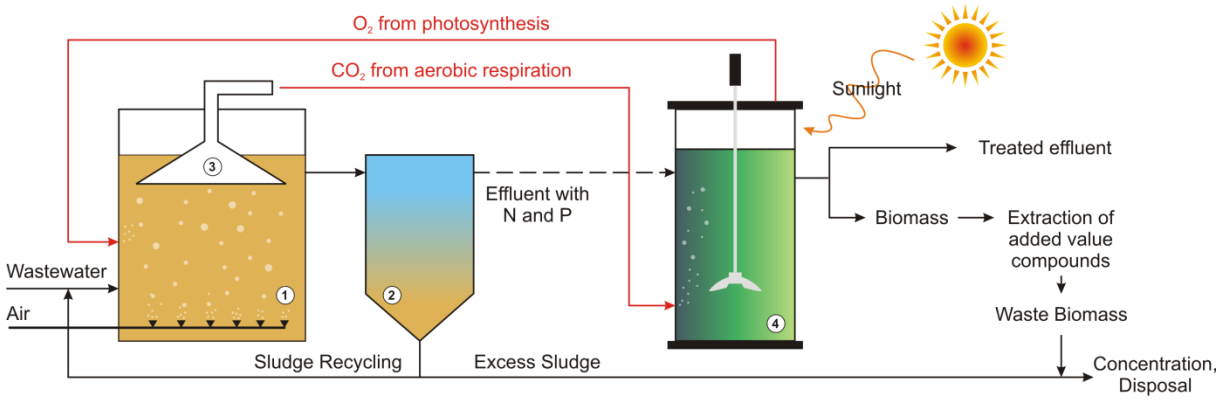

Fig.0.2.3. Coupling between a conventional aerobic treatment plant and a photobioreactor (1 – aerobic tank, 2 – clarifier, 3 – gas trap, 4 - photobioreactor)

The coupling between an aerobic plant and a photobioreactor can solve certain problems such as the elimination of the denitrification stage and the reduction of aeration costs. In the same spirit as the microalgal – bacterial consortiums, the CO_2 from the bacterial respiration can be used as substrate for microalgae that produce in its turn O_2 utilized by aerobes. The aerobic plant effluent, if loaded with nutrients, can be also a low cost substrate for microalgae. The air in the aerobic tank can be supplemented through mechanical ejectors while the CO_2 can be augmented for microalgae from other combustion processes (*e.g.* power plants).

PART I

MODELING AND CONTROL OF THE PHOTOAUTOTROPHIC GROWTH PROCESS OF MICROALGAE IN PHOTOBIOREACTOR

I.1. BASIC CONCEPTS REGARDING THE MODELING AND CONTROL OF PHOTOBIOREACTORS

***Abstract*:** In the present chapter the main concepts that lay the basis for further modeling and control of photobioreactors are briefly described. The modeling of photobioreactors is extended from the general approach of bioprocesses to specific class of models obtained through the coupling of radiative models with kinetic models. The state of the art in what regards photobioreactors' control is rendered with a view on the principal control strategies: chemostatic, lumostatic and pH control.

I.1.1. The Microalgae

The Earth's atmosphere before Life was rich in CO_2 and CH_4. In these hostile conditions the first microorganisms – cyanobacteria – emerged 3.5 billion years ago. For eons, they were the sole photosynthesizers which contributed with oxygen to the reducing and anaerobic atmosphere. The first eukaryote appeared only 1.5 – 2.2 billion years ago, so far no living organism ever grew larger than a single cell. The first photosynthetic eukaryotes – microalgae – played an essential role in the formation of the actual breathable atmosphere (Barsanti and Gualtieri, 2006). The microalgae (including cyanobacteria which are also known as blue-green algae) and the macroalgae contribute with approximately 40 – 50% of the oxygen in atmosphere.

The microalgae use photosynthesis in order to turn the sunlight energy into chemical energy required for the conversion of CO_2 into organic compounds. The process is underpinned by the photosynthetic reaction centers which contain chlorophyll, an extremely important biomolecule able to harvest the solar light. These proteins (*i.e.* chlorophylls) are incorporated inside organelles of eukaryotes, named chloroplasts, while in prokaryotes (*i.e.* cyanobacteria) they are embedded in the plasma membrane. During their evolution the photosynthetic microorganisms inhabited virtually every ecological niche on Earth illuminated with visible light, most of which being inhospitable. Thus, they can live at very low (psychrophiles) or very high temperature (thermophiles), in acidic (acidophiles) or alkaline environments (alkaliphiles), when the salt concentrations are extremely high (halophiles) or in conditions with low availability of water (xerophiles). Several others are able to resist at high levels of radiation, especially ultraviolet light, or to live in extremely low levels of light. The

thermophilic prokaryotes (*e.g. Thermosynechococcus elongatus*) and eukaryotes (*e.g. Cyanidium caldarium*) were found to live in hot springs at maximal temperatures of 74 °C (Yamaoka *et al.*, 1978) and 55 °C, respectively (Ford, 1986). Other microalgae abound in the Arctic and Antarctic zones at temperatures close to freezing (*e.g.* species of *Cymbella*, *Chlamydomonas nivalis*) (Armstrong 1987; Okuyama *et al.*, 1992). Certain species of microalgae are able to live at pH lower than 3 (*e.g. Chlamydomonas acidophila*) in environments such as volcanic waters, or at pH higher than 11 in soda lakes (*e.g. Spirulina platensis*) (Belkin and Boussiba, 1991; Spijkerman, 2005). Green algae such as *Dunaliella salina* can be found in hypersaline environments at NaCℓ concentrations up to saturation (Jiménez and Niell, 1991). Species such as *Trentepohlia umbrina* were found to survive on the tree bark almost without water for major part of the year because rain falls on the bark only during period without leaves (Raj *et al.*, 2010). In what regards the light availability the depth record is held by a dark purple red algae collected at a depth of 268 m where faint light is blue-green and its intensity is only 0.0005% of surface light. These types of microalgae are able to live in low-irradiance environments due to certain accessory pigments which are capable to harvest the light and channel the energy to chlorophyll *a*, the only pigment able to convert efficaciously the energy of absorbed light into high energy bonds of organic molecules (*e.g.* ATP). In contrast, the microalgae which live in high-irradiance environments have pigments that protect them against photodamage (*e.g. Dunaliella salina, Chlamydomonas nivalis*). The amount of accessory pigments confers to microalgae their large variety of colors, hence their common names such as brown algae, red algae and green algae.

The algae form the base of the marine food chain supporting directly or indirectly most life in oceans (which extend on 71% of Earth's surface) being also identified as the elemental resource of fossil carbon found in crude oil and natural gas (Andersen, 2005). The algae can be aquatic or subaerial (exposed to atmosphere instead of being submerged in water), planktonic (suspended in the lighted regions of any water bodies) or benthic (attached on stones, sand, plants or animals). The planktonic algae are not always a vector of life but sometimes a cause of death when their population becomes too large as result to the aquatic system pollution with artificial or natural substances such as nitrates and phosphates. The algal blooms are also known as water eutrophication and it is estimated that more than 50% of them produce poisons which affect the neuromuscular systems and are carcinogenic for vertebrates, frequently causing massive death of fish, birds, bovines, dogs and other animals and serious illness to humans (Carmichael, 1997). Even though the microalgae are typically aquatic microorganisms, a significant number are adapted to life on land (tree trunks, animal

fur, snow banks, hot springs, or even embedded within desert rocks). The subaerial microalgae are able to convert rock in soil, to minimize soil erosion and to increase water retention and nutrient availability for plants growing nearby.

Certain species of microalgae can establish mutually beneficial partnerships with other organisms. They furnish oxygen and complex organic compounds to their partners receiving back protection and simple nutrients. Arrangements which ensure both partners to survive in inhospitable conditions are created with fungi to form lichens or with reef-building corals.

Most algal groups are considered photoautotrophs, in other words they are depending completely on the photosynthetic apparatus for their metabolic requirements and on the availability of light in order to convert CO_2 into organic substances, producing at the same time O_2 as a residue in the water photolysis reaction. The majority of algal groups contain colorless heterotrophic species which are able to acquire organic carbon from the external environment through phagotrophy (*i.e.* ingesting particles) or through osmotrophy (*i.e.* uptake of dissolved organic compounds). Several types of microalgae have the capacity to augment the photosynthesis with sugars, acetate or other small organic compounds imported through the cell membrane-based transport proteins (*e.g. Chlamydomonas* is able to utilize acetate as unique source of carbon and energy).

There are also certain types of algae, termed auxotrophs, which are not able to synthesize essential compounds such as vitamins of B_{12} complex or fatty acids and are therefore forced to import them.

Various other types of algae use a complex spectrum of nutritional strategies combining photosynthesis with osmotrophy and/or phagotrophy modulating their different nutritional modes as the environment is changing. This capability of functioning sometimes as photoautotrophs (producers) and other times as heterotrophs (consumers) is known as mixotrophy.

Based on their nutritional strategies the microalgae can be classified in four groups (Barsanti and Gualtieri, 2006):

- Obligate heterotrophic algae – are mainly heterotrophs, but are able to support themselves through phototrophy when the organic compounds from the medium limit their growth;
- Obligate phototrophic algae – are mainly phototrophs, but are capable to supplement their growth through phagotrophy and/or osmotrophy when the light becomes limiting;
- Facultative mixotrophic algae – are able to grow equally as phototrophs and as heterotrophs;

- Obligate mixotrophic algae – are mainly phototrophs, but phagotrophy and/or osmotrophy furnishes essential compounds for growth (the photoauxotrophic algae can be included in this group).

The microalgae are able to reproduce by a variety of means, both sexual and asexual. The sexual reproduction consists in plasmogamy (*i.e.* fusion of gametes) followed by karyogamy (*i.e.* nuclear fusion) to form a diploid zygote. The asexual reproduction involves that an individual organism is able to produce additional copies of itself through cellular bisection, zoospore or autospore production, autocolony formation or even through fragmentation.

As a result of their abundance in almost every corner of this planet and of their ability to biosynthesize various components with high nutritional values certain species of microalgae are used for human and animal nutrition. For millennia species such as *Nostoc*, *Arthrospira* (*Spirulina*) and *Aphanizomenon* were collected for human consumption (Becker, 2004). Actually, certain microalgae are used in aquaculture for the breeding of various species of marine animals as a food source for all growth stages of bivalve mollusks, larval stages of some crustacean species, and very early growth stages of some fish species. Algae are furthermore used to produce mass quantities of zooplankton (rotifers, copepods, brine shrimp) which serve in turn as food for larval and early-juvenile stages of crustaceans and fish. The microalgae are also attractive for a wide range of biotechnological and environmental applications that are described for the specialized reader in Appendix 1 and 2. In addition, the definition and the classification of the photobioreactors along with the main design types and their operating modes are available in Appendix 3.

I.1.2. Photobioreactor Modeling – State of the art

For sustainable development of pilot or industrial photobioreactors, reliable operating protocols must be conceived in order to achieve stable performances and process traceability. These targets require quantifiable advanced knowledge in what regards the physicochemical and biological phenomena which take place within the facility. The mathematical models used for numerical simulation are the analytical tools which allow to predict the process behavior and to comprehend its significant mechanisms. They must accomplish certain conditions such as embedding the main variables involved in the process, describing as accurate as possible their dynamics, having numerical solutions in accordance with the technological reality and being handleable from a mathematical point of view. Thus, their degree of detail should be low enough to be tractable, but high enough to avoid the loss of realism.

The general process of photosynthesis lays the basis of photobioreactor's modeling and its understanding is fundamental in this context. A brief description of the global process of photosynthesis can be found in Appendix 4.

I.1.2.1. General Approach of Modeling Photobioreactors

The mathematical modeling of the photosynthetic growth of microalgae in photobioreactors can be realized by using the general approach elaborated for submerged cultures of microorganisms. The growth of a microalgae culture can be defined as the increase in mass, while the *growth rate* is the increase of microalgal cell mass per unit of time.
In batch cultures the growth of microbial populations follow the general growth curve depicted in Fig.I.1.1.

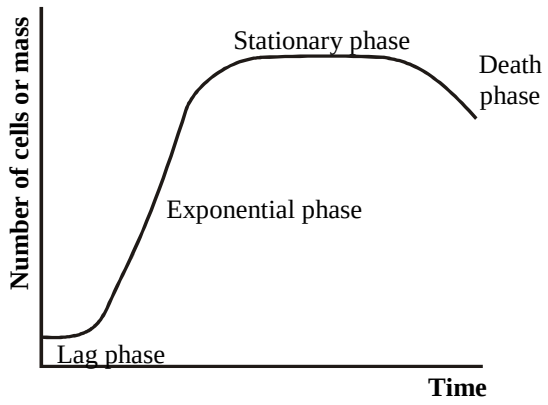

Fig.I.1.1. General growth curve of microorganisms

The general growth curve of microorganisms highlights four distinct phases which are identical for microalgae:

- *Lag phase*. The lag phase is a period of accommodation of algae to the new autotrophic medium. This phase can take up to two days while the microalgae start to synthesize various biochemicals without growing in mass. The lag phase is observed when the microalgae are inoculated on a different medium from the one on which they were preserved (*e.g.* from a heterotrophic medium used on Petri dishes to an autotrophic medium in photobioreactor).
- *Exponential growth phase (Log Phase)*. Once the microalgae cells have adapted to the photoautotrophic medium their number starts to increase exponentially:

$$X(t) = X(0)e^{\mu t} \quad \text{(I.1.1)}$$

where $X(t)$ is the biomass concentration at time *t*, $X(0)$ is the initial concentration of biomass and μ is the specific growth rate. The growth can be expressed also by using logarithms:

$$lnX(t) = lnX(0) + \mu t \quad \text{(I.1.2)}$$

where μ is given by:

$$\mu = \frac{lnX(t) - lnX(0)}{t} \quad \text{(I.1.3)}$$

- *Stationary phase*. When one of the substrates from the culture medium is consumed or certain secondary metabolites have accumulated, the growth is limited or inhibited and the microalgal population reaches a stationary phase.
- *Death phase*. When the culture does not have the proper growth conditions the cells start to die with a decay rate higher than the growth rate. If the culture analysis is made on optical basis (*e.g.* optical density, turbidity) the death phase may be confused with the stationary phase because the sensors will display a constant concentration regardless of the decay rate, therefore a microscopic exam must be done.

Taking into consideration the four phases described above, the proper modeling of bioprocesses can be done through zonal modeling approach due to the fact that various parameters of the model are different for each separate phase. Thus, in order to obtain a good fitting of models with experimental data is important to identify a different set of parameters for each phase.

Most of the models used currently for bioprocesses are proper only for the exponential growth phase and even though they are able to express mathematically a stationary phase it usually does not fit well with experimental data. Nevertheless, lag, stationary and death phases do not present interest from a technological point of view and are frequently neglected aiming maximum productivities.

If the photobioreactor is operated in continuous mode the stationary and death phases are eliminated by maintaining the culture in a continuous exponential phase for a long period of

time. The continuous mode aims to reach a steady state where the biomass concentration is constant and the specific growth rate μ equals the dilution rate *D*.

The mathematical representation of the main state variables of the photosynthetic growth process necessitates the simultaneous manipulation of two types of mechanisms:

- Physiological behavior which includes characterization of metabolic activity, determination of bioreactions' stoichiometries and determination of kinetics for the substrate conversion in biomass or products;
- Physical controlling measures which include the characterization of gas-liquid transfer rates, thermodynamic equilibria and light transfer inside the photobioreactor.

Considering that the photosynthetic processes depend on the light availability inside the culture, its attenuation by the microalgal cells must be well understood and characterized in order to obtain a reliable mathematical model of the photobioreactor. The description of the growth, consumption and production kinetics which lead to the derivation of the state variables must be thus associated with the transport phenomena and with the physical transfer of light energy described through radiative transfer equations.

The general approach can effectively be applied to photosynthetic growth of microalgae (*e.g. Chlamydomonas reinhardtii*) without significant modification.

I.1.2.2. Mass Balance Modeling

The lack of precise laws regarding the microalgae evolution makes the modeling this kind of bioprocesses complicated. However, the microalgal culturing processes must conform to certain rules such as the conservation of mass, electroneutrality of solutions etc.

Taking for example a component i inside the photobioreactor, its general balance equation can be described as:

$$\begin{bmatrix} Accumulation\ rate \\ of\ component\ i \end{bmatrix} = \begin{bmatrix} Transport\ rate \\ of\ component\ i \end{bmatrix} + \begin{bmatrix} Conversion\ rate \\ of\ component\ i \end{bmatrix} \quad \text{(I.1.4)}$$

One particularity of the microalgal cultures is the anisotropic medium, in terms of light, inside the photobioreactor given by the self-shading phenomenon. Thus, the kinetic rates are varying along the culture depth and therefore they must be considered as average values denoted by the < > operator. On the other hand a reactor may be well mixed or plug flow, but in the following lines only the first one will be considered because it is the most common. Except

the fed-batch mode, the reactors operated in discontinuous or continuous mode work at constant volume, and thus, the general expression of time-varying dissolved components (including the biomass) can be expressed as follows:

$$V_l \frac{dc_i}{dt} = \langle r_i \rangle V_l + F\left(c_{i,0} - c_i\right) \tag{I.1.5}$$

where c_i is the mass concentration of component i which is constant all over the reactor's volume and equal with the concentration in the output flow. V_l is the reactor's volume, F is the volumetric flow rate, $c_{i,0}$ is the mass concentration of component i in the feed and r_i is the mass volumetric conversion rate of component i.

By introducing the dilution rate $D = F/V_l$ and the specific mass conversion rate of component i, μ_i, the following relations can be obtained:

$$\langle r_i \rangle = \langle \mu_i \rangle c_i \tag{I.1.6}$$

hence the time variation of the mass concentration of component i can be written as:

$$\frac{dc_i}{dt} = \langle \mu_i \rangle c_i + D\left(c_{i,0} - c_i\right) \tag{I.1.7}$$

If the molar specific rate of reaction – J, the molar mass of component i – M_i and the stoichiometric coefficients – ν_i ($\nu_i > 0$ for a product and $\nu_i < 0$ for a substrate) are introduced (Cornet *et al.*, 1998), then:

$$\langle \mu_i \rangle = \nu_i M_i \langle \mathrm{J} \rangle \tag{I.1.8}$$

which gives the time variation of the molar concentration of component i:

$$\frac{dc_i'}{dt} = \nu_i M_i \langle \mathrm{J} \rangle c_i' + D\left(c_{i,0}' - c_i'\right) \tag{I.1.9}$$

where c_i' and $c_{i,0}'$ is the molar concentration of component i inside the reactor (into the liquid phase) and in the feed, respectively.

This formulation is somehow accurate only for the dissolved components (or solid components which are well homogenized into the culture) which have no exchange between liquid and gaseous phases. In other words, it is accurate for the components which are introduced into the photobioreactor exclusively through the liquid phase (*e.g.* ammonium, nitrates, phosphates, sulfates etc) or for the components which are formed into the liquid phase (*e.g.* biomass or other extracellular products), and do not leave the reactor in gaseous form as a result of a saturation process.

The microalgal culturing techniques involves also gaseous compounds such as O_2 which is produced in the water photolysis reaction. The O_2 will remain dissolved in the culture up to its saturation value above which it will leave the reactor in gaseous form. Commonly, the pH of photosynthetic cultures of microalgae is regulated by means of gaseous CO_2 bubbled into the reactor. In the same manner, the gas will be dissolved in the culture up to a specific concentration and the excess will leave the reactor in gaseous form. Thus, a phase equilibrium governed by Henry's law and determined by the molality of molecular solute will establish:

$$c'_{i,\text{gas}} \overset{f(P,T)}{\longleftrightarrow} c'_{i,\text{aq}} \tag{I.1.10}$$

where $c'_{i,\text{gas}}$ is the molar concentration of gaseous component *i* and $c'_{i,\text{aq}}$ is the molar concentration of dissolved species *i*. The equilibrium is a function of pressure *P* and temperature *T* and because the vapor dissociation of $c'_{i,\text{aq}}$ is appreciable only at very high temperatures which are not compatible with the microalgal growth process is therefore neglected. Thus, the general formulation considers only the gaseous component which leaves the reactor as a result of saturation and not due to vapor phase dissociation.

As a consequence, a term related to gas-liquid mass transfer must be added in order to derive a proper mathematical model expression for the dissolved gasses involved in the photosynthetic process.

$$\frac{dc'_i}{dt} = \nu_i M_i \langle \mathrm{J} \rangle c'_i + D\left(c'_{i,0} - c'_i\right) + N_i \tag{I.1.11}$$

where N_i is the volumetric mass transfer rate of component *i*.

By considering that all kinetic processes, whether they refer to substrates consumption or to products accumulation, take place only under the influence of biomass, the dynamic expression (I.1.11) accepts simplification. Thus, any reaction rate can be expressed as a

function of the mass volumetric conversion rate of biomass – $r_x = \langle\mu\rangle X$, where μ is the specific mass conversion rate of biomass and X is the mass concentration of biomass. The C-mole mass – M_x needs also to be introduced in order to express r_x in terms of molar conversion rate. By using the stoichiometric coefficients the molar conversion rate of component *i* can be written as:

$$r_i' = \nu_i \frac{\langle r_x \rangle}{M_x} \tag{I.1.12}$$

The general dynamic expression (I.1.11) will thus become:

$$\frac{dc_i'}{dt} = \nu_i \frac{\langle r_x \rangle}{M_x} + D\left(c_{i,0}' - c_i'\right) + N_i \tag{I.1.13}$$

N_i takes positive values only for dissolved gasses whereas for the components which do not establish any gas-liquid equilibrium it will be null.

Under certain circumstances the biomass growth can be influenced by various substrates or reaction products (*e.g.* inhibition), thus the specific growth rate can be expressed as a complex function of any component(s): $\mu = f(c_1, \cdots, c_i, \cdots, c_N)$.

However, the volumetric mass transfer rate is usually expressed as:

$$N_i = (K_L a)_i \left(c_{i,\text{sat}}' - c_i'\right) \tag{I.1.14}$$

where $(K_L a)_i$ is the overall volumetric mass transfer coefficient for component *i* and $c_{i,\text{sat}}'$ is the molar concentration of component *i* at saturation.

At gas-liquid equilibrium the concentration of a dissolved gas at saturation is related to pressure and can be expressed through its output molar fraction – y_{out}^i and Henry's constant – H_i.

$$c_{i,\text{sat}}' = \frac{y_{out}^i P}{H_i} \tag{I.1.15}$$

where $\sum y_{out}^i = 1$ and $y_{out}^i = 1/n_{out}^i$; n_{out}^i is the number of moles of component *i*. The number of gas moles which exit the photobioreactor can be computed by subtracting the

number of gas moles which remain dissolved in the liquid volume from the number of gas moles which enters into the reactor:

$$y_{out}^{i} G_{out} = y_{in}^{i} G_{in} - V_l N_i \quad \text{(I.1.16)}$$

where y_{in}^{i} is the input molar fraction of gaseous component *i*, and G_{in} and G_{out} are the input and output flow of gas mixtures. Thus, a simple balance equation can be written for any output molar fraction of any gaseous component *i* which intervenes in the culture dynamics, by using the ideal gas law:

$$\frac{dy_{out}^{i}}{dt} = \frac{RT}{PV_g}\left(y_{in}^{i} G_{in} - y_{out}^{i} G_{out} - V_l N_i\right) \quad \text{(I.1.17)}$$

The modeling approach described above ensures an accurate description of the main state variables of a multiphase photobioreactor under various circumstances, without any loss of realism. This model may be applied to various species of microalgae and to different types of photobioreactors by reidentifying the model parameters.

I.1.2.2.1. *The Droop Model*

Various researches were focused on the ability of microalgae to biosynthesize certain secondary metabolites (*e.g.* lipids, starch, hydrogen etc) under stress conditions. The results showed that the main mechanism of production is the nutrient starvation (*e.g.* nitrogen, sulfur, phosphorus). Certain nutrients are not used directly by the microalgal cells but absorbed and stored in intracellular pools which represent internal resources used only when there is a need to biosynthesize primary metabolites. In other words, when a nutrient is completely exhausted from the medium the photosynthetic activity of microalgae lasts another few days during this period being progressively limited (Fig.I.1.2). In order to introduce the concept of intracellular quota of nutrient Droop (1968) has undertaken a challenging approach describing its dynamics in relation with the biomass concentration and the extracellular nutrient concentration. The model was developed in the first instance for the dynamic representation of the effect of B_{12} vitamin internal quota on the phytoplankton growth rate (Droop, 1968), but proved afterward to be appropriate for other macronutrients. The Droop formulation is based on the fact that the growth rate of biomass is not directly linked to the absorption rate of

nutrient from the culture medium, but related equally with the intracellular quota of nutrient, denoted Q.

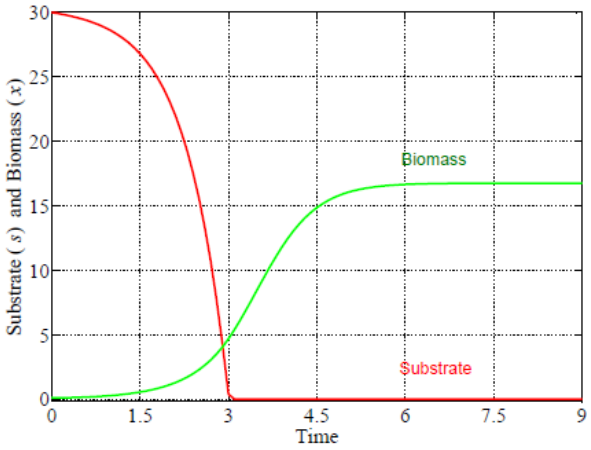

Fig.I.1.2. Typical growth curve for microalgae from Bernard, (2011)

Thus, mass balance equation of the Droop model for a well-mixed photobioreactor can be written as:

$$\frac{dX}{dt} = \langle r_x \rangle - DX \tag{I.1.18}$$

$$\frac{dS}{dt} = -\langle r_s \rangle - D(S_0 - S) \tag{I.1.19}$$

$$\frac{dQ}{dt} = \frac{\langle r_s \rangle - \langle r_x \rangle Q}{X} \tag{I.1.20}$$

Because the Droop model is more specific in comparison with the general approach the notations of the state variables are: X for biomass, S for the limiting substrate (*e.g.* nitrogen, sulfur, phosphate) and Q for intracellular quota of limiting substrate. $\langle r_s \rangle$ is the external substrate consumption rate. Other important state variables (*e.g.* non-limiting substrates, dissolved gases, products or components in gaseous phase) can be also added by using the general formulation described above.

The general models presented above are not available for the case of high density cultures and must be modified by:

- Including the irradiance effect on the microalgal growth,

- Considering a light gradient which establish inside the culture as a result of self-shading phenomenon.

I.1.2.2.2. *Matrix Representation*

The ordinary differential equations which describe the main state variables of the photosynthetic growth process can be expressed in matrix form. The general formulation of a continuous-time state-space model described by nonlinear differential equations can be written as:

$$\begin{cases} \dot{x} = f(x) + \sum_{i=1}^{m} g_i(x)u_i \\ y_i = h_j(x) \text{ with } j = 1, \dots, l \end{cases} \quad \text{(I.1.21)}$$

where $x \in \mathbb{R}^n$ is the state vector, $u \in \mathbb{R}^m$ is the vector of inputs and $y \in \mathbb{R}^m$ is the vector of outputs; $f(x)$ is an n-dimensional vector of nonlinear functions, $g(x)$ is an $(m\,x\,n)$-dimensional matrix of nonlinear functions and $h(x)$ is an m-dimensional vector of nonlinear functions.

For a well-mixed photobioreactor operated in continuous mode the input variable is $u = D$ and the output variable is $y = X$. In this case X needs to be measurable or estimable. It is assumed that the concentration of biomass in the feed is null, thus the matrix representation of a general model for photobioreactors can be written as follows:

$$\begin{cases} \dot{x} = \begin{bmatrix} \dot{X} \\ \dot{c}_i' \\ \dot{y}_{out}^i \end{bmatrix} = \begin{bmatrix} \langle r_x \rangle \\ \nu_i \frac{\langle r_x \rangle}{M_x} + N_i \\ \frac{RT}{pV_g}\left(y_{in}^i G_{in} - y_{out}^i G_{out} - V_l N_i\right) \end{bmatrix} + \begin{bmatrix} -X \\ c_{i,0}' - c_i' \\ 0 \end{bmatrix} D \\ y = X \end{cases} \quad \text{(I.1.22)}$$

As it can be observed the state vector x can contain, besides biomass concentration which is the center of any photosynthetic growth process, a series of substrates, dissolved gasses, products or molar fractions of gaseous components.

If other inputs which significantly influence the photosynthetic process are identified (*e.g.* $y_{in}^i G_{in} = G_{in}^i$ – the partial volume of gaseous component *i*, controlled in order to manipulate a

state or internal variable) the model can be rewriten resulting a multivariable system. These types of formulations are widely used for control purposes.

I.1.2.2.3. *Stoichiometric Parameters*

The conversion of substrate *i* into product *j* (including biomass) is usually expressed through the mass yield $Y_{i/j}$ which have the following general expression:

$$Y_{i/j} = \left|\frac{\langle \mu_j \rangle}{\langle \mu_i \rangle}\right| = \left|\frac{\nu_j}{\nu_i}\right| \frac{M_j}{M_i} \tag{I.1.23}$$

Thus, $Y_{i/j}$ is not dependent on the reaction rate J and therefore it must be expressed stoichiometrically rather than kinetically.

However, the model can be reduced in complexity by using a single stoichiometric equation which describes the elemental composition of dry cell material, either the global content of carbon, oxygen, hydrogen, nitrogen, phosphorus and sulfur, or the mass fractions of different groups of macromolecules such as proteins, lipids and carbohydrates. When the stoichiometric equation is not available, a pseudo-reaction scheme could be defined. In that case, $Y_{i/j}$ represents apparent yield coefficients, identified from experimental data (Bastin and Dochain, 1990).

I.1.2.3. Radiative Transfer Modeling

The microalgae are able to absorb photons only in the visible domain (400 – 700 nm) frequently named photosynthetic active radiation (PAR) and on the extreme red end of the visible spectrum (700 – 800 nm). Exclusively in this range the absorption of a photon can lead to the excitation of an electron and hence of a molecule (*e.g.* chromophore molecules) because the lower energy of an infrared photon could be confused with the energy derived by molecular collisions, eventually increasing the noise of the system and not its information. The higher energy of an UV photon could dislodge the electron from the electronic cloud and destroy the molecular bonds of the chromophore (Barsanti and Gualtieri, 2006).

The light is attenuated in a culture of microalgae, regardless of photobioreactor's shape or the lighting source, creating a heterogeneous radiant field. The light gradient is responsible for the

decreasing growth rates along the depth *z* of the culture, therefore the availability of light at each *z* must be determined in order to accurately calculate the local photosynthetic responses. The attenuation of light is induced by pigments of photosynthetic cells which absorb the photonic energy, and depends on various factors such as photobioreactor geometry, lighting source position, hemispherical incident flux density, emission spectrum, optical properties of culture medium, biomass concentration, pigmentation etc. A typical case of light attenuation is presented in Fig.I.1.3 for a rectangular photobioreactor lighted from one side. As it can be observed the attenuation of photonic energy inside the reactor takes place on one direction, which is the culture depth.

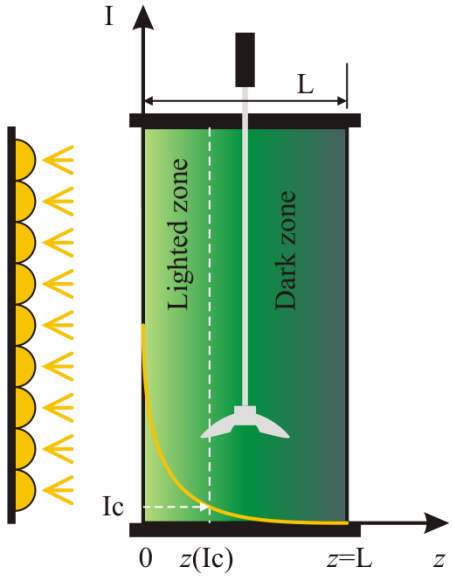

Fig.I.1.3. Schematic representation of light attenuation inside a photobioreactor lighted from one sight (*I* – irradiance, I_c – compensation point, *L* – photobioreactor depth, *z* – culture depth)

The available radiant light energy, for which photosynthesis compensates the respiration and thus the exchange rates for O_2 and CO_2 are equal to zero, is known as the compensation point. In order to characterize the attenuation of light inside photobioreactors various concepts were approached, starting from simple laws such as the Lambert-Beer law to complex radiative models such as the two-flux model.

The Lambert-Beer's law can describe mathematically the decrease of light as a function of depth:

$$q_z = q_0 \cdot e^{-kz} \tag{I.1.24}$$

where q_z is the intensity of light at depth *z*, q_0 is the intensity of light at depth 0 and *k* is the attenuation coefficient which describes how quickly the light is attenuated in a body of water (the Lambert-Beer's law can be expressed also in terms of irradiance *I*).

In order to model the light attenuation inside a microalgae culture two independent phenomena must be considered, namely the absorption of light by pigments and the scattering of light by cells.

One of the most accurate models for such complex media is the two-flux model which considers both absorption and scattering phenomena. Cornet *et al*., (1995, 1998) presented a handleable model by simplifying the radiative transfer equation based on a hypothesis of monodimensional attenuation (for rectangular reactors). The light propagation (for a wavelength λ) takes place exclusively along culture depth *z*, in both directions q_λ^+ and q_λ^-. Thus, for an incident flux which is perpendicular on the optical surface the following system can be written:

$$\begin{cases} \frac{dq_\lambda^+}{dz} = -E_{a\lambda} X q_\lambda^+ - E_{s\lambda} X b_{2\lambda} (q_\lambda^+ - q_\lambda^-) \\ \frac{dq_\lambda^-}{dz} = E_{a\lambda} X q_\lambda^- - E_{s\lambda} X b_{2\lambda} (q_\lambda^+ - q_\lambda^-) \end{cases} \quad \text{(I.1.25)}$$

where $E_{a\lambda}$ and $E_{s\lambda}$ are the mass absorption and the mass scattering coefficients, $b_{2\lambda}$ is the backward scattering fraction and *X* is the biomass concentration.

Imposing appropriate boundary conditions, the solution of the system gives the irradiance $I_\lambda(z)$ for any depth *z* of the culture:

$$I_\lambda(z) = q_\lambda^+(z) + q_\lambda^-(z) \quad \text{(I.1.26)}$$

The analytical expression of spectral irradiance was presented by Pottier *et al.*, (2005) considering a quasi-collimated incident flux and the two-flux model.

$$I(z) = 2q_0 \frac{(1+\alpha)e^{\delta(L-z)} - (1-\alpha)e^{-\delta(L-z)}}{(1+\alpha)^2 e^{\delta L} - (1-\alpha)^2 e^{-\delta L}} \quad \text{(I.1.27)}$$

with $\delta = X\sqrt{E_a(E_a + 2bE_s)}$ the two-flux extinction coefficient and $\alpha = \sqrt{(E_a)/(E_a + 2bE_s)}$ the linear scattering modulus.

The light attenuation modeling inside photobioreactors was approached by various other authors such as Molina Grima *et al.*, (1997), García Camacho *et al.*, (1999), Csőgör *et al.*, 2001, Sierra *et al.*, (2008) etc.

I.1.2.4. Kinetic Modeling

Kinetics is the domain of bioprocesses modeling concerned with the reaction rates or the speed of a reactant or product in a particular reaction. A simple formalism similar to that on chemistry may be adopted to illustrate the transformation of substrates – S_i into biomass – X and products – P_i:

$$\nu_{S_i} \sum_{i=1}^{p} S_i \xrightarrow{r} X + \nu_{P_i} \sum_{i=1}^{k} P_i \qquad \text{(I.1.28)}$$

ν_{S_i} is the consumption yield of S_i, ν_{P_i} is the production yield of P_i and r is the reaction rate.
Thus, the reaction rates are complex functions which describe the relation between the reactants and products. The reaction scheme I.1.28 is applicable for processes of microbial growth and biosynthesis of secondary metabolites, but various other schemes can be drawn for different other necessities (*e.g.* to describe the formation of products in anaerobic processes when the biomass does not accumulate, to describe the decay of biomass, to describe the internal quota of a substrate in relation with the its extracellular concentration etc).
Most of the kinetic models currently used are approximate relations based on empirical considerations, which fortunately work in many instances.
It should be noted here that most of the states variables, ratios or quotas of a biological model are constrained to remain positive because their negative values have no physical significance. This constraint applies also to the reaction rates r_i which must be always positive.

I.1.2.4.1. *Basic Growth Kinetics*

The specific growth rate, defined earlier for batch cultures, can be described through the most commonly used expression which is the Monod's empirical model (Monod, 1942) that uses a law introduced by Michaëlis-Menten at the beginning of 20th century for enzymatic kinetics:

$$\mu = \mu_{max} \frac{S}{K_s + S} \quad \text{(I.1.29)}$$

where S is the substrate concentration, μ_{max} is the maximum specific growth rate and K_s is the half-saturation constant. The Monod's model permits the description of growth limitation phenomenon given by the depletion of substrate.

I.1.2.4.2. *Substrate Inhibition Kinetics*

In certain cases high concentrations of substrate can inhibit the growth of microorganisms. For this particular case the Andrews-Haldane expression can be used (Andrews, 1968):

$$\mu = \mu_0 \frac{S}{K_s + S + \frac{S^2}{K_I}} \quad \text{(I.1.30)}$$

with

$$\mu_0 = \mu_{max} \left(1 + 2\sqrt{\frac{K_s}{K_I}}\right) \quad \text{(I.1.31)}$$

where K_I is the inhibition constant.
Other common kinetic equations can be found in Appendix 5.

I.1.2.5. Coupling of Growth Kinetics with Radiative Transfer

The light attenuation inside microalgal cultures produces (as stated in section I.1.2.3) a heterogeneous radiant field for which local kinetics in each point of the reactor must be considered. The light-driven processes result in using a particular class of models which can return an averaged photosynthetic response by expressing the specific growth rate in terms of light attenuation inside the photobioreactor. Thus, the coupling between radiative and kinetic models is fundamental in photobioreactor studies being researched by various authors.
In the following lines there are presented the most cited kinetic models used for the microalgal culturing of various species such as: *Arthrospira platensis*, *Chlorella vulgaris*, *Isochrysis galbana*, *Porphyridium purpureum*, *Chlamydomonas reinhardtii*, etc.

$$\mu = \mu_{max} \frac{\mathcal{I}}{\mu_{max}+\mathcal{I}}$$; (Tamiya *et al.*, 1953) (I.1.32)

$$\mu = \mu_{max} \left(1 - e^{-\frac{\mathcal{I}}{\mathcal{I}_{max}}}\right)$$; (Van Oorschot, 1955) (I.1.33)

$$\mu = \mu_{max} \frac{\mathcal{I}}{\mathcal{I}_{max}} e^{\left(1-\frac{\mathcal{I}}{\mathcal{I}_{max}}\right)}$$; (Steele, 1977) (I.1.34)

$$\mu = \mu_{max} \frac{\mathcal{I}}{(K_i^m+\mathcal{I}^m)^{\frac{1}{m}}}$$; (Bannister, 1979) (I.1.35)

$$\mu = \mu_{max} \frac{\mathcal{I}^n}{\mathcal{I}_k^n+\mathcal{I}^n}$$; (Molina Grima *et al.*, 1994) (I.1.36)

$$\mu = \mu_{max} \frac{\mathcal{I}}{K_S+\mathcal{I}}$$; (Cornet *et al.*, 1995) (I.1.37)

$$\mu = \mu_{max} \frac{I_{av}^{\left(b+\frac{c}{I_0}\right)}}{\left[I_k\left(1+\left(\frac{I_0}{K_i}\right)^{a}\right)\right]^{\left(b+\frac{c}{I_0}\right)}+I_{av}^{\left(b+\frac{c}{I_0}\right)}}$$; (Molina Grima *et al.*, 1999) (I.1.38)

$$\mu = \mu_{max} \frac{I}{K_S+I+\frac{I^2}{K_I}}$$; (Fouchard *et al.*, 2009) (I.1.39)

where $\mathcal{I}$ is the incident photosynthetic radiation on a horizontal surface, $\mathcal{I}_{max}$ is the saturation value of $\mathcal{I}$, $\mathcal{I}_k$ is the microalgal affinity for light, I_{av} is the photosynthetically active average irradiance inside culture I_0 is the solar photosynthetically active irradiance on the reactor's surface and I is the irradiance for a specific depth of the culture.

Most of the models used in photobioreactor studies are based on the assumption that all concentrations are homogeneous and only the light has a special distribution. It must be noted that the Lambert-Beer equation (I.1.24) and the two-flux model equation (I.1.27) are providing local values of irradiance and therefore, in order to be properly used in growth kinetic models, two directions are commonly attended:

- The irradiance is expressed as average irradiance received by the culture along the depth L of photobioreactor, based on which the average specific growth rate is calculated (Molina Grima *et al.*, 1996; Acién Fernández *et al.*, 2001; Li *et al.*, 2003; Sloth *et al.*, 2006):

$$\langle I \rangle = \frac{I_0}{L} \int_0^L I dz \quad \text{(I.1.40)}$$

In this case the specific growth rate is calculated based on the average value of I.

- The growth rate is expressed as average photosynthetic response $\langle \mu \rangle$ calculated all over the reactor volume, obtained by integrating all local photosynthetic responses on the direction of the culture depth (Cornet *et al.*, 1995, 1998; Favier-Teodorescu *et al.*, 2003; Pruvost *et al.*, 2008; Cornet and Dussap, 2009; Fouchard *et al.*, 2009):

$$\langle \mu \rangle = \frac{1}{L} \int_0^L \mu\big(I(z)\big) dz \quad \text{(I.1.41)}$$

The local irradiance is determined using radiative model previously described (Eq. I.1.17) The microalgal growth rates are modeled considering the light as major "substrate", which causes limitation (*e.g.* Eq.I.1.37) or even inhibition (*e.g.* Eg.I.1.39) effect. This formulation is consistent only if the concentrations of other substrates do not limit or inhibit the growth.

I.1.2.6. Other Considerations Regarding Photobioreactor Modeling

Besides the available irradiance inside the culture there might be other substrates which limit or inhibit the microalgal growth. Thus, the literature also furnishes specific models which take into consideration the light availability coupled with other substrates such as: total inorganic carbon, nitrogen, phosphorous, sulfur, phycocyanin etc (Baquerisse 1999; Nouals, 2000; Cornet, 1998; Martinez Sancho *et al.*, 1999; Spolaore, 2005; Becera-Celis *et al.*, 2008a; Haario *et al.*, 2009; Fouchard *et al.*, 2009).

Given that the photosynthetic processes require CO_2 for growth and release O_2 from water photolysis reaction, the modeling of dissolved gases inside the culture remains a mediated problem in photobioreactor studies (Cogne *et al.*, 2001; Eriksen *et al.*, 2007; Sierra *et al.*, 2008; Nedbal *et al.*, 2010).

The CO_2 dissolution in water leads to the formation of molecular (*i.e.* $CO_{2,aq}$ and H_2CO_3) and ionic species (*i.e.* HCO_3^- and CO_3^{2-}) whose sum is known as total inorganic carbon (TIC). The TIC species establish dynamic equilibria which were discussed in a number of papers (Cornet, 1998; Molina Grima *et al.*, 1999; Becera-Celis *et al.*, 2008a).

Most of microalgal culturing techniques utilize gaseous CO_2 for the regulation of pH which is considered one of the most important parameters. Nevertheless, the dynamic modeling of pH

is poorly discussed in literature. However, Camacho Rubio *et al.*, (1999) proposed an expression for the concentration of H^+ ions (antilogarithm of pH) as a function of dissolved CO_2 based on the electroneutrality of solution and chemical equilibria:

$$d[H^+] = \frac{\frac{K_1}{[H^+]} + 2\frac{K_1 K_2}{[H^+]^2}}{1 + \frac{K_w}{[H^+]^2} + \frac{K_1[CO_2]}{[H^+]^2} + 4\frac{2K_1 K_2[CO_2]}{[H^+]^3}} d[CO_2] \quad \text{(I.1.42)}$$

where K_1, K_2 and K_w are equilibrium constants.

Buehner *et al.*, (2009) developed a dynamic model for time-variation of pH in a flat panel photobioreactor which was used as I/O model for the manipulation of CO_2 to control the pH:

$$\frac{d\mathrm{pH}}{dt} = \frac{1}{\tau_{\mathrm{pH}}}\left(K_{\mathrm{pH}} m_{\mathrm{TIC}}(t) - \mathrm{pH}(t)\right) \quad \text{(I.1.43)}$$

where τ_{pH} is the lag time associated with TIC settling into the appropriate species, K_{pH} is the conversion factor TIC to pH units and m_{TIC} is the concentration of TIC.

It must be mentioned here the paper of Lee *et al.*, (2006) which defined the light uptake rate for lumostatic cultures in bubble column photobioreactors:

$$q_e = \frac{(I_{in} - I_{out})A}{V_l C} \quad \text{(I.1.44)}$$

where q_e is the specific light uptake rate, I_{in} and I_{out} are the average light input and output energy, A is the optical surface of photobioreactor, V_l is the reactor's volume and C is the parameter to calculate q_e. The researches were oriented on three parameters: the cell concentration, the fresh weight and the concentration of astaxanthin.

Mairet *et al.*, (2011) developed a reliable model completing the Droop model with an equation which describes the dynamics of neutral lipid quota and one for the relation between chlorophyll and particulate nitrogen.

The hydrogen production from microalgae is also a mediated problem, but the modeling of the process is a work in progress. Nevertheless, the literature furnishes few modeling ideas (Park and Moon, 2007; Obeid *et al.*, 2009; Fouchard *et al.*, 2009).

I.1.3. Photobioreactor Control – State of the Art

From a general point of view, the automatic control of photobioreactors aims to keep certain process state variables (or functions of the state variables, specific criteria etc) close to a prescribed setpoint value or a previously defined profile despite disturbances and variations in process kinetics.
The researches regarding photobioreactor control are very rare. Currently, the control of photobioreactors is mainly oriented to strategies such as chemostats, pH-stats and lumostats.

I.1.3.1. Chemostatic Control

The chemostats are systems with embedded optical devices (able to measure variables such as turbidity or optical density of the culture) through which the dilution rate and the concentration of microalgae in photobioreactor can be controlled. The chemostatic control assumes the continuous addition of fresh medium into the reactor while the culture liquid is continuously removed, maintaining thus a constant volume. The addition of fresh culture medium can be realized in open loop (the input flow is usually constant) or closed loop (the input flow is variable being precisely calculated through the feedback mechanism in order to maintain the biomass concentration constant). The general chemostatic control of bioreactors (Mailleret *et al.*, 2004; Deschênes *et al.*, 2005; Zhao *et al.*, 2010) can be applied without many changes to photobioreactors. The majority of studies refer to linear control of biomass (Benson and Rusch, 2006; Sandnes *et al.*, 2006; Benson *et al.*, 2009), but the sustained research regarding the coupling between growth kinetics and radiative transfer led to the development of reliable dynamical models based on which certain nonlinear control techniques were approached in simulation (Mailleret *et al.*, 2005; Becerra-Celis *et al.*, 2008b; Ifrim *et al.*, 2010).

I.1.3.2. pH Control

The pH is a fundamental variable of microalgal cultures which is practically controlled in almost every study by means of on-off controllers. Usually, the pH of a photosynthetic culture of microalgae is regulated through CO_2 injection, but there are also reported acid/base pH controllers (Granum and Myklestad, 2002). The pH control is a nonlinear problem which requires suitable dynamical models and their lack narrows the control design to standard

linear algorithms which were reported to give satisfactory results (García *et al.*, 2003; Berenguel *et al.*, 2004; Buehner *et al.*, 2009; Fernández *et al.*, 2010), but they have the disadvantage of being based on linear tangent models around specific steady-state points.

I.1.3.3. Lumostatic Control

Although the light transfer inside microalgal cultures is fundamental in photobioreactor modeling, the studies regarding light control are rare. Many researches are targeting the usage of direct solar radiation and thus it is rather a significant disturbance than a control variable. Most studies on laboratory photobioreactors artificially illuminated employ a constant incident light flux throughout experiments. For continuous cultures a constant incident light flux determined through radiative models may be suitable, but for batch cultures the optimization of energetic consumption based on the rationalization of light appears to be a good idea.

Suh and Lee, (2001) cultivated a photosynthetic microorganism *Synechococcus* PCC 6301in an internally radiating photobioreactor which was controlled in lumostatic mode through a model-based control technique. The protocol consisted in manipulating the incident light intensity (input variable) to control the average irradiance calculated with the light distribution model. Batches piloted in lumostatic mode presented better productivities in comparison with the ones operated at constant incident light, thus eliminating the photoinhibition effect.

Choi *et al.*, (2003) operated in lumostatic mode a bubble column photobioreactor inoculated with *Haematococcus pluvialis*. The control variable, the specific light uptake defined earlier (Eq. I.1.44), was controled through the incident light flux manipulation. The authors reported cell concentrations with up to 250% higher than those obtained under constant light intensities. The research was continued by Lee *et al.*, (2006) who determined the best specific light uptake rates for the same type of photobioreactor.

I.1.3.4. Other Controllable Variables

The temperature is a variable which may significantly affect the development of microalgal cells and which is involved in the molecular thermodynamics of the dissolved chemical species. Its control is practically reported in most of the papers regarding microalgal culturing in laboratory devices, through thermal agents such as water or air (fans installed on the back

side of the reactors). The temperature is kept constant to an optimum value through on-off or PID controllers. The temperature of solar photobioreactors are hard to be controlled because of their dimensions, but there are reported pilot equipments immersed in water pools (Buehner *et al.*, 2009) for adequate control.

An innovative concept is the strategy developed by Marxen *et al.*, (2005) for the cultivation of *Synechocystis* sp. under controlled physiological conditions. The closed loop system named physiostat used as output variable the physiological state of microalgae measured online by recording the chlorophyll fluorescence parameters, while the light was used as input signal.

I.1.4. Further Objectives

The first chapter introduces a series of basic concepts regarding the modeling and control of bioreactors and photobioreactors which will lay the basis for the further studies presented in this thesis. The modeling and control concepts presented above can be also applied for the wastewater treatment plants with minimal modifications. However, most of the methods presented in the following chapters, used to model and to control the photobioreactors will be extended for wastewater treatment processes.

In what regards the photobioreactor studies the main objectives are to derive and to validate a dynamic model for the photoautotrophic growth of *Chlamydomonas reinhardtii* in an artificially lighted torus photobioreactor. The model must describe the dynamics of the main variables of the biological system which lead to the accurate prediction of the culture pH, a fundamental property of the system.

Based on the proposed model, which is a reliable tool for research, monitoring and control purposes, nonlinear multivariable control algorithms will be designed and validated in practice for the chemostatic, pH-static and lumostatic operation of photobioreactors.

I.2. MATERIALS AND METHODS

***Abstract*:** The present chapter details the materials and the methods used to fulfill the objectives regarding the validation of the proposed model and the practical implementation of the derived control algorithms. The experimental bench which consists in a torus photobioreactor and a suite of devices for monitoring and control is also presented.

I.2.1. The Biological Agent and the Culture Medium

The biological agent utilized in all experiments presented in this section was a wild type *Chlamydomonas reinhardtii* strain, referred as 137AH, which was used as a model microorganism. This strain originates from a culture collection of French Atomic Energy Center (Cadarache, France), where it is preserved in liquid nitrogen to prevent possible genetic mutations. For research purposes the strain is preserved by GEPEA laboratory in axenic conditions on Petri dishes with tris-acetate-phosphate (TAP) medium (Harris, 1989). The Petri dishes are kept in a refrigerated incubator at 4°C and low light intensity (40 $\mu mol \cdot m^{-2} \cdot s^{-1}$) being replicated each month. To adapt the microalgae to grow on liquid TAP medium and to prepare a sufficient quantity of cells to inoculate the reactor a successive cultivation in 500 mL Erlenmeyer flasks at 25°C and 100 $\mu mol \cdot m^{-2} \cdot s^{-1}$ light intensity is needed. These precultures are replicated with a permanent character at GEPEA laboratory to serve as inoculum in various research activities. The composition of standard TAP medium is presented in Table I.2.1.

Table I.2.1. Heterotrophic TAP medium (Harris, 1989)

Component	*Concentration*
$NH_4C\ell$	0.4 $g \cdot L^{-1}$
$MgSO_4 \cdot 7H_2O$	0.1 $g \cdot L^{-1}$
$CaC\ell_2 \cdot 2H_2O$	0.05 $g \cdot L^{-1}$
KH_2PO_4	0.056 $g \cdot L^{-1}$
K_2HPO_4	0.108 $g \cdot L^{-1}$
Tris-Base	2.42 $g \cdot L^{-1}$
Glacial acetic acid	1 $mL \cdot L^{-1}$
Hutner's trace elements (Hutner *et al.*, 1950)	1 $mL \cdot L^{-1}$

In what regards the experiments developed on photobioreactor it was chosen an autotrophic minimum growth medium (MGM) whose composition is presented in Table I.2.2.

Tabel I.2.2. Autotrophic MGM composition

Component	*Concentration*
$NaHCO_3$	1.68 $g \cdot L^{-1}$
$NH_4C\ell$	1.45 $g \cdot L^{-1}$
$MgSO_4 \cdot 7H_2O$	0.28 $g \cdot L^{-1}$
$CaC\ell_2 \cdot 2H_2O$	0.05 $g \cdot L^{-1}$
KH_2PO_4	0.61 $g \cdot L^{-1}$
Hutner's trace elements (Hutner *et al.*, 1950)	1 $mL \cdot L^{-1}$

According to Roels (1983) 1 mol of fixed CO_2 leads to 1 C-mol of biomass, and hence the following stoichiometry can be established:

$$CO_2 + 0.576H_2O + 0.181NH_3 + 0.006H_2SO_4 + 0.021P_i \rightarrow$$
$$CH_{1.771}O_{0.472}N_{0.181}S_{0.006}P_{0.021}(\text{biomass}) + 1.107O_2 \qquad \text{(I.2.1)}$$

Based on the nitrogen concentration in the above described culture medium results that it will become limiting when the biomass concentration will reach 2 $g \cdot L^{-1}$; the sulfur and the phosphorus will remain non-limiting at the same concentration of biomass. The use of a non-limiting culture medium lets the light to be the single "substrate" which limits the photosynthetic growth of microalgae, thus simplifying the expression of the specific growth rate.

In order to provide an inorganic environment for autotrophic growth of microalgae the cellular mass from the Erlenmeyer flasks was separated through centrifugation (2000 rpm, 5 minutes at 25°C) and resuspended in fresh autotrophic medium.

I.2.2. The Experimental Plant

The experimental bench presented in Fig. I.2.1. was realized in order to study and model the behavior of a *Chlamydomonas reinhardtii* culture and to control the photosynthetic growth process. The kernel of the plant is a lab-scale torus-shape photobioreactor (7) where the growth process takes place. Being a photosynthetic process the culture is lighted by an

electroluminescent diode panel (8) with variable light intensity which can be controlled through a voltage generator (9). The torus photobioreactor can be operated in discontinuous mode (batch mode), semi-continuous mode or continuous mode. The protocols for discontinuous mode operation consist in filling the entire reactor with concentrated fresh medium, inoculation and biomass development up to a stationary phase given by the exhaustion of a substrate or by the osmotic pressure exerted by high concentrations of biomass. In semi-continuous mode the reactor is partially filled with fresh medium and inoculated with a culture of cells. As the biomass is growing more medium is added up to a maximum working volume. This type of operating protocol is preferred when one of the substrates or products inhibit the growth. The continuous mode involves a constant feeding of the reactor with fresh medium by means of a pump. The volume of the reactor will remain constant which means that the same quantity of entered liquid will exit the reactor. The experimental bench is prepared to be operated in all three regimes, the montage consisting in a container of fresh medium (12), a feeding diaphragm pump (13), an evacuation peristaltic pump (14) and a container for the harvested biomass (15). The pH of the microalgae culture is usually regulated with gaseous CO_2 which is stored in a bottle under pressure (2). The addition of CO_2 is monitored with a mass flow meter (4) and controlled through a proportional valve (6). It is also used N_2 gas as vector gas in order to transport other gases (bubbled CO_2, produced O_2 or H_2 if formed) to the mass spectrometer for analysis, given that it is non-reactive. The N_2 installation consists in a N_2 gas bottle (1), a mass flow meter (3) to monitor the added gas and a proportional control valve (5). The composition of the output mixture of gases can be measured with a mass spectrometer (11) and converted in volumetric units by means of a mass flow meter (10) mounted at the exit of the photobioreactor. The pH and the temperature of the culture are measured with a gel pH electrode immersed in the reactor and attached to a transmitter (16). In the same manner the turbidity of the culture is measured with an optical turbidity probe connected to a transmitter (17). The marine impeller is actuated by an engine whose speed can be controlled by a source (18). The data from the plant are acquired through a data acquisition board (19) and transmitted to the process computer (20).

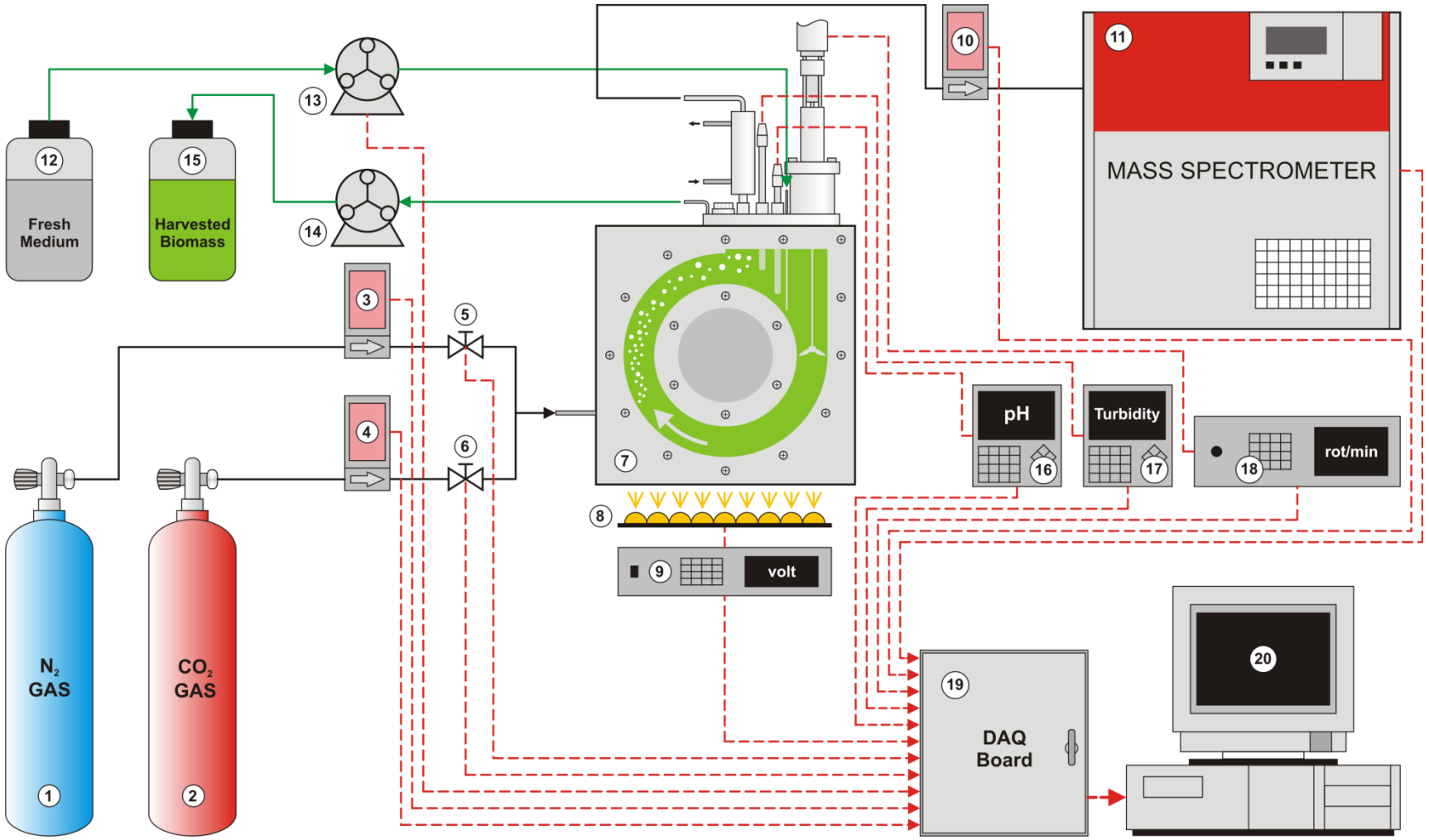

Fig.I.2.1. The experimental bench for monitoring and control the photobioreactor: ——— - gas lines; ——— - liquid lines; - - - - - - data transmission lines; 1 – N_2 gas bottle; 2 – CO_2 gas bottle; 3 – N_2 mass flow meter; 4 – CO_2 mass flow meter; 5 – N_2 proportional control valve; 6 – CO_2 proportional control valve; 7 – photobioreactor; 8 – electroluminescent diode panel; 9 – voltage generator for diode panel; 10 – output mass flow meter; 11 – mass spectrometer; 12 – fresh medium container; 13 – feeding diaphragm pump; 14 – evacuation peristaltic pump; 15 – harvested cells suspension container; 16 – pH transmitter; 17 – turbidity transmitter; 18 – stirrer engine controller; 19 – data acquisition board; 20 – process computer.

I.2.2.1. The Photobioreactor

The experiments presented in this section were developed in a lab-scale torus-shape photobioreactor (Fig.I.2.2) elaborated by GEPEA laboratory mainly for studying the hydrogen production by *Chlamydomonas reinhardtii* (Fouchard, 2005; Degrenne 2009). The reactor has a working volume of 1.47 L and a thickness of 4 cm. The torus shape presents a series of advantages, mainly in what regards its hydrodynamics, already highlighted in the technical literature (Pruvost *et al.*, 2004a; Pruvost *et al.*, 2004b; Pruvost *et al.*, 2006).

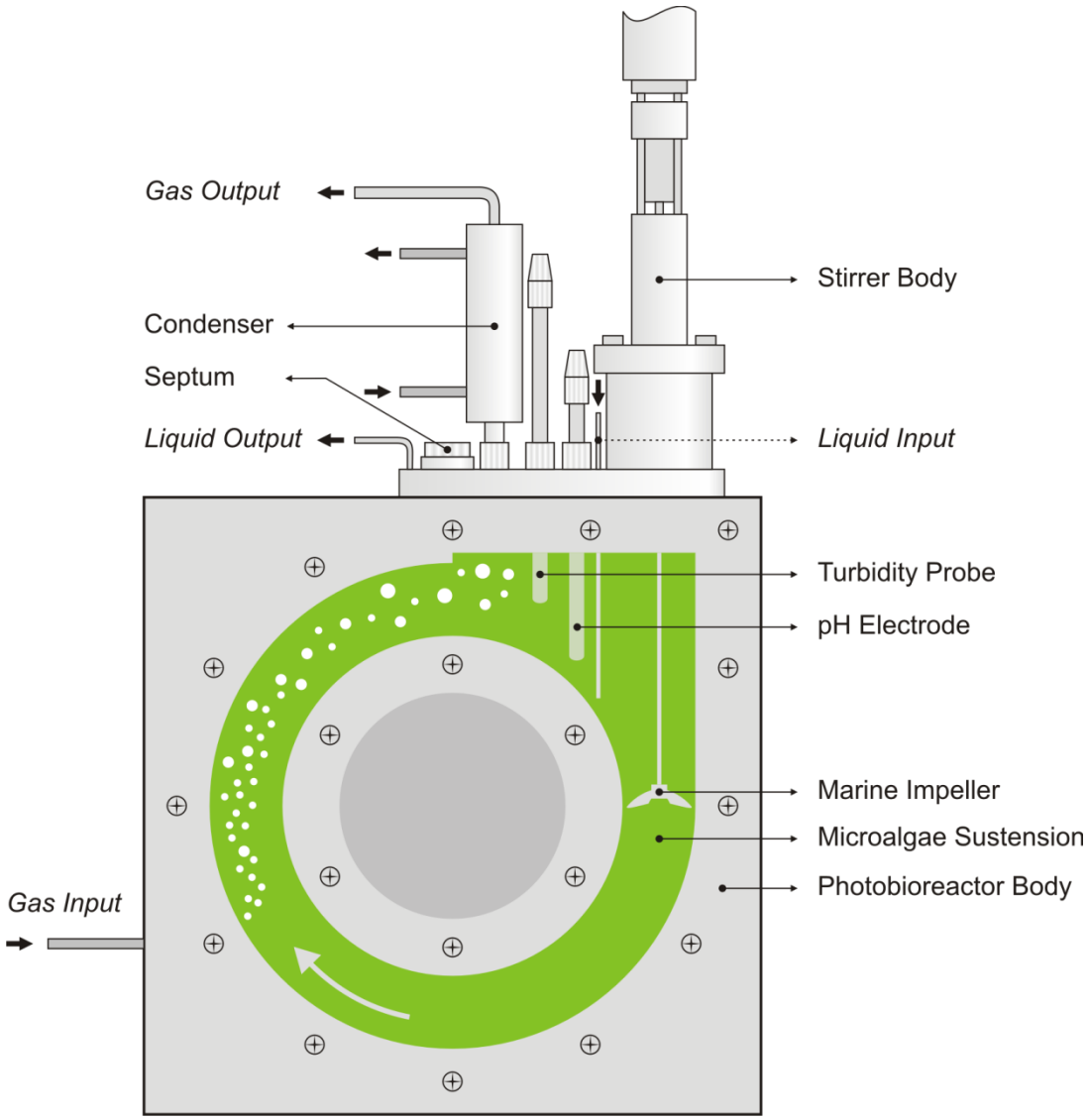

Fig.I.2.2. Lab-scale torus-shape photobioreactor

The reactor is provided with a marine impeller which, associated with the torus geometry, confers a tridimensional vortex flow which is adequate for the access of algae to the available

light and which results also in a proper homogenization of the medium in terms of concentrations. The photobioreactor has a stainless steel 316L body with a transparent polycarbonate front side which makes possible the steam sterilization-in-place (SIP). The incident light flux falls perpendicularly on the front side of the reactor whereas the back side is polished, giving a mirroring effect. The geometry of the reactor allows considering that the light attenuation is monodimensional which results in an easier manner of modeling the light transfer (Pottier *et al.*, 2005). Due to the fact that the culture is well homogenized the photoinhibition which takes place in the dark zone of the reactor (back side) can be treated as overall value and not distributed in layers, because the cells are rapidly shifted between dark to light zones.

The reactor is sealed with EDPM gaskets which are resistant to high temperature, physical wear and corrosion. In addition, the upper plate of the reactor allows the mounting of a condenser for the output gas, a pH electrode, a turbidity probe, a septum for sampling and nozzles for alimentation and evacuation of the culture.

I.2.2.2. The Light Intensity Loop

The light is the most important parameter in what regards the photobioreactor operation, being practically the limiting substrate of the photosynthetic growth of the microalgae thus conducting the process in terms of specific growth rate. The microalgae are able to capture light on visible domain (400 – 700 nm), frequently named *Photosynthetic Active Radiation* (PAR).

The photobioreactor is lighted by means of an electroluminescent diode panel (LED panel) (Fig.I.2.3) which has certain advantages in comparison with the classical fluorescent tubes; namely it gives collimated nature and homogeneity to the emitted light, it has a moderate heating, it is easy controllable and robust.

The LED panel was conceived through the attachment of 750 white and 750 far-red diodes on a printed circuit board. The white diodes emit light on entire visible domain while the far-red diodes emit light on the extreme red end of the visible spectrum (700 – 800 nm). The far-red diodes are usually required for studies regarding the decoupling of PSII dependent and independent pathways which can be realized by using a specific emission spectrum with wavelengths above 680 nm (*e.g.* hydrogen production protocols). The LED panel can be controlled through a voltage generator IT 6832 32V 6A which delivers 192W maximal power. The maximum allowable current which passes through a diode is 20mA.

The LED panel was installed at a distance of 2.5 cm from the transparent side of the reactor. The hemispherical incident light flux q_0 (or photon flux density PFD, as commonly named in photobioreactor studies), expressed in $\mu mol \cdot m^{-2} \cdot s^{-1}$, was measured with a plan sensor LI-COR LI-190-SA attached to a portable data logger LI-COR LI-250A. The measurements were done on six equidistant points on the internal wall of the transparent front side of the reactor. Their average was found to be linearly dependent of the supply current, thus being easily correlated through linear regression.

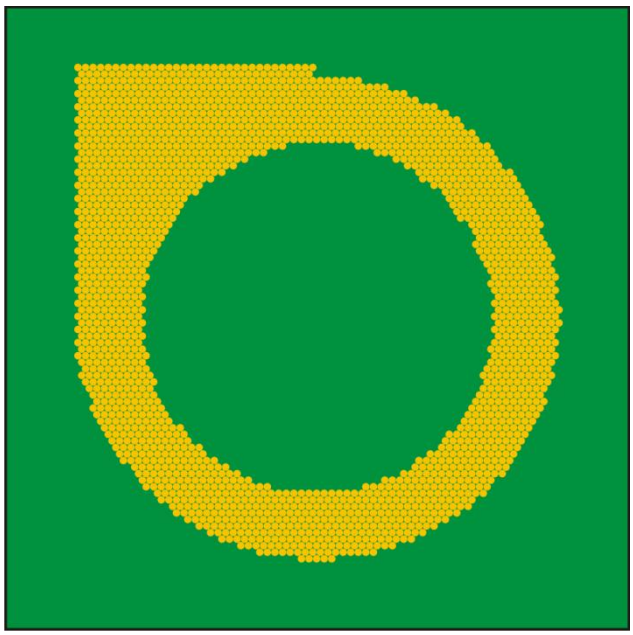

Fig.I.2.3. Electroluminescent diode panel (LED panel)

The voltage generator can be controlled remotely if connected to the process computer. In a closed loop with light as control variable, the output variable can be the lighted volume fraction or the specific light uptake rate, both based on measurable (or estimated) online values of incident light flux and biomass.

I.2.2.3. The Biomass Loop

The photobioreactor is provided with a Mettler Toledo® InPro8000 fiber optic sensor connected to a Mettler Toledo® Trb8300 transmitter, being able to measure the turbidity of a microalgae culture or its concentration of suspended particles. The turbidity and the suspended particles measurements take advantage of the interaction of light and particles. The light source installed in the transmitter is a near infrared light emitting diode (NIR-LED)

with a wavelength of 880 nm and the receiver is a silicon photodiode. The Trb8300 determines the turbidity value 500 times per second ensuring optimum compensation of external light. The signal is measured over an average time of 100 milliseconds in order to ensure a good signal-to-noise ratio. To eliminate interferences, additional zero point and reference signals are measured. The transmitter has four standard 0/4 – 20 mA outputs, 500 ohm load maximum, isolated from the measurement circuitry with an accuracy of ± 0.05 mA. The Trb8300 sensor is able to measure: FTU – Formazin Turbidity Units, NTU – Nephelometric Turbidity Units, EBC – European Brewery Convention, ppm – Parts per Million, g/L – Grams per Liter and % - Percents. The turbidity values FTU, NTU or EBC are used if the system is calibrated with formazin or the corresponding turbidity value of the process media is known, *i.e.* by grab sample measurements with laboratory turbidimeters calibrated in FTU, NTU or EBC. The % are used for samples with unknown turbidity characteristics by defining "turbidity" units on a relative 0-100 % scale. The ppm or g/L are used when the undissolved solid content has been determined by an alternative measurement, *i.e.* dry mass measurements of grab samples.

Due to the fact that a separate turbidity value is not available and the concentration of biomass (*i.e.* dry matter) is an offline analysis which is lengthy, it was more convenient to use percents. There was found a linear dependence between percents and dry matter, the correlation being realized offline through linear regression.

The biomass concentration can be controlled by manipulating the feeding flow of fresh medium. The fluid is immersed into the reactor by means of a diaphragm metering pump Stepdos® FEM 1.08 dedicated to laboratory use. The pump provides a quasi-continuous steady flow on a range of 0.01 to 30 mL·min^{-1} with an accuracy of 2% of set value. Knowing that the dilution D is the ratio between the feeding flow F and the working volume V of the reactor ($D = F/V$), it results that the pump can operate at dilutions between 0 to 1.22 h^{-1}. However, the calculated wash out dilution of the reactor is 0.1 h^{-1} which makes the pump operating range more than sufficient. The pump can be controlled remotely if connected to the process computer. The biomass loop can be let open by imposing a certain feeding flow to the pump or it can be closed by measuring online the biomass concentration, comparing it with a reference value and actuating the feeding flow (or indirectly the dilution) accordingly. A continuous operating regime requires a constant volume inside the photobioreactor which was assured by installing an evacuation nozzle in the upper part and a peristaltic evacuation pump.

A dispense mode is also available in order to deliver a certain volume of medium in a specified amount of time which is totally adequate for semi-continuous operating protocol of the reactor.

I.2.2.4. The pH Loop

The pH of the microalgae culture was measured with a Mettler Toledo® Inpro 3253SG/120/Pt100 gel-electrolyte pH electrode with integrated temperature sensor for the automatic compensation during calibration and measurement. Simultaneous measurement of pH value and temperature facilitates operation and increases calibration and measurement accuracy. The sensor is designed to allow autoclaving and in-situ sterilization. The electrical potential difference between the immersed electrode and microalgae culture, which is proportional with the ions concentration, is measured mV. The signal is passed to a Mettler Toledo® M400 transmitter which furnishes in turn a signal between 4 – 20 mA acquired through the DAQ board and converted in pH units. The pH measuring range is 0 – 14 with an accuracy of ± 0.02 units.

The photosynthetic microalgae growth protocols usually require gaseous CO_2 for pH regulation which decreases the pH, counterbalancing its increase under the influence of biomass growth. The pH regulation with gaseous CO_2 is more convenient because it is used also as carbonaceous substrate for microalgae. The CO_2 gas is furnished from a bottle under pressure with a purity of app. 90%. The gas is monitored by means of a Bronkhörst® HIGH TECH EL-FLOW mass flow meter which is virtually independent of pressure and temperature changes. The flow meter operates according to the by-pass measurement principle. A part of the total flow passes through a heated capillary tube, the temperature difference (ΔT), sensed by the upstream and downstream temperature sensors on the capillary, being directly proportional with the mass (or volumetric) flow rate of the gas according to the following relation:

$$\Delta T = k \cdot C_p \cdot G_m \qquad \text{(I.2.2)}$$

The mass flow rate can be converted to volumetric flow rate dividing it by the density of the gas:

$$G_m = G_v \cdot \rho \qquad \text{(I.2.3)}$$

where k is a constant factor, C_p is the specific heat, ρ is the gas density and $G_{m|v}$ is the mass or volumetric flow rate of the gas.

These types of flow meters are calibrated for a specific gas (in this case for CO_2) therefore they furnish values directly converted in volumetric flow rate. The measuring range of the CO_2 flow meter is between 0 and 3 $mL_n \cdot min^{-1}$, working at pressures up to maximum 2 bar.

The CO_2 gas flow is controlled by a proportional control valve mounted on the mass flow meter whose aperture (0 – 100%) is linearly dependent on the working range of the flow meter.

Thus, the pH loop can be closed by controlling the pH with the partial input volumetric flow of CO_2 noted hereinafter $G_{in}^{CO_2}$.

I.2.2.5. The Temperature Loop

As stated above the temperature of the culture is measured with the Pt100 sensor incorporated in the pH electrode. The measuring temperature range is 0 – 100 °C for operation and 0 – 140 °C for sterilization. The Pt100 signal is also acquired by the Mettler Toledo® M400 transmitter, sent to the DAQ board and processed by the computer. According to the set temperature, the sensor actuates a fan mounted on the back side of the reactor, usually through an on-off controller.

I.2.2.6. The Output Gas Analysis System

The molar composition of the output gas was measured by a QMS 200 PFEIFFER VACUUM® mass spectrometer calibrated for N_2, CO_2, O_2 and H_2. The measurement frequency of the gas samples requires a volume of 3 – 4 $mL_n \cdot min^{-1}$ which can be achieved only by adding a vector gas (N_2). The N_2 gas is preserved in a pressurized bottle wherefrom is bubbled into the reactor with a constant flow of 10 $mL_n \cdot min^{-1}$. The N_2 line is provided with a Bronkhörst® HIGH TECH EL-FLOW mass flow meter with a range of 0 – 100 $mL_n \cdot min^{-1}$ – max. 2 bar (calibrated for N_2) and a proportional control valve mounted on the flow meter. Due to the fact that water vapors may be drive off along with the output gas, harming the

mass spectrometer, the photobioreactor is provided with a condenser maintained at 5°C with cold water, and a dryer tube in addition.

The gas leaving the PBR headspace is introduced in the mass spectrometer through a capillary tube of 150 µm core diameter. The gas enters in the analysis chamber through an on-off valve where the pressure for precise measurement must be between 10^{-8} – 10^{-6} mbar. This pressure is achieved by means of a pumping group which consists of one membrane pump and two turbomolecular pumps which create vacuum by evacuating the gas molecules from the analysis chamber. The gas is ionized by an electron bombardment unit using tungsten filaments. The molecular ions obtained (resulted by removing one electron from the molecule) are separated in the analysis chamber according to the ratio between their mass and their charge by applying an electric field. The ions are analyzed separately by a detector which returns an electric signal linearly proportional to their concentration.

The total volume of gas that exits the photobioreactor is measured with a Bronkhörst® HIGH TECH EL-FLOW mass flow meter calibrated for CO_2 on a range of 0 – 100 $mL_n \cdot min^{-1}$ – max. 2 bar. Knowing that 10 $mL_n \cdot min^{-1}$ of N_2 gas, that does not suffer any change, are constantly bubbled into the reactor, a correction factor must be imposed for the signal of the output flow meter:

$$C = \frac{C_{p(CO_2)} \cdot \rho_{CO_2}}{C_{p(N_2)} \cdot \rho_{N_2}} \quad \text{(I.2.4)}$$

Based on the measurement of the mass spectrometer and of the mass flow meter the exact volume of each gas component of the output mixture can be determined:

$$G_m^i = G_m^{tot} \cdot y^i \quad \text{(I.2.5)}$$

where G_m^i is the mass flow rate of i^{th} component, G_m^{tot} is the mass flow rate of the output mixture of gases and y^i is the molar fraction of i^{th} component.

I.2.3. The Online Measurements

The data which can be measured online and registered on the process computer are:

- The voltage imposed to the LED panel which can be converted in incident light intensity q_0 ($\mu mol \cdot m^{-2} \cdot s^{-1}$)

- The turbidity (%) of the culture which can be converted into biomass concentration based on dry matter measurements ($g \cdot L^{-1}$)
- The pH of the culture (pH units)
- The feeding pump flow ($mL \cdot min^{-1}$)
- The aperture (%) of the N_2 proportional valve which can be converted in volumetric flow ($mL_n \cdot min^{-1}$)
- The aperture (%) of the CO_2 proportional valve which can be converted in volumetric flow ($mL_n \cdot min^{-1}$)
- The volumetric flow of the output flow meter ($mL_n \cdot min^{-1}$)
- The molar fractions of the output gas components ($mol \cdot h^{-1}$)

I.2.4. The Offline Measurements

I.2.4.1. Dry Matter

The dry matter of the culture was measured once a day in order to establish a good correlation with the online turbidity value or to monitor the experimental plant. The analysis consists in filtering a known volume of sample and drying it 24 hours (or up to constant mass) at 110°C in an oven. The filters (Whatman GF/F) were dried before sampling in an oven and preserved in a desiccator at room temperature. The filtration was performed with a laboratory vacuum pump on 5 – 10 mL of sample depending on the biomass concentration. Each sample was made in triplicate and weighted on a precision balance. The difference between the empty filter and the filter with dried biomass gives the concentration of biomass as follows:

$$DM = \frac{m_2 - m_1}{V_{sample}} \quad \text{(I.2.6)}$$

where DM – dry matter ($g \cdot L^{-1}$), m_1 – the empty filter (g) and m_2 – the filter with dried biomass.

While the fresh culture medium does not contain suspended solids, the dry matter was associated with the biomass concentration.

I.2.4.2. Total Inorganic Carbon

The total dissolved inorganic carbon (TIC) was measured on the supernatant with an analyzer Shimadzu® TOC-5000A. The samples preparation involved a centrifugation at 5000 rpm for 5 minutes and eventually filtration. The analysis consists in passing the sample through a solution of phosphoric acid which converts all inorganic forms of carbon in CO_2 whose concentration is read by a non-dispersive infrared detector cell (NDIR). The device furnishes the concentration of TIC in $mg \cdot L^{-1}$.

I.2.4.3. Anions (sulfates – SO_4^{2-} and phosphates – PO_4^{3-})

The sulfates and the phosphates ions present in the microalgae culture were determined through anionic chromatography (DIONEX) by using concentration precolumn (AG12A) and a separation column (AS12A). The eluent is a mixture of $NaHCO_3$ 30mM and Na_2CO_3 270mM. The concentration of anions is determined through the peak surface associated with a previously established internal calibration. The samples must be centrifuged or filtered before their injection into the columns. The device furnishes concentration values expressed in $mg \cdot L^{-1}$.

I.2.4.4. Ammonium Ions

The ammonium ions from the microalgae culture were determined through the salicylate method by using Hach Lange® TNT plus 832 analysis kits. The salicylate method involves a three-step reaction sequence. The first reaction involves the conversion of ammonia to monochloroamine by chlorine addition. Then, the monochloroamine reacts with salicylate to form 5-aminosalicylate. Finally, the 5-aminosalicylate is oxidized in the presence of sodium nitroferriccyanide to form a blue-green colored dye that absorbs light at 650 nm. The absorbance of the analysis kit was measured with a Hach Lange® DR2800 spectrophotometer which converts it into concentration units expressed in $mg \cdot L^{-1}$.

I.2.5. Process Computer

All signals transmitted by the devices described above and acquired through the DAQ board, USB or RS-232 ports are processed in a custom piloting program designed in LabVIEW®. Due to the fact that LabVIEW® can work with Matlab® scripts this program was installed also in order to work in tandem.

I.3. A KNOWLEDGE-BASED MODEL OF PH EVOLUTION DURING MICROALGAL GROWTH IN PHOTOBIO-REACTOR: A TOOL FOR MONITORING AND CONTROL PURPOSES

***Abstract*:** The aim of this chapter is to develop and to validate a global model for the photoautotrophic growth process of *Chlamydomonas reinhardtii*, in order to delineate the principal variables of the biological system which conduct to the precise prediction of the culture pH. The dynamic behavior of the biological system was expressed through a multi-state model in continuous-time formulation, based on mass balance equations and on local photosynthetic responses of the anisotropic medium, further associated with a suite of algebraic equations which describe the thermodynamic properties of the ternary solute system ammonia – carbon dioxide – water. The simulation results were compared with the results obtained on two experiments piloted in batch mode at 100 and 300 $\mu mol \cdot m^{-2} \cdot s^{-1}$ incident light intensities. The model response was studied in simulation for the most influent input variables (*i.e.* dilution, incident light intensity and carbon dioxide volume) which can be designated as control variable.

I.3.1. Introduction

Chlamydomonas reinhardtii serves as model organism in studies regarding the photosynthetic apparatus and its associated pigments, due to its genetic and physiological features (Grossman *et al.*, 2003). During the last decades the microalga was used in various applications such as kinetic studies (Jansen *et al.*, 1999), pigments production (Grossman *et al.*, 2004), immobilized cell systems (Garbayo *et al.*, 2005), wastewater treatment processes (Kong *et al.*, 2010), hydrogen production (Fouchard *et al.*, 2005; 2008; Melis, 2007; Degrenne *et al.*, 2011), electricity production (Rosenbaum *et al.*, 2005) and many others. *Chlamydomonas* is able to sustain photoautotrophic, photoheterotrophic and chemoheterotrophic metabolisms, but in this study only the first one will be considered, being of increased interest in the actual context of expanding CO_2 production derived from human activities. The photoautotrophic metabolism implies that the microalga is capable to convert inorganic substances into organic substances further used in cellular functions as biosynthesis

and respiration, using light as energy source. Thus, it absorbs CO_2 as major substrate and generates O_2 as a residue in the water photolysis reaction (Harris, 2009).

For sustainable development of pilot or industrial photobioreactors, reliable operating protocols must be conceived in order to achieve stable performances and process traceability. These targets require quantifiable advanced knowledge in what regards the physicochemical and biological phenomena which take place within the facility. The mathematical models used for numerical simulation are the analytical tools which allow to predict the process behavior and to comprehend its significant mechanisms. They must accomplish certain conditions such as embedding the main parameters involved in the process, describing as accurate as possible their dynamics, having numerical solutions in accordance with the technological reality and being handleable from a mathematical point of view. Thus, their degree of detail should be low enough to be tractable, but high enough to avoid the loss of realism.

The aim of this chapter is to propose and to validate a global model for the photoautotrophic growth process of *Chlamydomonas reinhardtii*, to describe the main variables of the system laying the foundation for an accurate prediction of the pH. The global photoautotrophic growth model consists in the coupling of a radiative, a biological and a thermodynamic model.

The light-driven processes result in using a particular class of models which return local photosynthetic responses by expressing the specific growth rate in terms of light attenuation inside the photobioreactor. Thus, the radiative models are fundamental in photobioreactor studies being researched by various authors (Cornet *et al.*, 1995; Cornet and Dussap, 2009; Molina Grima *et al.*, 1999; Pottier *et al.*, 2005). The biological model describes the dynamic behavior of the system through a multi-state model in a continuous-time formulation. The set of nonlinear differential equations introduced are mainly deduced from mass balance considerations on both liquid and gaseous phases. The scientific literature furnishes numerous approaches concerning the photosynthetic growth models, as a result of the active research in this area during last decades (Cornet *et al.*, 1998; Rubio *et al.*, 1999; Fouchard *et al.*, 2009).

The photoautotrophic microorganisms are cultivated in aqueous solution in which the inorganic carbonaceous substrate is provided through the dissolution of CO_2 gas in water or through the speciation of carbonates from the culture media. The dissolved carbon dioxide reacts with the water forming ionic species such as bicarbonate (HCO_3^-) and carbonate (CO_3^{2-}) among which dynamic equilibria are established. The dissolved ammonia (NH_3) from the

culture media reacts in its turn with the HCO_3^- ions to form the carbamate ions (NH_2COO^-), composing thus a ternary solute system $NH_3 - CO_2 - H_2O$. In what regards the microalgal culturing only the $CO_2 - H_2O$ solute system was approached, even though the thermodynamic properties of the ternary solute system $NH_3 - CO_2 - H_2O$ was extensively studied during the last decades due to its potential use in industrial and environmental applications such as urea and melamine production or CO_2 removal from flue gas in post combustion carbon capture processes (Derks and Versteeg, 2009; Jilvero *et al.*, 2011). The ternary solute system is also important for the aquaculture recycling installations (Colt *et al.*, 2009). The proper knowledge regarding the light attenuation inside the reactor, the dynamic behavior of the biological system and the electrolytic properties of the liquid phase lead to an accurate prediction of the pH which is known to be a key feature in microalgae culturing.
The chapter is organized as follows: after its detailed description the photoautotrophic growth model is validated on experimental data. The discussion focuses on model behavior in order to illustrate its ability to be used as a tool for monitoring and control purposes.

I.3.2. Bioprocess Modeling

I.3.2.1. The Biological Phenomenon

The model presented hereunder describes the main variables of the photosynthetic growth process of green microalga *Chlamydomonas reinhardtii* under light limiting conditions. The eukaryote organism is able to sustain photoautotrophic metabolism, in other words it is capable to convert inorganic substances into organic substances further used in cellular functions as biosynthesis and respiration, using light as energy source. In order to capture light, photoautotrophic organisms carry out photosynthesis, a process which is initiated through the absorption of a photon by the chlorophyll, leading to the excitation of an electron hence transferred through an electron transport chain, up to the ultimate reduction of NADP to NADPH. The electron deficient molecule of chlorophyll receives back its electrons from the photo-induced oxidation of water ($2H_2O + \text{light} \rightarrow 4e^- + 4H^+ + O_2$). The microalgae are able to capture light on visible domain (400 – 700 nm), frequently named photosynthetic active radiation (PAR) and on the extreme red end of the visible spectrum (700 – 800 nm), also referred as light, even though is dimly visible to some eyes. Besides the electron flux, a proton gradient is created and leads to ATP synthesis. The NADPH and ATP molecules

represent the assimilatory power required to reduce CO_2 to carbohydrates during the light independent phase (Barsanti and Gualtieri, 2006). Thus, the microalgae are able to absorb CO_2 as major substrate and to generate O_2 as a residue in the water oxidation reaction induced by the light as source of energy.

In vitro, this type of organism is often cultivated in aqueous solution in which the inorganic carbonaceous substrate is provided exclusively through the injection of the CO_2 gas into the reactor or through the addition of carbonates in the culture medium. When CO_2 gas dissolves in water it forms other species such as dissolved carbon dioxide ($CO_{2,aq}$), carbonic acid (H_2CO_3), bicarbonate (HCO_3^-) and carbonate (CO_3^{2-}), whose sum is known as total inorganic carbon (TIC). The ionic species represent potential sources of $CO_{2,aq}$ for photosynthesis as a result of their interconversion through a series of reactions such as hydration, dehydration and protonation. The carbonates, usually used in research studies (*e.g.* sodium hydrogen carbonate – $NaHCO_3$ used in the performed experiments), behave alike at dissolution forming the same species. The phase equilibrium (Eq.I.3.1) is governed by Henry's law and is determined by the molality of molecular solute. Vapor phase dissociation of $CO_{2,aq}$ is appreciable only at very high temperatures and can be therefore neglected (Edwards *et al.*, 1978).

$$CO_{2,gas} \overset{f(P,T)}{\longleftrightarrow} CO_{2,aq} \tag{I.3.1}$$

The weak electrolyte $CO_{2,aq}$ reacts with water establishing the following chemical equilibria:

$$CO_{2,aq} + H_2O \leftrightarrow H_2CO_3 \leftrightarrow H^+ + HCO_3^- \leftrightarrow 2H^+ + CO_3^{2-} \tag{I.3.2}$$

Being hard to distinguish between $CO_{2,aq}$ and H_2CO_3, the two species will be considered a single dissolved gas (Colt *et al.*, 2009). The ratio between $CO_{2,aq}$ and HCO_3^- has a strong dependence on pH making the bicarbonate to become the dominant species in solutions with pH exceeding 6.3. When $CO_{2,aq}$ is removed from medium as a result of photosynthetic growth the equilibrium (Eq.I.3.2) will shift to the left and the pH will increase. *Chlamydomonas* developed mechanisms which enable both $CO_{2,aq}$ and HCO_3^- to support photosynthesis (Harris, 2009), but they still require $CO_{2,aq}$ which will be obtained by splitting the bicarbonate ($H^+ + HCO_3^- \leftrightarrow CO_{2,aq} + OH^-$), a reaction that releases OH^- causing again

the increase of the pH. The algae cultivating techniques imply the pH regulation by means of CO_2 gas bubbled into the reactor. This fresh share of CO_2 will shift back the equilibrium to the right, and consequently the pH will decrease.

The slow conversion of HCO_3^- into $CO_{2,aq}$ is rapidly overreached by the photosynthetic consumption of $CO_{2,aq}$ leading to pH increase. Therefore, small volumes of CO_2 gas need to be continuously immersed into the reactor in order to maintain the pH around the prescribed value.

Besides the bicarbonate buffer system, the pH is also influenced by the ammonium (NH_4^+) ions present in the culture medium. A certain amount of NH_4^+ ions dissociates to form molecular ammonia (NH_3) establishing thus a dynamic equilibrium (Eq.I.3.3). *Chlamydomonas reinhardtii* uses NH_4^+ as inorganic nitrogen source for growth and when it becomes limiting, other forms of nitrogen – both organic and inorganic – may be used, but after their conversion into NH_4^+ ions (Harris, 2009). The ratio between NH_4^+ and NH_3 is strongly dependent on pH making the ammonia dominant in solutions with pH higher than 9.3. The self-ionization of water must be also considered here (Eq.I.3.4).

$$NH_3 + H_2O \leftrightarrow NH_4^+ + OH^- \quad \text{(I.3.3)}$$

$$H_2O \leftrightarrow H^+ + OH^- \quad \text{(I.3.4)}$$

NH_3 interferes with the HCO_3^- ions in solution forming carbamate. Thus, additional ionic equilibria must be considered:

$$NH_3 + HCO_3^- \leftrightarrow NH_2COO^- + H_2O \quad \text{(I.3.5)}$$

The sum of NH_3, NH_4^+ and NH_2COO^- molar concentrations is known as total inorganic nitrogen (TIN). In order to estimate an accurate value of pH in photoautotrophic algal cultures it is necessary to develop a computational package for the prediction of the thermodynamic properties of the $NH_3 - CO_2 - H_2O$ multisolute system along with a multi-state model in continuous-time formulation, which describes the dynamic behavior of the biological system.

I.3.2.2. Model Structure and Assumptions

The global model of the photoautotrophic growth process associates three models briefly depicted in Fig.I.3.1, namely a radiative model, a biological model and a thermodynamic model. Being a photoautotrophic process, all biological phenomena described above are driven by the light available inside the culture and therefore a radiative model is required to express its attenuation. Heterogeneous in terms of light availability, the culture is treated as a system with distributed parameters on its depth *z*. The radiative model will thus return local photosynthetic responses $\mu_I\big(I(z)\big)$ based on the input values of photon flux density q_0 and biomass concentration *X*. However, the culture is homogeneous in terms of concentrations therefore the local photosynthetic responses are integrated in order to calculate the average photosynthetic response $\langle\mu_I\rangle$ all over the volume of the reactor.

The biological model describes the time variation of main state variables of the system balancing kinetics of production and consumption and gas-liquid mass transfers. The state vector $x^T = \left[X\ c_{\mathrm{TIN}}\ c_{\mathrm{TIC}}\ c_{\mathrm{O_2}}\ y_{out}^{\mathrm{CO_2}}\ y_{out}^{\mathrm{O_2}}\right]$ integrates six variables, namely biomass concentration, total inorganic nitrogen concentration, total inorganic carbon concentration, dissolved oxygen concentration, $\mathrm{CO_2}$ and $\mathrm{O_2}$ molar fractions in the output gas; first four being characteristic to liquid phase whereas the last two are specific to gaseous phase.

The thermodynamic model is a computational package which enables the quantitative description of dissolved molecular and ionic species of $\mathrm{NH_3 - CO_2 - H_2O}$ multisolute system, providing values of activity coefficients. The ternary solute system was extensively studied in the last decades, the literature offering several models dedicated to mathematical description of electrolyte solution. A comparative study of thermodynamic electrolyte models was published by Jaworski *et.al.*, (2011) for the same system. In this study it was considered Pitzer's (1973) ionic model which is a complex virial expansion of the excess Gibbs free energy which characterizes interactions among ions and solvent. The thermodynamic model returns the vector of the internal variables $w^T = \left[c_{\mathrm{CO_2}} c_{\mathrm{HCO_3^-}}\ c_{\mathrm{CO_3^{2-}}}\ c_{\mathrm{NH_3}}\ c_{\mathrm{NH_4^+}}\ c_{\mathrm{NH_2COO^-}}\ c_{\mathrm{OH^-}}\ c_{\mathrm{H^+}}\ \mathrm{pH}\right]$ which are function of states.

The vector of inputs $u = \left[X\ q_0\ D\ G_{in}^{\mathrm{CO_2}}\ G_{in}^{\mathrm{O_2}}\ T\right]$ includes some variables (*i.e.* q_0, D and $G_{in}^{\mathrm{CO_2}}$) with increased influence over the system which can be designated as control variable. *p* is the set of model parameters which will be rendered later on in the article.

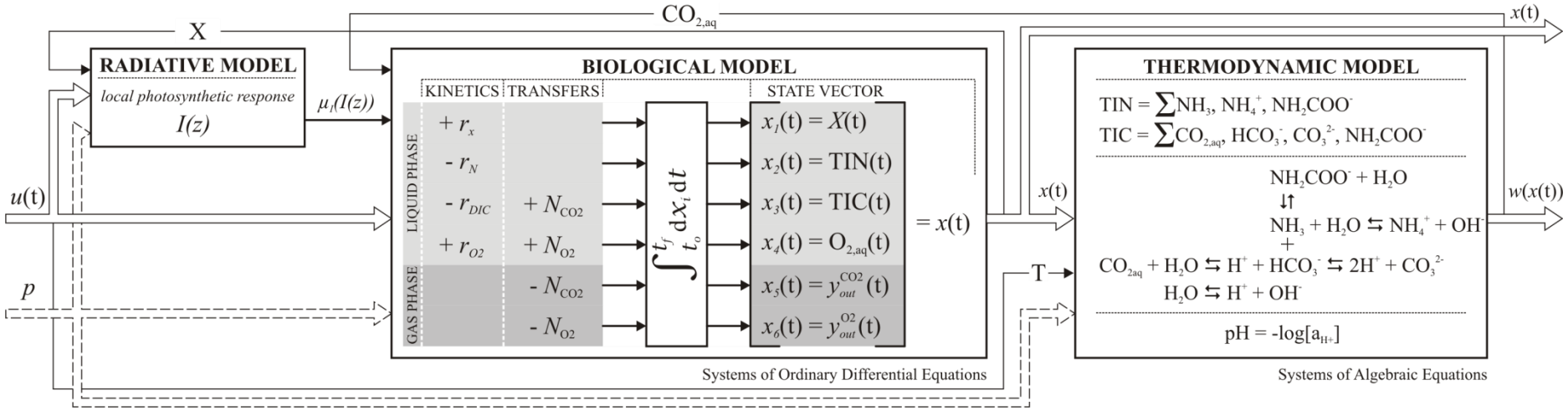

Fig.I.3.1. The structure of the global model of photoautotrophic growth process

where

$x^T = \left[X\ c_{\mathrm{TIN}}\ c_{\mathrm{TIC}}\ c_{\mathrm{O_2}}\ y_{out}^{\mathrm{CO_2}}\ y_{out}^{\mathrm{O_2}}\right]$

$u = \left[X\ q_0\ D\ G_{in}^{\mathrm{CO_2}}\ G_{in}^{\mathrm{O_2}}\ T\right]$

$w^T = \left[c_{\mathrm{CO_2}} c_{\mathrm{HCO_3^-}}\ c_{\mathrm{CO_3^{2-}}}\ c_{\mathrm{NH_3}}\ c_{\mathrm{NH_4^+}}\ c_{\mathrm{NH_2COO^-}}\ c_{\mathrm{OH^-}}\ c_{\mathrm{H^+}}\ \mathrm{pH}\right]$

Based on the reactor geometry it is assumed that it is perfectly stirred, and consequently the suspended algae can access equally the inorganic substrate and the dissolved gases in order to synthesize new mass cell. The experiments were carried out on nutrients in excess (C, N, S, P sources), but below their inhibition level, so that the specific growth rate to be a function of light and not of chemical substrate, since light is considered to be the main "substrate" which regulates the growth of photoautotrophs. The gas phase distribution inside the reactor was considered heterogeneous which is why the molar fractions of the dissolved gases are functions of the average between the input and output gas.

I.3.2.3. The Radiative Model – Light Transfer in the Photobioreactor

The photosynthetic growth of *Chlamydomonas reinhardtii* is governed by the light availability inside the culture. In order to determine the attenuation of light inside the photobioreactor the radiative model proposed by Pottier *et al.,* (2005) was used. This model describes the irradiance *I* distribution (Eq.I.3.6) inside the photobioreactor and, for the torus one under study, the analytical solution was obtained as follows:

$$I(z) = 2q_0 \frac{(1+\alpha)e^{\delta(L-z)} - (1-\alpha)e^{-\delta(L-z)}}{(1+\alpha)^2 e^{\delta L} - (1-\alpha)^2 e^{-\delta L}} \quad \text{(I.3.6)}$$

with $\delta = X\sqrt{E_a(E_a + 2bE_s)}$ the two-flux extinction coefficient and $\alpha = \sqrt{(E_a)/(E_a + 2bE_s)}$ the linear scattering modulus. E_a and E_s are the mass absorption and the mass scattering coefficients while b is the backward scattering fraction (dimensionless). q_0 represents the hemispherical incident light flux or photons flux density (PFD). X represents the biomass concentration inside the photobioreactor and L is the photobioreactor depth.

I.3.2.4. The Biological Model

I.3.2.4.1. *Photoautotrophic Growth Kinetics*

The algal growth results from the difference between the anabolic and catabolic processes, the biomass increase through photosynthesis and the partial degradation through respiration. The global volumetric rate is expressed as follows:

$$r_x = r_{x_p} - r_{x_s} = (\mu_p - \mu_s)X \quad \text{(I.3.7)}$$

with: r_{x_p} – volumetric growth rate due to photosynthesis, r_{x_s} – volumetric decrease rate due to respiration, μ_p – specific growth rate and μ_s describes the respiration kinetics. The term related to photosynthesis (μ_p) is a function of available light inside the culture and thus a function of local value of irradiance $I(z)$ (Eq.I.3.6) and μ_s is constant and not significantly affected by the culture medium evolution (Melis *et al.*, 2000). Thus, $\mu_p \equiv \mu_I$ is represented by a photosynthetic growth model with inhibitory term (Andrews, 1968; Fouchard *et al.*, 2009).

$$\mu_I = \mu_0 \frac{I}{K_I + I + \frac{I^2}{K_{II}}} \quad \text{(I.3.8)}$$

where: K_I is the half-saturation constant, K_{II} the inhibition constant and μ_0 is related to the maximum specific growth rate μ_{max} – $\mu_0 = \mu_{max}\left(1 + 2\sqrt{K_I/K_{II}}\right)$ – (Dochain, 2008). By coupling the kinetic model of photosynthesis (Eq.I.3.8) with the radiative model (Eq.I.3.6) there are allowed to be determined the local photosynthetic responses $\mu_I(I(z))$. The average photosynthetic response $\langle \mu_I \rangle$ calculated all over the reactor volume is obtained by integrating the local photosynthetic responses on the direction of culture depth z, thus obtaining (Fouchard *et al.*, 2009):

$$\langle \mu_I \rangle = \frac{1}{L} \int_0^L \mu_I\big(I(z)\big) dz \quad \text{(I.3.9)}$$

where: < > denotes a spatial averaging.

I.3.2.4.2. *Total Inorganic Carbon Kinetics*

The TIC consumption rate $\langle r_{\mathrm{TIC}} \rangle$ is proportional with the global volumetric growth rate $\langle r_x \rangle$ whereas the biomass is synthesized exclusively from inorganic carbon:

$$\langle r_{\mathrm{TIC}} \rangle = \frac{1}{M_x} \langle r_x \rangle = \frac{X\langle \mu_I \rangle - X\mu_s}{M_x} \quad \text{(I.3.10)}$$

where M_x is the C-mole mass.

I.3.2.4.3. *Stoichiometry of Chlamydomonas reinhardtii Photoautotrophic Growth*

An overall stoichiometry characterizing the yields of conversion of substrates into products has been established based on the elemental conservation relations (C, H, O, N, S, P) considering that 1 mol CO_2 fixed leads to 1 C-mol biomass (Roels, 1983):

$$CO_2 + 0.576\ H_2O + 0.181\ NH_3 + 0.006\ H_2SO_4 + 0.021\ P_i \rightarrow$$
$$CH_{1.771}O_{0.472}N_{0.181}S_{0.006}P_{0.021}(\text{biomass}) + 1.107\ O_2 \qquad \text{(I.3.11)}$$

The total inorganic nitrogen (TIN) is considered to be the main substrate, after carbon, which limits the photosynthetic growth of microalgae. According to the stoichiometric Eq.I.3.11 the TIN consumption rate $\langle r_{\mathrm{TIN}} \rangle$ can be computed as follows:

$$\langle r_{\mathrm{TIN}} \rangle = \frac{Y_{N/X}}{M_x} \langle r_x \rangle \qquad \text{(I.3.12)}$$

where $Y_{N/X}$ is the yield of TIN conversion which represents the uptake rate of TIN by produced biomass unit.

The oxygen is produced through water photolysis and partially consumed through respiration, therefore its kinetic rate $\langle r_{O_2} \rangle$ is supposed to be proportional to the growth rate as follows (Fouchard *et al.*, 2009):

$$\langle r_{\mathrm{O_2}} \rangle = \frac{Q_P}{M_x} \langle r_x \rangle \qquad \text{(I.3.13)}$$

where Q_P is the photosynthetic quotient which represents the number of moles of O_2 produced divided by the moles of CO_2 (Eq.I.3.11).

I.3.2.4.4. *Gas-Liquid Mass Transfers*

The gas-liquid mass transfer is modeled using the two-film theory assuming the gas phase to be in plug-flow and the liquid phase well-stirred. The volumetric mass transfer rate for oxygen N_{O_2} can then be expressed as follows:

$$N_{O_2} = (K_L a)_{O_2}\left(c_{O_2,\text{sat}} - c_{O_2}\right) = (K_L a)_{O_2}\left(\frac{y_{O_2}^{\text{lm}}\, P}{H_{O_2}} - c_{O_2}\right) \quad \text{(I.3.14)}$$

where $c_{O_2,\text{sat}}$ and c_{O_2} are respectively the saturation and actual concentration of dissolved oxygen in the liquid phase. $(K_L a)_{O_2}$ is the overall volumetric mass transfer coefficient for oxygen, $y_{O_2}^{\text{lm}}$ is the logarithmic mean (lm) between input and output oxygen molar fractions and P is the total pressure in the gas phase. The Henry's constant H_{O_2} is estimated trough the method given by Schumpe (1985), taking into account the decrease in solubility of gases due to electrolytes in the culture medium.

In the same way, the volumetric mass transfer rate for carbon dioxide N_{CO_2} is given by:

$$N_{CO_2} = (K_L a)_{CO_2}\left(\frac{y_{CO_2}^{\text{lm}}\, P}{\gamma_{CO_2} H_{CO_2}} - c_{CO_2}\right) \quad \text{(I.3.15)}$$

where $(K_L a)_{CO_2}$, $y_{CO_2}^{\text{lm}}$, H_{CO_2} and c_{CO_2} have the same significance as above except that they are expressed for CO_2. $(K_L a)_{CO_2}$ is estimated from the molecular diffusivities of carbon dioxide and oxygen (D_{CO_2} and D_{O_2}) as follows (Nielsen *et al.*, 2003):

$$(K_L a)_{CO_2} = (K_L a)_{O_2} \frac{D_{CO_2}}{D_{O_2}} \quad \text{(I.3.16)}$$

I.3.2.5. The Thermodynamic Model – The Multisolute System

In the multisolute $NH_3 - CO_2 - H_2O$ system, nine distinct species exist: NH_3 (molecular), NH_4^+, NH_2COO^-, CO_2 (molecular), HCO_3^-, CO_3^{2-}, H_2O (molecular), OH^- and H^+; resulting thus 17 unknowns (c_i and γ_i for all species except water which is expressed in terms of activity a_w). To solve these unknowns, 17 independent equations are needed:

(*i*) Five chemical equilibria:

$$K_1 = \frac{a_{H^+} a_{HCO_3^-}}{a_{CO_2} a_w} \quad K_2 = \frac{a_{H^+} a_{CO_3^{2-}}}{a_{HCO_3^-}}$$
$$K_3 = \frac{a_{NH_4^+} a_{OH^-}}{a_{NH_3} a_w} \quad K_4 = \frac{a_{NH_3} a_{HCO_3^-}}{a_{NH_2COO^-} a_w} \qquad \text{(I.3.17)}$$
$$K_w = \frac{a_{H^+} a_{OH^-}}{a_w}$$

where $a_i = \gamma_i c_i$ is the activity of component i, γ_i is the molal activity coefficient of component i and c_i is the concentration of component i. The equilibrium constants K_1, K_2, K_3, K_4 and K_w in relation with temperature are available in literature (Edwards *et al.*, 1978).

(*ii*) Two mass balances:

$$c_{TIC} = c_{CO_2} + c_{HCO_3^-} + c_{CO_3^{2-}} + c_{NH_2COO^-} \qquad \text{(I.3.18)}$$

$$c_{TIN} = c_{NH_3} + c_{NH_4^+} + c_{NH_2COO^-} \qquad \text{(I.3.19)}$$

(*iii*) Electroneutrality relation:

The concentration of anions balanced by the number of charges must equalize the concentration of cations balanced in the same manner (Dochain, 2008).

$$c_{NH_4^+} + c_{H^+} + c_{Na^+} = c_{HCO_3^-} + 2c_{CO_3^{2-}} + c_{NH_2COO^-} + c_{OH^-} + c_{Cl^-} \qquad \text{(I.3.20)}$$

Thus, the electroneutrality is written for the main species present in the culture medium. The molar concentration of the associated counterions Na^+ and Cl^- can be assumed to be constant in the given experimental conditions.

(*iv*) In addition, the Eq. (I.3.21) is used for eight activity coefficients, one for each species except water. Finally, the Eq. (I.3.22) is used for the activity of water.

$$\ln\gamma_i = -A_\phi z_i^2 \left[\frac{\sqrt{I}}{1+1.2\sqrt{I}} + \frac{2}{1.2}\ln\left(1+1.2\sqrt{I}\right)\right] + 2\sum_{j\neq w} m_j \left\{\beta_{ij}^0 + \frac{\beta_{ij}^1}{2I}\left[1-\left(1+2\sqrt{I}\right)\exp\left(-2\sqrt{I}\right)\right]\right\} - \frac{z_i^2}{4I^2}\sum_{j\neq w}\sum_{k\neq w} m_j m_k \beta_{jk}^1 \quad \text{(I.3.21)}$$

where $I = \frac{1}{2}\sum_j z_j^2 m_j$, is the ionic strength of the solution. The parameters β_{ij}^0, and β_{ij}^1, are molecule-molecule, molecule-ion and ion-ion interaction parameters, given in Edwards *et al.* (1978). A_ϕ can be expressed for temperatures ranging 0 to 100°C through the following relation (Zemaitis *et al.*, 1986):

$$A_\phi = -61.44534\exp\left(\frac{T-273.15}{273.15}\right) + 2.864468\left[\exp\left(\frac{T-273.15}{273.15}\right)\right]^2 + 183.5379\ln\left(\frac{T}{273.15}\right) - 0.6820223(T-273.15) + 0.0007875695(T^2-(273.15)^2) + 58.95788\left(\frac{273.15}{T}\right) \quad \text{(I.3.22)}$$

The activity of water is determined from the Gibbs-Duhem equation:

$$\ln a_w = M_w\left\{\frac{2A_\phi I^{\frac{3}{2}}}{1+1.2\sqrt{I}} - \sum_{i\neq w}\sum_{j\neq w} m_i m_j\left[\beta_{ij}^0 + \beta_{ij}^1\exp\left(-2\sqrt{I}\right)\right]\right\} - M_w\sum_{i\neq w} m_i \quad \text{(I.3.23)}$$

In the end, the pH was calculated through the following relation:

$$\text{pH} = -\log\left(a_{\text{H}^+}\right) \quad \text{(I.3.24)}$$

I.3.3. The Mass Balance Model

The mass balance model regroups two types of components: conversion terms (which describe the kinetics of various biochemical reactions of the process and conversion yields of various substrates in terms of biomass and products) and terms for the dynamics of transport (which regroup transit of matter within the process in liquid or gaseous form and the transfer phenomena between phases) (Dochain, 2008).

I.3.3.1. Liquid Phase

The states characteristic to liquid phase ($X\ c_{\mathrm{TIN}}\ c_{\mathrm{TIC}}\ c_{\mathrm{O_2}}$) which describe the photoautotrophic growth process can be expressed in terms of mass balance equations as follows:

$$\frac{dX}{dt} = \langle r_x \rangle(t) - D(t)X(t) \tag{I.3.25}$$

$$\frac{dc_{\mathrm{TIN}}}{dt} = -\langle r_{\mathrm{TIN}} \rangle(t) + D(t)\big(c_{\mathrm{TIN},i} - c_{\mathrm{TIN}}(t)\big) \tag{I.3.26}$$

$$\frac{dc_{\mathrm{TIC}}}{dt} = -\langle r_{\mathrm{TIC}} \rangle(t) + N_{\mathrm{CO_2}}(t) + D(t)\big(c_{\mathrm{TIC},i} - c_{\mathrm{TIC}}(t)\big) \tag{I.3.27}$$

$$\frac{dc_{\mathrm{O_2}}}{dt} = \langle r_{\mathrm{O_2}} \rangle(t) + N_{\mathrm{O_2}}(t) - D(t)c_{\mathrm{O_2}}(t) \tag{I.3.28}$$

where D represents the dilution, $c_{\mathrm{TIN},i}$ the concentration of total inorganic nitrogen in the feed and $c_{\mathrm{TIC},i}$ the concentration of total inorganic carbon in the feed. The volumetric rates $\langle r_x \rangle$, $\langle r_{\mathrm{TIC}} \rangle$, $\langle r_{\mathrm{TIN}} \rangle$ and $\langle r_{\mathrm{O_2}} \rangle$ are given by Equations (I.3.7), (I.3.10), (I.3.12) and (I.3.13). The volumetric mass transfer rates $N_{\mathrm{O_2}}$ and $N_{\mathrm{CO_2}}$ are given by Equations (I.3.14) and (I.3.15).
The biological model uses as input the dissolved carbon dioxide concentration $c_{\mathrm{CO_2}}$ (required for the computation of $N_{\mathrm{CO_2}}$) furnished by the thermodynamic model and determined through the mass balance Equation (I.3.18). The concentration of ammonia $c_{\mathrm{NH_3}}$ is also determined through a mass balance Equation (I.3.19). Water, the last molecular species of the multisolute system, is expressed in terms of activity through Equation (I.3.23). The concentrations of ionic species ($c_{\mathrm{HCO_3^-}}\ c_{\mathrm{CO_3^{2-}}}\ c_{\mathrm{NH_4^+}}\ c_{\mathrm{NH_2COO^-}}\ c_{\mathrm{OH^-}}$) present in the ternary solute system $\mathrm{NH_3 - CO_2 - H_2O}$ can be computed from the chemical equilibria (I.3.17). The hydrogen ions concentration $c_{\mathrm{H^+}}$ results from the electroneutrality Equation (I.3.20), whose logarithm gives the pH (Eq.I.3.24).

I.3.3.2. Gaseous Phase

The water has a limited capacity to solvate gases (*i.e.* saturation point) therefore the overflow remained in gaseous form leaves the reactor. Based on the ideal gas law and gas balance

equations the molar fractions of output gases can be computed, assuming that the flow and concentration of all input gasses are known and measurable. Thus, the time variation of the states specific to gas phase, $y_{out}^{CO_2}$ and $y_{out}^{O_2}$, can be expressed as:

$$\frac{dy_{out}^{CO_2}}{dt} = \frac{RT}{PV_g}\left(y_{in}^{CO_2}(t)G_{in}(t) - y_{out}^{CO_2}(t)G_{out}(t) - V_l N_{CO_2}(t)\right) \quad \text{(I.3.29)}$$

$$\frac{dy_{out}^{O_2}}{dt} = \frac{RT}{PV_g}\left(y_{in}^{O_2}(t)G_{in}(t) - y_{out}^{O_2}(t)G_{out}(t) - V_l N_{O_2}(t)\right) \quad \text{(I.3.30)}$$

where R is the universal gas constant, T the temperature and V_g and V_l the gas and liquid volumes. G_{in} and G_{out} are the input and the output total volumetric flow rates.

The vector gas N_2 is also present in the input gas and consequently in the output gas. In comparison to CO_2 and O_2, the N_2 gas has lower solubility in water and that is why its volume is assumed to remain unchanged; even more, it does not participate to any consumption of production processes during photoautotrophic growth. The N_2 molar fraction in the outgoing gas $y_{out}^{N_2}$ is given by:

$$y_{out}^{N_2} = 1 - y_{out}^{CO_2} - y_{out}^{O_2} \quad \text{(I.3.31)}$$

All molar fractions in G_{in} are known and equal with:

$$y_{in}^{CO_2} = \frac{G_{in}^{CO_2}}{G_{in}};\ y_{in}^{O_2} = \frac{G_{in}^{O_2}}{G_{in}};\ y_{in}^{N_2} = \frac{G_{in}^{N_2}}{G_{in}} \quad \text{(I.3.32)}$$

where: $G_{in}^{CO_2}$, $G_{in}^{O_2}$ and $G_{in}^{N_2}$ are the volumetric feeding flow rates of CO_2, O_2 and N_2. G_{in} is the input gas flow rate, being the sum of all input gases. The same relations can be written for the output gas flow rate G_{out} which can be estimated through a gas balance equation on N_2 gas:

$$G_{out} = \frac{y_{in}^{N_2}}{y_{out}^{N_2}} G_{in} \quad \text{(I.3.33)}$$

I.3.4. Model Parameters

The model parameters can be divided into seven groups of parameters:

- the absorption and scattering coefficients (E_a, E_b and b) used in the radiative model were identified in a previous study (Pottier *et al.*, 2005);
- the kinetic model parameters (μ_0, K_I, K_{II} and μ_s) were identified through multi-parameter regression on experimental data as presented in Fouchard *et al.*, (2009); Degrenne *et al.*, (2011);
- the yield conversion coefficients ($Y_{N/X}$ and Q_P) result from Roels (1983) stoichiometry equation whereas M_x was estimated by Loubière *et al.*, (1997);
- the mass transfer and diffusion coefficients ($(K_La)_{O_2}$, D_{CO_2}, D_{O_2}) – the overall volumetric mass transfer coefficient for oxygen $(K_La)_{O_2}$ was determined in a previous study by Degrenne (2009) according to a method presented in Roustan (2003), whereas the diffusion coefficients can be found in Denny (1993);
- the ideal gas law parameters (p, T, R) – the pressure and the temperature are measurable and the universal gas constant can be found in Mohr *et al.*, (2008)
- the parameters characterizing the reactor geometry (V_l, V_g and L) are measurable;
- phase and chemical equilibria parameters (H_{CO_2}, H_{O_2}, K_1, K_2, K_3, K_4 and K_w) – the Henry's constants are estimated through the method given by Schumpe (1985) and the equilibrium constants are found in Edwards *et al.*, (1978) for 25°C.

The parameters values used in the numerical simulations of the photoautotrophic growth process are summarized in Table I.3.1.

Table I.3.1. Model parameters

Group	*Parameter*	*Value*	*Unit*
Radiative model	E_a	172	$m^2 \cdot kg^{-1}$
	E_b	870	$m^2 \cdot kg^{-1}$
	b	0.0008	-
Kinetic model	μ_0	0.16	h^{-1}
	K_I	120	$\mu mol \cdot m^{-2} \cdot s^{-1}$
	K_{II}	2500	$\mu mol \cdot m^{-2} \cdot s^{-1}$
	μ_s	0.013	h^{-1}
Stoichiometric values	$Y_{N/X}$	0.181	-
	M_x	$27.8 \cdot 10^{-3}$	$kg \cdot C\text{-}mole^{-1}$
	Q_P	1.107	-

Mass transfer and diffusion coefficients	$(K_L a)_{O_2}$	0.46	h^{-1}
	D_{CO_2}	$1.92 \cdot 10^{-9}$	$m^2 \cdot s^{-1}$
	D_{O_2}	$2.38 \cdot 10^{-9}$	$m^2 \cdot s^{-1}$
Ideal gas law	P	$1.013 \cdot 10^{5}$	Pa
	T	298.15	K
	R	8.3145	$J \cdot mol^{-1} \cdot K^{-1}$
Photobioreactor geometry	V_l	$1.47 \cdot 10^{-3}$	m^3
	V_g	$0.12 \cdot V_l$	m^3
	L	0.04	m
Phase and chemical equilibria	H_{CO_2}	2903.8	$Pa \cdot m^3 \cdot mol^{-1}$
	H_{O_2}	$8.385 \cdot 10^{4}$	$Pa \cdot m^3 \cdot mol^{-1}$
	K_1	$4.38 \cdot 10^{-7}$	-
	K_2	$4.65 \cdot 10^{-11}$	-
	K_3	$1.76 \cdot 10^{-5}$	-
	K_4	3.09	-
	K_w	10^{-14}	-

The global model of photoautotrophic growth process is highly sensitive to three parameters: μ_0, V_g and $(K_L a)_{O_2}$. While μ_0 was easily confirmed on offline experimental values of biomass *X* and incident light flux q_0, and V_g was precisely estimated by measuring the empty volume of reactor head and gas lines, $(K_L a)_{O_2}$ remained the single parameter used to fit the model with the available experimental data. In comparison with the value of 0.46 h^{-1} measured by Degrenne (2009) which corresponds to an air flow of 10 $mL_n \cdot min^{-1}$, the best fitting was achieved with 0.9 h^{-1} (corresponding to ~20 $mL_n \cdot min^{-1}$).

I.3.5. Model Validation

Two experiments were conducted in order to validate the model afore-described and, due to the fact that the specific growth rate is a complex function of light, each procedure considered a different incident light intensity (*i.e.* 110 $\mu mol \cdot m^{-2} \cdot s^{-1}$ and 300 $\mu mol \cdot m^{-2} \cdot s^{-1}$ respectively). The other cultivating conditions (*e.g.* substrate composition, temperature, stirring velocity) were maintained identical in both experiments which unfolded 200 hours in discontinuous mode ($D = 0$). As it can be observed in Fig.I.3.2 and I.3.3 the microalgal culture presents a lag phase (or accelerated growth phase) during the first 2 days. This behavior is also confirmed by the output O_2 gas dynamics, rendered in Fig.I.3.6 and I.3.11, respectively. Thus, in order to obtain a proper fitting of the global photoautotrophic growth model on

experimental data μ_0 was considered equal to 0.09 h^{-1} during the first 40 hours of cultivation for the first experiment and 48 hours for the second one. Nevertheless, low concentrations of biomass do not present interest from a technological point of view and the accommodation phase is frequently neglected on the evidence that it is a short transitory phase and, that is why, a zonal modeling oriented on the exponential growth phase is usually aimed. The limitation in applying this model to other types of photobioreactors consists in adapting the radiative model according to their geometry and optical properties of the cultivated microorganism.

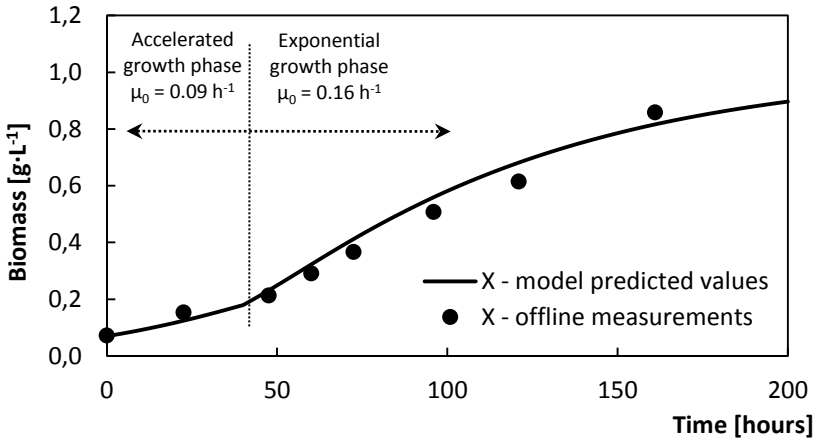

Fig.I.3.2. Biomass evolution at 110 µmol·m^{-2}·s^{-1} incident light intensity

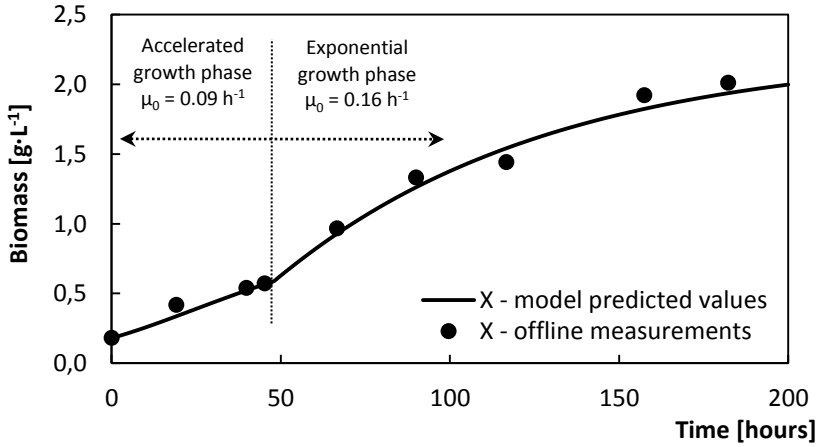

Fig.I.3.3. Biomass evolution at 300 µmol·m^{-2}·s^{-1} incident light intensity

To evaluate the pH response and furthermore the gas dynamics, the CO_2 was bubbled into the reactor by means of a pulse width modulation controller which aimed to maintain the pH around 7.5. The amplitude of each CO_2 pulse corresponds to 100% aperture of the CO_2 proportional valve.

The input CO_2 gas (Fig.I.3.4 and Fig.I.3.9) was used as input variable in the global photoautotrophic growth model along with its correspondent acquired experimental time. The CO_2 used in this purpose was found to be impure, 2.8 % being identified as O_2 which was also used as input variable in the model.

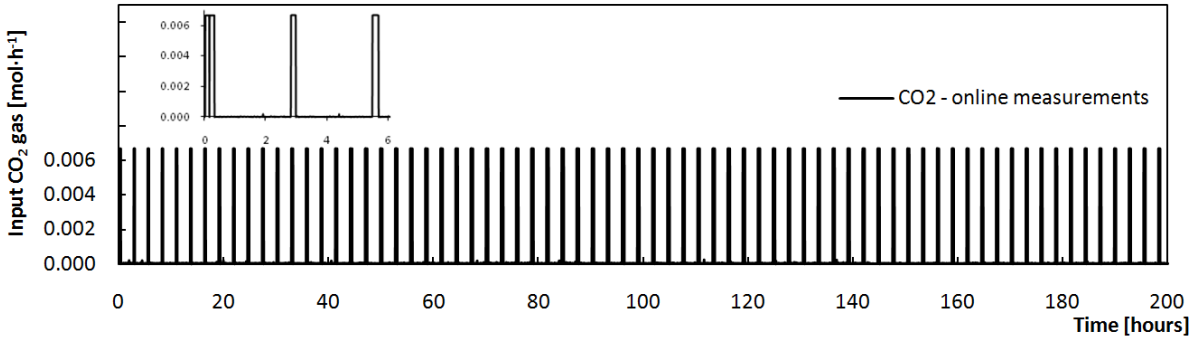

Fig.I.3.4. The input CO_2 gas at 110 µmol·m^{-2}·s^{-1} incident light intensity

The incoming N_2 gas was also measured and known to be constant at 10 mL·min^{-1}. The volumetric flow rate of the output mixture of gases G_{out} was continuously measured and the molar fractions of each component were analyzed by means of a mass spectrometer, thus, the partial volumes of each gas (except $G_{in}^{N_2}$ which is assumed to be constant and to remain unchanged) are available.

As it can be observed in Fig.I.3.5 and Fig.I.3.10 the output partial CO_2 gas predicted values are properly fitted to the experimental values acquired online for both experiments.

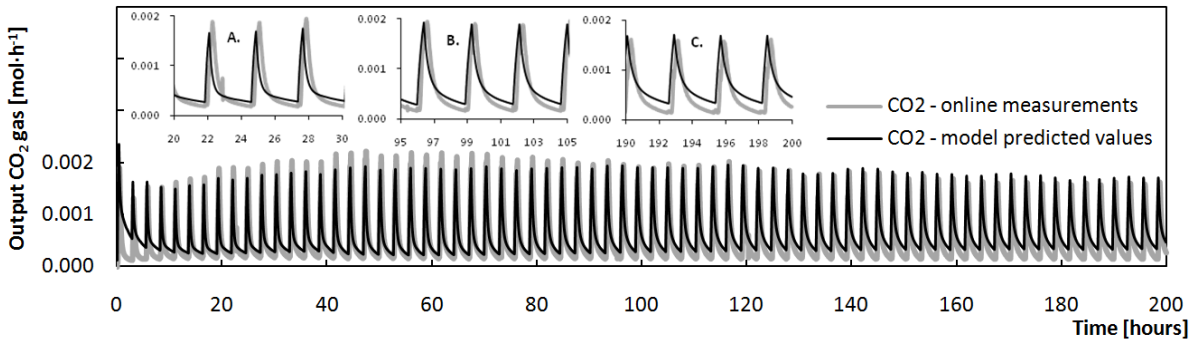

Fig.I.3.5. The output CO_2 gas at 110 µmol·m^{-2}·s^{-1} incident light intensity

The output O_2 gas dynamics (Fig.I.3.6 and Fig.I.3.11) were satisfactory predicted, but its evolution rather suggest a linear evolution which is not fully proportional with the specific growth rate. However, if r_{O_2} is desired to be used in the estimation of biomass, based on the

assumption that water photolysis is strictly associated with biomass growth, further studies must be undertaken. The high values of output O_2 gas observed at the beginning of both experiments correspond to the air existent in the head of the reactor, which requires a specific amount of time for its complete depletion.

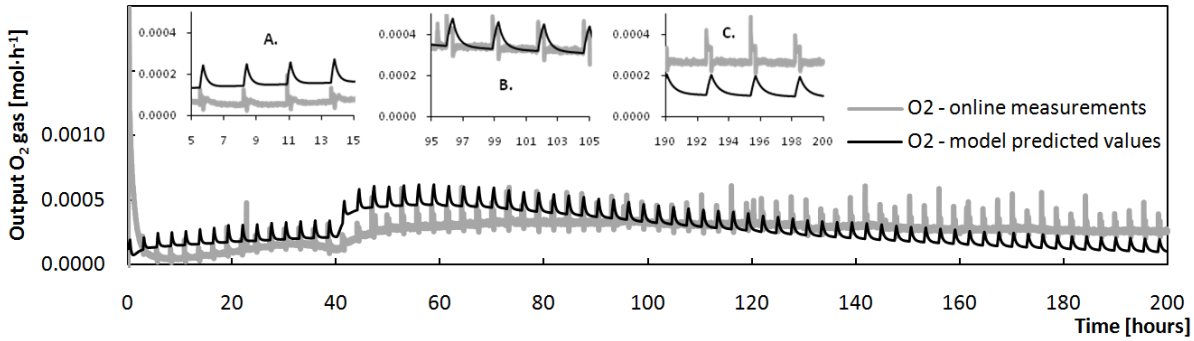

Fig.I.3.6. The output O_2 gas at 110 µmol·m^{-2}·s^{-1} incident light intensity

The limitation in implementing the gas balance model on other devices consist in adapting the liquid volume V_l, the gas volume V_g and the volumetric mass transfer coefficient $(K_L a)_{O_2}$ to new technological conditions. V_l/V_g ratio has a strong influence over the gaseous phase – output CO_2 and O_2 gas dynamics – and no influence over the liquid phase because V_l will always be constant. A higher ratio (thus a higher V_g) tends to predict lower output gas values than the ones found in practice. V_g was approximated at 12% of V_l counting the head of the reactor and the gas lines up to the measuring device. The volumetric mass transfer coefficient $(K_L a)_{O_2}$ on the other hand influences the variables of the liquid phase (TIC, $CO_{2,aq}$, $O_{2,aq}$ and implicitly the pH). $(K_L a)_{O_2}$ was identified in other works for the exact same type of reactor – 0.46 h^{-1} (Fouchard *et al.*, 2009) – but, in order to obtain a proper fitting of the model predicted values to the experimental data, a higher value of 0.9 h^{-1} was required.

A set of offline measures for TIC is available only for the experiment piloted at 110 µmol·m^{-2}·s^{-1} incident light intensity. Fig.I.3.7 shows a satisfactory match between the predicted and the experimental values with an error of max. 10%. The dominant specie of TIC is the HCO_3^- which represents app. 95% at a pH close to 7.5, thus making the $CO_{2,aq}$ contribution very low, which is why the TIC expression is insensitive to $(K_L a)_{O_2}$ variations on an ample range. Conclusively, the lack of data regarding the $CO_{2,aq}$ and $O_{2,aq}$ narrows the re-identification of $(K_L a)_{O_2}$ based exclusively on the pH dynamics.

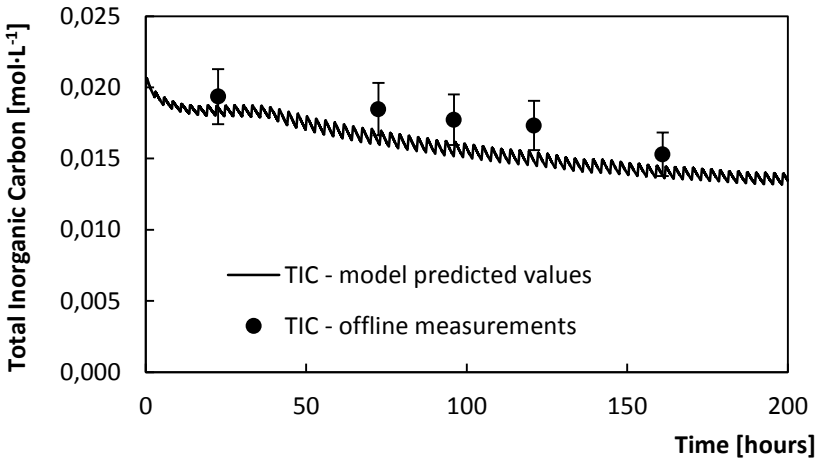

Fig.I.3.7. TIC consumption at 110 µmol·m^{-2}·s^{-1} incident light intensity

The model has the tendency to predict higher values for the pH during the first hours of cultivation (Fig.I.3.8) when the biomass concentration is very low. The thermodynamic model which predicts the pH is very sensitive and needs to be properly initialized. A proper initialization of the thermodynamic model, along with an accurate photosynthetic growth model, will result in an excellent capacity of prediction.

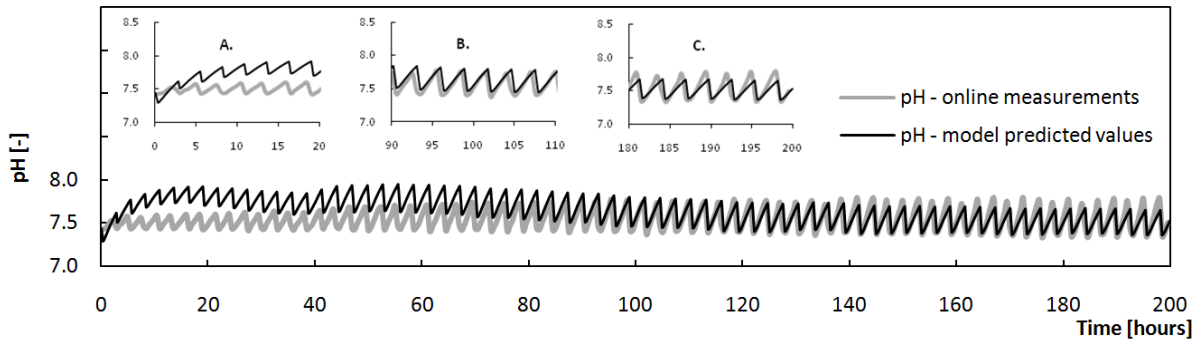

Fig.I.3.8. pH evolution at 110 µmol·m^{-2}·s^{-1} incident light intensity

Hereinafter, there are rendered the dynamics of the available input and output gases and the pH for the second experiment operated at 300 µmol·m^{-2}·s^{-1} incident light intensity which does not deflect from the assertions afore made.

However, a particular aspect on this one is worth being discussed: the incident occurred during the third day of operation (app. between the 50th to 70th hours). As it can be observed in the detail of Fig.I.3.9, the input CO_2 gas loses its periodicity for a period of time sufficient to let examine the prediction accuracy of the gas balance and pH models.

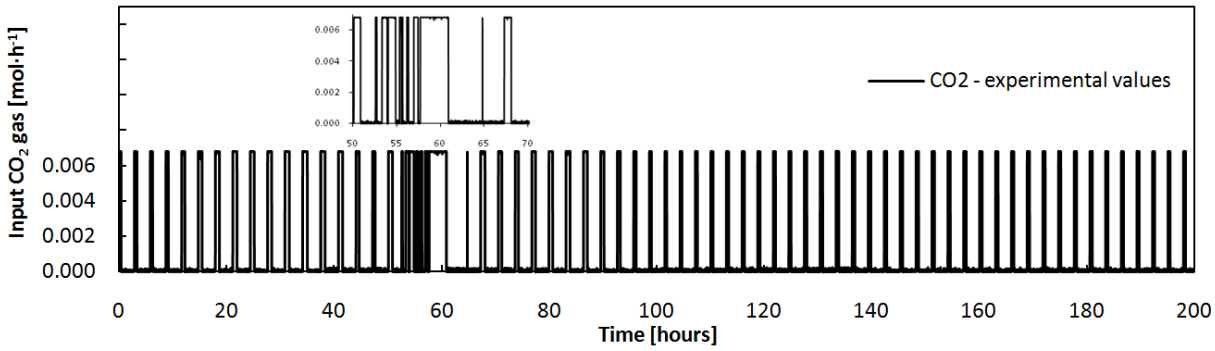

Fig.I.3.9. The incoming CO_2 gas at 300 µmol·m^{-2}·s^{-1} incident light intensity

The output CO_2 gas (Detail B., Fig.I.3.10) and the output O_2 gas (Detail B., Fig.I.3.11) are very well predicted by the gas balance model all the more so as the incident is projected on the exponential growth phase. On the other hand the thermodynamic model has a good ability to predict the pH (Fig.I.3.12) on a wide range of incoming CO_2 gas volumes.

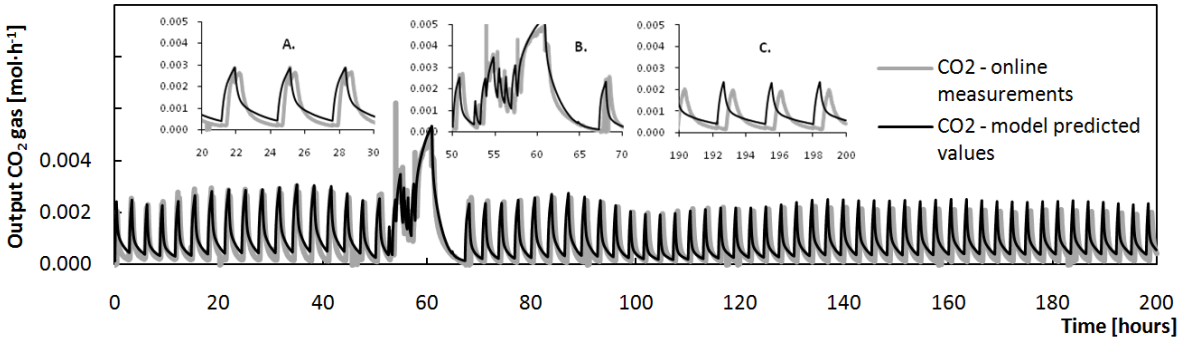

Fig.I.3.10. The output CO_2 gas at 300 µmol·m^{-2}·s^{-1} incident light intensity

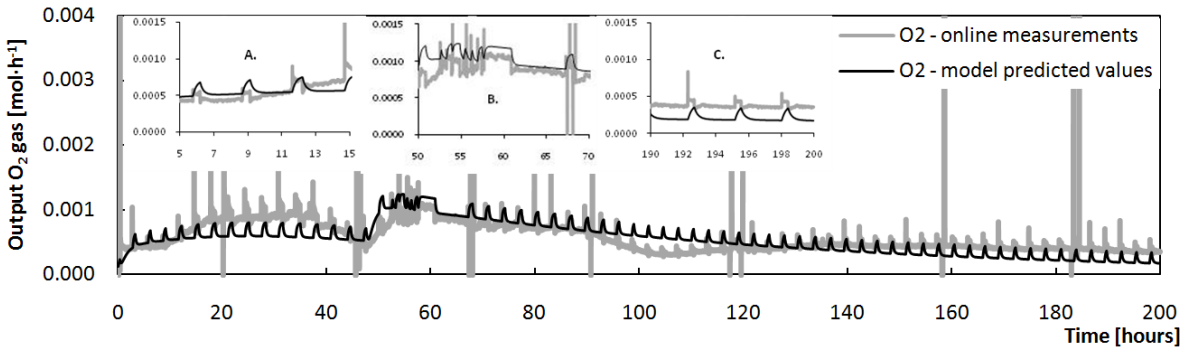

Fig.I.3.11. The output O_2 gas at 300 µmol·m^{-2}·s^{-1} incident light intensity

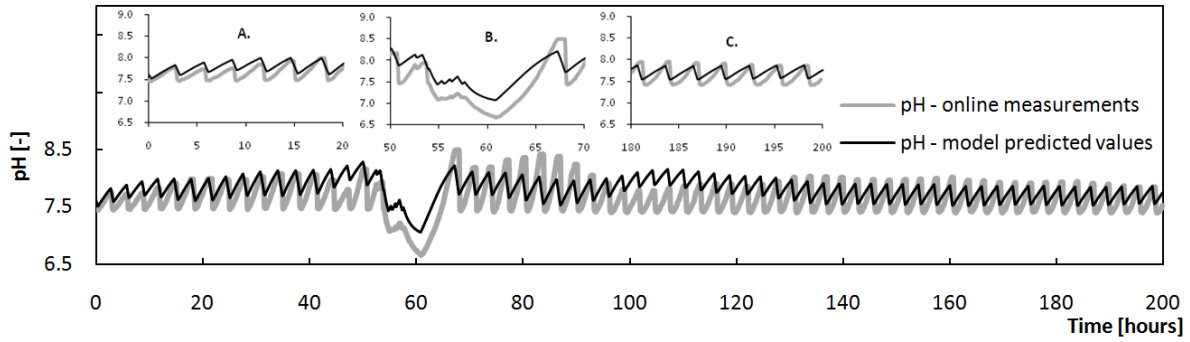

Fig.I.3.12. pH evolution at 300 µmol·m^{-2}·s^{-1} incident light intensity

From a biological point of view the optimal pH for the growth of *Chlamydomonas reinhardtii* is 7.5 (Kong *et al.*, 2010; Kosourov *et al.*, 2003) that is why a pH controller has rather to reject various disturbances than to work on other pH regimes; an important aspect to be considered for control purposes. The TIN has also a strong influence over the pH in the sense that a model based exclusively on TIC and biomass kinetics will predict even higher values discordant with the experimental reality.

I.3.6. Model Behavior

To analyze the response of the model to the most influent input variables (*i.e.* q_0, D and $G_{in}^{CO_2}$), designatable as control variables, the following operating conditions were selected for numerical simulation:

Dynamics 1: ——— Solid Line – corresponds to the basic simulation of the model in batch mode over 300 hours, thus with null dilution *D*. The incident light flux q_0 and the incoming CO_2 gas flow $G_{in}^{CO_2}$ were kept constant at 300 µmol·m^{-2}·s^{-1} and 0.0011 mol·h^{-1} (15% aperture of the corresponding proportional valve), respectively.

Dynamics 2: ..... Round Dot Line – considers the same conditions as *dynamics 1* with the difference that *D* is increased to 0.02 h^{-1} after the 100th hour of simulation. The system is thus set up to work in continuous mode with a constant dilution ≠ 0 which results in a constant volume of the reactor, assembly known in literature as open loop chemostat.

Dynamics 3: – – – – Dash Line – considers the same conditions as *dynamics 1* with the difference that q_0 is decreased to 200 µmol·m^{-2}·s^{-1} after the 100th hour of simulation.

Dynamics 4: ▬ . ▬ Long Dash Dot Line – considers the same conditions as *dynamics 1* with the difference that $G_{in}^{CO_2}$ is increased to 0.00368 mol·h^{-1} (50% aperture of the CO_2 proportional valve) after the 100th hour of simulation.

The numerical simulations of the global photoautotrophic growth model, presented in this section, were initialized with the values mentioned in Table I.3.2.

Table I.3.2. Initial conditions used for the numerical simulation of the global photoautotrophic growth model

Variable at t = 0*	*Value*	*Unit*
Biomass conc. – $X(0)$	0.200	g·L^{-1}
TIN conc. – $c_{\mathrm{TIN}}(0)$	0.027	mol· L^{-1}
TIC conc. – $c_{\mathrm{TIC}}(0)$	0.020	mol· L^{-1}
Dissolves O_2 conc. – $c_{O_2}(0)$	0.000	mol· L^{-1}
Out. CO_2 molar fraction – $y_{out}^{CO_2}(0)$	0.005	-
Out. O_2 molar fraction – $y_{out}^{O_2}(0)$	0.005	-
Out. N_2 molar fraction – $y_{out}^{N_2}(0)$	0.990	-
Output gas – $G_{out}(0)$	0.2452	mol· h^{-1}
Dissolved CO_2 conc. – $c_{CO_2}(0)$	1.32E-2	mol· L^{-1}
Bicarbonate conc. – $c_{HCO_3^-}(0)$	1.11E-3	mol· L^{-1}
Carbonate conc. – $c_{CO_3^{2-}}(0)$	5.69E-3	mol· L^{-1}
Ammonia conc. – $c_{NH_3}(0)$	6.98E-3	mol· L^{-1}
Ammonium conc. – $c_{NH_4^+}(0)$	2.00E-2	mol· L^{-1}
Carbamate con. – $c_{NH_2COO^-}(0)$	1.71E-5	mol· L^{-1}
Hydroxyl conc. – $c_{OH^-}(0)$	8.24E-6	mol· L^{-1}
Hydrogen conc. – $c_{H^+}(0)$	3.16E-8	mol· L^{-1}
pH – $pH(0)$	7.500	-

* The initial values used for numerical simulations represent the real experimental concentrations used also for the above-described validation of the global photoautotrophic model with experimental data, thus $c_{\mathrm{TIN},i} \equiv c_{\mathrm{TIN}}(0)$ and $c_{\mathrm{TIC},i} \equiv c_{\mathrm{TIC}}(0)$.

Fig.I.3.13, I.3.14, I.3.15 and I.3.16 display the kinetics of the states which are characteristic to the liquid phase in various operating conditions: the biomass, the TIN, the TIC and the dissolved oxygen. A variance of q_0 leads to a modification of μ_I and hence of X in the sense that a negative step of light (*e.g.* from 300 µmol·m^{-2}·s^{-1} to 200 µmol·m^{-2}·s^{-1}) will lead to a lower volumetric growth or to complete inhibition (Fig.I.3.13, Dyn.3) and, on the contrary, a positive light step is expected to increase X.

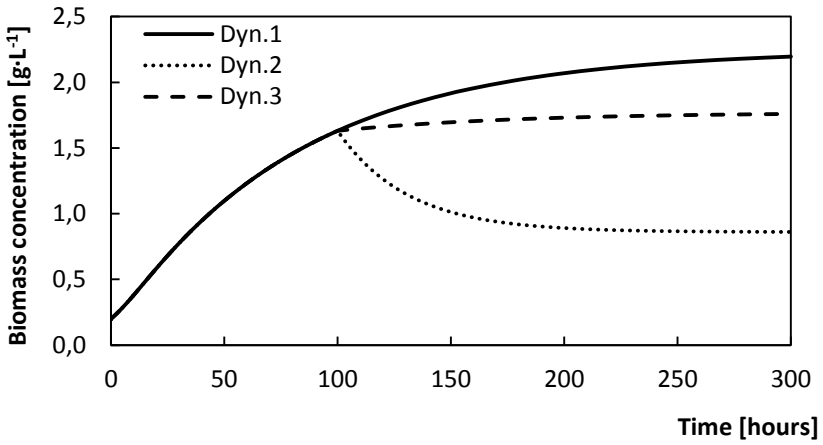

Fig.I.3.13. The kinetics of biomass

The dilution rate on the other hand does not inhibit the photosynthetic growth, but decreases *X* as a result of the hydraulically depletion of the reactor (Fig.I.1.13, Dyn.2). Due to the fact that the photosynthetic growth rate is a complex function of light which does not consider other factors (TIN, TIC) a variation of $G_{in}^{CO_2}$ will have no influence on *X*; the growth model is not sensitive to any other kinetics apart from light (this simplification is valid only if the dissolved substrates exist in the culture at concentrations which do not inhibit the growth).

The TIN concentration is inverse proportional with *X* that is to say any increase of biomass will be attended by substrate (TIN) consumption (Fig.I.3.14, Dyn.1, Dyn.3). A positive dilution step (*e.g.* from null to 0.02 h^{-1}) will increase the ammonium concentration due to the fresh quotient of medium which is continuously added (Fig.I.3.14, Dyn.2). Due to the fact that the biomass is not influenced by the $G_{in}^{CO_2}$ variation, the ammonium concentration will remain accordingly unchanged.

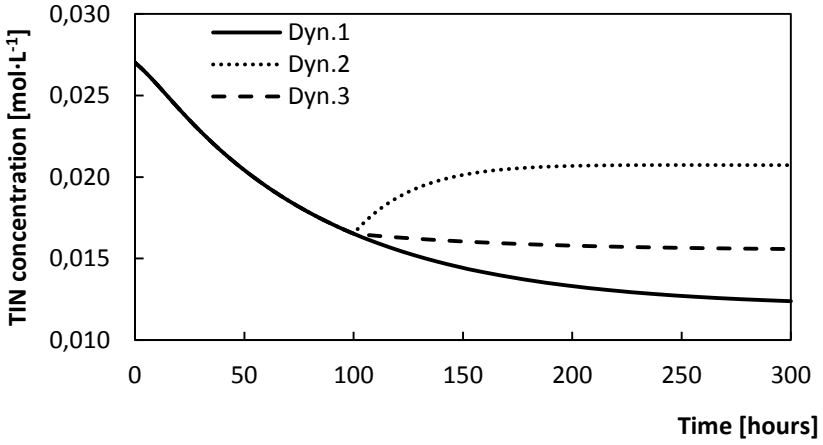

Fig.I.3.14. The kinetics of total inorganic nitrogen

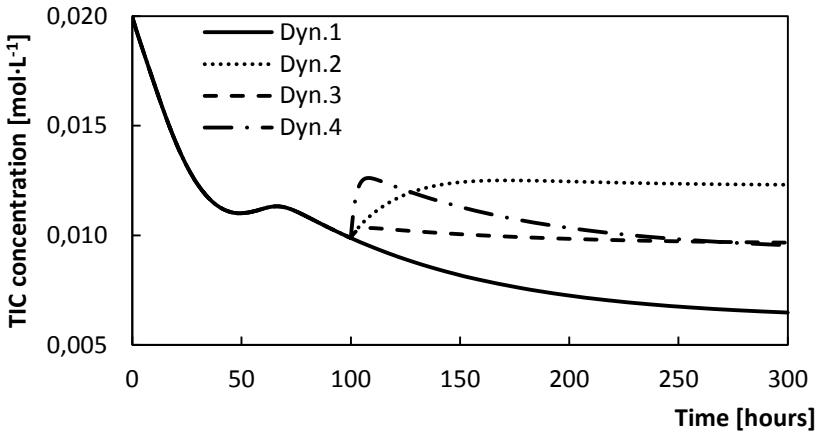

Fig.I.3.15. The kinetics of total inorganic carbon

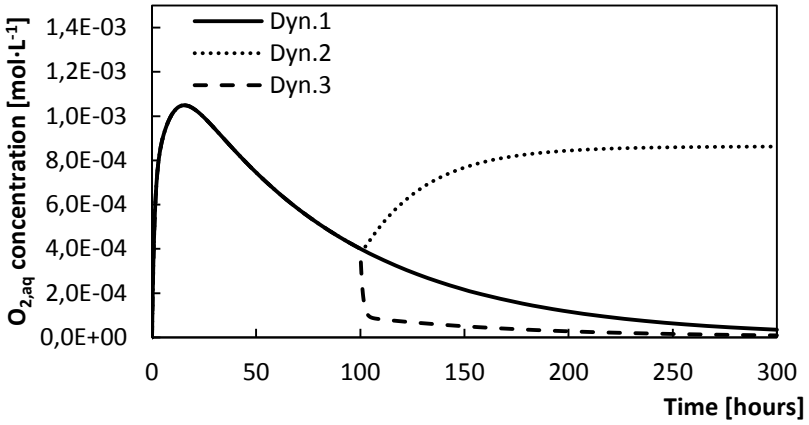

Fig.I.3.16. The kinetics of dissolved oxygen

The TIC concentration (Fig.I.3.15) follows the same dynamics as TIN being in inverse ratio with *X*. A positive *D* will add to the existent amount of TIC a fresh quotient (Fig.I.3.15, Dyn.2). The difference consists in the fact that the input CO_2 gas is also a constituent of TIC, therefore a positive step of $G_{in}^{CO_2}$ (*e.g.* from 0.0011 mol·h^{-1} to 0.00368 mol·h^{-1}) will increase its quantity (Fig.I.3.15, Dyn.4).

The oxygen is produced during water photolysis under growth conditions and, whether it is dissolved or in gaseous form, it is an excellent indicator of the photosynthetic growth. The maximal production rate of oxygen takes place during the exponential growth phase that is why a negative light step will inhibit the oxygen production (Fig.I.3.16, Dyn.3). A positive *D* (lower than the *D* which corresponds to the reactor wash out) will increase the $O_{2,aq}$ concentration (Fig.I.3.16, Dyn.2). The term related to the *D* in Eq. (I.3.28) describes only the oxygen which leaves the reactor assuming that there is no $O_{2,aq}$ in the fresh medium, thus the

$O_{2,aq}$ gained after a positive step of *D* derives from the continuous exponential phase in which the culture is maintained. Q_P is expressed as stoichiometric coefficient and not as a complex function of O_2 and CO_2 and therefore the oxygen kinetics will not be sensitive to any variation of $G_{in}^{CO_2}$.

The variables related to gas phased are presented in Fig.I.3.17, I.3.18, I.3.19 and I.3.20. The negative light step (Fig.I.3.17, I.3.18, I.3.19, Dyn.3) and the positive dilution step (Fig.I.3.17, I.3.18, I.3.19, Dyn.2) are influencing directly only the O_2 gas dynamics which, whether it is decreasing or increasing, affects the other two molar fractions (of CO_2 and N_2) in opposite direction. O_2 in comparison with CO_2 and N_2 shares max. 5% of the output mixture flow which makes its visibility low (Fig.I.3.20, Dyn.1, 2, 3).

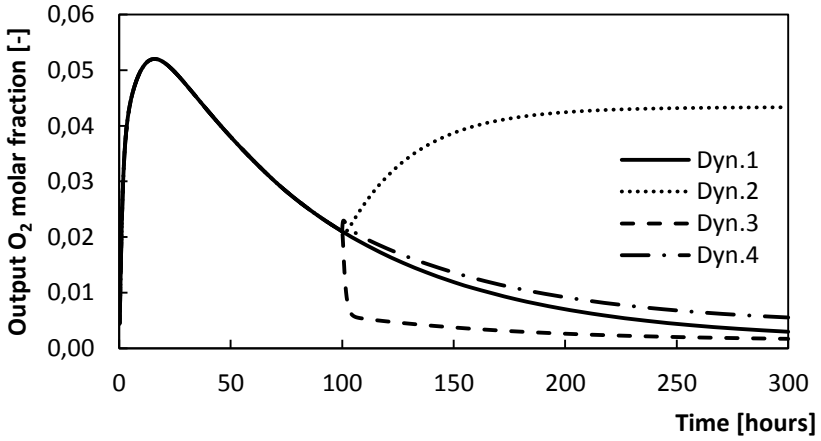

Fig.I.3.17. Molar fraction of O_2 in the output gas

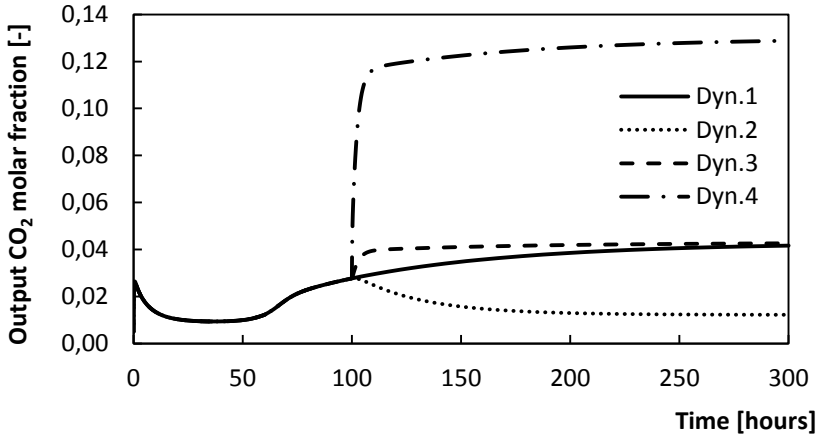

Fig.I.3.18. Molar fraction of CO_2 in the output gas

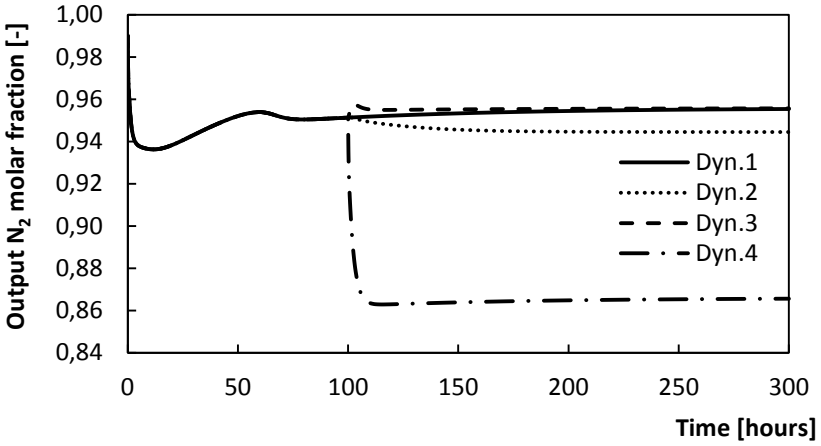

Fig.I.3.19. Molar fraction of N_2 in the output gas

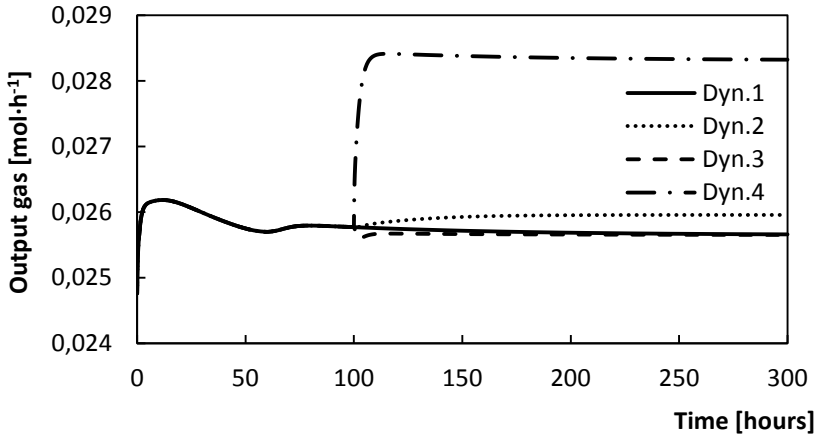

Fig.I.3.20. Total output gas

The $G_{in}^{CO_2}$ positive step can be observed in the dynamics of the output CO_2 molar fraction (Fig.I.3.18, Dyn.4) reflecting thus the limited capacity of water to dissolve this gas. At the same time the output mixture flow augments accordingly (Fig.I.3.20, Dyn.4).

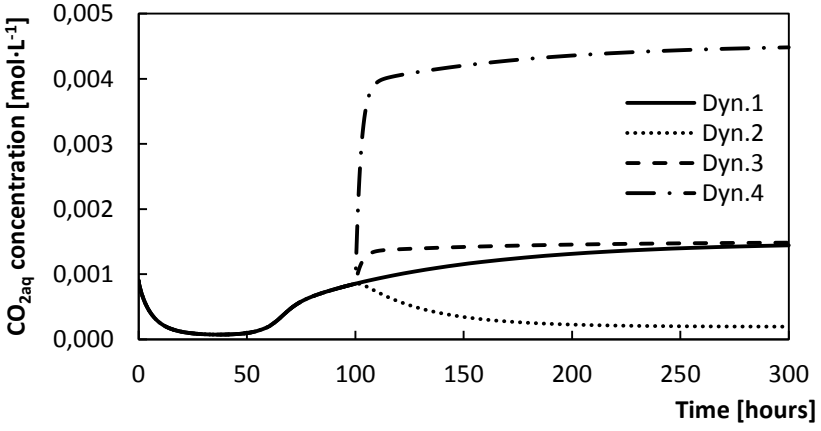

Fig.I.3.21. The dynamics of dissolved carbon dioxide

The bicarbonate buffer system consists in the chemical equilibria established between $CO_{2,aq}$, HCO_3^-, CO_3^{2-} and NH_2COO^-, whose dynamics are presented in Fig.I.3.21, I.3.22, I.3.23 and I.3.26.

At a pH of ~7.5 the HCO_3^- is the dominant species representing ~94.19% of TIC, while $CO_{2,aq}$ shares only ~5.57%, the CO_3^{2-} ~0.23% and NH_2COO^- ~0.01%. HCO_3^- follows the exact dynamics of TIC (Fig.I.3.22) with the exception that it is not influenced by the $G_{in}^{CO_2}$ positive step due to the slow interconversion between $CO_{2,aq}$ and HCO_3^-. A part of the CO_2 immersed into the reactor will remain dissolved in molecular form (Fig.I.3.21, Dyn.4) while the excess will exit the reactor (Fig.I.3.18, Dyn4). A positive step of *D* will bring fresh HCO_3^- and CO_3^{2-} in the reactor while the $CO_{2,aq}$ will decrease as result of a prolonged preservation of the culture in exponential phase (Fig.I.3.21, I.3.22, I.3.23, Dyn.2).

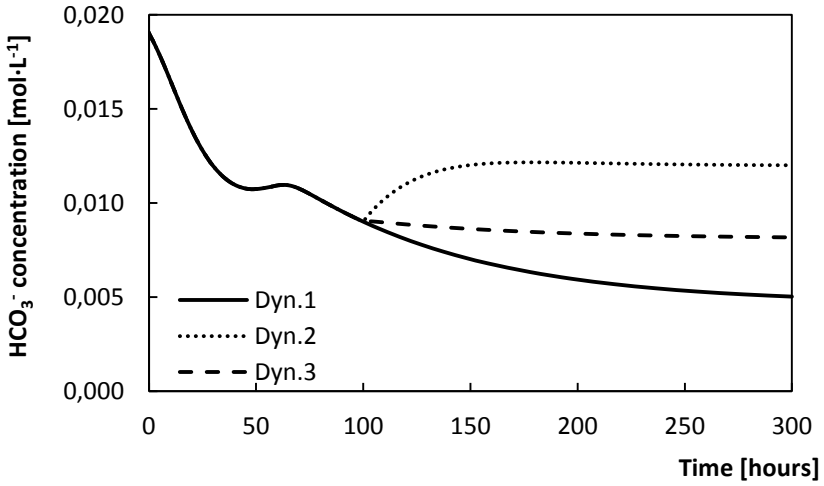

Fig.I.3.22. The dynamics of bicarbonate ions

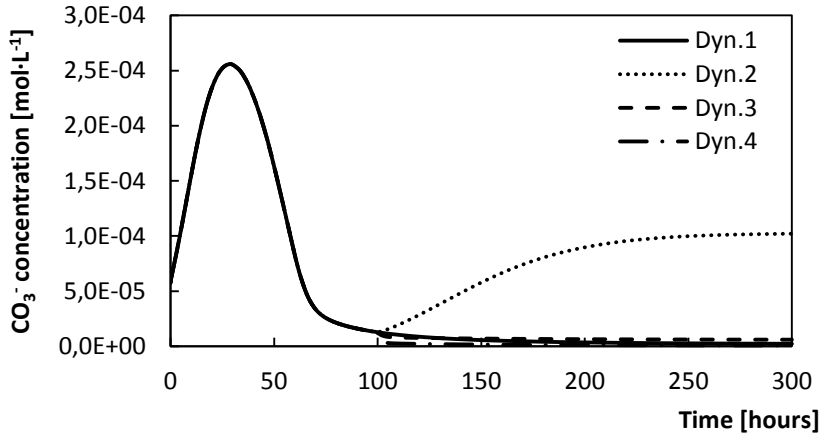

Fig.I.3.23. The dynamics of carbonate ions

$CO_{2,aq}$ kinetics is closely linked to biomass evolution and thus its lowest concentration is observed during the exponential growth phase (Fig.I.3.21, Dyn.1).

NH_4^+ is the dominant species among the nitrogen ionic species summing ~98.4% of TIN. A small part of NH_4^+ dissociates into NH_3 (~1.59% of TIN) which reacts with HCO_3^- to form the NH_2COO^- (~0.01 of TIN). A positive *D* step will increase the concentration of all TIN species (Fig.I.3.24, I.3.25, I.3.26, Dyn.2) whereas the negative q_0 step is observable only in the dynamics of NH_4^+ (Fig.I.3.25, Dyn.3). $G_{in}^{CO_2}$ does not influence visibly the TIN species.

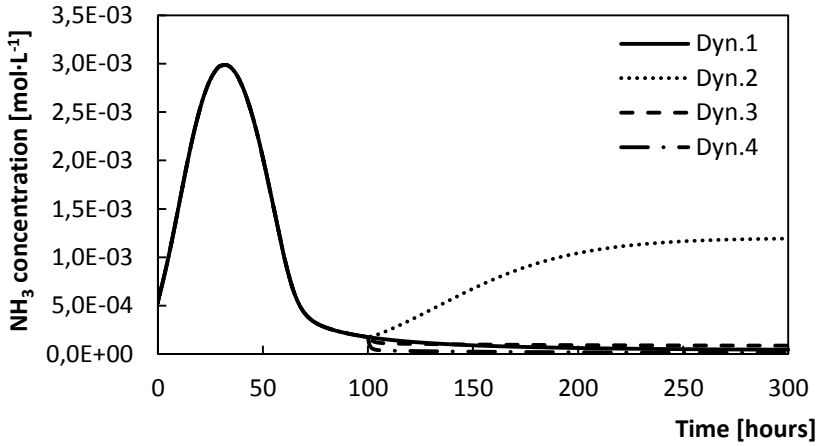

Fig.I.3.24. The evolution of ammonia concentration

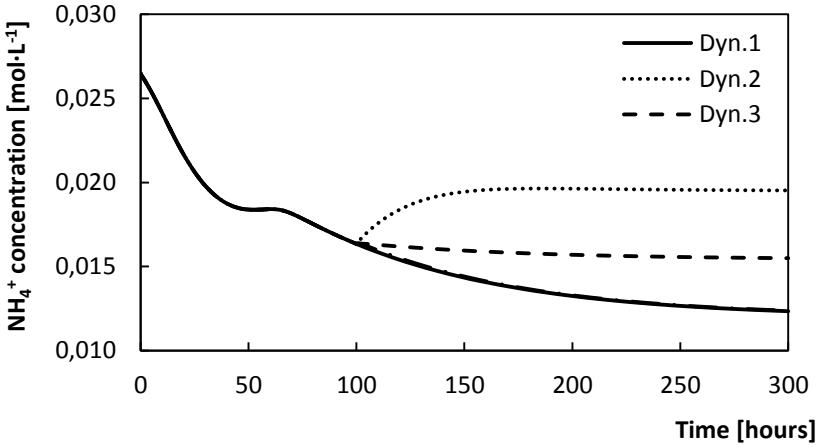

Fig.I.3.25. The evolution of ammonia ions concentration

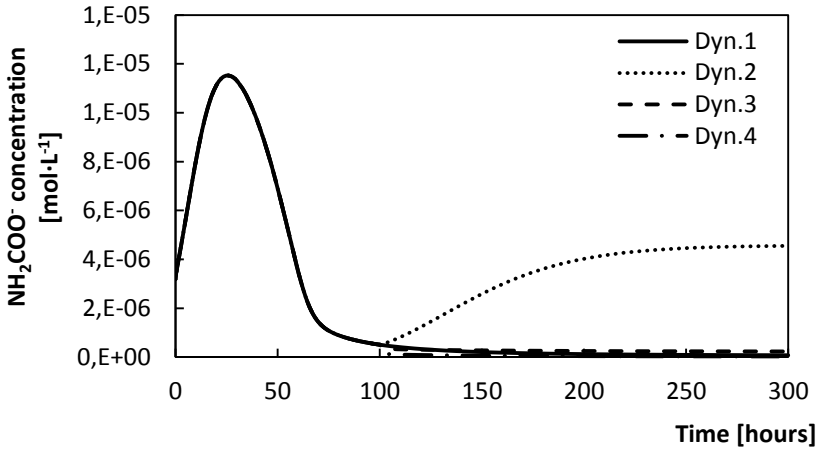

Fig.I.3.26. The evolution of carbamate ions concentration

The self-ionization of water is extremely important in establishing the chemical equilibria (I.3.2) and (I.3.3).

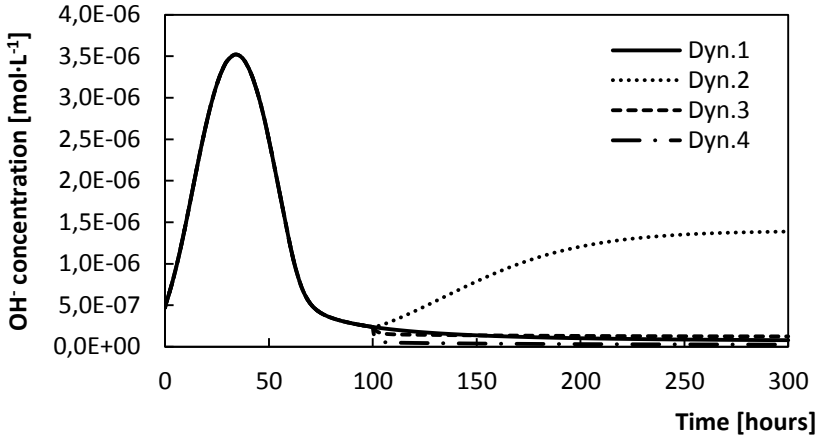

Fig.I.3.27. Hydroxyl ions concentration

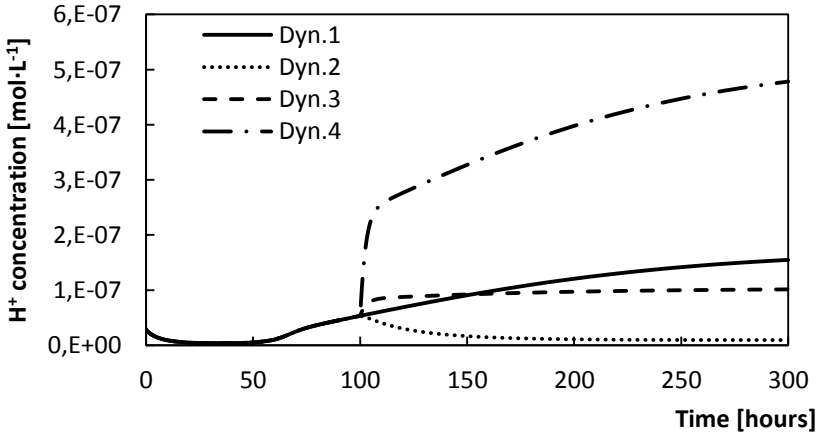

Fig.I.3.28. Hydrogen ions concentration

The H^+ ions concentration represents practically the negative antilogarithm of pH which is one of the most important parameters of the photoautotrophic growth process.

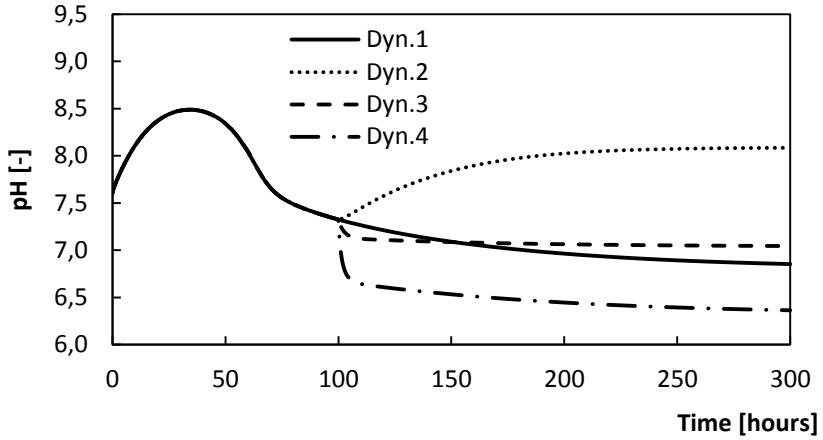

Fig.I.3.29. The pH evolution

The pH (Fig.I.3.29) is a complex function of μ_I, TIN and TIC. The biomass consumes $CO_{2,aq}$ shifting the equilibria (Eq. I.3.2) to the left and increasing the pH (Fig.I.3.29, Dyn.1), whereas more $G_{in}^{CO_2}$ brought to the culture shifts back the equilibria (Eq. I.3.2) determining the pH to decrease (Fig.I.3.29, Dyn.4), thus the $CO_{2,aq}$ is acting as a weak acid. A positive *D* step increases the pH due to a stronger biomass growth and due to the NH_3 from the feed which acts as a weak base (Fig.I.3.29, Dyn.2).

Another series of parameters which influence the nine chemical species of the thermodynamic model, and hence the pH, are the activity coefficients γ_i (Eq.I.3.21) and the water activity a_w (Eq.I.3.23). They account the deviation of the chemical species concentration in mixture from ideal behavior, being complex functions of ionic strength and temperature, and therefore not constant in time. However, their variation is extremely low and can be expressed as average values. Table I.3.3 renders the average values of the activity coefficients and water activity along with the overall relative standard deviation.

Table I.3.3. The variation of the activity coefficients and of water activity.

Activity coefficient	*Average value @ 25°C*[*]	*Relative Standard Deviation* (σ_r)
$\bar{\gamma}_{NH_3}$	1.00	0.0 %
$\bar{\gamma}_{NH_4^+}$	0.88	1.8 %
$\bar{\gamma}_{NH_2COO^-}$	0.88	6.4 %

$\bar{\gamma}_{CO_2}$	1	1.5 %
$\bar{\gamma}_{HCO_3^-}$	0.86	1.4 %
$\bar{\gamma}_{CO_3^{2-}}$	0.57	1.4 %
$\bar{a}_w$	1	0.0 %
$\bar{\gamma}_{OH^-}$	0.88	1.4 %
$\bar{\gamma}_{H^+}$	0.87	0.0 %

* Valid for all conditions presented in this paper

Whether they are recalculated for each integration step or used as constant average values, the global model response in terms of pH will be quite similar, with a mismatch lower than 0.1 pH units. However, if the thermodynamic model is supposed to be simplified, the activity coefficients can be neglected (*i.e.* $\gamma_i = 1$), working directly with concentrations. Figure I.3.30 depicts the pH mismatch between the simulations of the global model with activities versus concentrations on a range of pH from 6 to 8. Thus, it can be observed a difference of 0.1 pH units at a constant temperature of 25 °C.

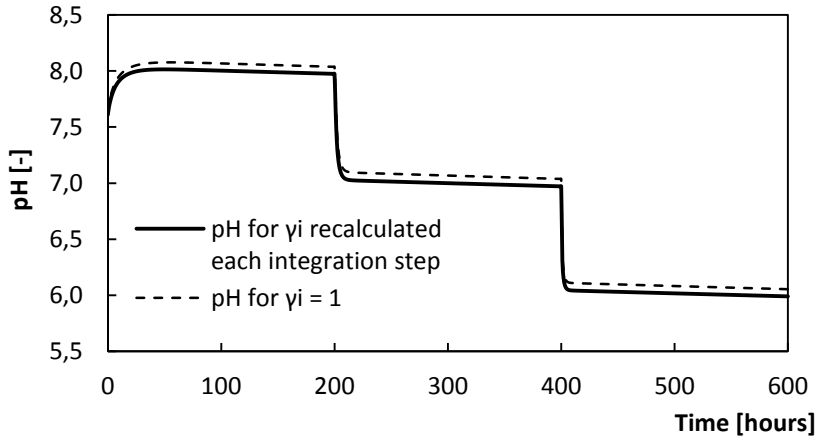

Fig.I.3.30. pH mismatch between the numerical simulations of the global model with activities versus concentrations

If the temperature cannot be measured online it will interpose as a disturbance further increasing the mismatch. It must be noted that the simulations in Fig.I.3.30 were made on nutrients in excess, expecting a different behavior of the system when one of them become limiting. Therefore, precisely calculated activity coefficients for appropriate temperatures will significantly increase the prediction accuracy of the global photoautotrophic growth model.

Conclusions Regarding the Modeling of Photobioreactors

The association between a radiative model, a biological model and a thermodynamic model presented an excellent capacity of predicting the main variables of the photoautotrophic growth process which are characteristic both to the liquid and gaseous phase, thus making the global photoautotrophic growth model an excellent tool for monitoring, research and control purposes. The D, q_0 and $G_{in}^{\mathrm{CO_2}}$ are the main input variables which influence the photoautotrophic growth process and can be designated as control variables in various control strategies for photobioreactors. The presented model can be applied to other types of photobioreactors and photosynthetic organisms by adapting the radiative model to their geometry and by re-identifying the parameters which depend strictly on the shape of the reactor (*e.g.* $(K_L a)_{\mathrm{O_2}}$ and $H_{\mathrm{O_2|CO_2}}$).

I.4. NONLINEAR MULTIVARIABLE CONTROL OF PHOTOBIO-REACTORS

***Abstract*:** The present chapter aims the design of nonlinear multivariable control algorithms based on the exact linearizing control theory. The nonlinear multivariable control of photobioreactors is discussed both for continuous and discontinuous cultures targeting the control of measurable or estimable output variables such as biomass, pH, specific light uptake rate and lighted volume fraction. Their control can be realized by manipulating the dilution – chemostatic control, the injected CO_2 gas – pH-static control and the incident light flux intensity – lumostatic control, respectively. The chemostatic control which is applicable to continuous cultures and the lumostatic control which is more appropriate for batches were associated with the pH-stat. Because the model proposed is too complex to allow the synthesis of proper algorithms, it was reduced by differentiating the states with slow dynamics from the ones with fast dynamics which were converted into algebraic expressions. In addition, a dynamic time-varying expression was derived for the concentration of hydrogen ions (negative antilogarithm of pH) obtaining thus an I/O model appropriate for control purposes. The degree of interaction between I/O signals was determined for continuous cultures in order to establish if the system allows the implementation of decentralized SISO controllers or requires a centralized MIMO controller. The efficacy of the proposed nonlinear controllers is demonstrated in simulation.

I.4.1. Introduction

The relevance of microalgae cultivation became undisputed during last decades. Whether they are bred for human or animal nutrition, involved in biotechnological production of metabolites (Spolaore *et al.*, 2006) or employed in environmental applications (Pittman *et al.*, 2011) the processes need to be monitored and controlled in order to achieve optimal performances and process traceability. The huge popularity of microalgae culturing techniques thus far originates mainly from their potential to sustain photoautotrophic metabolism that is the use of light as energy source and the CO_2 mitigation, abilities which involve several new challenges for modeling and control in comparison with other microorganisms such as yeasts or bacteria (Bernard, 2011). However, the microalgae industry develops cautiously expecting new protocols from the researches undertaken in the

biotechnological and control fields regarding process optimization, many applications still referring to small scale facilities. The efficiency of such processes can increase significantly if accurate nonlinear control models are to be developed.

In this context, the present chapter aims to derive I/O models suitable for the simultaneous control in closed loop of three measurable outputs, namely the biomass concentration, the pH and the specific light uptake (or the lighted volume fraction), by manipulating the dilution, the input CO_2 gas and the incident light intensity.

In what regards the continuous cultures a square system with two controllable inputs (*i.e.* D and $G_{in}^{CO_2}$) and two measurable outputs (*i.e.* X and pH) was considered. The continuous operation of photobioreactors is more convenient in terms of biomass productivity, in comparison with the discontinuous regime, thus avoiding stationary or even death phases by preserving the culture in a continuous exponential growth phase. The continuous microalgae culture systems that embed optical devices (able to measure the turbidity or the optical density of the culture), through which the microalgae concentration in the photobioreactor and the dilution rate can be controlled are referred in literature as turbidostats or closed loop chemostats (Marxen *et al.*, 2005; Sandnes *et al.*, 2006). Practically, the turbidostatic control involves the compensation of biomass growth by diluting the algal culture with a feed rate precisely calculated through the feedback mechanism, which is equal to the output rate keeping thus the reactor's volume constant (Benson and Rusch, 2006). Usually, the pH of a photosynthetic culture of microalgae is regulated through CO_2 injection which can be designated as control variable in pH-static control. Until now the pH control in photobioreactors was approached through standard linear algorithms which have the disadvantage of working around specific steady-state points. Nevertheless, the pH control remains a nonlinear problem which requires suitable dynamical models. In this respect, the present chapter proposes a dynamic time-varying expression for the concentration of hydrogen ions (negative antilogarithm of pH) based on the previously developed model, thus obtaining an I/O model appropriate for control purposes.

Nevertheless, the batch cultures present certain advantages in comparison with the continuous cultures, such as safety against contaminants and ease at implementation. The batch cultures are also treated as square systems with two inputs (*i.e.* q_0 and $G_{in}^{CO_2}$) and two outputs (*i.e.* q_e or Γ and pH). The lumostats are practically systems in which the incident light intensity is manipulated in closed loop in order to control outputs such as specific light uptake, average irradiance inside the culture or lighted volume fraction. The lumostatic control targets the

minimization of the self-shading effect by increasing the light intensity with the biomass growth and also the rationalization of energy consumption with light.

The present chapter is organized as follows: in the first instance the simultaneous chemostatic and pH-static control is investigated in detail by approaching their control scheme, the identification of the main operating points, the reduction of the global photoautotrophic growth model, the evaluation of the interactions between I/O signals, the development of the feedback linearizing algorithms and their validation in simulation. Based on the same considerations the lumostatic control is proposed in two variants, for specific light uptake rate and for lighted volume fraction control. The lumostatic algorithms performance is also presented in simulation.

I.4.2. Chemostatic and pH-static Control

I.4.2.1. The Global Photoautotrophic Growth Model

Chlamydomonas reinhardtii is able to sustain photoautotrophic metabolism and hence to assimilate inorganic forms of carbon (*i.e.* CO_2, HCO_3^-) and to convert them into requisite organic substances for cellular functions, generating at the same time O_2 as a residue in the water oxidation reaction induced by light as source of energy. More than a substrate, gaseous CO_2 which acts as a weak acid is usually used to decrease the pH culture. The CO_2 consumption under the influence of biomass growth increases the pH, thus the partial volume of gaseous carbon dioxide ($G_{in}^{CO_2}$) can be designated as controllable input in order to manipulate the pH. The dilution (D) which was found to have a significant impact over the bioprocess (Section I.3.6) can be also assigned as control variable in order to regulate the biomass concentration (X).

A general continuous-time state-space model is described by the following nonlinear differential equations:

$$\begin{cases} \dot{x} = f(x) + \sum_{i=1}^{m} g_i(x)u_i \\ y_i = h_j(x) \text{ with } j = 1, \dots, l \end{cases} \quad \text{(I.4.1)}$$

In what regards the experimental bench presented in section I.2.2 the two outputs, namely the biomass concentration X and the concentration of hydrogen ions c_{H^+} (negative antilogarithm

of pH) are measurable, and thus the global photoautotrophic growth model can be rewritten in state-space form (Eq.I.4.2) according to the general nonlinear model (Eq.I.4.1):

$$\begin{cases} \dot{x} = \begin{bmatrix} \dot{X} \\ \dot{c}_{\mathrm{TIN}} \\ \dot{c}_{\mathrm{TIC}} \\ \dot{c}_{\mathrm{O_2}} \\ \dot{y}_{out}^{\mathrm{CO_2}} \\ \dot{y}_{out}^{\mathrm{O_2}} \end{bmatrix} = \begin{bmatrix} \langle r_x \rangle \\ -\langle r_{\mathrm{TIN}} \rangle \\ -\langle r_{\mathrm{TIC}} \rangle + N_{\mathrm{CO_2}} \\ \langle r_{\mathrm{O_2}} \rangle + N_{\mathrm{O_2}} \\ RT/PV_g \left(-y_{out}^{\mathrm{CO_2}} G_{out} - V_l N_{\mathrm{CO_2}} \right) \\ RT/PV_g \left(G_{in}^{\mathrm{O_2}} - y_{out}^{\mathrm{O_2}} G_{out} - V_l N_{\mathrm{O_2}} \right) \end{bmatrix} + \begin{bmatrix} -X \\ c_{\mathrm{TIN},i} - c_{\mathrm{TIN}} \\ c_{\mathrm{TIC},i} - c_{\mathrm{TIC}} \\ -c_{\mathrm{O_2}} \\ 0 \\ 0 \end{bmatrix} D + \begin{bmatrix} 0 \\ 0 \\ 0 \\ 0 \\ RT/PV_g \\ 0 \end{bmatrix} G_{in}^{\mathrm{CO_2}} \\ y_1 = X \\ y_2 = c_{\mathrm{H^+}} = \frac{1}{\gamma_{H^+} 10^{\mathrm{pH}}} \end{cases} \quad \text{(I.4.2)}$$

A suite of algebraic equations, which were already described in section I.3.2, is associated with the dynamic model:

- The expression of irradiance – $I(z)$ – Eq.I.3.6;
- The expressions of kinetic rates – $\langle r_x \rangle$, $\langle r_{\mathrm{TIN}} \rangle$, $\langle r_{\mathrm{TIC}} \rangle$ and $\langle r_{O_2} \rangle$ – Eq. I.3.7 (with I.3.8 and I.3.9), I.3.12, I.3.10 and I.3.13, respectively;
- The gas-liquid mass transfers – $N_{\mathrm{O_2}}$ and $N_{\mathrm{CO_2}}$ – Eq.I.3.14 and I.3.15,
- The output $\mathrm{N_2}$ molar fraction – $y_{out}^{\mathrm{N_2}}$ – Eq.I.3.31,
- The total output gas – G_{out} – I.3.33.

The relations which describe the ternary solute system $\mathrm{NH_3 - CO_2 - H_2O}$ were rewritten as follows:

$$c_{\mathrm{CO_2}} = c_{\mathrm{TIC}} - c_{\mathrm{HCO_3^-}} - c_{\mathrm{CO_3^{2-}}} - c_{\mathrm{NH_2COO^-}} \quad \text{(I.4.3)}$$

$$c_{\mathrm{HCO_3^-}} = K_1 \frac{\gamma_{\mathrm{CO_2}} c_{\mathrm{CO_2}} a_w}{\gamma_{\mathrm{HCO_3^-}} \gamma_{\mathrm{H^+}} c_{\mathrm{H^+}}} \quad \text{(I.4.4)}$$

$$c_{\mathrm{CO_3^{2-}}} = K_2 \frac{\gamma_{\mathrm{HCO_3^-}} c_{\mathrm{HCO_3^-}}}{\gamma_{\mathrm{CO_3^{2-}}} \gamma_{\mathrm{H^+}} c_{\mathrm{H^+}}} \quad \text{(I.4.5)}$$

$$c_{\mathrm{NH_3}} = c_{\mathrm{TIN}} - c_{\mathrm{NH_4^+}} - c_{\mathrm{NH_2COO^-}} \quad \text{(I.4.6)}$$

$$c_{\mathrm{NH_4^+}} = K_3 \frac{\gamma_{\mathrm{NH_3}} c_{\mathrm{NH_3}} a_w}{\gamma_{\mathrm{NH_4^+}} \gamma_{\mathrm{OH^-}} c_{\mathrm{OH^-}}} \quad \text{(I.4.7)}$$

$$c_{\mathrm{NH_2COO^-}} = \frac{\gamma_{\mathrm{NH_3}} c_{\mathrm{NH_3}} \gamma_{\mathrm{HCO_3^-}} c_{\mathrm{HCO_3^-}}}{K_4 \gamma_{\mathrm{NH_2COO^-}} a_w} \tag{I.4.8}$$

$$c_{\mathrm{OH^-}} = K_w \frac{a_w}{\gamma_{\mathrm{OH^-}} \gamma_{\mathrm{H^+}} c_{\mathrm{H^+}}} \tag{I.4.9}$$

$$c_{\mathrm{H^+}} = c_{\mathrm{HCO_3^-}} + 2c_{\mathrm{CO_3^{2-}}} + c_{\mathrm{OH^-}} - c_{\mathrm{NH_4^+}} + ct \tag{I.4.10}$$

$$\mathrm{pH} = -log(\gamma_{\mathrm{H^+}} c_{\mathrm{H^+}}) \tag{I.4.11}$$

The gaseous phase inside the reactor is considered homogeneous by reasons of mathematical simplicity, thus $y_{\mathrm{CO_2}}^{\mathrm{lm}} = y_{out}^{\mathrm{CO_2}}$. The activity coefficients γ_i are calculated with relation (I.3.21), whereas the water activity a_w is determined with the Gibbs-Dunhem equation (I.3.23).

I.4.2.2. The Control Scheme

The objective is to control simultaneously in closed loop both measurable outputs, *X* and pH, by manipulating the dilution *D* and the input $\mathrm{CO_2}$ gas volume, $G_{in}^{\mathrm{CO_2}}$, as shown in Fig.I.4.1. The controller structure is intended to be nonlinear so that conjoined with the nonlinear process to achieve a linear closed loop which is unconditionally stable regardless of the operating point or the transitory trajectory, thus being capable to globally stabilize the photoautotrophic growth process. The feedback linearizing control requires the derivation of a proper I/O model which must be handleable from a mathematical point of view (*i.e.* having the lowest admissible relative degree). Thus, in order to reduce the relative degree of the nonlinear system (Eq.I.4.2), the number of states from the global photoautotrophic growth model must be decreased. The global model reduction can be done if the states with faster dynamics are identified and their derivatives equalized with zero, by analyzing the response of the system to varying frequencies (Ogata, 1997; Chau, 2002; D'Azzo and Houpis, 2003). The frequency response of the system is directly linked to the time domain and has a clear physical interpretation, but requires the linearization of the system around certain steady-state operating points which must be also identified (Skogestad and Postlethwaite, 2001; Paraskevopoulous, 2001). In what regards the controller synthesis the degree of interaction between I/O signals can be quantified through a RGA analysis in order to evaluate the necessity of developing centralized MIMO or decentralized SISO controllers.

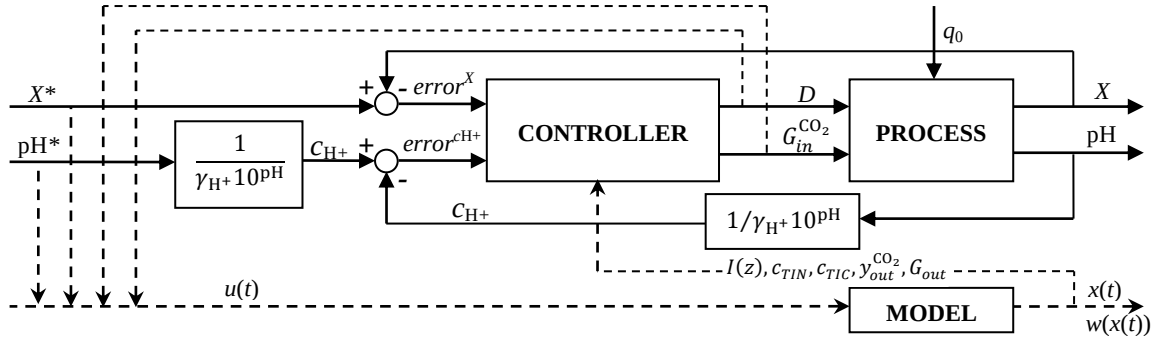

Fig.I.4.1. Chemostatic and pH-static control design scheme of photobioreactor

In Fig.I.4.1 the input vector of the model $u(t) = [X\ \text{pH}\ D\ G_{in}^{CO_2}\ G_{in}^{O_2}\ T]$ consists in real measurable variables. The model returns the state vector $x^T(t) = [X\ c_{\text{TIN}}\ c_{\text{TIC}}\ c_{O_2}\ y_{out}^{CO_2}\ y_{out}^{O_2}]$ and the vector of internal variables $w^T(t) = [c_{CO_2} c_{HCO_3^-}\ c_{CO_3^{2-}}\ c_{NH_3}\ c_{NH_4^+}\ c_{NH_2COO^-}\ c_{OH^-}\ c_{H^+}\ \text{pH}]$, some of them being required at the computation of the control algorithm.

The operation of a photobioreactor in continuous mode is more convenient, in terms of biomass productivity, in comparison with the discontinuous regime, thus avoiding the delays given by washing, sterilizing and inoculating the reactor and by the lag or the accelerated growth phases which can take up to 48 hours. The objective of the biomass controller is to preserve the culture in a continuous exponential growth phase by adding constantly precisely calculated volumes of fresh medium, hence evacuating in the same time portions of biomass equivalent with the dilution *D* imposed, thus preventing a stationary phase caused by the depletion of the nutrients or by the osmotic pressure encountered at high concentrations of biomass.

The photoautotrophic organisms consume CO_2 as principal source of carbon which has also the property of decreasing the pH, therefore proper volumes of CO_2 are used to keep the pH around an optimal prescribed value. The pH controller (Fig.I.4.1) is practically conceived around the concentration of hydrogen ions (c_{H^+}) for reasons of mathematical simplicity in expressing a handleable I/O model.

In this context a simultaneous nonlinear feedback control for biomass and pH appears to be an efficient solution to stabilize the photoautotrophic growth process. However, because a nonlinear controller requires certain immeasurable variables in order to precisely calculate the controls, the prediction capacity of the global photoautotrophic growth model (Eq.I.4.2) can be employed to this end (Fig.I.4.1).

I.4.2.3. The Main Steady-State Operating Points

The photobioreactor can be operated at various concentrations of biomass in accordance with the selected working protocol. If the objective is, for example, the biomass productivity, then from the simulation of the hourly productivity as a function of dilution on a wide range of light intensities, one can conclude from Fig.I.4.2 that the optimal dilution in terms of productivity ranges between 0.4 to 0.6 h^{-1}.

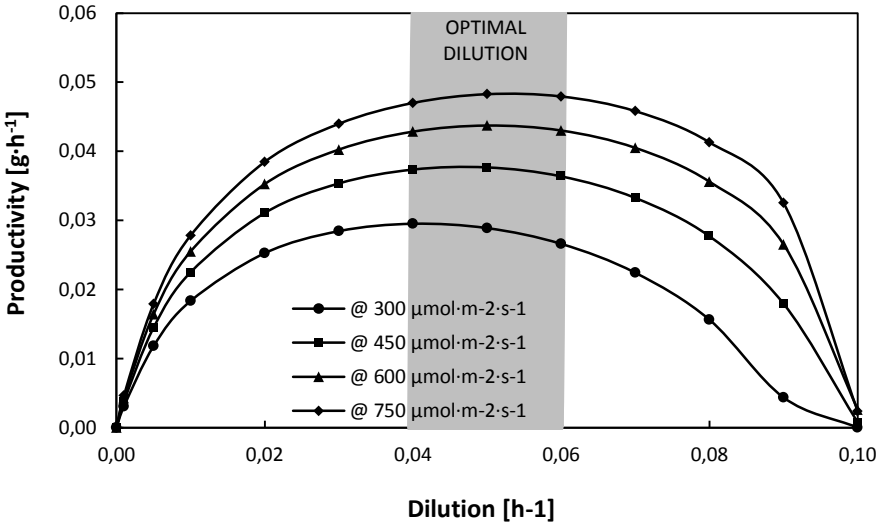

Fig.I.4.2. Optimal dilution in terms of productivity for a wide range of light intensities

On the other hand there are various protocols which require high concentrations of biomass to be furnished – achieved at low dilution rates – thus saving space and optimizing the water/medium consumption (Degrenne *et al.*, 2011).

In what regards the pH no study was performed in this thesis in the sense of finding the best pH value for optimal biomass production, therefore it was always considered 7.5 as it has been suggested by other authors (Kong *et al.*, 2010; Kosourov *et al.*, 2003) for *Chlamydomonas reinhardtii*. Thus, the setpoint tracking function of the pH controller must be robust enough to reject the disturbances given by eventual transitory regimes of biomass.

Based on the above mentioned conditions two operating points were identified:

1) Low dilution – 0.01 h^{-1} (one tenth of washout dilution) – associated with a high concentration of biomass in the reactor and optimal $G_{in}^{CO_2}$ consumption – $1.2184 \cdot 10^{-3}$ $mol \cdot h^{-1}$ – to adjust the pH at 7.5 which leads to the following steady-state values: X =

1.2460 g·L^{-1}, c_{TIN} = 0.0180 mol·L^{-1}, c_{TIC} = 0.0110 mol·L^{-1}, $c_{\mathrm{O_2}}$ = 6.3480·10^{-4} mol·L^{-1}, $y_{out}^{\mathrm{CO_2}}$ = 0.0238 and $y_{out}^{\mathrm{O_2}}$ = 0.0323.

2) Optimal dilution – 0.05 h^{-1} – associated with the best biomass productivity (Fig.I.4.2.) and optimal $G_{in}^{\mathrm{CO_2}}$ consumption – 1.9686·10^{-3} mol·h^{-1} – to adjust the pH at 7.5 which leads to the following steady-state values: X = 0.3929 g·L^{-1}, c_{TIN} = 0.0241 mol·L^{-1}, c_{TIC} = 0.0174 mol·L^{-1}, $c_{\mathrm{O_2}}$ = 9.5446·10^{-4} mol·L^{-1}, $y_{out}^{\mathrm{CO_2}}$ = 0.0375 and $y_{out}^{\mathrm{O_2}}$ = 0.0473.

The two identified steady-state operating points will be used to obtain the linear tangent models for the frequency response and RGA analysis.

I.4.2.4. Model Reduction

According to the control scheme (Fig.I.4.1) the input, state and output vectors of the global model (Eq.I.4.2) are: $u = [u_1\ u_2] = \left[D\ G_{in}^{\mathrm{CO_2}}\right]$ (the controllable inputs considered for control purposes and not all inputs used for the integration of the global photoautotrophic growth model), $x^T = [x_1\ x_2\ x_3\ x_4\ x_5\ x_6] = \left[X\ c_{\mathrm{TIN}}\ c_{\mathrm{TIC}}\ c_{\mathrm{O_2}}\ y_{out}^{\mathrm{CO_2}}\ y_{out}^{\mathrm{O_2}}\right]$ and $y = [y_1\ y_2] = [X\ c_{\mathrm{H^+}}]$. The synthesis of nonlinear controllers requires proper I/O models, in other words the output measurable variables, X and $c_{\mathrm{H^+}}$, must be explicit functions of the input measurable variables, D and $G_{in}^{\mathrm{CO_2}}$ respectively. The relative degree d_i is a fundamental characteristic of a nonlinear system and practically represents the number of times the output y needs to be differentiated before the input u appears explicitly. In what regards the biomass equation (*in* Eq.I.4.2) the input variable D appears explicitly after the first derivation, therefore the relative degree associated with the output y_1 is equal to d_1 = 1. The second output y_2, described by the algebraic electroneutrality relation (Eq.I.4.10), is not an explicit function of u_2 and must be derived two times for the output to appear and thus the relative degree will be d_2 = 2. However, the final expression of the control algorithm will be unnecessarily complex pointing to the reduction of the relative degree to 1 and hence the reduction of the model. In addition, the algebraic loops must be simplified, on the basis of certain assumptions, in order to produce a dynamic model for $c_{\mathrm{H^+}}$.

I.4.2.4.1. *Frequency Response of Global Photoautotrophic Model*

Based on the model response to various frequencies the states with slow dynamics can be differentiated from the ones with fast dynamics which can be reduced to algebraic equations by equalizing their derivatives with zero.

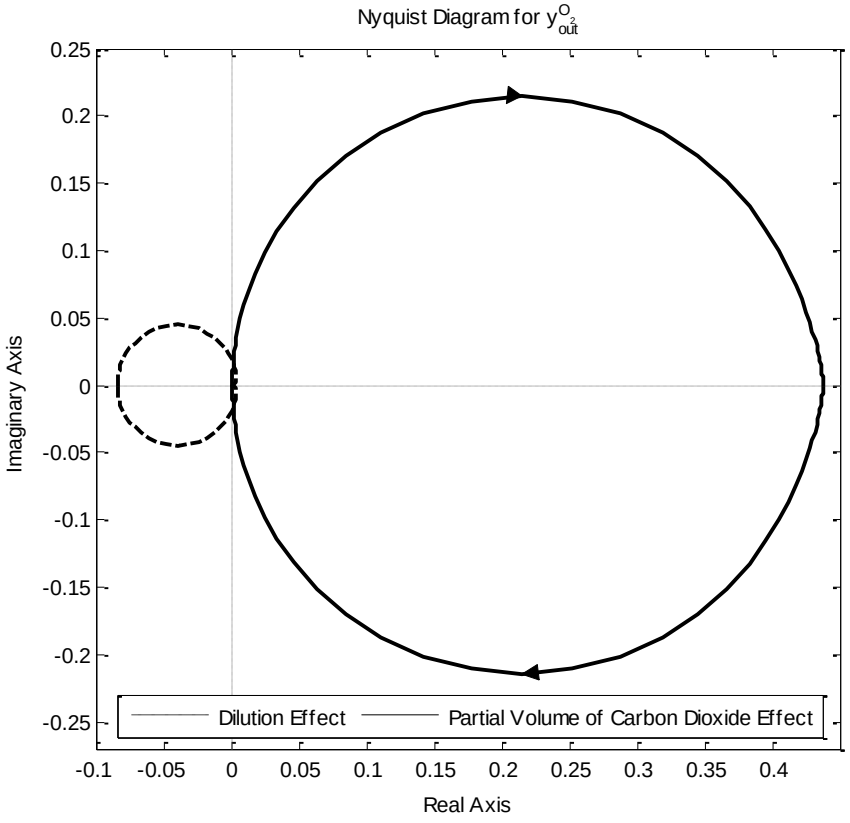

Fig.I.4.3. Comparison between Nyquist plots for $H_{2,D-y_{out}^{O_2}}(j\omega)$ and $H_{2,G_{in}^{O_2}-y_{out}^{O_2}}(j\omega)$

The frequency response analysis requires steady-state linear models which can be obtained through the linearization of the dynamic nonlinear model (Eq.I.4.2) around the two operating points identified above (section I.4.2.3). In this particular case the measurable or estimable outputs y of the system are the states x, thus resulting two sets of transfer functions $H_{i,u-y}(s)$ (one per operating point) each consisting in twelve transfer functions (one for every $u-y$ pair). For graphical representation only one point was considered (D = 0.05 h^{-1} & $G_{in}^{CO_2}$ = $1.9686 \cdot 10^{-3}$ $mol \cdot h^{-1}$), noting that the other operating point gives a similar response. To select the appropriate transfer functions it is important to determine how much the input variables u (*i.e.* D and $G_{in}^{CO_2}$) influence the outputs y.

The association between a specific input and an output can be done by comparing their Nyquist diagrams. Fig.I.4.3 shows the comparison between the D and $G_{in}^{\mathrm{CO}_2}$ effects over $y_{out}^{\mathrm{O}_2}$ dynamics, highlighting that $G_{in}^{\mathrm{CO}_2}$ is the most influent input.

By comparing the Nyquist plots which depict the effect of the inputs over each of the outputs it was found that D has a major influence over X and c_{TIN}, whereas $G_{in}^{\mathrm{CO}_2}$ mainly influences the rest of the states, thus the following transfer functions were obtained:

$$H_{2,D-X}(s) = \frac{0.3929 \cdot s^5 + 7.8220 \cdot s^4 + 42.4800 \cdot s^3 + 36.5100 \cdot s^2 + 3.3360 \cdot s + 0.0808}{s^6 + 19.9500 \cdot s^5 + 108.9000 \cdot s^4 + 97.2500 \cdot s^3 + 12.2100 \cdot s^2 + 0.5455 \cdot s + 0.0082} \quad \text{(I.4.12)}$$

$$H_{2,D-c_{\mathrm{TIN}}}(s) = \frac{3.5530 \cdot 10^{-15} \cdot s^5 + 2.8690 \cdot 10^{-5} \cdot s^4 + 5.737 \cdot 10^{-4} \cdot s^3 + 0.0031 \cdot s^2 + \cdot 0.0025 \cdot s + 1.1800 \cdot 10^{-4}}{s^6 + 19.9500 \cdot s^5 + 108.9000 \cdot s^4 + 97.2500 \cdot s^3 + 12.2100 \cdot s^2 + 0.5455 \cdot s + 0.0082} \quad \text{(I.4.13)}$$

$$H_{2,G_{in}^{\mathrm{CO}_2}-c_{\mathrm{TIC}}}(s) = \frac{3.5530 \cdot 10^{-15} \cdot s^5 + 3.4150 \cdot s^4 + 38.1100 \cdot s^3 + 35.5600 \cdot s^2 + 2.9700 \cdot s + 0.0648}{s^6 + 19.9500 \cdot s^5 + 108.9000 \cdot s^4 + 97.25000 \cdot s^3 + 12.2100 \cdot s^2 + 0.5455 \cdot s + 0.0082} \quad \text{(I.4.14)}$$

$$H_{2,G_{in}^{\mathrm{CO}_2}-c_{\mathrm{O}_2}}(s) = \frac{0.0047 \cdot s^4 + 0.0418 \cdot s^3 + 0.0058 \cdot s^2 + 2.6830 \cdot 10^{-4} \cdot s + 4.1210 \cdot 10^{-6}}{s^6 + 19.9500 \cdot s^5 + 108.9000 \cdot s^4 + 97.25000 \cdot s^3 + 12.2100 \cdot s^2 + 0.5455 \cdot s + 0.0082} \quad \text{(I.4.15)}$$

$$H_{2,G_{in}^{\mathrm{CO}_2}-y_{out}^{\mathrm{CO}_2}}(s) = \frac{138.7000 \cdot s^5 + 1555.0000 \cdot s^4 + 1532.0000 \cdot s^3 + 194.2000 \cdot s^2 + 8.6470 \cdot s + 0.1307}{s^6 + 19.9500 \cdot s^5 + 108.9000 \cdot s^4 + 97.25000 \cdot s^3 + 12.2100 \cdot s^2 + 0.5455 \cdot s + 0.0082} \quad \text{(I.4.16)}$$

$$H_{2,G_{in}^{\mathrm{CO}_2}-y_{out}^{\mathrm{O}_2}}(s) = \frac{4.3350 \cdot s^5 + 42.6000 \cdot s^4 + 41.8900 \cdot s^3 + 5.3120 \cdot s^2 + 0.2382 \cdot s + 0.0036}{s^6 + 19.9500 \cdot s^5 + 108.9000 \cdot s^4 + 97.25000 \cdot s^3 + 12.2100 \cdot s^2 + 0.5455 \cdot s + 0.0082} \quad \text{(I.4.17)}$$

To discriminate among the states with slow and fast dynamics the most widely used means of displaying their frequency responses are the Bode plots. Fig.I.4.4 displays the Bode characteristics of the linear model (I.4.12-I.4.17), in terms of magnitude versus frequency and, as it can be observed, the X, c_{TIN} and c_{TIC} responds too slowly to let the high frequencies inputs to have substantial effect on the outputs and the sinusoidal inputs with $\omega > \omega_{\mathrm{cf}}$ are attenuated by the system dynamics.

Thus, X, c_{TIN} and c_{TIC} are states with slow dynamics, whereas c_{O_2}, $y_{out}^{\mathrm{CO}_2}$ and $y_{out}^{\mathrm{O}_2}$ are states with fast dynamics which can be converted into algebraic equations by equalizing their derivatives with zero, obtaining:

$$c_{\mathrm{O}_2} = \frac{\langle r_{\mathrm{O}_2} \rangle}{(K_L a)_{\mathrm{O}_2} + D} + \frac{(K_L a)_{\mathrm{O}_2} y_{out}^{\mathrm{O}_2} P}{H_{\mathrm{O}_2}\left((K_L a)_{\mathrm{O}_2} + D\right)} \tag{I.4.18}$$

$$y_{out}^{\mathrm{CO}_2} = \frac{G_{in}^{\mathrm{CO}_2} + V_l (K_L a)_{\mathrm{CO}_2} c_{\mathrm{CO}_2}}{G_{out} + \frac{V_l (K_L a)_{\mathrm{CO}_2} P}{\gamma_{\mathrm{CO}_2} H_{\mathrm{CO}_2}}} \tag{I.4.19}$$

$$y_{out}^{\mathrm{O}_2} = \frac{G_{in}^{\mathrm{O}_2} + V_l (K_L a)_{\mathrm{O}_2} c_{\mathrm{O}_2}}{G_{out} + \frac{V_l (K_L a)_{\mathrm{O}_2} P}{H_{\mathrm{O}_2}}} \tag{I.4.20}$$

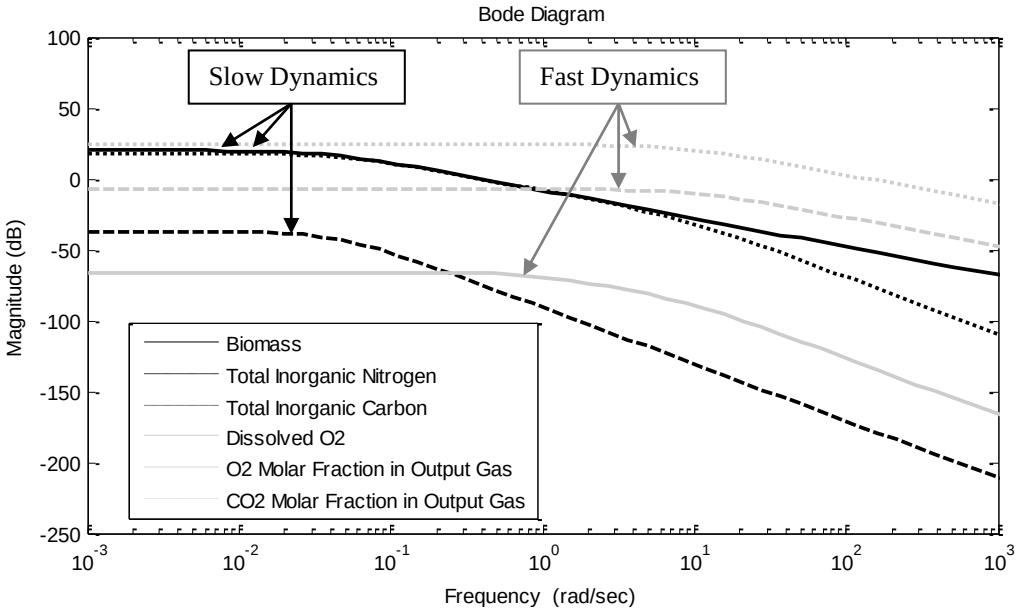

Fig.I.4.4. Bode plots for $H_{2,D-X}(j\omega)$, $H_{2,D-c_{\mathrm{TIN}}}(j\omega)$, $H_{2,G_{in}^{\mathrm{CO}_2}-c_{\mathrm{TIC}}}(j\omega)$, $H_{2,G_{in}^{\mathrm{CO}_2}-c_{\mathrm{O}_2}}(j\omega)$, $H_{2,G_{in}^{\mathrm{CO}_2}-y_{out}^{\mathrm{CO}_2}}(j\omega)$ and $H_{2,G_{in}^{\mathrm{CO}_2}-y_{out}^{\mathrm{O}_2}}(j\omega)$

The dynamic model (Eq.I.4.2) was reconstructed in Simulink® and linearized in Matlab® by using the `linmod` function. The Nyquist and Bode diagrams were also plotted in Matlab® by employing the specific `nyquist` and `bode` functions.

I.4.2.4.2. *Algebraic Loops Reduction*

In order to compile a dynamical time-varying expression for the second output variable c_{H^+} some algebraic loops of the nonlinear model (Eq.I.4.2) must be simplified on the basis of

certain assumptions. First of all the electroneutrality relation (Eq.I.4.10) must be derived (Eq.I.4.21) and all its terms, which are implicit functions of states, need to be substituted.

$$\dot{c}_{H^+} = \dot{c}_{HCO_3^-} + 2\dot{c}_{CO_3^{2-}} + \dot{c}_{OH^-} - \dot{c}_{NH_4^+} + \dot{c}t \tag{I.4.21}$$

It is assumed that all activity coefficients γ_i are constant, which is close to reality because even though they are neglected (γ_i = 1) the pH will not vary with more than 0.1 units (on a pH range of ~6 to 8) (Fig.I.3.30). Thus, the constants of equation (I.4.4) can be regrouped in the term $\varepsilon = K_1\gamma_{CO_2}a_w/\gamma_{HCO_3^-}$ and by substituting equation (I.4.3) in (I.4.4) the following relation will be obtained:

$$c_{HCO_3^-} = \frac{\varepsilon}{\gamma_{H^+}c_{H^+}}c_{CO_2} = (\varepsilon 10^{pH} + 1)\left(c_{TIC} - c_{CO_3^{2-}} - c_{NH_2COO^-}\right) \tag{I.3.22}$$

HCO_3^- is the dominant species of TIC summing approximate 94.19% at a pH of 7.5, whereas $CO_{2,aq}$ counts 5.57%, CO_3^{2-} 0.23% and NH_2COO^- shares only 0.01%. Due to their concentration the dynamics of CO_3^{2-} and NH_2COO^- can be neglected even though they vary in time, thus $\dot{c}_{CO_3^{2-}} = 0$ and $\dot{c}_{NH_2COO^-} = 0$.

In what regards the TIN, its dominant specie is NH_4^+ summing up to 98.40% at a pH of 7.5, while NH_3 counts 1.59% and NH_2COO^- remains with 0.01%. Consequently, to simplify the dynamic expression of c_{H^+}instead of $c_{NH_4^+}$ it can be directly used the c_{TIN} differential equation.

The objective of a pH controller is to keep the pH around a prescribed value, and hence c_{H^+} should be constant, thus it can be admitted that $\dot{c}_{H^+} = 0$ which determines as well $\dot{c}_{OH^-} = 0$.

By equalizing with zero the derivatives of all negligible components (*i.e.* $c_{CO_3^{2-}}$, $c_{NH_2COO^-}$ and $\dot{c}_{OH^-}$) and replacing $c_{NH_4^+}$ with c_{TIN}, the expression (I.4.21) will become:

$$\dot{c}_{H^+} = (\alpha 10^{pH} + 1)\dot{c}_{TIC} - \dot{c}_{TIN} \tag{I.4.23}$$

In order to express the TIC as an explicit function of $G_{in}^{CO_2}$, the expression (I.4.19) can be rearranged as follows:

$$N_{\mathrm{CO_2}} = \frac{G_{in}^{\mathrm{CO_2}} - G_{out}^{\mathrm{CO_2}}}{V_l} \tag{I.4.24}$$

By substituting equation (I.4.24) into the general relation of c_{TIC} (*in* Eq.I.4.2) it will be obtained:

$$\dot{c}_{\mathrm{TIC}} = -\langle r_{\mathrm{TIC}} \rangle + \frac{G_{in}^{\mathrm{CO_2}} - G_{out}^{\mathrm{CO_2}}}{V_l} + D\left(c_{\mathrm{TIC},i} - c_{\mathrm{TIC}}\right) \tag{I.4.25}$$

Finally, the dynamic expression of $\dot{c}_{\mathrm{H^+}}$ can be obtained by substituting the $\dot{c}_{\mathrm{TIC}}$ equation (I.4.24) and the $\dot{c}_{\mathrm{TIN}}$ equation (*in* I.4.2) into (I.4.23):

$$\dot{c}_{\mathrm{H^+}} = -\left(\frac{1}{M_x} - \frac{Y_{N/X}}{M_x(\varepsilon 10^{\mathrm{pH}}+1)}\right)\langle r_{\mathrm{x}} \rangle - \frac{1}{V_l} G_{out}^{\mathrm{CO_2}} + \frac{1}{V_l} G_{in}^{\mathrm{CO_2}} + \left(c_{\mathrm{TIC},i} - c_{\mathrm{TIC}} - \frac{c_{\mathrm{TIN},i} - c_{\mathrm{TIN}}}{(\varepsilon 10^{\mathrm{pH}}+1)}\right) D \tag{I.4.26}$$

I.4.2.4.3. *Matrix Representation of the Reduced Model*

The reduced model which is meant to be used for control techniques consists in four states $x^T = [x_1\ x_2\ x_3\ x_4] = [X\ c_{\mathrm{TIN}}\ c_{\mathrm{TIC}}\ c_{\mathrm{H^+}}]$ and the same input and output vectors as the global model: $u = [u_1\ u_2] = \left[D\ G_{in}^{\mathrm{CO_2}}\right]$ and $y = [y_1\ y_2] = [X\ c_{\mathrm{H^+}}]$. To this model a suite of algebraic equations are added: equations (I.3.6 – I.3.10; I.3.12 – I.3.15, I.3.31, I.3.33, I.4.3 – I.4.11 and I.4.18 – I.4.20). The analytical nonlinear functions $f(.)$, $g_1(.)$ and $g_2(.)$ of the reduced model rewritten in matrix form are:

$$f(x) = \begin{bmatrix} \langle r_x \rangle \\ -\frac{Y_{N/X}}{M_x}\langle r_x \rangle \\ -\frac{G_{out}^{\mathrm{CO_2}}}{V_l} - \frac{1}{M_x}\langle r_x \rangle \\ -\frac{G_{out}^{\mathrm{CO_2}}}{V_l} - \left(\frac{1}{M_x} - \frac{Y_{N/X}}{M_x(\varepsilon 10^{\mathrm{pH}}+1)}\right)\langle r_{\mathrm{x}} \rangle \end{bmatrix}, \quad g_1(x) = \begin{bmatrix} -X \\ c_{\mathrm{TIN},i} - c_{\mathrm{TIN}} \\ c_{\mathrm{TIC},i} - c_{\mathrm{TIC}} \\ c_{\mathrm{TIC},i} - c_{\mathrm{TIC}} - \frac{c_{\mathrm{TIN},i} - c_{\mathrm{TIN}}}{(\varepsilon 10^{\mathrm{pH}}+1)} \end{bmatrix}, \quad g_2(x) = \begin{bmatrix} 0 \\ 0 \\ \frac{1}{V_l} \\ \frac{1}{V_l} \end{bmatrix}$$

I.4.2.4.4. *The Response of the Reduced Model vs. Global Model*

In terms of pH, the reduced model will predict slightly higher values in comparison with the global photoautotrophic growth model (Fig.I.4.5) because of the simplifications imposed to the algebraic system.

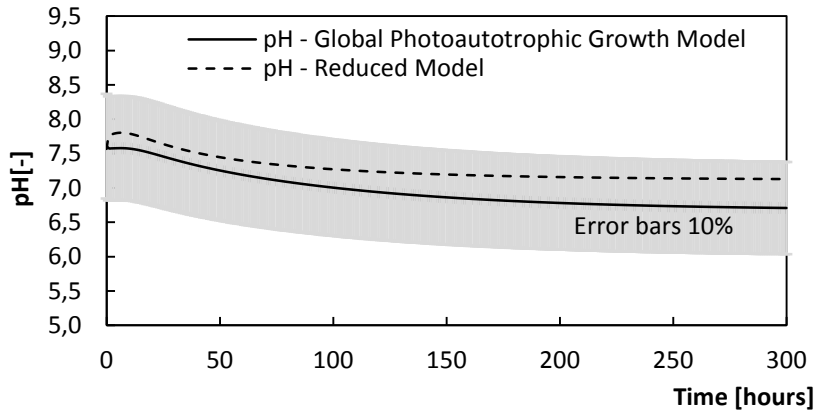

Fig.I.4.5. pH response of the global photoautotrophic growth model vs. reduced model

The simulations (Fig.I.4.5) were done for a batch culture (D = 0) on 300 hours with a constant $G_{in}^{CO_2}$ = 1.5·10^{-3} and q_0 = 300 μmol·m^{-2}·s^{-1}. The results obtained showed a mismatch of 0.2 – 0.4 pH units (< 10%) as it can be observed in Fig.I.4.5.

I.4.2.5. The RGA Analysis

I.4.2.5.1. *Formulation and Properties*

To evaluate the simultaneous control of X and pH and their practical implementation through centralized MIMO or through decentralized SISO controllers a RGA analysis was employed. The RGA was developed by Bristol (1966) as a steady-state measure to quantify the degree of interaction between I/O signals, giving relevant suggestions in what regards the I/O pairings for decentralized control. The array was initially defined for a $n \times n$ square system, whose elements λ_{ij} (*i.e.* relative gains) are the ratio between the gain of an element $[H(s)]_{ij}$ in the transfer matrix $H(s)$ when all the other loops are open, and the gain of the same element when all the other loops are perfectly controlled. The RGA of a non-singular square matrix $H(s)$ is a square matrix frequently computed as:

$$\mathrm{RGA}(H) = \Lambda(H) \triangleq H(s) \times (H(s)^{-1})^T \tag{I.4.27}$$

where × denotes element-by-element multiplication (Schur product). Subsequently, other authors (Kinnaert, 1995; Skogestad and Postlethwaite, 2001) extended its field of application to dynamic processes allowing to be computed for any frequency ω, retrieving the same

properties as the classical approach. The RGA can be denoted $\Lambda(H)$ in both cases, with the Laplace-variable s being equal to 0 for steady-state measurement and $j\omega$ for frequency-dependent systems.

For a $n \times n$ square system the transfer function matrix $H(s)$ with elements $[H(s)]_{ij} = h_{ij}(s)$, denoting input j by u_j and output i by y_i (the Laplace-variable s will be omitted for $H(s)$, $H_{ij}(s)$ and $\lambda_{ij}(s)$):

$$\begin{pmatrix} Y_1 \\ Y_2 \\ \vdots \\ Y_n \end{pmatrix} = H(s) \cdot \begin{pmatrix} U_1 \\ U_2 \\ \vdots \\ U_n \end{pmatrix} \tag{I.4.28}$$

- The *open loop gain* between input u_j and output y_i, h_{ij}, can be obtained by letting all other inputs except u_j, be constant:

$$h_{ij} = \left(\frac{\partial y_i}{\partial u_j}\right)_{u_k=0,\forall\, k\neq j} \tag{I.4.29}$$

- The *closed loop gain*, $\hat{h}_{ij}$ is obtained, by holding all outputs except y_i constant, using feedback control:

$$\hat{h}_{ij} \triangleq \left(\frac{\partial y_i}{\partial u_j}\right)_{y_k=0,\forall\, k\neq i} \tag{I.4.30}$$

Ideally, if no interaction between the loops are present, the gain between input u_j and output y_i would remain the same when the other loops are closed, so the *relative gain* $h_{ij}/\hat{h}_{ij} = 1$. On the other hand, if there is loop interaction in the system, h_{ij} and $\hat{h}_{ij}$ will differ. Hence, the quotient

$$\lambda_{ij} = h_{ij}/\hat{h}_{ij} \tag{I.4.31}$$

can be used as an interaction measure, and a relative gain array (RGA) with elements $[\Lambda(\mathrm{H})]_{ij} = \lambda_{ij}$ can be formed. $y = Hu$ gives $h_{ij} = [H]_{ij}$, and similarly, $u = H^{-1}y$ gives

$$\frac{1}{\hat{h}_{ij}} = \left(\frac{\partial u_j}{\partial y_i}\right)_{y_k=0,\forall\, k\neq i} = [H^{-1}]_{ji} \tag{I.4.32}$$

Each element in the RGA can therefore be calculated using:

$$\lambda_{ij} \triangleq \frac{h_{ij}}{\hat{h}_{ij}} = [H]_{ij}[H^{-1}]_{ji} \tag{I.4.33}$$

Hence, the whole RGA matrix can directly be calculated using Eq.I.4.27.

The RGA has a number of attractive algebraic properties, of which the most important are (Skogestad and Postlethwaite, 2001):

- It is independent of input and output scaling;
- Its rows and columns sum is equal to one: $\sum_{i=1}^{m} \lambda_{ij} = \sum_{j=1}^{m} \lambda_{ij} = 1$;
- A relative change of an element in $H(s)$, equal to the negative inverse of its corresponding RGA-element, gives singularity.
- The RGA is the identity matrix if $H(s)$ is upper or lower triangular.

From the last property results that the RGA (or more precisely $\Lambda - I$) yields a measure of *two-way interaction*.

Besides the algebraic properties above-mentioned, the RGA has a number of useful control properties (Skogestad and Postlethwaite, 2001) such as:

- The RGA is a good indicator of sensitivity to uncertainty,
  - *Uncertainty in the input channels (diagonal input uncertainty)*. Systems with large RGA-elements around the cutting frequency are fundamentally difficult to control because of sensitivity to input uncertainty (*e.g.* caused by uncertain or neglected actuator dynamics).
  - *Element uncertainty*. Large RGA-elements denote sensitivity to element-by-element uncertainty as it results from algebraic property no.3. However, this type of uncertainty may not occur in practice due to physical couplings between the transfer function elements. The diagonal input uncertainty (which is always present) is usually of more concern for plants with large RGA-elements.
- *Non-square plants.* The RGA can be generalized for non-square systems by employing the pseudo inverse.
- RGA and the *decentralized control*. It must be avoided the input-output pairing on negative steady-state RGA-elements in order to obtain stable plants. Otherwise, if the

sub-controllers are designed independently each with integral action, the interactions will create instability either when all of the loops are closed, or when the loop corresponding to the negative relative gain becomes inactive (*e.g.* due to saturation).

I.4.2.5.2. *Pairing Suggestions*

For a 2 × 2 matrix (two controlled variables and two manipulated variables) with elements h_{ij}, the corresponding RGA for a steady-state system is:

$$H = \begin{bmatrix} h_{11} & h_{12} \\ h_{21} & h_{22} \end{bmatrix} \Rightarrow \Lambda(H) = \begin{bmatrix} \lambda_{11} & \lambda_{12} \\ \lambda_{21} & \lambda_{22} \end{bmatrix} = \begin{bmatrix} \lambda_{11} & 1-\lambda_{11} \\ 1-\lambda_{11} & \lambda_{11} \end{bmatrix} \tag{I.4.34}$$

where

$$\lambda_{11} = \frac{1}{1-\kappa} \tag{I.4.35}$$

$$\kappa \triangleq \frac{h_{12}h_{21}}{h_{11}h_{22}} \tag{I.4.36}$$

κ is referred as the interaction measure and is a singular point for the RGA when is equal to 1. The uncertainty of the model, and hence of the transfer function matrix H, may produce uncertainties in the computed RGA (Chen and Seborg, 2002).

The general rules of I/O signal pairing suggest that (Kinnaert, 1995) a system might be decoupled if λ_{11} is close to unity, that is the interaction with other loops ($u_j \rightarrow y_{i,\forall i \neq j}$) is minimal and the pairing may be done along the diagonal. On the other hand, a λ_{11} close to 0 describes the same situation except that now the suggested pairing should be done along the anti-diagonal. Negative elements of the RGA imply that the sign of the steady-state gain will change when the other loops in the remaining subsystem are perfectly controlled case that should be avoided because the plant is ill-conditioned and it may lead to instabilities. Otherwise, if $0 < \lambda_{11} < 1$ the performance of a decentralized controller can be poor due to the strong interactions and, in such situations, the multivariable control is recommended to be approached through centralized MIMO controllers.

I.4.2.5.3. *The Non-square Relative Gain Array (NRG)*

The biological processes naturally have an unequal number of inputs and outputs, therefore the RGA may be generalized to a non-square $l \times m$ matrix H by use of the Moore-Penrose pseudo inverse $H^{\dagger}$ (Chang and Yu, 1990; Skogestad and Postlethwaite, 2001). These multivariable systems can be controlled either through centralized MIMO or through decentralized SISO controllers. The NRG method has as additional goal the conversion of the non-square systems to square systems through the algebraic decoupling of the I/O pairs with the smallest influence over the system (Reeves and Arkun, 1989). The RGA of a non-square multivariable system described through the transfer matrix H has the following form:

$$\Lambda(H) = H \times (H^{\dagger})^{T} \tag{I.4.37}$$

The properties of the non-square matrices were stated initially by Chang and Yu (1990) and completed by other authors (Cao, 1995).

The RGA for non-square systems has the following properties:

- If the rank of the system is the row rank - $rank(A) = l$ (the number of inputs is higher than the number of outputs which are linear independent), $AA^{\dagger} = I$ and:
  - The RGA is independent of output scaling, $\Lambda(D \cdot A) = \Lambda(A)$
  - Each RGA row sums to one, $\sum_{j=1}^{m} \lambda_{ij} = 1$
  - In this case $m - l$ inputs might be eliminated by identifying the smallest sum of elements on each column, having as result a square system of l^{th} order.
- If the rank of the system is the column rank - $rank(A) = m$ (the number of outputs is higher than the number of inputs which are linear independent), $A^{\dagger}A = I$ and:
  - The RGA is independent of input scaling, $\Lambda(A \cdot D) = \Lambda(A)$
  - Each RGA column sums to one, $\sum_{i=1}^{l} \lambda_{ij} = 1$
  - In this case $l - m$ inputs can be excluded by identifying the smallest sum of elements on each row, having as result a square system of m^{th} order.

Unlike the square systems, the inputs and/or outputs of a non-square system must be scaled in order to withdraw useful conclusions. At a steady-state operating point ($s = 0$) the scaling of a model can be done by introducing the scaled variables:

$$u = D_u^{-1}u^0 \text{ and/or } y = D_y^{-1}y^0 \tag{I.4.38}$$

where D_u and D_y are the diagonal scaling matrices.
If the original model is given by the equation:

$$y^0(t) = G^0(s) \cdot u^0(t) \tag{I.4.39}$$

where $G^0(s)$ is the original transfer matrix between $u^0(t)$ and $y^0(t)$, the model becomes:

$$G(s) = S_1 \cdot G^0(s) \cdot S_2 \tag{I.4.40}$$

where $S_1 = D_u$ and $S_2 = D_y^{-1}$.
There are no general scaling procedures (Waller and Waller, 1995) that is why the scaling must be done carefully since a bad scaling can make the model ill-conditioned even though the plant itself is well-conditioned.

I.4.2.5.4. *RGA Analysis for the Photoautotrophic Growth Process*

A simplistic representation of the control strategy (*i.e.* simultaneous control of *D* and $G_{in}^{CO_2}$ to manipulate the *X* and c_{H^+}) would result in a 2×2 square system which can be unconditionally decoupled because *X* is not a function of c_{H^+}, and $G_{in}^{CO_2}$ cannot possibly interpose in its relation, thus no $G_{in}^{CO_2} \rightarrow X$ interaction will exist. Whereas the nonlinear manipulation of the dilution to control *X* in a photobioreactor is a mediated problem resembling to other applications, the nonlinear control of the pH requires further insight. As stated above, the $G_{in}^{CO_2}$ action is to decrease the pH of an algae culture when it is bubbled into the photobioreactor, whereas the pH increase is ensured through the photoautotrophic growth of biomass. At the same time the pH is influenced by the TIN present in the culture medium. In conclusion, the pH is a complex nonlinear function of all other three states of the reduced dynamic model (*i.e. X*, TIN and TIC), fact which can be deduced from its dynamic relation (I.4.26). Hence, to evaluate the interactions between the main variables of the system the pH relation must be uncoupled and thus a non-square system (I.4.41) with two manipulable inputs, *D* and $G_{in}^{CO_2}$, and three controllable outputs, *X*, TIN and TIC, is considered:

$$\begin{bmatrix} X \\ c_{\mathrm{TIN}} \\ c_{\mathrm{TIC}} \end{bmatrix} = \begin{bmatrix} H_{i,D-X} & H_{i,G_{in}^{\mathrm{CO_2}}-X} \\ H_{i,D-\mathrm{TIN}} & H_{i,G_{in}^{\mathrm{CO_2}}-\mathrm{TIN}} \\ H_{i,D-\mathrm{TIC}} & H_{i,G_{in}^{\mathrm{CO_2}}-\mathrm{TIC}} \end{bmatrix} \begin{bmatrix} D \\ G_{in}^{\mathrm{CO_2}} \end{bmatrix} \tag{I.4.41}$$

The RGA and NRG analyses are calculated for steady-state ($s = 0$) and, in order to obtain the value of each element $[H(0)]_{ij}$ of the transfer function matrix the system was linearized around the same two operating points afore-identified, but using the reduced model which returns:

1) for D = 0.01 $\mathrm{h^{-1}}$ and $G_{in}^{\mathrm{CO_2}}$ = 1.7550·10^{-3} mol·$\mathrm{h^{-1}}$ (for pH = 7.5) – X = 1.2461 g·$\mathrm{L^{-1}}$, c_{TIN} = 0.0180 mol·$\mathrm{L^{-1}}$, c_{TIC} = 0.0195 mol·$\mathrm{L^{-1}}$ and $c_{\mathrm{H^+}}$ = 3.6451·10^{-8} mol·$\mathrm{L^{-1}}$;
2) for D = 0.05 $\mathrm{h^{-1}}$ and $G_{in}^{\mathrm{CO_2}}$ = 2.3107·10^{-3} mol·$\mathrm{h^{-1}}$ (for pH = 7.5) – X = 0.3929 g·$\mathrm{L^{-1}}$, c_{TIN} = 0.0241 mol·$\mathrm{L^{-1}}$, c_{TIC} = 0.0198 mol·$\mathrm{L^{-1}}$ and $c_{\mathrm{H^+}}$ = 3.6839·10^{-8} mol·$\mathrm{L^{-1}}$.

The transfer functions obtained for the first operating point by using the reduced model are the following:

$$H_{1,D-X}(s) = \frac{1.25 \cdot s^3 + 3.60 \cdot 10^{-2} \cdot s^2 + 3.45 \cdot 10^{-4} \cdot s + 1.10 \cdot 10^{-6}}{s^4 + 5.12 \cdot 10^{-2} \cdot s^3 + 9.23 \cdot 10^{-4} \cdot s^2 + 7.09 \cdot 10^{-6} \cdot s + 1.98 \cdot 10^{-8}} \tag{I.4.42}$$

$$H_{1,D-\mathrm{TIN}}(s) = \frac{1.13 \cdot 10^{-4} \cdot s^2 + 2.13 \cdot 10^{-6} \cdot s + 10^{-8}}{s^4 + 5.12 \cdot 10^{-2} \cdot s^3 + 9.23 \cdot 10^{-4} \cdot s^2 + 7.09 \cdot 10^{-6} \cdot s + 1.98 \cdot 10^{-8}} \tag{I.4.43}$$

$$H_{1,D-\mathrm{TIC}}(s) = \frac{-6.24 \cdot 10^{-4} \cdot s^2 - 1.18 \cdot 10^{-5} \cdot s - 5.53 \cdot 10^{-8}}{s^4 + 5.12 \cdot 10^{-2} \cdot s^3 + 9.23 \cdot 10^{-4} \cdot s^2 + 7.09 \cdot 10^{-6} \cdot s + 1.98 \cdot 10^{-8}} \tag{I.4.44}$$

$$H_{1,G_{in}^{\mathrm{CO_2}}-X}(s) = 0 \tag{I.4.45}$$

$$H_{1,G_{in}^{\mathrm{CO_2}}-\mathrm{TIN}}(s) = 0 \tag{I.4.46}$$

$$H_{1,G_{in}^{\mathrm{CO_2}}-\mathrm{TIC}}(s) = \frac{6.90 \cdot 10^{-1} \cdot s^3 + 2.84 \cdot 10^{-2} \cdot s^2 + 3.52 \cdot 10^{-4} \cdot s + 1.37 \cdot 10^{-6}}{s^4 + 5.12 \cdot 10^{-2} \cdot s^3 + 9.23 \cdot 10^{-4} \cdot s^2 + 7.09 \cdot 10^{-6} \cdot s + 1.98 \cdot 10^{-8}} \tag{I.4.47}$$

which lead to the following steady-state coefficients transfer matrix:

$$H_1(0) = \begin{bmatrix} 1.10 \cdot 10^{-6}/1.98 \cdot 10^{-8} & 0 \\ 10^{-8}/1.98 \cdot 10^{-8} & 0 \\ -5.53 \cdot 10^{-8}/1.98 \cdot 10^{-8} & 1.37 \cdot 10^{-6}/1.98 \cdot 10^{-8} \end{bmatrix} \quad \text{(I.4.48)}$$

Unlike the square systems, the inputs and/or outputs of a non-square system must be scaled in order to withdraw useful conclusions. Because the rank of the system is the column rank – $rank(H) = m$ the system is not independent of output scaling, therefore the diagonal inverse matrix of the steady-state values (I.4.49) used for the linearization of the reduced model can be considered as scaling matrix:

$$S_{1,y}^{-1} = \begin{bmatrix} 1/1.2461 & 0 & 0 \\ 0 & 1/0.0180 & 0 \\ 0 & 0 & 1/0.0195 \end{bmatrix} \quad \text{(I.4.49)}$$

Thus, for the first operating point the following NRG matrix results:

$$\Lambda_1 = \begin{bmatrix} 0.7173 & 0.0000 \\ 0.2827 & 0.0000 \\ 0.0000 & 1.0000 \end{bmatrix} \quad \text{(I.4.50)}$$

Similarly, the NRG matrix was calculated for the second operation point obtaining comparable results:

$$\Lambda_2 = \begin{bmatrix} 0.9994 & 0.0000 \\ 0.0006 & 0.0000 \\ 0.0000 & 1.0000 \end{bmatrix} \quad \text{(I.4.51)}$$

In this case $l - m$ inputs can be excluded by identifying the smallest sum of elements on each row having as result a square matrix system of m^{th} order. Summing each row of Λ_1 (I.4.50) and Λ_2 (I.4.51) it can be observed that the smallest value is taken by the second row which means that TIN will be poorly controlled when using D and $G_{in}^{CO_2}$ in the given configuration, thus the system can be squared by neglecting its interactions. Because λ_{23} is equal to 1 it results that the concentration of TIC is the main state which influences the pH.

The system thus squared (Fig.I.4.6) will give, for any D and $G_{in}^{CO_2}$, $H_{1|2,G_{in}^{CO_2}-X} = h_{12} = 0$ for the same reason that μ_I (I.3.8) is not a function of c_{TIC}, and $G_{in}^{CO_2}$ does not interpose in

biomass relation. In this case, $\lambda_{12} = \lambda_{21} = 0$ and $\lambda_{11} = \lambda_{22} = 1$, the RGA is the identity matrix (I.4.52) which points that there are no cross-interactions, its diagonal dominance allowing the decentralized control on $D \rightarrow X$ and $G_{in}^{\mathrm{CO_2}} \rightarrow c_{\mathrm{TIC}}$ channels.

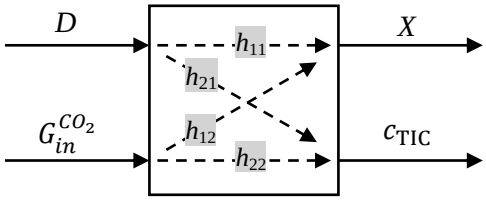

Fig.I.4.6. The square system of the photobioreactor

$$\Lambda_{1|2} = \begin{bmatrix} 1 & 0 \\ 0 & 1 \end{bmatrix} \tag{I.4.52}$$

Nevertheless, the mathematical formulation of μ_I as an exclusive function of available irradiance inside the photobioreactor is consistent only if the carbonaceous substrate (TIC) is non-limiting. The working protocol presented in this paper consists in using a culture medium enriched in $\mathrm{NaHCO_3}$ with a constant addition of $\mathrm{CO_2}$ for pH regulation, but there are various other facilities operated exclusively with gaseous $\mathrm{CO_2}$ (Buehner *et al.*, 2009) where the TIC can easily become limiting. The carbonaceous substrate can also become limiting at high concentration of biomass leading to substrate depletion. In order to describe that the photoautotrophic growth process takes place only in the presence of light, but is inhibited when the carbon source becomes limiting, a mathematically continuous switching function, to turn process rate equation on and off, must be added in the expression of μ_I (Eq.I.4.53). The TIC half-saturation coefficient has only mathematical significance and must have a small value for switching purpose (K_{TIC} = 0.001 mol·L^{-1}).

$$\mu_I = \mu_0 \frac{I}{K_I + I + \frac{I^2}{K_{II}}} \frac{c_{\mathrm{TIC}}}{K_{\mathrm{TIC}} + c_{\mathrm{TIC}}} \tag{I.4.53}$$

To estimate the I/O interactions in a biological system where the carbon source can be also a limiting factor, the reduced model was linearized around the same two operating points presented earlier except that the dynamics of the specific growth rate was calculated with Eq. (I.4.53). Thus, the transfer functions for the first operating point are:

$$H_{1,D-X}(s) = \frac{1.25 \cdot s^3 + 3.96 \cdot 10^{-2} \cdot s^2 + 4.14 \cdot 10^{-4} \cdot s + 1.43 \cdot 10^{-6}}{s^4 + 5.42 \cdot 10^{-2} \cdot s^3 + 1.01 \cdot 10^{-3} \cdot s^2 + 7.91 \cdot 10^{-6} \cdot s + 2.24 \cdot 10^{-8}} \quad \text{(I.4.54)}$$

$$H_{1,D-c_{\mathrm{TIC}}}(s) = \frac{-6.24 \cdot 10^{-4} \cdot s^2 - 1.18 \cdot 10^{-5} \cdot s - 5.54 \cdot 10^{-8}}{s^4 + 5.42 \cdot 10^{-2} \cdot s^3 + 1.01 \cdot 10^{-3} \cdot s^2 + 7.91 \cdot 10^{-6} \cdot s + 2.24 \cdot 10^{-8}} \quad \text{(I.4.55)}$$

$$H_{1,G_{in}^{\mathrm{CO_2}}-X}(s) = \frac{4.95 \cdot 10^{-2} \cdot s^2 + 9.34 \cdot 10^{-4} \cdot s + 4.39 \cdot 10^{-6}}{s^4 + 5.42 \cdot 10^{-2} \cdot s^3 + 1.01 \cdot 10^{-3} \cdot s^2 + 7.91 \cdot 10^{-6} \cdot s + 2.24 \cdot 10^{-8}} \quad \text{(I.4.56)}$$

$$H_{1,G_{in}^{\mathrm{CO_2}}-c_{\mathrm{TIC}}}(s) = \frac{6.90 \cdot 10^{-1} \cdot s^3 + 2.85 \cdot 10^{-2} \cdot s^2 + 3.53 \cdot 10^{-4} \cdot s + 1.37 \cdot 10^{-6}}{s^4 + 5.42 \cdot 10^{-2} \cdot s^3 + 1.01 \cdot 10^{-3} \cdot s^2 + 7.91 \cdot 10^{-6} \cdot s + 2.24 \cdot 10^{-8}} \quad \text{(I.4.57)}$$

and the transfer function matrix at steady-state for the linear model (I.4.54 – I.4.57) which corresponds to the first operating point is:

$$H_1(0) = \begin{bmatrix} 1.43 \cdot 10^{-6}/2.24 \cdot 10^{-8} & 4.39 \cdot 10^{-6}/2.24 \cdot 10^{-8} \\ -5.54 \cdot 10^{-8}/2.24 \cdot 10^{-8} & 1.37 \cdot 10^{-6}/2.24 \cdot 10^{-8} \end{bmatrix} \quad \text{(I.4.58)}$$

The transfer functions obtained for the second operating point are:

$$H_{2,D-X}(s) = \frac{3.93 \cdot 10^{-1} \cdot s^3 + 4.05 \cdot 10^{-2} \cdot s^2 + 1.08 \cdot 10^{-3} \cdot s + 1.72 \cdot 10^{-6}}{s^4 + 1.43 \cdot 10^{-1} \cdot s^3 + 6.84 \cdot 10^{-3} \cdot s^2 + 1.14 \cdot 10^{-4} \cdot s + 1.75 \cdot 10^{-7}} \quad \text{(I.4.59)}$$

$$H_{2,D-c_{\mathrm{TIC}}}(s) = \frac{-1.58 \cdot 10^{-4} \cdot s^2 - 8.11 \cdot 10^{-6} \cdot s - 1.33 \cdot 10^{-8}}{s^4 + 1.43 \cdot 10^{-1} \cdot s^3 + 6.84 \cdot 10^{-3} \cdot s^2 + 1.14 \cdot 10^{-4} \cdot s + 1.75 \cdot 10^{-7}} \quad \text{(I.4.60)}$$

$$H_{2,G_{in}^{\mathrm{CO_2}}-X}(s) = \frac{4.14 \cdot 10^{-2} \cdot s^2 + 2.12 \cdot 10^{-3} \cdot s + 3.49 \cdot 10^{-6}}{s^4 + 1.43 \cdot 10^{-1} \cdot s^3 + 6.84 \cdot 10^{-3} \cdot s^2 + 1.14 \cdot 10^{-4} \cdot s + 1.75 \cdot 10^{-7}} \quad \text{(I.4.61)}$$

$$H_{2,G_{in}^{\mathrm{CO_2}}-c_{\mathrm{TIC}}}(s) = \frac{6.90 \cdot 10^{-1} \cdot s^3 + 6.26 \cdot 10^{-2} \cdot s^2 + 1.45 \cdot 10^{-3} \cdot s + 2.30 \cdot 10^{-6}}{s^4 + 1.43 \cdot 10^{-1} \cdot s^3 + 6.84 \cdot 10^{-3} \cdot s^2 + 1.14 \cdot 10^{-4} \cdot s + 1.75 \cdot 10^{-7}} \quad \text{(I.4.62)}$$

and the transfer function matrix at steady-state for the linear model (I.4.59 – I.4.62) which corresponds to the second operating point is:

$$H_2(0) = \begin{bmatrix} 1.72 \cdot 10^{-6}/1.75 \cdot 10^{-7} & 3.49 \cdot 10^{-6}/1.75 \cdot 10^{-7} \\ -1.33 \cdot 10^{-8}/1.75 \cdot 10^{-7} & 2.30 \cdot 10^{-6}/1.75 \cdot 10^{-7} \end{bmatrix} \quad \text{(I.4.63)}$$

The RGA is independent of input and output scaling and therefore it can easily be calculated for both operating points (I.4.64):

$$\Lambda_1 = \begin{bmatrix} 0.8893 & 0.1107 \\ 0.1107 & 0.8893 \end{bmatrix}; \qquad \Lambda_2 = \begin{bmatrix} 0.9883 & 0.0117 \\ 0.0117 & 0.9883 \end{bmatrix} \tag{I.4.64}$$

The matrices maintain their diagonal dominance thus the control channels $D \rightarrow X$ and $G_{in}^{\mathrm{CO_2}} \rightarrow c_{\mathrm{TIC}}$ were well chosen and the values of their relative gains show that the plant is well-conditioned. Practically, the second control channel is $G_{in}^{\mathrm{CO_2}} \rightarrow$ pH because the objective is not to control the TIC but to control the pH, nevertheless acting on the TIC system appears to be the main mechanism of pH manipulation whereas TIN may be treated as disturbance. If the photobioreactor is operated at optimal dilution in terms of productivity (*e.g.* 0.05 h^{-1}), in other words at low biomass concentration, the interferences are small enough – $[\Lambda_2(0)]_{12} = [\Lambda_2(0)]_{21} = 0.0117$ – to allow the use of decentralized SISO controllers. The more dilution decreases, the more interferences increase – $[\Lambda_1(0)]_{12} = [\Lambda_1(0)]_{21} = 0.1107$ – because higher concentrations of biomass consume more carbon. High concentrations of biomass are required in various operating protocols such as hydrogen production (Degrenne *et al.*, 2011) therefore the experiments performed for validation of the control algorithm were designed to maintain the biomass around 1.8 and 2.0 $g \cdot L^{-1}$. The protocol allows investigating the behavior of the pH controller on a wide range of biomass concentrations. The RGA correlated with 1.8 $g \cdot L^{-1}$ (Λ_3) and 2.0 $g \cdot L^{-1}$ (Λ_4) biomass and pH of 7.5 show, as expected, significant interferences (I.4.65) which recommend caution at the decentralization of the system or safer, the use of centralized MIMO controllers.

$$\Lambda_3 = \begin{bmatrix} 0.7172 & 0.2828 \\ 0.2828 & 0.7172 \end{bmatrix}; \qquad \Lambda_4 = \begin{bmatrix} 0.6292 & 0.3708 \\ 0.3708 & 0.6292 \end{bmatrix} \tag{I.4.65}$$

In conclusion, if the photoautotrophic growth process takes place under non-limiting conditions in terms of carbonaceous substrate, the system can be easily decoupled, but under limiting conditions is safer to use centralized MIMO controllers.

I.4.2.6. Multivariable Feedback Linearizing Control

I.4.2.6.1. *Basic Principles*

The feedback linearizing control is a nonlinear control technique which can produce a linear model that is an exact representation of the original nonlinear model over a large set of operating conditions (Henson and Seborg, 1997).

The first step in developing a feedback linearizing control strategy is to derive an I/O model (I.4.66) through appropriate manipulations that is deriving y with respect to time until the input u appears.

$$\begin{aligned} y_i^{(k)} &= L_f^k h_i, k = 1, \dots, d_i - 1 \\ y_i^{(d_i)} &= L_f^{d_i} h_i + \sum_{j=1}^{m} L_{gj} L_f^{d_i - 1} h_i u_j \; ; \; i = 1, \dots, m \end{aligned} \tag{I.4.66}$$

where $L_f h$ and $L_g h$ are the Lie derivatives of h with respect to f and g, and d_i is the relative degree of output y_i with respect to input u_i.

The general model (Eq.I.4.1) can thus be rewritten in a matrix form as:

$$\underbrace{\begin{bmatrix} y_1^{(r_1)} \\ \vdots \\ y_m^{(r_m)} \end{bmatrix}}_{dy/dt} = \underbrace{\begin{bmatrix} L_f^{d_1} h_1(x) \\ \vdots \\ L_f^{d_m} h_m(x) \end{bmatrix}}_{a(x)} + \underbrace{\begin{bmatrix} L_{g1} L_f^{d_1 - 1} h_1(x) & \cdots & L_{gm} L_f^{d_1 - 1} h_1(x) \\ \vdots & \ddots & \vdots \\ L_{g1} L_f^{d_m - 1} h_m(x) & \cdots & L_{gm} L_f^{d_m - 1} h_m(x) \end{bmatrix}}_{B(x)} \underbrace{\begin{bmatrix} u_1 \\ \vdots \\ u_m \end{bmatrix}}_{u} \tag{I.4.67}$$

$B(x)$ is the characteristic matrix of the system (Eq.I.4.1) and, only if it is nonsingular, the linearizing control law is given by the following expression:

$$u = -B(x)^{-1} a(x) + B(x)^{-1} v \tag{I.4.68}$$

which renders a linear I/O map between the new input v and the output y, thus leading to the following linear closed loop system:

$$\begin{bmatrix} y_1^{(r_1)} \\ \vdots \\ y_m^{(r_m)} \end{bmatrix} = \begin{bmatrix} v_1 \\ \vdots \\ v_m \end{bmatrix} \quad \text{(I.4.69)}$$

Secondly, it must be defined a stable linear reference model of the tracking error $\left(y^*(t) - y(t)\right)$. For this purpose it is assumed that the regulation error decreases according to the following stable linear time varying first order dynamics (Bastain and Dochain, 1990):

$$\frac{d}{dt}(y^* - y) = -\Phi(y^* - y) \quad \text{(I.4.70)}$$

where $\Phi = diag(\varphi_1, \varphi_2)$ with $\varphi_i > 0$ is the matrix which contains the poles of the system that impose the error dynamics. The coefficients φ_i are arbitrary with the exception that they need to be chosen so that the differential equation (I.4.67) to be stable. The reference model is independent of the particular process operating point.

Finally, the control design consists in calculating the control action u so that the I/O model (I.4.67) to exactly match the reference model (I.4.70). The control u is obtained by substituting (I.4.67) into (I.4.70):

$$u = B(x)^{-1}\left\{\Phi(y^* - y) + \frac{dy^*}{dt} - a(x)\right\} \quad \text{(I.4.71)}$$

I.4.2.6.2. *Nonlinear Control Algorithms for the Photoautotrophic Growth Process*

The dynamical model (I.4.67) which corresponds to the photoautotrophic growth process is:

$$\begin{bmatrix} \dot{X} \\ \dot{c}_{H^+} \end{bmatrix} = \begin{bmatrix} \langle r_x \rangle \\ -\frac{G_{out}^{\mathrm{CO_2}}}{V_l} - \left(\frac{1}{M_x} - \frac{Y_{N/X}}{M_x(\varepsilon 10^{\mathrm{pH}}+1)}\right)\langle r_x \rangle \end{bmatrix} + \begin{bmatrix} -X & 0 \\ c_{\mathrm{TIC},i} - c_{\mathrm{TIC}} - \frac{c_{\mathrm{TIN},i} - c_{\mathrm{TIN}}}{\varepsilon 10^{\mathrm{pH}}+1} & \frac{1}{V_l} \end{bmatrix} \begin{bmatrix} D \\ G_{in}^{\mathrm{CO_2}} \end{bmatrix} \quad \text{(I.4.72)}$$

The characteristic matrix of the system is noticeable nonsingular because X and V_l are always positive (X = 0 corresponds to the wash-out of the reactor). The objective of the control algorithm is to maintain the biomass and the pH at the prescribed values $y^* = [y_1^* \; y_2^*]$ by actuating D and $G_{in}^{CO_2}$.

Eq.I.4.71 furnishes the following expression for the control laws:

$$u = \begin{bmatrix} u_1 = (\langle r_x \rangle - \varphi_X er_X)/X \\ u_2 = -V_l \left(c_{\mathrm{TIC},i} - c_{\mathrm{TIC}} - \frac{c_{\mathrm{TIN},i} - c_{\mathrm{TIN}}}{\varepsilon 10^{\mathrm{pH}} + 1} \right) u_1 + V_l \left(\frac{1}{M_x} - \frac{Y_{N/X}}{M_x(\varepsilon 10^{\mathrm{pH}} + 1)} \right) \langle r_x \rangle + G_{out}^{\mathrm{CO_2}} + V_l \varphi_{\mathrm{H^+}} er_{\mathrm{H^+}} \end{bmatrix} \quad \text{(I.4.73)}$$

where:

$$er_X = X^* - X \quad \text{(I.4.74)}$$

and

$$er_{\mathrm{H^+}} = c_{\mathrm{H^+}}^* - c_{\mathrm{H^+}} = \frac{1}{\gamma_{\mathrm{H^+}} 10^{\mathrm{pH}^*}} - \frac{1}{\gamma_{\mathrm{H^+}} 10^{\mathrm{pH}}} \quad \text{(I.4.75)}$$

The activity coefficient $\gamma_{\mathrm{H^+}}$ is a function of temperature and ionic strength of the solution and therefore it can vary in time resulting in a variable $c_{\mathrm{H^+}}^*$. However, its variation is extremely low in the given experimental condition.

I.4.2.6.3. *Results in Simulation*

The nonlinear control algorithm (Eq.I.4.73) which was implemented in simulation was found to be able to globally stabilize the photoautotrophic growth process of a *Chlamydomonas reinhardtii* culture (Fig.I.4.7). The initial conditions used for simulation were presented in the previous chapter. The efficiency of biomass controller in tracking various setpoints can be better observed for positive D steps because if the actual biomass value is significantly smaller than its setpoint the controller will respond with null dilution letting the biomass to grow naturally. The tuning parameter φ_X was set to 1 h^{-1}. Even though the pH is usually kept constant around an optimal value which is specific to each microalgae species, two steps (*i.e.* a negative and a positive step) were imposed in order to analyze the controller response. As it can be observed the pH is accurately controlled being able to reject any perturbation given by the biomass variation. The tuning parameter $\varphi_{\mathrm{H^+}}$ was set to $3 \cdot 10$ h^{-1}. The maximum input CO_2 flow is 3 $mL \cdot min^{-1}$, being no risk of saturation of the control even at lower pHs. Fig.I.4.7 displays the response of all states and internal variables to the D and input CO_2 steps.

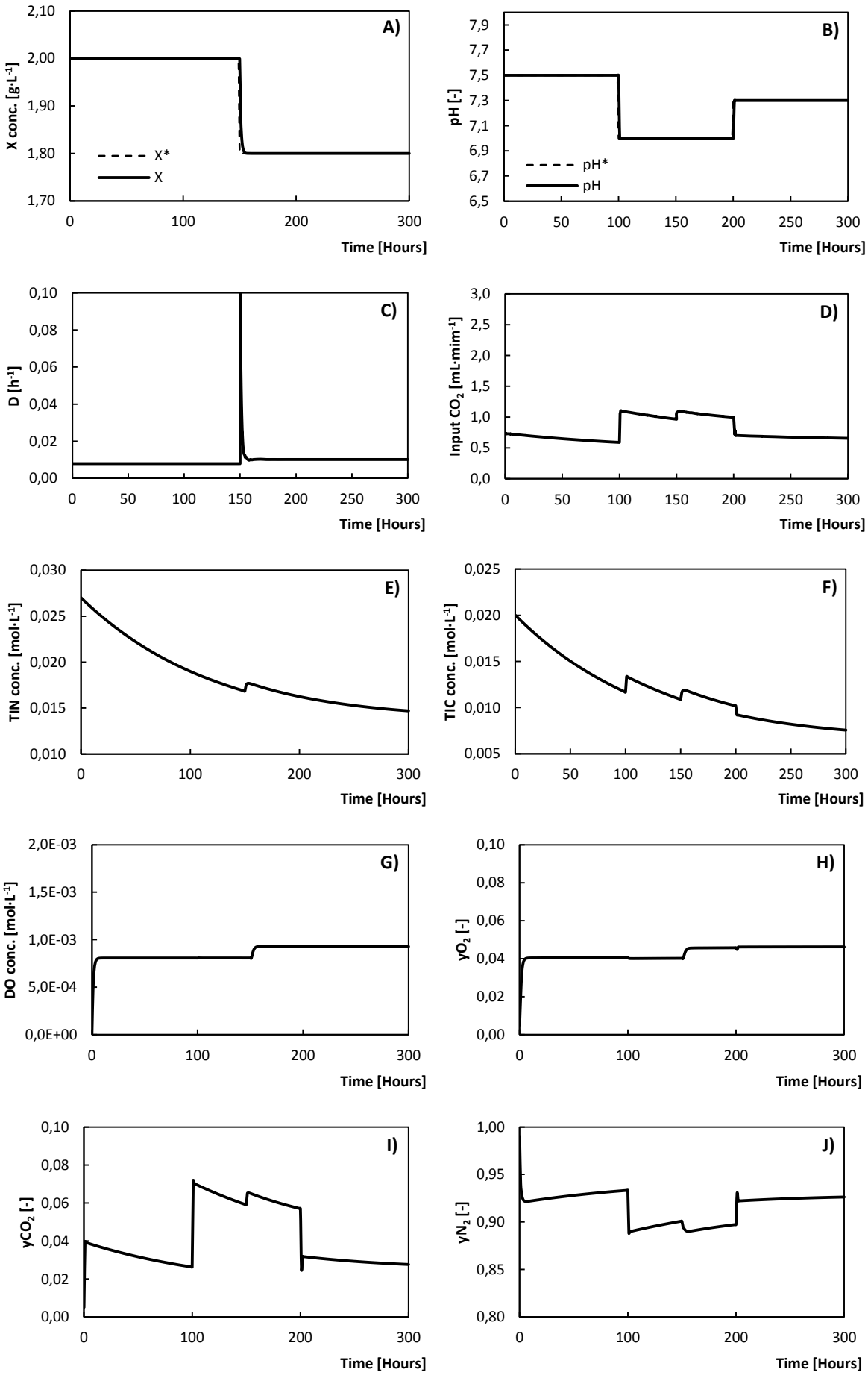
A)
X conc. [g·L-1]
2,10
2,00
1,90
1,80
1,70
X*
X
0
100
200
300
Time [Hours]
B)
pH [-]
7,9
7,7
7,5
7,3
7,1
6,9
6,7
6,5
pH*
pH
0
50
100
150
200
250
300
Time [Hours]
C)
D [h-1]
0,10
0,08
0,06
0,04
0,02
0,00
0
50
100
150
200
250
300
Time [Hours]
D)
Input CO2 [mL·mim-1]
3,0
2,5
2,0
1,5
1,0
0,5
0,0
0
50
100
150
200
250
300
Time [Hours]
E)
TIN conc. [mol·L-1]
0,030
0,025
0,020
0,015
0,010
0
100
200
300
Time [Hours]
F)
TIC conc. [mol·L-1]
0,025
0,020
0,015
0,010
0,005
0
50
100
150
200
250
300
Time [Hours]
G)
DO conc. [mol·L-1]
2,0E-03
1,5E-03
1,0E-03
5,0E-04
0,0E+00
0
100
200
300
Time [Hours]
H)
yO2 [-]
0,10
0,08
0,06
0,04
0,02
0,00
0
100
200
300
Time [Hours]
I)
yCO2 [-]
0,10
0,08
0,06
0,04
0,02
0,00
0
100
200
300
Time [Hours]
J)
yN2 [-]
1,00
0,95
0,90
0,85
0,80
0
100
200
300
Time [Hours]

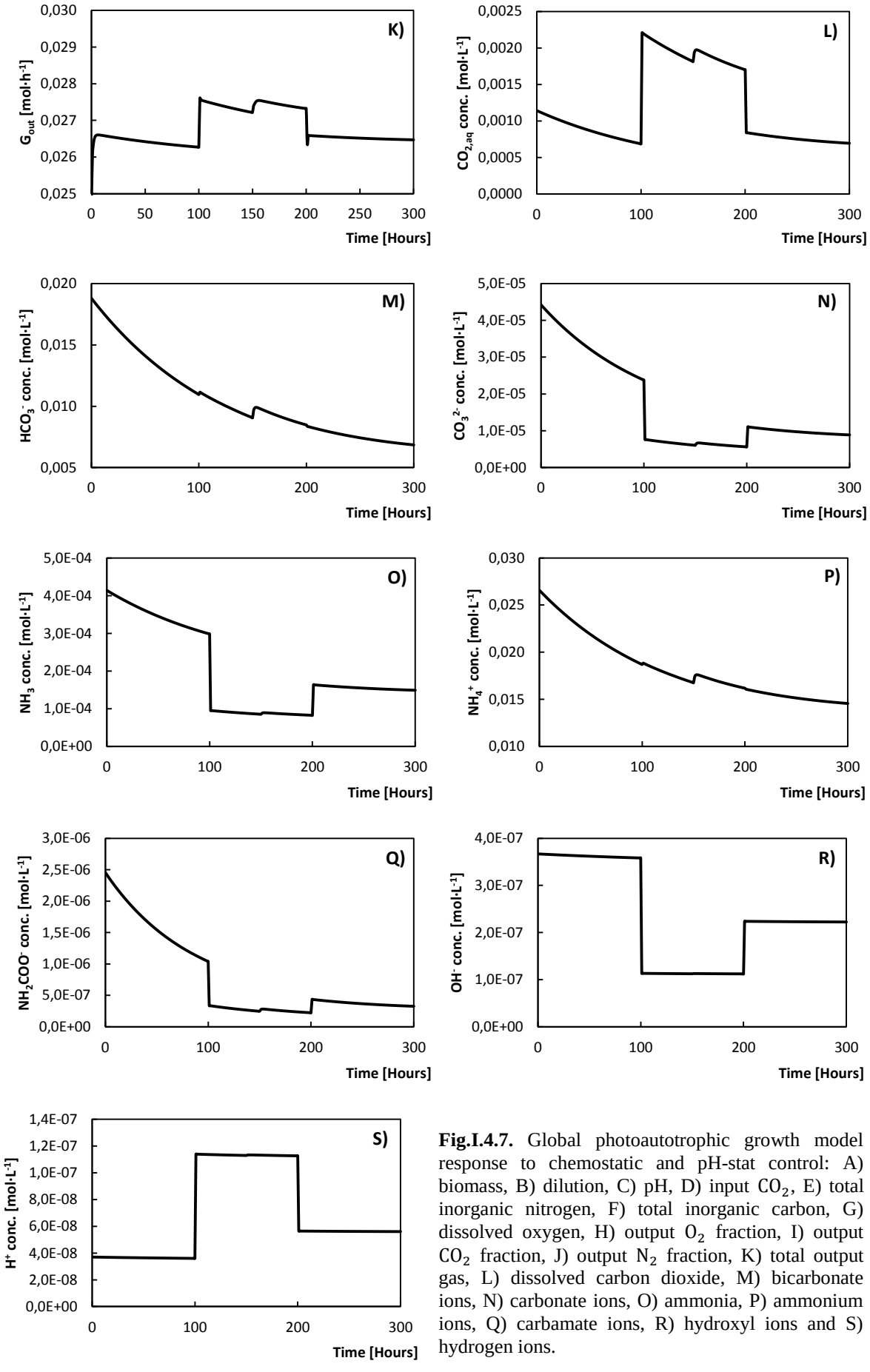

Fig.I.4.7. Global photoautotrophic growth model response to chemostatic and pH-stat control: A) biomass, B) dilution, C) pH, D) input CO_2, E) total inorganic nitrogen, F) total inorganic carbon, G) dissolved oxygen, H) output O_2 fraction, I) output CO_2 fraction, J) output N_2 fraction, K) total output gas, L) dissolved carbon dioxide, M) bicarbonate ions, N) carbonate ions, O) ammonia, P) ammonium ions, Q) carbamate ions, R) hydroxyl ions and S) hydrogen ions.

I.4.3. Lumostatic Control

The lumostatic operation of photobioreactors assumes the manipulation of the incident light flux (q_0) to control output variables such as specific light uptake, average irradiance inside the culture or lighted volume fraction. Such objectives can be achieved only in closed loop systems because at constant q_0 the light availability inside the culture will decrease with the growth of biomass concentration. As long as the input variable is q_0, this type of control is proper only for artificially illuminated photobioreactors. In addition, the lumostatic control aims the rationalization of energy consumption with light during the long transitory phase of batch cultures. The lumostatic control can be also applied to continuous cultures, but working at constant biomass concentration makes it is easier to impose a convenient constant incident light, therefore this type of control will be discussed mainly for batch cultures.

I.4.3.1. Specific Light Uptake Rate Control

The specific light uptake rate (q_e) was first defined by Van Liere and Mur, (1979) as the total amount of energy absorbed by the culture divided by the total biomass present in the culture. The concept was applied by other authors (Sánchez and Mas, 1996; Choi *et al.*, 2003; Lee *et al.*, 2006) in practical researches. The q_e expression was presented in section I.1.5.8 (Eq.I.1.54), but for reasons of mathematical simplicity in expressing a handleable I/O model base on measurable variables its dynamic expression can be reduced to:

$$\frac{dq_e}{dt} = \frac{q_0(t)}{X(t)} - q_e(t) \tag{I.4.76}$$

Thus, q_e will be the ratio between the incident light flux and the biomass concentration, and the control variable q_0 will have the same dynamics as the biomass whereas its range will be given by its prescribed value. The simplification is based on the assumption that the amount of photonic energy absorbed by the culture is proportional with the concentration of biomass and thus represented by a constant parameter multiplied with $\langle r_x \rangle$. Nevertheless, for the case of a photobioreactor lighted on one side, the measurement of the output light energy (I_{out}) in the back side of the reactor can be done only at low biomass concentrations when the entire volume of the culture gets to be lighted. At higher biomass concentrations the culture will be partially lighted and the limit between the lighted and the dark volumes (Fig.I.1.15),

represented through the compensation point (I_c), being situated inside the reactor (*i.e.* $0 < I_c < L$). In addition, for the case of two side lighted photobioreactors the I_{out} measurement is impracticable, narrowing its determination exclusively through radiative models. The neglect of all constant parameters (including the optical surface – A and the reactor's working volume – V_l) is done only for control purposes. However, the simplification will have effect only over the setpoint value in the sense that a different setpoint will be obtained for the same dynamics. In Eq.I.4.76 q_0 can be replaced with the average irradiance inside the culture $\langle I(z) \rangle$. However, Suh and Lee, (2001) used $\langle I(z) \rangle$ as output variable manipulated through q_0 by employing a model-based control technique.

It must be mentioned here that the automatic control of pH to an optimum value for microalgae growth must be done also during the lumostatic control. Because the RGA analysis presented in section I.4.2.5 can be applied to steady-state operation points and a batch culture will not achieve a convenient one, the multivariable control of q_e and pH through q_0 and $G_{in}^{\mathrm{CO_2}}$, respectively, must be accomplished through decentralized SISO controllers. Given that the nonlinear pH controller was designed for the continuous operation of a photobioreactor at constant light intensity, this configuration allows its validation at variable light intensity on a wide range of biomass concentrations. In batch mode D = 0 and thus the nonlinear control algorithm for pH is reduced to:

$$G_{in}^{\mathrm{CO_2}} = V_l \left(\frac{1}{M_x} - \frac{Y_{N/X}}{M_x(\varepsilon 10^{\mathrm{pH}}+1)} \right) \langle r_x \rangle + G_{out}^{\mathrm{CO_2}} + V_l \varphi_{\mathrm{H^+}} er_{\mathrm{H^+}} \tag{I.4.77}$$

The global photoautotrophic growth model is not needed for the decentralized control of q_e because its simple expression consists in two measurable variables (*i.e.* q_0 and X). Rewritten in space-state form, Eq.I.4.86 will give:

$$\begin{cases} \dot{x} = [\dot{q}_e] = [-q_e] + [1/X] q_0 \\ y = q_e \end{cases} \tag{I.4.78}$$

As it can be seen in Fig.I.4.8 the objective is to control the specific light uptake rate in closed loop by actuating the incident light flux intensity. Considering that the experimental bench presented in section I.2.2 is provided with a turbidity probe which can be associated with the biomass concentration and with a LED panel which can be set to a precise light intensity by

imposing a known voltage on its power source, the q_e can be calculated online making the automatic control issue easily approachable.

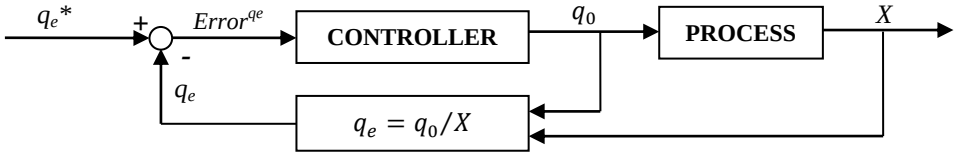

Fig.I.4.8. q_e control scheme

In what regards the control algorithm synthesis, the feedback linearizing control method presented in section I.4.2.6 can be applied. In consequence, the control expression will be:

$$q_0 = X\left(\varphi_{q_e} er_{q_e} - q_e\right) \tag{I.4.79}$$

with

$$er_{q_e} = q_e^* - q_e \tag{I.4.80}$$

where er_{q_e} is the error between the calculated value of q_e and its prescribed value q_e^*, and φ_{q_e} is a tuning parameter which is related with the pole of the system that impose the error dynamics.

The LED panel presented in section I.2.2.2 is upper bounded to 800 μmol·m^{-2}·s^{-1}, light intensity at which the maximal concentration of biomass reaches ~2.8 g·L^{-1} (Fig.I.4.9). In these culturing conditions the TIC concentration from the MGM will be almost depleted after 120 hours (Fig.I.4.10).

As it can be observed in Fig.I.4.11, the batch culture piloted at constant light intensity of 800 μmol·m^{-2}·s^{-1} reaches a q_e of ~350 after 60 hours of cultivation. Nevertheless, if q_e would be maintained constant throughout the entire cultivation period, significant light energy could be saved, because at low biomass concentrations the light energy exceeds the cell absorption capacity and the excess is converted to heat. The lumostatic control leads to lower biomass concentration (< with 0.45 g·L^{-1}), but is only a matter of optimization.

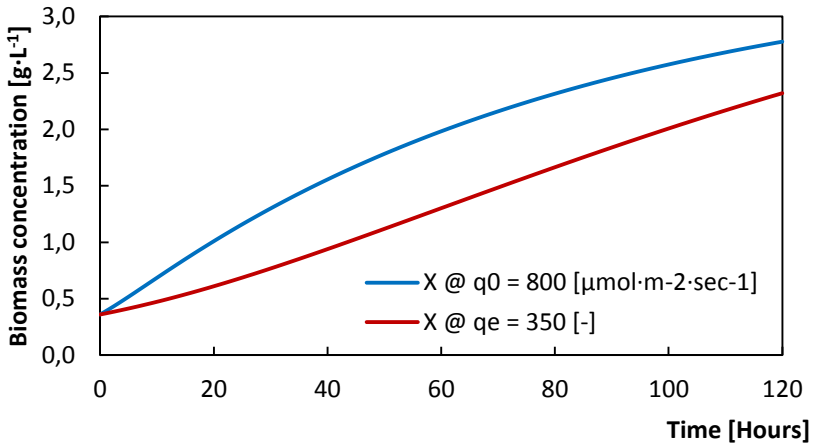

Fig.I.4.9. Biomass kinetics in a batch piloted at constant incident light intensity vs. a batch operated in lumostatic mode (numerical simulation)

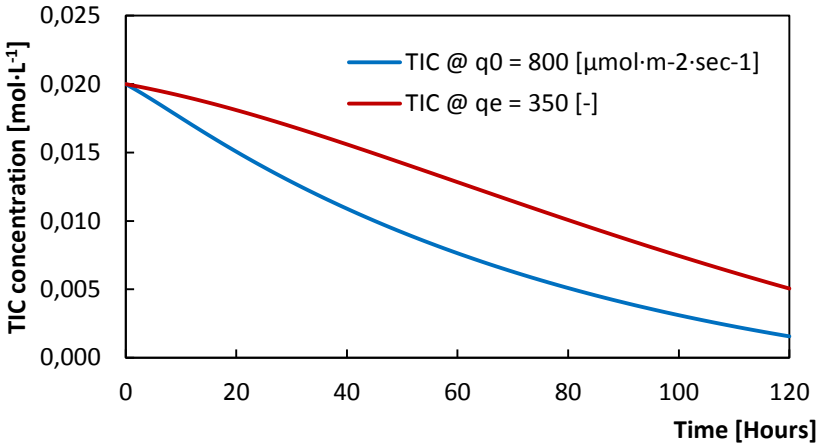

Fig.I.4.10. TIC dynamics in a batch piloted at constant incident light intensity vs. a batch operated in lumostatic mode (numerical simulation)

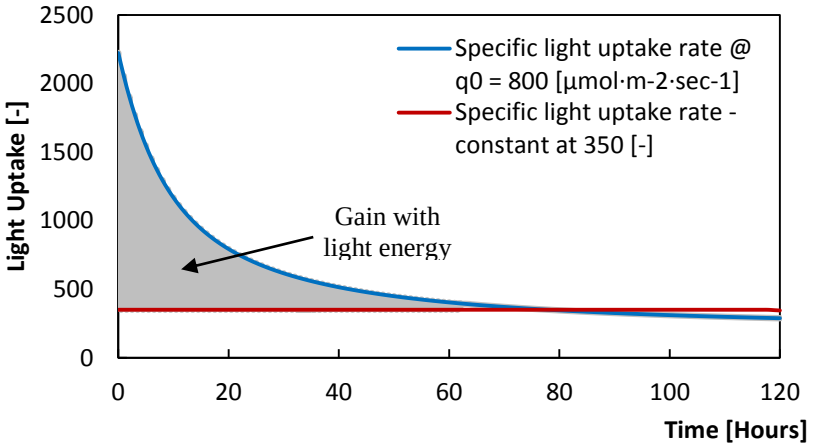

Fig.I.4.11. Specific light uptake rate evolution in a batch piloted at constant incident light intensity vs. lumostatic control (numerical simulation)

Finding the optimal q_e^* depends on various factors such as photobioreactor geometry, light transfer inside the reactor, capacity of light source, the objective of the cultivation, etc.

In Fig.I.4.12 the input variable q_0 is plotted for a wide range of q_e^*. If the prescribed value is too elevated the control variable will be quickly saturated and the controller will work with an increasing error. Contrarily, if the set-point is too small, lower biomass concentrations will be obtained and longer culturing periods.

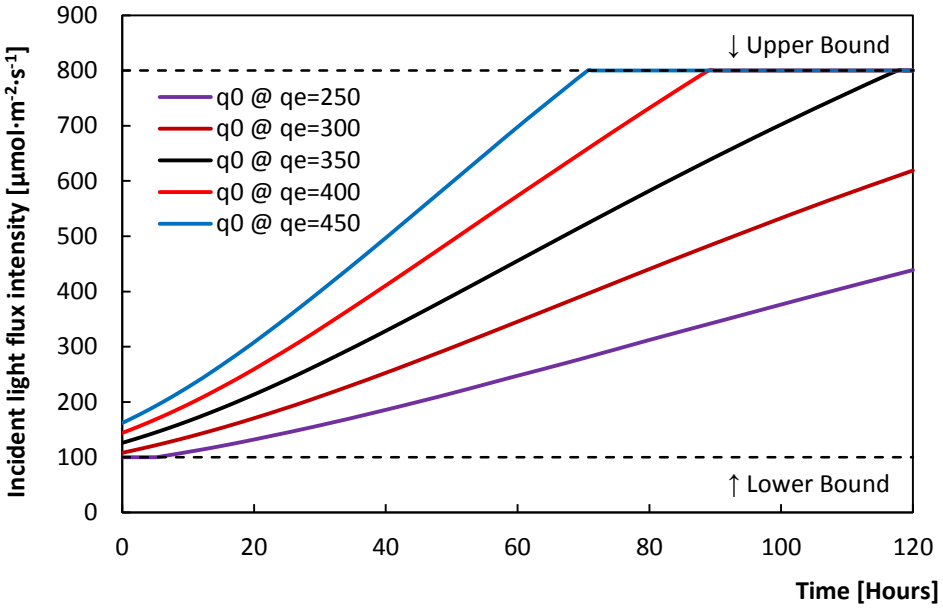

Fig. I.4.12. Control variable (q_0) evolution for a wide range of specific light uptake rate setpoints (q_e^*)

The lower bound of 100 µmol·m^{-2}·s^{-1} corresponds to the minimum light intensity used for startup (lag phase). For the given configuration the best balance between saving energy and good biomass productivity lies around a q_e^* of 350. However, there is no general rule of choosing a proper q_e^* because it is characteristic to each system and depends on many technological aspects, but it can be taken into consideration in optimal control techniques.

For the same q_e range there are rendered the expected concentrations of biomass (Fig.I.4.13) and TIC (Fig.I.4.14). The TIC concentration must not reach too low values because after the inoculation of the reactor the microalgae need approximately one day for adaptation, period in which they consume carbon even though no mass increase is registered. During the accommodation phase the incident light is maintained at low intensities (*e.g.* 100 µmol·m^{-2}·s^{-1} – for *Chlamydomonas reinhardtii*) in order to avoid photoinhibition, but the accommodation period is not usually modeled.

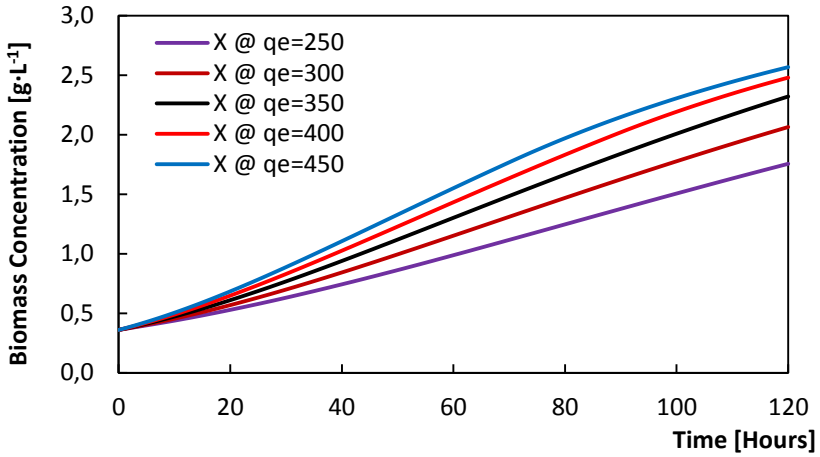

Fig.I.4.13. The expected biomass concentration for a wide range of specific light uptake rates

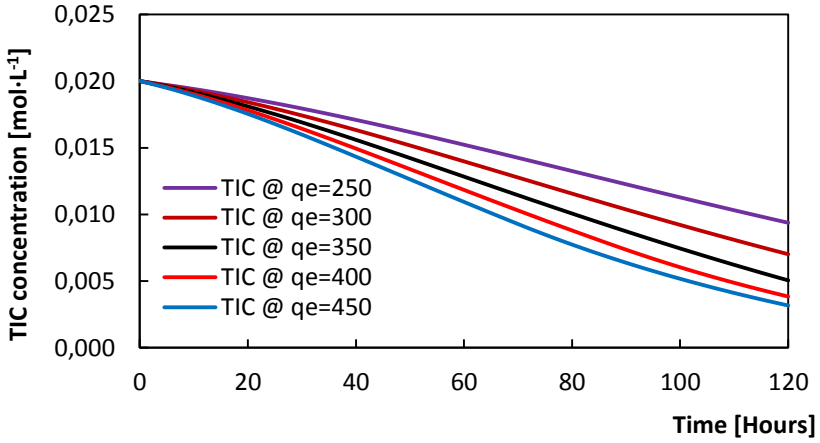

Fig.I.4.14. The expected TIC concentration for a wide range of specific light uptake rates

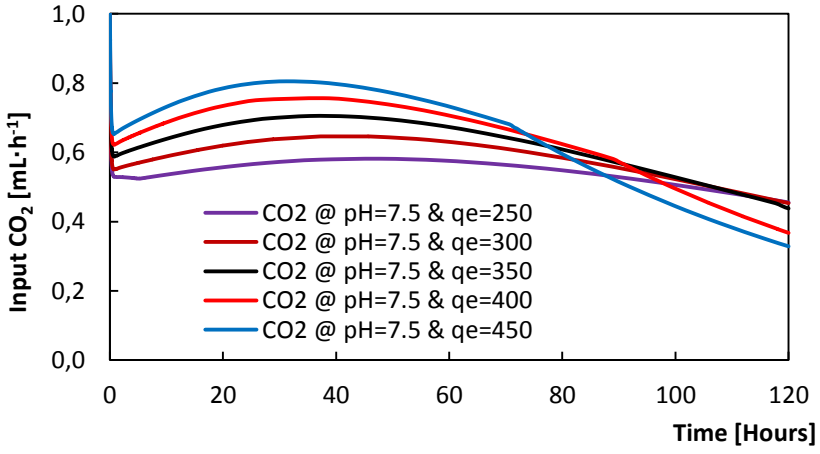

Fig.I.4.15. Expected CO_2 consumption for pH regulation at 7.5 for a wide range of specific light uptake rates

The expected CO_2 consumption for pH control at 7.5, on the same q_e range (*i.e.* 250 to 450), is plotted in Fig.I.4.15. As it can be observed the input CO_2 does not vary much considering that the proportional valve capacity is 0 – 3 mL·H^{-1}.

I.4.3.2. Lighted Volume Fraction Control

As it was depicted earlier in Fig.I.1.15 the working volume of the reactor (V_l) can be divided in lighted volume and dark volume, based on the light distribution inside the culture. The boundary between the two volumes is the compensation point (I_c) where $\mu_p = \mu_s$. In a rectangular photobioreactor lighted from one side, the lighted volume fraction (Γ) can be expressed as the ratio between the culture depth which corresponds to the compensation point (z_{I_c}) and the total length of the photobioreactor (L):

$$\Gamma = \frac{z_{I_c}}{L} \tag{I.4.81}$$

z_{I_c} can be determined with the simplified irradiance formula presented by Cornet and Dussap, (2009):

$$\frac{I_c}{q_0} = exp\left[-\frac{1+\alpha}{2\alpha} E_a X z_{I_c}\right] \tag{I.4.82}$$

Which lead to:

$$\frac{d\Gamma}{dt} = \frac{ln\left(\frac{I_c}{q_0(t)}\right)}{-\frac{1+\alpha}{2\alpha} E_a X(t) L} - \Gamma(t) \tag{I.4.83}$$

This type of lumostatic control must be also associated with a pH controller as mentioned in the previous section. The multivariable control is realized as well through decentralized nonlinear SISO controllers and all comments made for the specific light uptake rate control are applicable here. Practically, Γ is not directly measurable, but based on a proper knowledge regarding the light transfer inside the photobioreactor, it can be easily calculated from online X and q_0 values.

The control objective, as presented in Fig.I.4.16, is to maintain Γ at a prescribed value by actuating the incident light flux intensity based on a feedback mechanism. Both values (*i.e. X* and q_0) needed to compute Γ, are measurable.

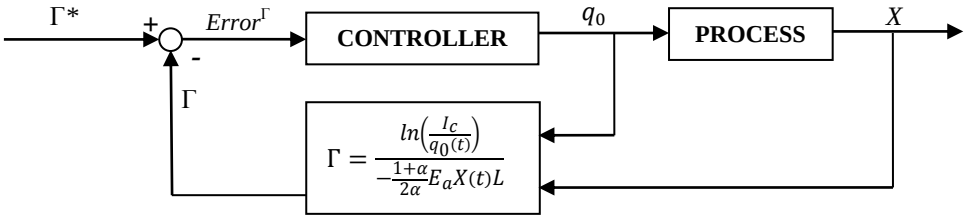

Fig.I.4.16. Γ control design scheme

The synthesis of the control algorithm follows the same steps of feedback linearizing method presented in section I.4.2.6, the expression of the control variable taking the following form:

$$q_0 = \frac{I_c}{exp\left((\varphi_\Gamma er_\Gamma + \Gamma)\left(-\frac{1+\alpha}{2\alpha}E_a X L\right)\right)} \tag{I.4.84}$$

with

$$er_\Gamma = \Gamma^* - \Gamma \tag{I.4.85}$$

where er_Γ is the error between the calculated value of Γ and its setpoint Γ^*, and φ_Γ is a tuning parameter related with the pole of the system which imposes the error dynamics.

It is obvious that the best growth rates are to be obtained at $\Gamma^* = 1$, that is when the entire volume of the reactor is lighted. Unfortunately, this objective requires huge light intensities which are not available in many cases. Taking the example presented in Fig.I.4.9 where the biomass develops in batch mode at constant light intensity of 800 μmol·m^{-2}·s^{-1} (which represents the input variable saturation) it can be observed (Fig.I.4.17) that Γ registers a sharp decreasing tendency soon after inoculation. Thus, a controller set to $\Gamma^* = 1$ will take less than 10 hours to reach the saturation of the input variable, working thereafter with an increasing error.

Consequently, the Γ controller can be set to one, only at low biomass concentrations which require continuous operation of the photobioreactor. Thus, the lumostat (Fig.I.4.16) must be

associated with the chemostat and pH-stat (Fig.I.4.1) resulting a system with three inputs $u(t) = \left[D\ G_{in}^{CO_2}\ q_0\right]$ and three outputs $y = [X\ \text{pH}\ \Gamma]$.

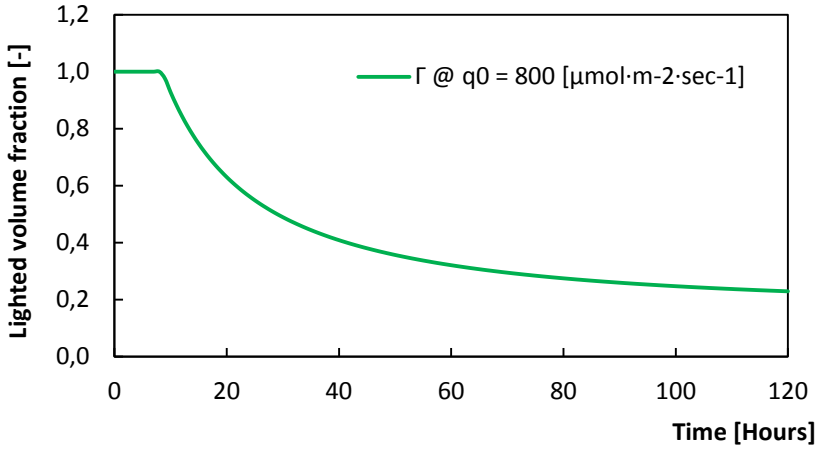

Fig.I.4.17. Γ evolution in a batch culture at constant light intensity of 800 µmol·m^{-2}·s^{-1}

Recalling that q_0 is bounded to 800 µmol·m^{-2}·s^{-1}, the highest biomass concentration at which Γ can be maintained to one is 0.64 g·L^{-1}. Few steps were applied for X (Fig.I.4.18) and Γ (Fig.I.4.19) in order to evaluate the response of the control algorithms.

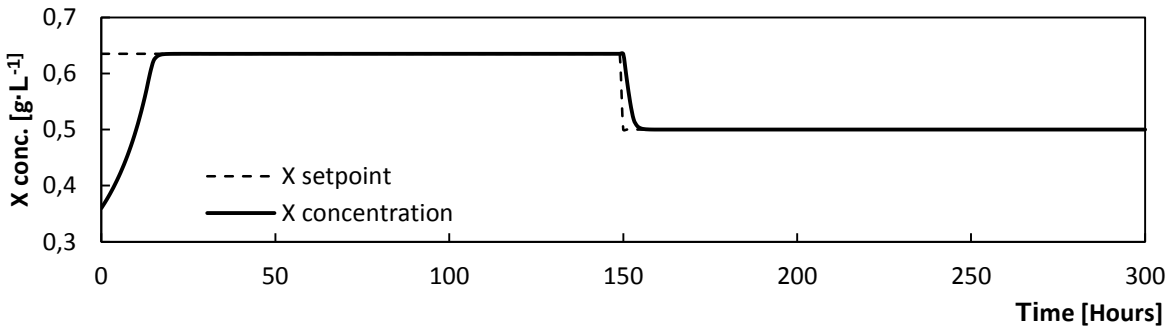

Fig.I.4.18. Biomass concentration in multivariable $X - \Gamma - \text{pH}$ control

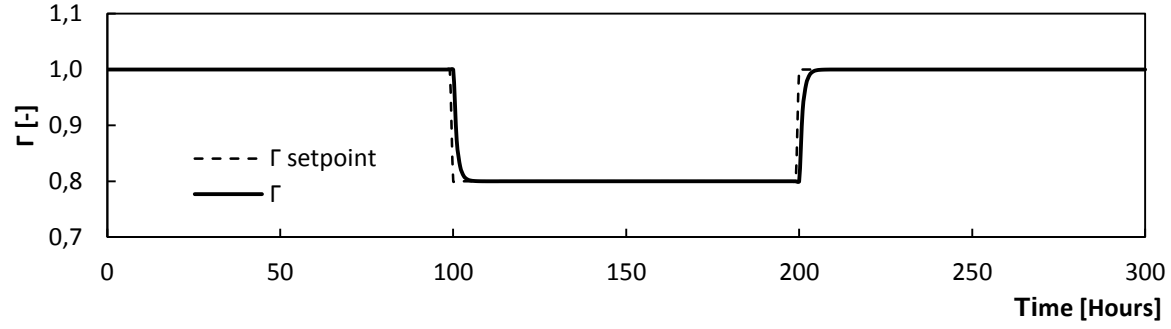

Fig.I.4.19. Lighted volume fraction steps in multivariable $X - \Gamma - \text{pH}$ control

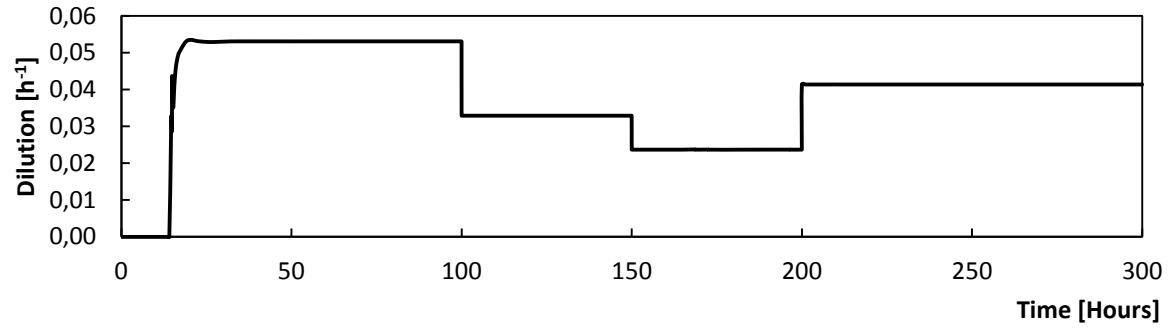

Fig.I.4.20. Dilution – the control variable of biomass

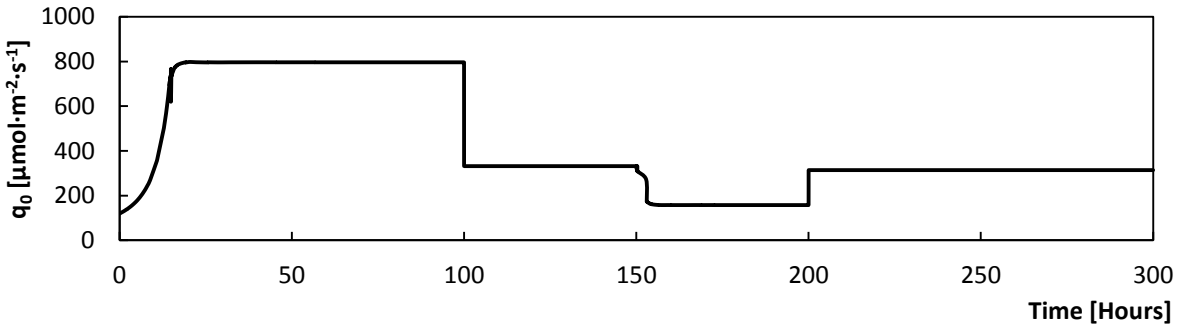

Fig.I.4.21. Incident light intensity – the control variable of lighted volume fraction

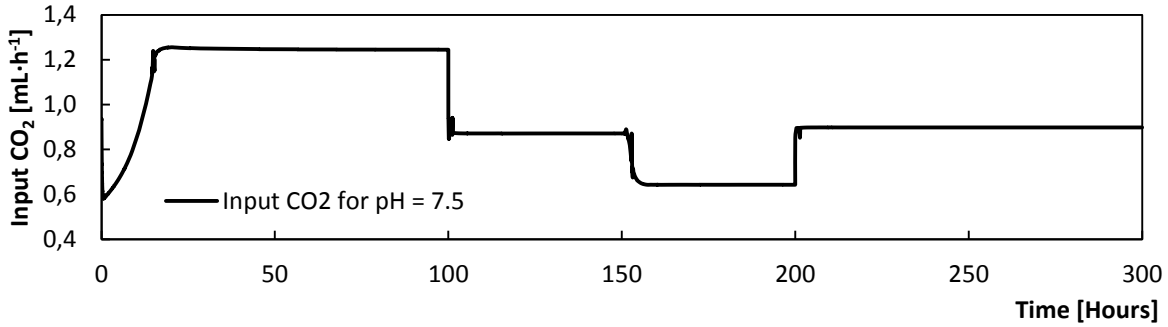

Fig.I.4.22. Input CO_2 – the control variable of pH (maintained constant at 7.5)

The pH is controlled to 7.5 as usually, and the evolution of the input CO_2 is plotted in Fig.I.4.22. It can be observed that all inputs (D, $G_{in}^{CO_2}$ and q_0) present the same dynamics due to the fact that they are related to the specific growth rate, thus highlighting the importance of a proper photosynthetic growth model.

Nevertheless, there are specific cases in which Γ needs to be maintained at setpoints lower than one, for example the hydrogen production protocol proposed by Degrenne *et al.*, (2011). The method consists in maintaining a batch culture in constant light conditions up to a high biomass concentration (*e.g.* ~2 g·L^{-1}) followed by the decrease of light intensity to achieve a

$\Gamma < 0.25$. The abrupt decrease of light leads to the establishment of an anoxic regime as a result of biomass decrease. The anoxic conditions activate the hydrogenase which is responsible for the production of molecular hydrogen. Fig.I.4.23 depicts the biomass concentration during the first 60 hours of batch in constant light intensity (*i.e.* 800 $\mu mol \cdot m^{-2} \cdot s^{-1}$) along with its slight decrease during the last 60 hours of lumostatic control to $\Gamma^* = 0.23$. The oxygen production stops immediately after the decrease of light intensity leading to anoxia which promotes the production of molecular hydrogen.

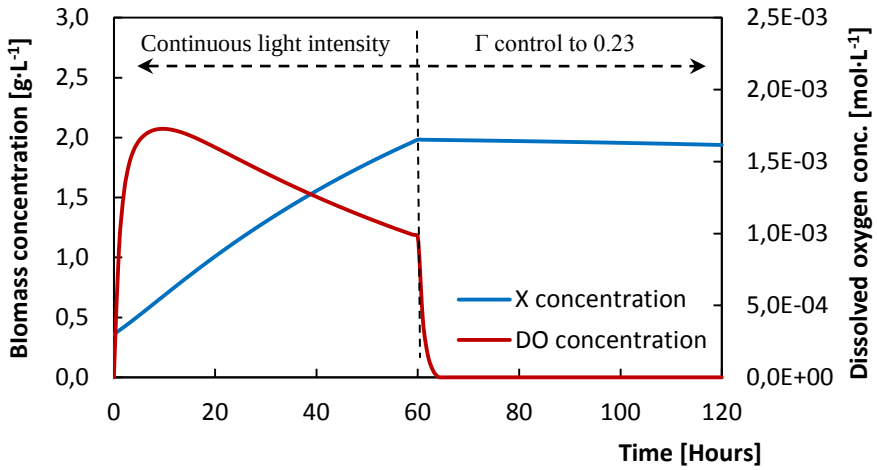

Fig.I.4.23. Biomass and dissolved oxygen evolution during batch culturing in constant light intensity and lumostatic control

The protocol can be applied also to lower incident light intensities the difference lying in the period of achieving high biomass concentrations.

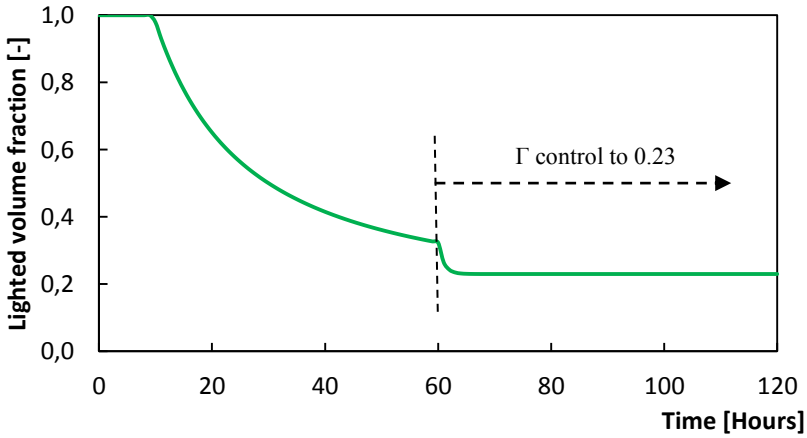

Fig.I.4.24. Γ – output variable evolution during batch culturing in constant light intensity and lumostatic control

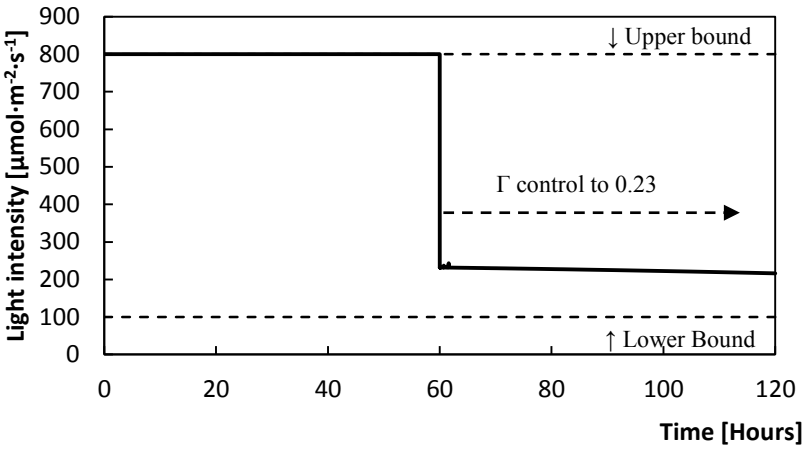

Fig.I.4.25. q_0 – input variable evolution during batch culturing in constant light intensity and lumostatic control

Fig.I.4.24 shows the evolution of lighted volume fraction during both batch at constant incident light intensity and lumostatic control, whereas fig.I.4.25 displays the evolution of the input variable q_0.

I.5. PRACTICAL IMPLEMENTATION

I.5.1. Validation of Chemostatic and pH-static Controllers

To validate the synthesized control algorithms (I.4.73), cells of *Chlamydomonas reinhardtii* were cultivated in photobioreactor and maintained in photoautotrophic growth conditions at constant light of 300 $\mu mol \cdot m^{-2} \cdot s^{-1}$. The first 160 hours of cultivation were assigned for batch regime cultivation ($D = 0$) that was necessary to achieve a high biomass concentration of 2.0 $g \cdot L^{-1}$ (Fig.I.5.1). The biomass concentration was practically estimated from online turbidity measurements through linear regression. The correlation was realized offline by comparing the turbidity probe signal with offline dry matter values analyzed daily. The dry matter was found to be well fitted on the response of the global photoautotrophic growth model which, in its turn, is excellently fitted with online measurements, as it can be clearly observed in Fig.I.5.1. Thus, having a reliable online biomass signal, the experimental bench was piloted in continuous mode for the next 72 hours: 32 hours to keep the biomass concentration at $y_1^* = 2.0\ g \cdot L^{-1}$ whereas the last 32 hours to maintain it at $y_1^* = 1.8\ g \cdot L^{-1}$. Even though the correlation between turbidity and dry matter was realized during the batch regime, three other dry matter values were determined pending the continuous regime reconfirming its validity (Fig.I.5.1). The turbidity signal is very noisy imposing the implementation of a moving average filter with a period of 600 samples/10 minutes that led to a control precision of ± 0.02 σ.

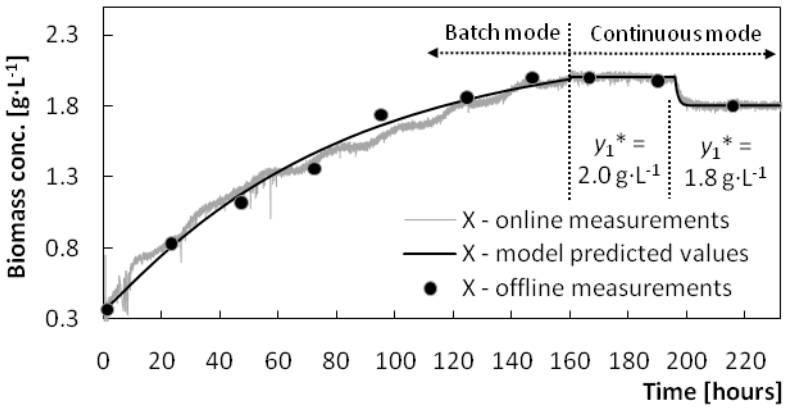

Fig.I.5.1. Time evolution of biomass concentration in batch and continuous operation: online values vs. simulation results

The pH was restrained at y_2^* = 7.5 during both discontinuous and continuous regimes with excellent results as it can be seen in Fig.I.5.2. The noise in the first day of experimentation is not caused by ill-conditioning of the controller but by the exhaustion of the CO_2 bottle over the night that led to erroneous value. The pH was regulated with a precision of ± 0.005 σ (excluding the noise in the first day) which is found at the accuracy limit of the pH electrode. Such control precision qualifies as more accurate in comparison with the values reported so far in the literature for this type of application (Berenguel *et al.*, 2004; Buehner *et al.*, 2009). A moving average filter with a period of 60 samples/1 minute was also implemented for the pH signal.

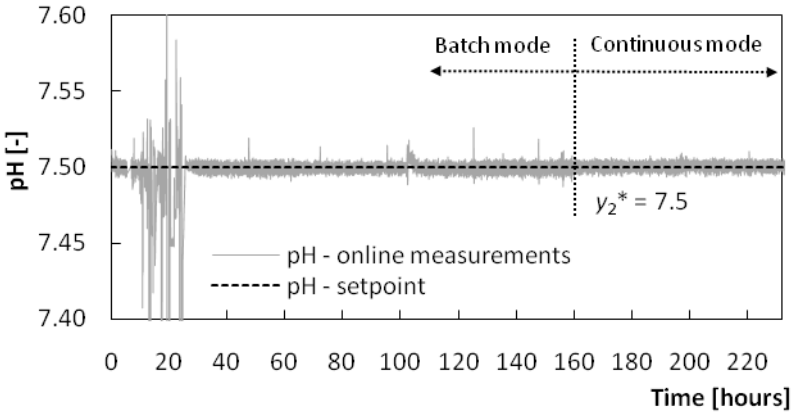

Fig.I.5.2. Time evolution of pH in batch and continuous operation

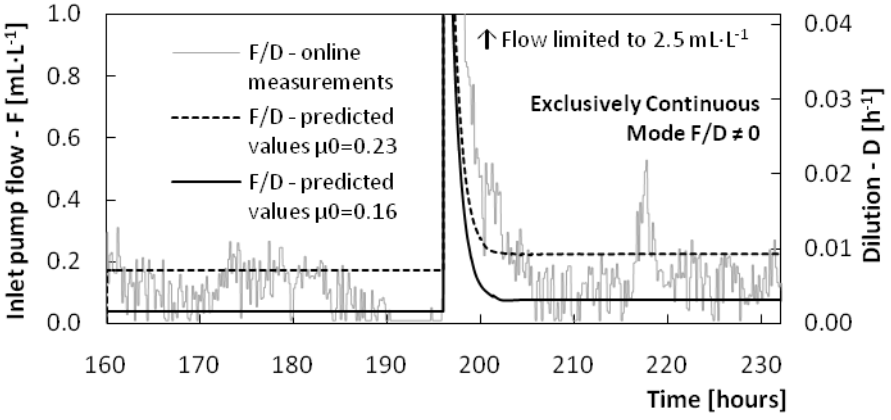

Fig.I.5.3. *D* in continuous regime used to control *X* concentration: online values vs. simulation results

Fig.I.5.3. presents the control variable for biomass manipulation exclusively for the continuous regime (in batch mode $D/F = 0$). The chart presents data expressed both as

dilution rate D (secondary axis) which is used by the model and as flow rate $F = DV$ which is the real parameter used by the feeding pump (primary axis). The control variable D was recalculated with the same periodicity of 600 samples/10 minutes due to the slow dynamics of X growth. The tuning parameter φ_X was determined empirically aiming the stabilization of the system. In practice φ_X was found to be higher (24 h^{-1}) in comparison with the numerical simulation where it can be equal to unity in order to predict the same profile.

Fig.I.5.4 presents the control variable for pH manipulation for both discontinuous and continuous regimes. The plot expresses data both as $G_{in}^{CO_2}$, which is directly measured by the flow meter, and as aperture of the proportional valve, which is the real control action. The control variable $G_{in}^{CO_2}$ was recalculated with a periodicity of 60 samples/1 minute due to the fact that the proportional valve requires several seconds to stabilize its aperture. In practice, the tuning parameter φ_{H+} was found to be $3 \cdot 10^6$ h^{-1} which is also suitable for numerical simulation. During the last 40 hours of batch regime the amplitude of $G_{in}^{CO_2}$ increases, pointing to a lower φ_{H+} or better to its schedule according to the operating points.

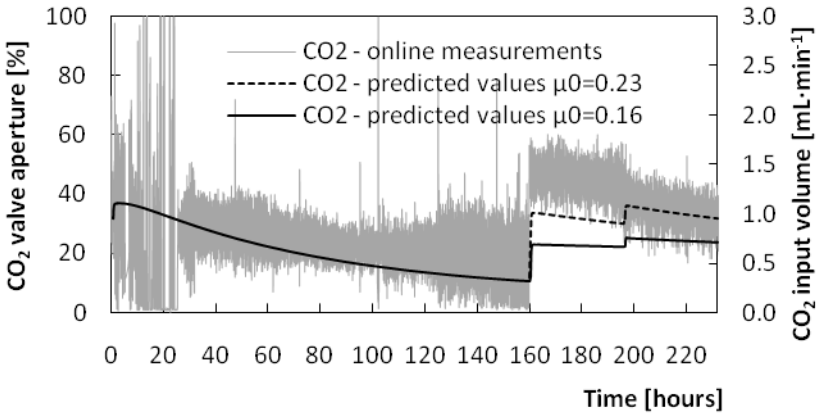

Fig.I.5.4. The injected CO_2 gas for pH control in batch and continuous operation: online values vs. simulation results

$G_{in}^{CO_2}$ consumption required to maintain the pH at 7.5 is well predicted by the global photoautotrophic growth model only in batch mode, whereas in continuous regime the model predicts lower values. Recalling that pH is a complex non-linear function of X, TIN and TIC, the lower predicted values might have been a result of the biomass dynamics because the CO_2 source remained unchanged and no component of the substrate was exhausted from the medium (*e.g.* TIN). μ_0 (from Eq.I.3.8), the term related to $\mu_{max} - \mu_0 = \mu_{max}\left(1 + 2\sqrt{K_I/K_{II}}\right)$

– (Dochain, 2008), which was identified to be 0.16 h^{-1} in batch mode may have a higher value in continuous regime. Fig.I.5.4 shows that the model response at higher μ_0 (square dot line) is closer to the measured values. The value used for numerical simulation (*i.e.* μ_0 = 0.2274 h^{-1}) is provided in a previous work of Fouchard *et al.*, (2009) who identified it on continuous cultures.

Certain variables such as $I(z)$, c_{TIN}, c_{TIC}, $y_{out}^{\mathrm{CO_2}}$ and G_{out} which are required for computing the control algorithms u_1 and u_2 (Eq.I.4.73) are predicted by the global photoautotrophic growth model in real time. $I(z)$, for instance is not measured neither offline nor online, but it can be calculated for any depth z of photobioreactor with the relation (I.3.6) based on known light intensities and biomass values acquired online. c_{TIN} is practically the sum of $c_{\mathrm{NH_4^+}}$, $c_{\mathrm{NH_3}}$ and $c_{\mathrm{NH_2COO^-}}$ and cannot be measured online as such, however there are specific chemical methods which consist in converting all species into $\mathrm{NH_4^+}$ that is thereafter quantified. Nevertheless, direct $\mathrm{NH_4^+}$ analyses are faster and cheaper and are good approximations of TIN, being its dominant species (*i.e.* $\mathrm{NH_4^+}$: ~98% of TIN). Fig.I.5.5 presents the comparison between $\mathrm{NH_4^+}$ offline measurements, available only for the batch regime, and the model response; the error bars being set to ± 0.002 mol·L^{-1}.

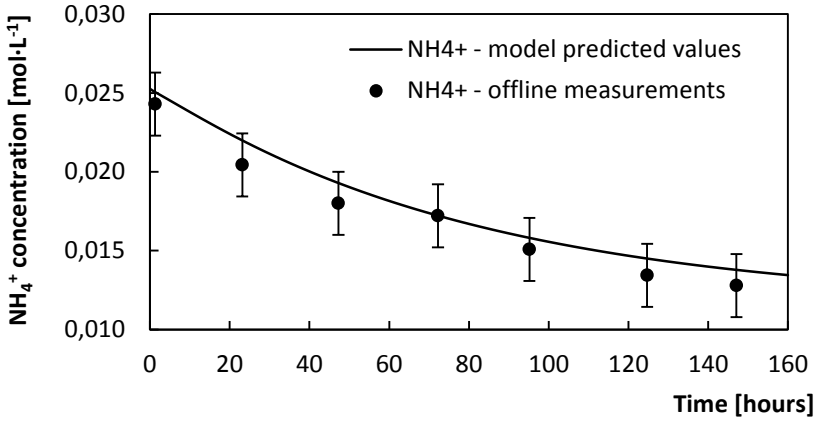

Fig.I.5.5. $\mathrm{NH_4^+}$ concentration in batch regime: offline values vs. simulation results

c_{TIC} was measured offline during the batch regime due to the lack of specific sensors and presented satisfactory fitting with the global model response. Fig.I.5.6 depicts the TIC offline measurements and the numerical simulation results; the error bars are set to ± 0.002 mol·L^{-1}.

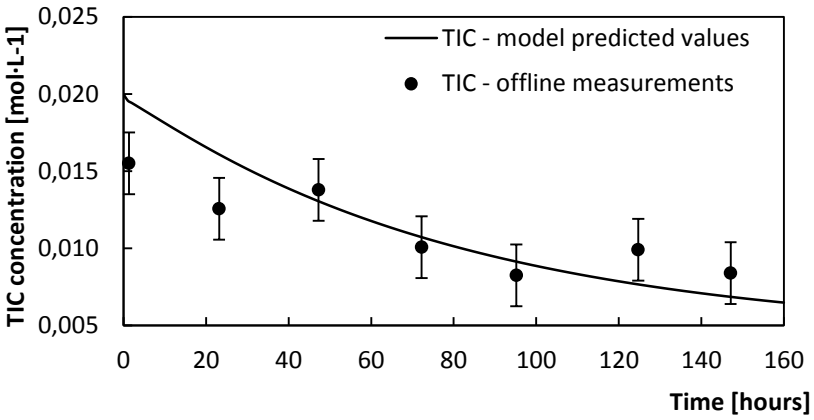

Fig.I.5.6. TIC concentration in batch regime: offline values vs. simulation results

$y_{out}^{CO_2}$ and $y_{out}^{N_2}$ were measured online by means of a mass spectrometer being observational variables not integrated in the control routine. They are available exclusively for batch regime because in continuous mode the evacuation pump, which has the role of maintaining a constant level in the photobioreactor, creates vacuum, stopping the gas to reach the mass spectrometer. $y_{out}^{CO_2}$ is a feed-forward component in u_2 and, as it can be seen in Fig.I.5.7, it is well predicted by the global photoautotrophic growth model.

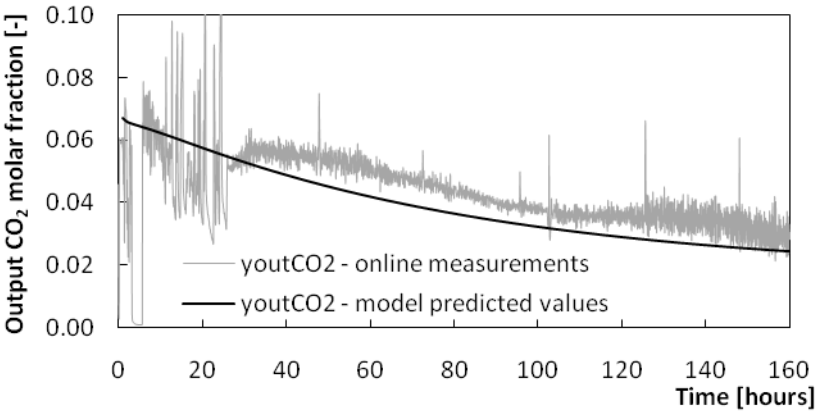

Fig.I.5.7. $y_{out}^{CO_2}$ in batch regime: online values vs. simulation results

Even though the experimental bench is provided with a flow meter for measurement of output mixture of gases G_{out} the acquired values were unsatisfactory as a result of a possible inappropriate fitting. However, it can be easily calculated through its specific relation (I.3.33) based on known values of $y_{in}^{N_2}$ and G_{in}, which are certainly measurable, and $y_{out}^{N_2}$ values.

Fig.I.5.8 displays online measurements for $y_{out}^{N_2}$ (exclusively for batch regime) which were predicted by the global photoautotrophic growth model with acceptable accuracy.

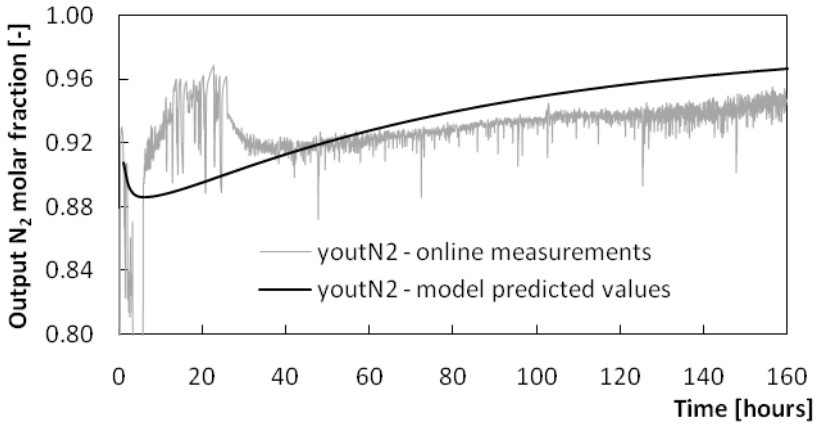

Fig.I.5.8. $y_{out}^{N_2}$ in batch regime: online values vs. simulation results

In perspective, the online measurements of $y_{out}^{CO_2}$ and $y_{out}^{N_2}$ can be integrated as input variables in the control routine.

Nevertheless, integrating the model with real measurable inputs such as X, pH, D, $G_{in}^{CO_2}$, $G_{in}^{O_2}$, $G_{in}^{N_2}$ and T will increase its precision capacity. The feedback mechanism of the FLC compensates for the prediction errors due to possible structural mismatch between the model and the process, thus, leading to precise manipulation of the output variable as in can be seen in Fig.I.5.1 and I.5.2. It must be noted that X represented a measurable input only in continuous mode because the batch was reserved to establish the correlation of offline dry mass measurements with the turbidity, thus, the pH controller giving good results in both cases. The pH controller proved its robustness on a wide range of biomass concentrations, thus, rejecting any perturbations given by variable concentration of components in the culture medium. Conclusively, even though the interferences were found to be significant when working at low dilution rates (I.4.65) the nonlinear pH controller proved its efficiency in rejecting the perturbations (both in discontinuous and continuous regimes) and thus the control of the photobioreactor can be decentralized using independent SISO controllers.

I.5.2. Validation of Lumostatic Controller

In order to validate the specific light uptake rate algorithm (Eq.I.4.79) the torus photobioreactor was inoculated with cells of *Chlamydomonas reinhardtii* that were cultivated in discontinuous mode. The culture medium and the initial conditions are identical with the previous experiment except that the incident light was not maintained constant but controlled for the manipulation of light uptake rate. The batch was conducted for 120 hours in lumostatic mode, q_e being maintained at 350 (Fig.I.5.9). q_e was calculated online based on measurable biomass and incident light intensity values. The lumostatic controller tracked the prescribed value with a global accuracy of ± 8.4 σ (± 2.4 % σ_r) that decreased to ± 4.5 σ (± 1.3 % σ_r) during last 80 hours.

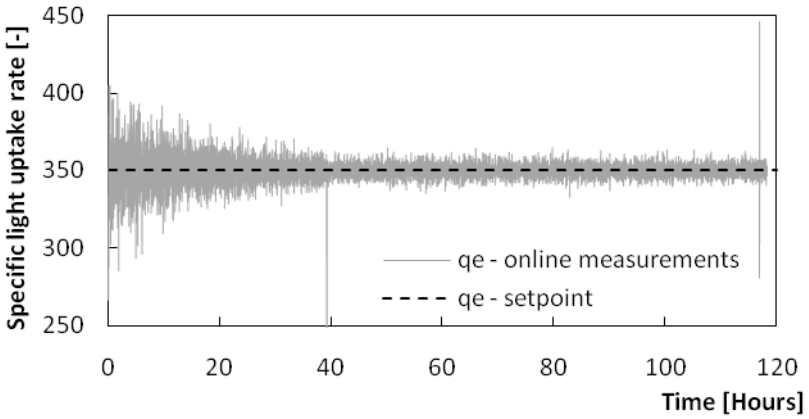

Fig.I.5.9. Time variation of q_e in a lumostatic batch: online measurements

The second output variable, the pH, was maintained at 7.5 throughout the experiment obtaining the same good results (Fig.I.5.10). The moving average filter with period of 60 samples/1 minute was retained for this experiment also. The pH peak registered around the 40th hour of cultivation is the result of a technical failure which blocked the input CO_2 valve to an insufficient volumetric flow rate. However, after the problem was solved the controller reached the prescribed value in less than half of hour. The controller can be set to act faster but the control variable will be noisier. The precision of control was as good as the one obtained for the previous experiment demonstrating that the nonlinear pH controller gives excellent results in batches with varying incident light intensities as well.

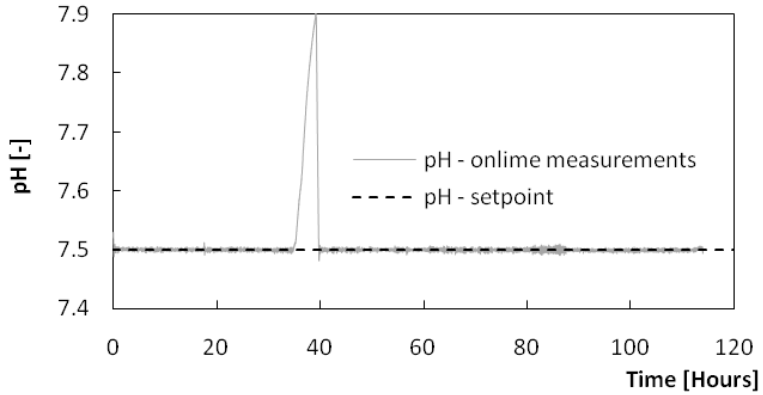

Fig.I.5.10. Time variation of pH in a lumostatic batch: online measurements

The biomass concentration was estimated online based on the signal of a turbidity probe using the same correlation obtained for the previous experiment. A moving average filter with a period of 60 samples/1 minute was also implemented for the noisy turbidity signal. Dry mass analyses were made once a day in order to verify the validity of the correlation under varying light intensities. The global photoautotrophic growth model fits well the experimental data only during the first 70 hours when the biomass reaches ~1.4 $g \cdot L^{-1}$ and the incident light intensity 500 $\mu mol \cdot m^{-2} \cdot s^{-1}$. Above this point the growth rate appears to decrease in comparison with the values predicted by the global photoautotrophic growth model. The slight growth inhibition might be a result of the high incident light intensities or of the depletion of a substrate.

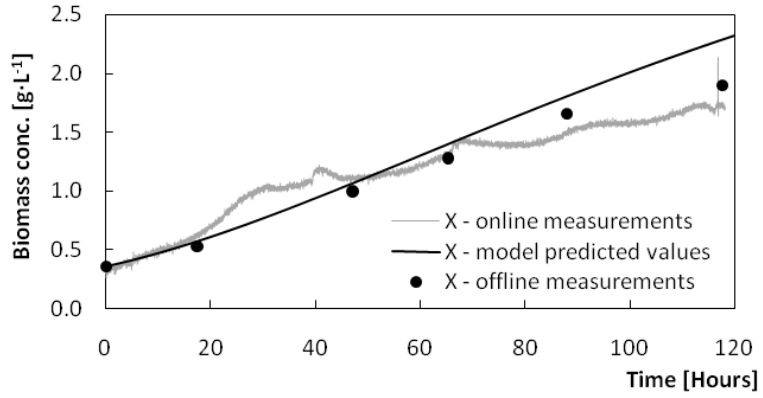

Fig.I.5.11. Time variation of biomass concentration in a lumostatic batch: online measurements vs. offline and simulated values

Fig.I.5.12 displays the control variable for light uptake rate manipulation, expressed both as voltage, which is the real parameter used by the power source of LED panel and as light

intensity given in μmol·m^{-2}·s^{-1}, which is used by the model. The two variables were found to be linearly dependent, the panel being operated in the range 17 to 24 V which corresponds to 100 to 800 μmol·m^{-2}·s^{-1} (Voltage $= 0.01 \cdot q_0 + 16$). Due to the slow biomass dynamics the incident light intensity was recalculated with the same periodicity of 60 samples/1 minute based on a feedback mechanism (Fig.I.4.8). The tuning parameter φ_{q_e} was determined empirically as being equal to unity both in practice and simulation. Because q_e is a simple ratio between q_0 and X, the incident light intensity profile overlaps the biomass registering the same mismatch during last 50 hours when compared with the photoautotrophic growth model response.

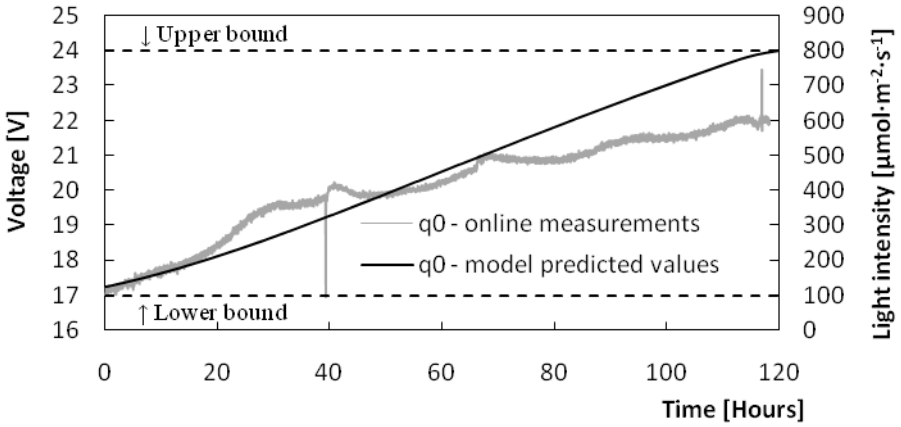

Fig.I.5.12. Time variation of input variable q_0 in a lumostatic batch: online measurements vs. model predicted values

As mentioned in section I.1.5.7 the coupling of growth kinetics with radiative transfer can be approached in two manners which differ in the sense that the irradiance, calculated for each z along reactor's depth – $I(z)$, is introduced in the formulation:

- whether it is averaged – $\langle I(z) \rangle$ and used as a single value in the kinetic equation of the specific growth rate $\mu(\langle I(z) \rangle)$,
- or used to compute local photosynthetic responses – $\mu\big(I(z)\big)$ which are thereafter averaged – $\langle \mu\big(I(z)\big) \rangle$.

By using the online measured values of q_0 (Fig.I.5.12) and X (Fig.I.5.11), the average irradiance – $\langle I(z) \rangle$ can be reconstructed. Fig.I.5.13 displays the offline reconstructed $\langle I(z) \rangle$ evolution which appears to be quasi-constant during q_e control and furthermore well predicted by the global photoautotrophic growth model.

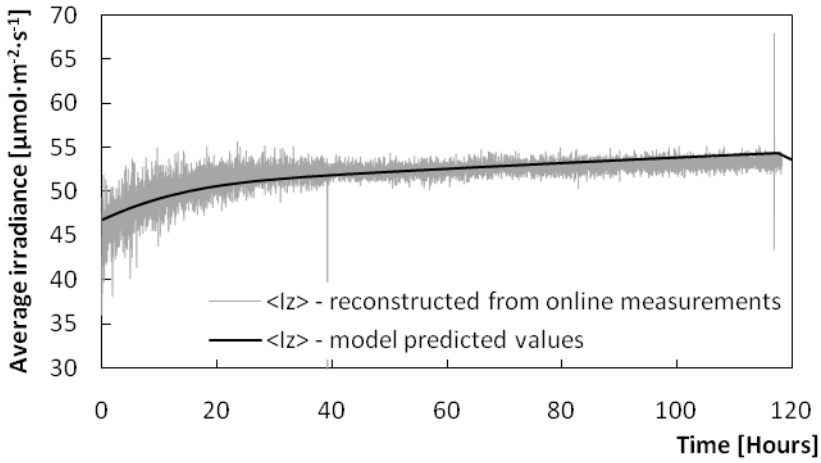

Fig.I.5.13. Time variation of reconstructed $\langle I(z) \rangle$ vs. model predicted values in a lumostatic batch

Another important parameter which can be reconstructed offline from q_0 and X values is the lighted volume fraction – Γ which can be calculated with Eq.I.4.83.

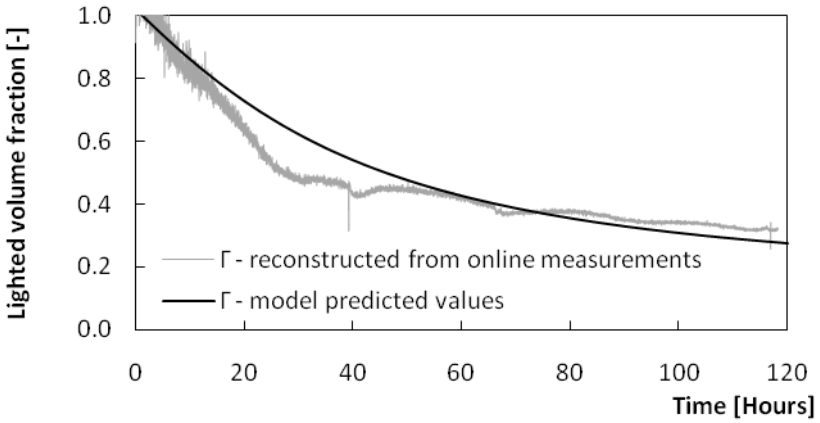

Fig.I.5.14. Time variation of reconstructed Γ vs. model predicted values in a lumostatic batch

Most of its parameters were discussed earlier (*i.e.* E_a, E_s and b) except the compensation point – I_c which corresponds to the minimum value of irradiance at which a positive photosynthetic growth rate can be obtained. The I_c value was determined in Takache *et al.*, (2010) to 10 ± 3 µmol·m^{-2}·s^{-1}. In this particular case I_c was used as fitting parameter since it is not directly measurable, thus the best match between experimental and simulated values was obtained for 5 µmol·m^{-2}·s^{-1}. However, the data may be submitted to small systematic errors given by the approximations made to correlate turbidity with dry matter and voltage with light intensity.

As it can be observed in Fig.I.5.14 Γ has a decreasing tendency, the lighted volume reaching down to 30% of reactor's volume. The lumostatic control of q_e ensures a quasi-constant $\langle I(z) \rangle$ but not a constant Γ because its control would require a faster increase of the input variable q_0 due to its exponential structure.

Fig.I.5.15 presents the control variable for pH regulation during a batch culture exposed to variable light intensities that appears to be well predicted by the phototrophic growth model. The variable is expressed both as aperture of the CO_2 proportional valve which is the real control action and as $G_{in}^{CO_2}$ which is measured by a specific flow meter. The input variable was recalculated with a periodicity of 60 samples/1 minute because the stabilization of CO_2 proportional valve requires several seconds. The tuning parameter φ_{H^+} was maintained identical with the previous experiment (*i.e.* $3 \cdot 10^6$ h^{-1}) during the first 90 hours. The pH is strongly related to the specific growth rate and therefore its decrease leads to lower $G_{in}^{CO_2}$ requirements, the input becoming noisier. During the last hours of cultivation φ_{H^+} was decreased to 10^6 h^{-1} resulting a smoother $G_{in}^{CO_2}$ with the same pH control precision. Thus, $G_{in}^{CO_2}$ evolution points once again to the schedule of φ_{H^+} according to $\langle \mu_I \rangle$.

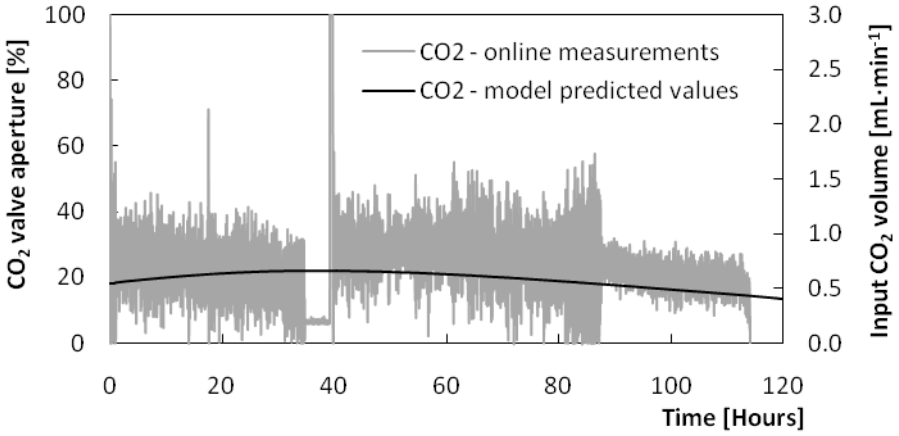

Fig.I.5.15. Time variation of input variable $G_{in}^{CO_2}$: online measurements vs. model predicted values

The variables required for the computation of the pH algorithm (*i.e.* c_{TIN}, c_{TIC}, $y_{out}^{CO_2}$ and G_{out}) were once again predicted by the phototrophic growth model in real time. Offline measurements for $c_{NH_4^+}$ (the dominant species of c_{TIN}) and c_{TIC} were realized in order to monitor the culture and are presented in Fig.I.5.16 and I.5.17. $c_{NH_4^+}$ present satisfactory

fitting with the model response mainly during the first part of the batch; the error bars being set to ± 0.002 mol·L^{-1}. The offline TIC values on the other hand are not well fitted with the global model, but the errors might appear at the conditioning of the samples which lose the dissolved CO_2 soon after sampling. The error bars in Fig.I.5.17 are also set to ±0.002 mol·L^{-1}.

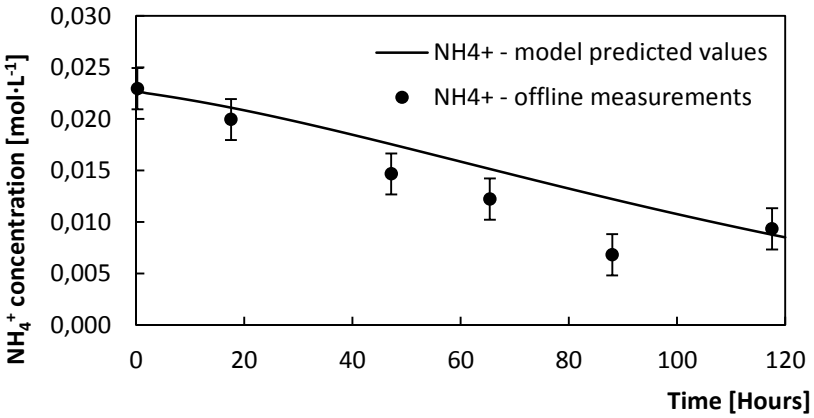

Fig.I.5.16. Time variation of $c_{\mathrm{NH_4^+}}$ in a lumostatic batch: offline vs. model predicted values

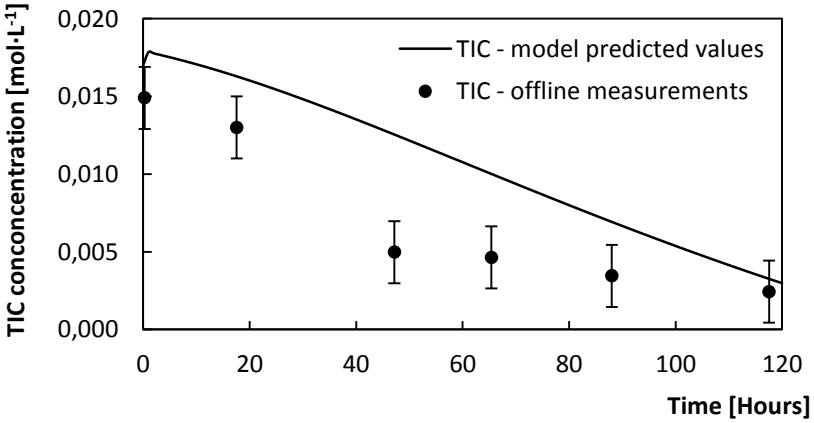

Fig.I.5.17. Time variation of c_{TIC} in a lumostatic batch: offline vs. model predicted values

In order to understand better the dynamics of the microalgae growth two more variables were measured offline, namely the sulfate (Fig.I.5.18) and phosphate (Fig.I.5.19) ions. They can be easily modeled by using the stoichiometric equation (I.3.11):

$$\frac{d\mathrm{SO_4^{2-}}}{dt} = \frac{Y_{S/X}}{M_x}\langle r_x \rangle \tag{I.5.1}$$

$$\frac{d\mathrm{PO_4^{3-}}}{dt} = \frac{Y_{P/X}}{M_x}\langle r_x \rangle \tag{I.5.2}$$

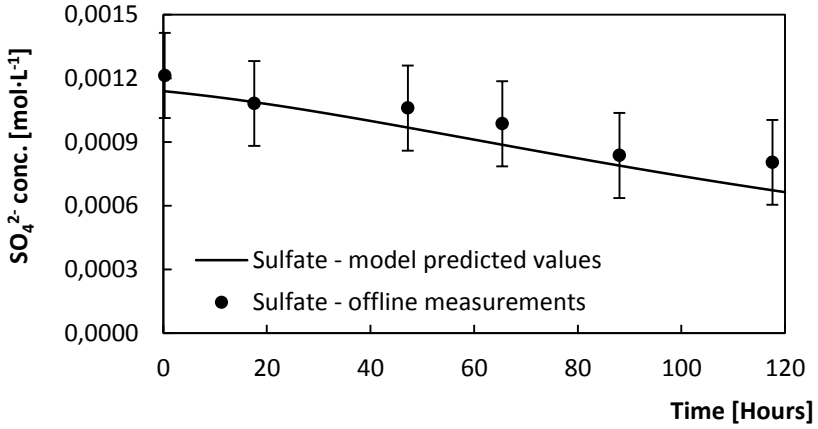

Fig.I.5.18. Time variation of SO_4^{2-} in a lumostatic batch: offline vs. model predicted values (error bars: ± 0.0002 mol·L^{-1})

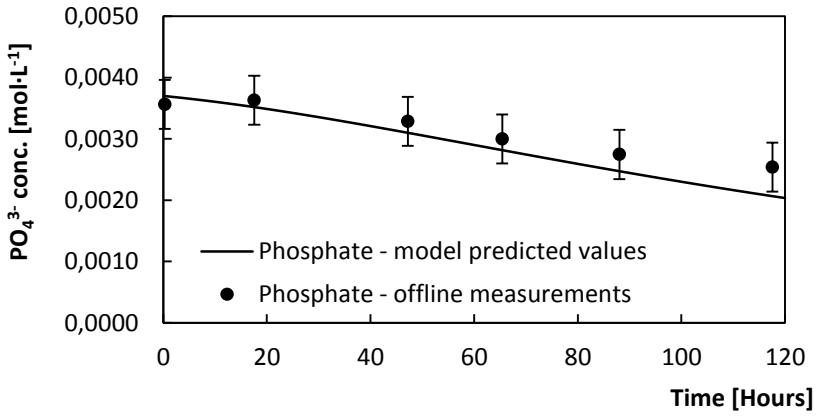

Fig.I.5.19. Time variation of PO_4^{3-} in a lumostatic batch: offline vs. model predicted values (error bars: ± 0.0004 mol·L^{-1})

As it can be observed no major substrate (*i.e.* C, N, S and P) is depleted thus the suspicion regarding the inhibition from the last hours of cultivation remains on the high light intensities.

Even though $y_{out}^{CO_2}$ and $y_{out}^{N_2}$ were measured online they remained observational variables which were not integrated in the control routine. They are acceptably predicted by the global photoautotrophic growth model (Fig.I.5.20 and Fig.I.5.21) and even though they deviate with few percents from the measurable values they preserve the same tendency. If they are integrated as measurable variables for the computation of the control algorithms the mismatches can be easily compensated by the feedback mechanism of FLC.

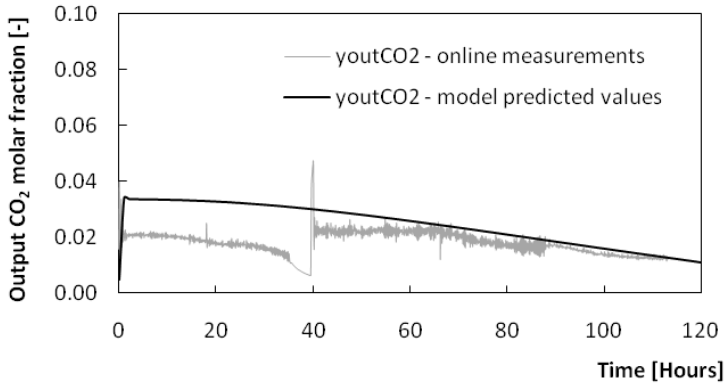

Fig.I.5.20. Time variation of $y_{out}^{CO_2}$ in a lumostatic batch: online vs. model predicted values

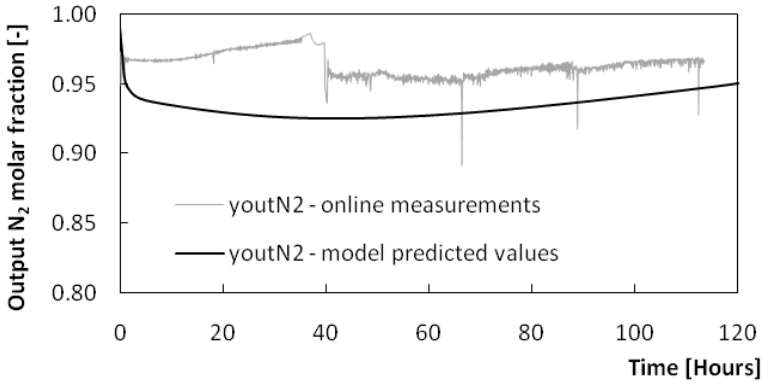

Fig.I.5.21. Time variation of $y_{out}^{N_2}$ in a lumostatic batch: online vs. model predicted values

Conclusions Regarding the Photobioreactor Control

The feedback linearizing control technique proved to globally stabilize the photoautotrophic growth process of *Chlamydomonas reinhardtii* in photobioreactor, known as being strongly nonlinear. A reduced model proper for control purposes was derived through the reducing of the global model by analyzing its response to various frequencies and simplifying its algebraic loops. The global phototrophic growth model integrated with real measurable inputs appeared to be an excellent tool for the prediction of certain immeasurable variables required for the computation of the control algorithm. The *X*, q_e and pH controllers evidenced their robustness and their accuracy in tracking the prescribed values. The $G_{in}^{CO_2}$ expression suggests that a proper growth model is fundamental in the control of pH. Particularly the pH controller presented good abilities in rejecting the disturbances given by variable biomass concentration even though the interactions in certain operating points are significant thus allowing the usage of decentralized SISO controllers.

PART II

MODELING AND CONTROL OF AEROBIC WASTEWATER TREATMENT PROCESSES

II.1. STATE OF THE ART REGARDING THE MODELING AND CONTROL OF WASTEWATER TREATMENT PROCESSES

***Abstract*:** The present chapter represents a brief state of the art regarding the modeling and the control of wastewater treatment processes. In addition, the main factors that influence the activated sludge processes are recalled.

The wastewater treatment plants are considered large nonlinear systems that are exposed to high disturbances in terms of influent flow rate and organics load, also associated with uncertainties regarding the composition of the wastewater, which are operated in continuous mode and must meet rigorous regulations.

In 1982, IWA (International Water Association) formed a task group on Mathematical Modeling for Design and Operation of Activated Sludge Processes. Their objective was to develop a platform that could be used for future development of model for nitrogen removal activated sludge processes. The research was concluded in ASM1 (Activated Sludge Model 1) (Henze *et al.*, 1987), a model which describes the organic carbon and nitrogen removal and consist in 13 state variables. ASM1 was subsequently extended by the same task group by including the biological phosphorus removal process – ASM2 (Henze *et al.*, 1995). Two other models (ASM2d and ASM3) were proposed afterwards including the denitrifying PAOs (phosphorus-accumulating organisms) and the internal storage compounds, respectively (Henze *et al.*, 1999; 2000).

Nowadays, the ASM family models are widely accepted and are the kernel of many other models with various added details. The degree of complexity of ASM models is however the main disadvantage in being used for automatic control purposes and therefore they must be simplified in accordance with each specific situation. Simplified versions of ASM models were obtained by considering the variables with slow dynamics constant and neglecting the ones with fast dynamics (Jeppsson, 1996). Such simplifications allowed their usage in automatic control applications.

Various control strategies were proposed in the technical literature but their evaluation and comparison (in practice or in simulation) are often difficult due to a series of motives such as the complexity of the biological process, the variability of the influent, the large range of time constants (which varies from minutes to days) and the lack of standard evaluation criteria (Alex *et al.*, 2008).

From 1998 to 2004 the development of benchmark tools used for the evaluation (based on simulation) of control strategies for WWTPs has been undertaken in Europe by Working Groups of COST Action 682 and 624 under the aegis of IWA Task Group on Benchmark of Control Strategies for WWTPs (Alex *et al.*, 1999).

Based on the benchmark models, which met a huge acceptance, more than 200 reports were published (*e.g.* Spanjers *et al.*, 1998; Copp, 2002; Jeppson and Pons, 2004).

The modeling of these processes is made globally, considering the nonlinear dynamics, but trying at the same time to simplify the models for their use in control techniques (Barbu, 2009). Due to the factors mentioned above the control problematics faces a certain degree of difficulty. The low repeatability rate, slow responses and the lack or high cost of the measuring instruments for the state variables of the bioprocesses (biomass concentration, COD concentration etc) also contribute to the difficulty of the wastewater treatment process control. Therefore, advanced and robust control laws that usually include in their structure state and parameter observers are currently used to control these processes.

According to (Larsson and Skogestad, 2000) two approaches in choosing the control structure of the process are taken into consideration: the approach oriented to the process and the one based on mathematical model. The first approach assumes the separated control of the main interest variables: dissolved oxygen concentration, nitrate and phosphate. One of the major and oldest problems encountered in wastewater treatment processes with direct impact on performance requirements is the dissolved oxygen concentration control. One can state that a satisfactory level of the dissolved oxygen concentration allows the developing of the microorganism' populations (the sludge) used in the process (Olsson, 1985; Ingildsen, 2002). Taking into account the importance of this problem, there are many approaches regarding the dissolved oxygen control in the literature: PI and PID-control, fuzzy logic, robust control, model based control etc. (Garcia-Sanz *et al.*, 2008; Olsson and Newell, 1999). Recently, the control problem of nitrate and phosphate level also became a priority. The control of the wastewater treatment processes, based on mathematical models, has known a large development both for strategies employing the use of the mathematical model in the control algorithm design, as well as for the case of state estimators. There can be mentioned the classic structures of PI and PID type (Katebi *et al.*, 1999) where the non-linear model linearized around an operating point is used for the controller design, up to exact linearizing control, multivariable or in an adaptive version together with a state and a parameter estimator (Nejjari *et al.*, 1999). The use of this model leads to the design of an indirect control structure of the process. It can be concluded that the control of the dissolved oxygen

concentration in the aerated tank practically assures a satisfactory level for the organic substrate. This problem - the control of the dissolved oxygen concentration - has been approached with good results in the control of a non-linear process using multi-model techniques (Barbu *et al.*, 2004).

Based on the ASM1 model in (Brdys and Zang, 2001) a non-linear predictive control technique for the indirect control of organic substrate through the control of dissolved oxygen concentration has been used. For the same model (Brdys and Konarczak, 2001) proposes a hierarchic control structure. This structure contains three levels: a higher level where a stable trajectory for the process on a time horizon is calculated, a mean level where the optimization of the trajectories for the dissolved oxygen concentration, the recycled active sludge flow and the recycled nitrate flow takes place and the lower level where the control of the dissolved oxygen concentration based on the setpoint imposed by the mean level is done. Another approach that now is very popular is the control based on artificial intelligence. It uses the knowledge and the expertise of the specialists about the process management. Expert systems, fuzzy and neuro-fuzzy systems have been used for the wastewater treatment processes control (Manesis *et al.*, 1998; Yagi *et al.*, 2002).

Generally, the wastewater treatment processes, as well as biotechnological processes, are characterized by parametric uncertainties that are determined by the operating conditions and the biomass growth.

II.2. MATERIALS AND METHODS

***Abstract*:** This chapter treats the materials and the methods used to accomplish the validation of the proposed model for the aerobic wastewater treatment pilot plant and the practical implementation of the developed control algorithms. The aerobic wastewater treatment pilot is based on a classical process with activated sludge and consists in a feeding tank, an aerobic tank and a clarifier. There are also presented the composition of the synthetic wastewater and the analyses made to monitor the plant.

II.2.1. The Biological Agent and the Culture Medium

The biological agent which led to the aerobic wastewater treatment in the experiments presented in this section was an activated sludge acquired from a plant which treats the effluents of a bakery yeasts factory. The sludge was preserved refrigerated in bottles and used whenever necessary for the pilot inoculation.

The wastewater used in experiments was a synthetic one, whose composition is presented in Table II.2.1:

Table II.2.1. Synthetic wastewater composition

Component	*Concentration*
Soluble starch	0.260 $g \cdot L^{-1}$
Glucose	0.260 $g \cdot L^{-1}$
Maltose	0.260 $g \cdot L^{-1}$
Peptone	0.043 $g \cdot L^{-1}$
Urea	0.092 $g \cdot L^{-1}$
Yeast extract	0.054 $g \cdot L^{-1}$
Malt extract	0.025 $g \cdot L^{-1}$
$NaH_2PO_4 \cdot H_2O$	0.042 $g \cdot L^{-1}$
$MgSO_4 \cdot 7H_2O$	$0.536 \cdot 10^{-3}$ $g \cdot L^{-1}$
$NaC\ell$	$0.357 \cdot 10^{-3}$ $g \cdot L^{-1}$
$CaC\ell_2$	$0.133 \cdot 10^{-3}$ $g \cdot L^{-1}$
$MnSO_4 \cdot H_2O$	$0.130 \cdot 10^{-3}$ $g \cdot L^{-1}$

The synthetic wastewater assures a concentration of COD of app. 800 mg/L in a ratio C:N:P of 100:5:1.

II.2.2. The Wastewater Treatment Pilot Plant

Fig.II.2.1 displays the wastewater treatment pilot plant and its main components: feeding tank, aerobic tank, anoxic tank, clarifier, electrical panel, pumps compartment and process computer.

The feeding tank has a capacity of 100 L and is provided with a mixer in order to deliver a homogeneous influent. The tank can be refrigerated to (2 – 4°C), thus avoiding the initiation of the biological processes pending the experiments. The feeding tank level can be monitored by means of an ultrasonic level sensor. The influent is transported with a peristaltic pump into the aerobic tank which is the core of the treatment process. The tank has a capacity of 35 L and is also provided with a stirrer. Air ejectors are installed at the bottom of the reactor furnishing dissolved oxygen to the biological mineralization process. The tank is equipped with a series of sensors for measuring various variables of the process such as pH, dissolved oxygen, ORP and temperature. The anoxic tank has the same capacity, but was not used for the experiments presented in this section. The clarifier has a cylindrical shape and a capacity of 60 L, assuring the sludge flocks sedimentation. The settled sludge can be recycled between the aerobic tank and the clarifier, and eliminated by means of two distinct peristaltic pumps.

Fig.II.2.1. The wastewater treatment pilot plant

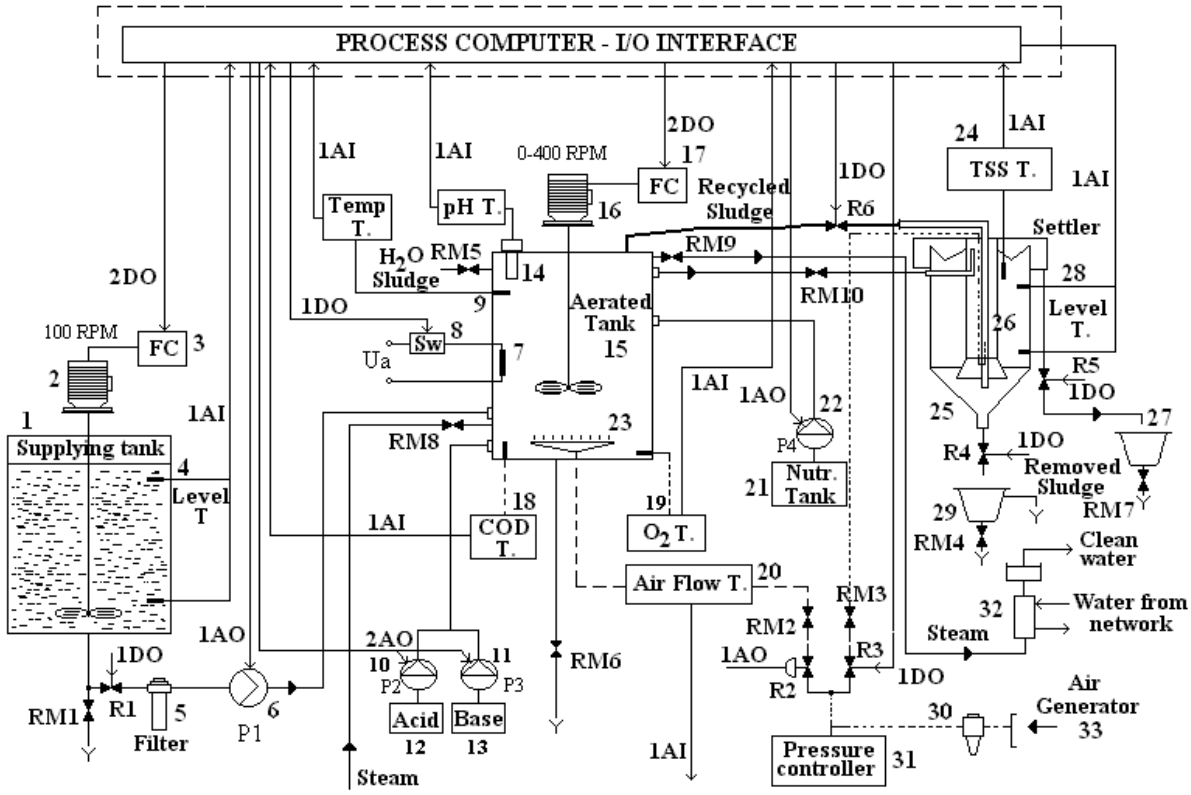

Fig.II.2.2. The operational scheme of the biological wastewater treatment pilot plant

Figure II.2.2 shows the operational scheme of the biological wastewater treatment plant. All elements are marked out, both technological and automation, together with the lines between them (wastewater lines, air, electrical lines):

1. wastewater feeding tank, refrigerated at 2 – 4°C, 150 L capacity;
2. stirring system for feeding tank, a.c., 100RPM, 100W;
3. frequency converter for the stirring system from the feeding tank;
4. ultrasonic level transducer for the feeding tank, 0 – 1000mm, 2 – 10mA output;
5. input filter for wastewater supply;
6. the pump P_1 (supplying the aerated tank with wastewater, 0 – 12 $L \cdot h^{-1}$);
7. heating resistance for the aerated tank, 2000W;
8. switch for temperature control in the aerated tank, nominal temperature 25 – 30°C;
9. temperature transducer, 0 – 100°C;
10. pump P_2 for pH correction (with acid), 0 – 100 $mL \cdot h^{-1}$ capacity;
11. pump P_3 for pH correction (with base), 0 – 100 $mL \cdot h^{-1}$ capacity;
12. tank for acid correction, 1 L capacity;
13. tank for base correction, 1L capacity;

14. pH transducer, 0 – 14, 2 – 10mA output;
15. aerated tank, 45 L capacity;
16. stirring system for the aerated tank, a.c., 0 – 400RPM, 200W;
17. frequency converter for the stirring system from the aerated tank;
18. ORP transducer, 0 – 300mg·L^{-1}, 2 – 10mA output;
19. DO transducer, 0 – 10 mg·L^{-1}, 2 – 10mA output;
20. air flow transducer, 0 – 200 L·h^{-1}, 2 – 10mA output;
21. tank for nutrient (*e.g.* phosphorus) supply, 1L capacity;
22. pump P_4 for nutrient supply, 0 – 100 mL·h^{-1} capacity;
23. aeration system for the aerobic tank;
24. total suspended solids transducer (TSS), 0 – 1000 FTU, 2 – 10mA output.
25. settler, 60 L capacity.
26. air-lift system for the sludge recycling from the settler to the aerated tank;
27. effluent evacuation tank, 40 L capacity;
28. level transducer for the clarifier tank, 0 – 1000 mm, 2 – 10mA output;
29. sludge evacuation system, 25 L capacity;
30. air filter (< 0,1μm);
31. pressure indicator, 0 – 6 bar;
32. condenser;
33. compressed air generator.

The system contains electrical and manual valves as follows:

- R_1: on-off electrical-valve for plant wastewater supply;
- R_2: continuous driven electrical-valve for air flow control in the aerated tank;
- R_3: on-off electrical-valve for sludge recycled system air supply;
- R_4: on-off electrical-valve for excess sludge evacuation;
- R_5: on-off electrical-valve for treated water evacuation;
- R_6: on-off electrical-valve for sludge recycled system from the settler to the aerated tank;
- RM_1: manual valve for the water evacuation from the supply tank;
- RM_2: manual valve for the aerated tank supplied with air;
- RM_3: manual valve for the sludge recycled system supplying with air;
- RM_4: manual valve for tank discharging with excess sludge;
- RM_5: manual valve for the aerated tank washing;
- RM_6: manual valve for water evacuation from the aerated tank;
- RM_7: manual valve for tank discharging of effluent;

- RM_8: manual valve for sterilization with steam (steam input);
- RM_9: manual valve for sterilization with steam (steam output);
- RM_{10}: manual valve for the effluent transfer from the aerated tank to the settler.

II.2.3. The Online Measurements

The data which can be measured online and registered in the process computer are:

- The turbidity (NTU) of the mixed liquor suspended solids (MLSS) in the aerobic tank which can be correlated with dry mass offline measurements;
- The pH of MLSS (pH units);
- The ORP of MLSS (mV);
- The DO of MLSS ($mg \cdot L^{-1}$);
- The temperature of MLSS (°C);
- The aeration rate ($L \cdot min^{-1}$);
- The pumps flow ($L \cdot h^{-1}$).

II.2.4. The Offline Measurements

II.2.4.1. Dry Matter

The dry matter of MLSS was measured once a day in order to monitor the activated sludge concentration. The analysis was realized by sampling 50 mL of MLSS and drying them in specific weighting vials at 105°C up to constant mass. The dry mass measurements were found to be well correlated with the turbidity signal only locally. Relation I.2.6 was employed to determine the dry mass concentration. The total suspended solids (TSS) concentration from the influent was very small and therefore neglected.

II.2.4.2. Chemical Oxygen Demand

Chemical Oxygen Demand (COD) represents the amount of oxygen consumed for complete chemical oxidation of the organic compounds into inorganic compounds. COD was determined through the potassium dichromate method with HI 93754B reagents. The analysis assumes the mineralization of the organic components at 150°C in a HI839800 tube test

heater. After mineralization and cooling the absorbance of the samples is read by means of a photometer HI83214.

II.2.5. Process Computer

The signals transmitted by the transducers are acquired on the process computer. The piloting program is built in Matlab®'s Simulink® which can be operated through a human-machine interface (HMI) which mediates the dialog between the human operator and the pilot plant. The HMI was developed in C++ while for the data storage regarding the process state and the future data analysis, the facilities offered by the system MS SQL SERVER 2005 are used.

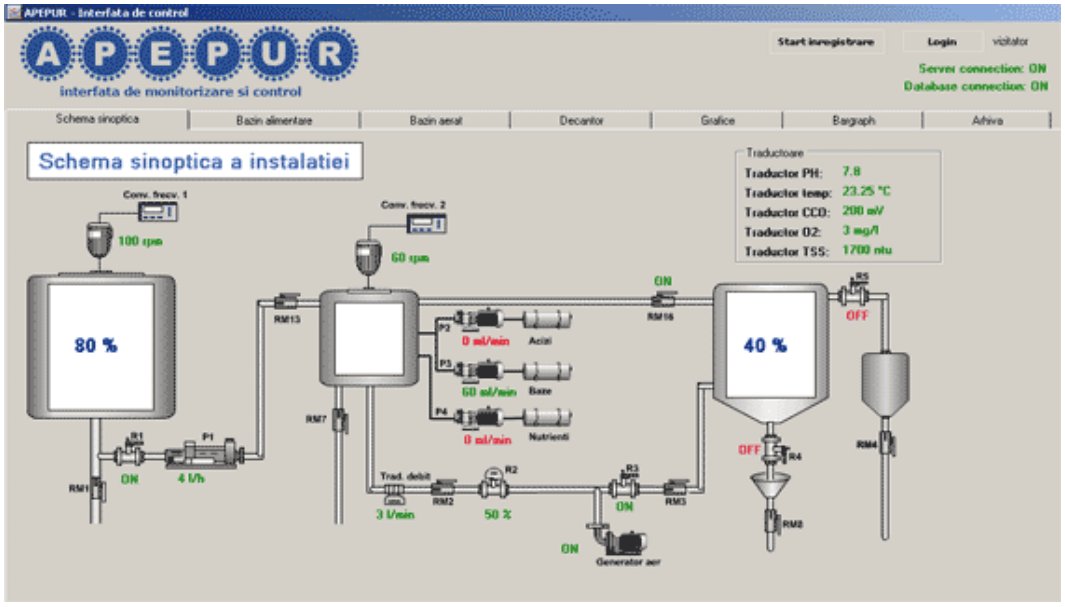

Fig.II.2.3. General overview of the pilot plant

The information transmitted between HMI and the control software is of two types: dynamic data, provided by sensors (temperature, pH, air flow etc.) and the commands transmitted to the treatment plant by the operator. This bidirectional data transfer is done every 250msec. as an UDP package that contains variables of double type (64bits). When the data package is received, HMI is updated with the new values which are memorized at pre-specified moments in an archive (database). The program that stores the data in the archive runs independently of the HMI meaning that both programs are not conditioned one another.

II.3. AEROBIC WASTEWATER TREATMENT MODELING

***Abstract*:** The present chapter proposes a simple and reliable nonlinear model to describe the dynamics of a conventional aerobic wastewater treatment pilot with sludge recycling. An empirical model for secondary clarifiers is also proposed in this chapter. The model parameters were identified on experimental data acquired from the wastewater treatment pilot plant.

II.3.1. Introduction

The wastewater treatment is more than a necessity it is a responsibility towards every producer which must sustainable improve the treatment processes. Various types of treatment were developed during the past years and this domain has almost no technological secrets, but the big challenge is the process control. The wastewater treatment processes are very complex, strongly non-linear and characterized by uncertainties regarding its parameters (Belia *et al.*, 2009). In the technical literature there are many models that try to capture as closely as possible the evolution of the wastewater treatment processes with activated sludge (Henze, *et al.*, 1987; 1995; 1999; 2000). The modeling of these processes is made globally, considering the nonlinear dynamics, but trying at the same time to simplify the models used in the control (Barbu, 2009).

II.3.2. Modeling of the Aerobic Wastewater Treatment Process

II.3.2.1. Bioprocess Description

The main objective of aerobic wastewater treatment process is to transform the organics present in wastewaters into stable oxidized end products which can be securely disposed without having any detrimental effect over the environment. In other words, the aerobic suspended growth process is a conventional wastewater treatment technique which consists in the oxidation of organics to CO_2, H_2O, NH_4^+ and new cells. A biological wastewater treatment installation is an association of distinct treatment processes or units designed to generate an effluent of specified quality from an influent with known composition and flow rate. The aerobic wastewater treatment, also known as secondary treatment, employs naturally

occurring microorganisms for the conversion of soluble and colloidal organics into dense microbial biomass that can be easily separated from the treated liquid by means of conventional settling processes. The aerobic treatment of wastewaters is accomplished mainly by heterotrophs which split the organics through two different processes, oxidation and biosynthesis, both resulting in their removal from influent. Oxidation or respiration (Eq.II.3.1) leads to mineralized end products, while biosynthesis (Eq.II.3.2) transforms the colloidal and soluble organics into particulate biomass which can be removed through settling. If one of the organic substrates becomes limiting the microbial cell tissue will be endogenously respired by microorganisms in order to obtain energy for maintenance (*i.e.* auto-oxidation – Eq.II.3.3). All three processes take place simultaneously in the aerobic tank and can be expressed stoichiometrically as follows (Gray, 2005):

- oxidation:

$$COHNS + O_2 + \text{Microorganisms} \rightarrow CO_2 + NH_3 + \text{other end products} + \text{energy} \quad \text{(II.3.1)}$$

- biosynthesis:

$$COHNS + O_2 + \text{Microorganisms} \rightarrow C_5H_7NO_2 \quad \text{(II.3.2)}$$

- auto-oxidation:

$$C_5H_7NO_2 + 5O_2 \rightarrow 5CO_2 + NH_3 + 2H_2O + \text{energy} \quad \text{(II.3.3)}$$

where $COHNS$ and $C_5H_7NO_2$ are the general expressions of organic matter and microorganisms.

In order to assure the organics mineralization, the MLSS is enriched in dissolved oxygen which is provided mechanically by means of air blowers. The microbial cells are forming flocs which are allowed to settle in a clarifier. A portion of the settled sludge is usually recycled back to the aerobic compartment. Thus, a conventional activated sludge process consists in (Fig.II.3.1):

- Aerobic tank in which the oxidation of the organic matter takes place. The input wastewater is mixed with return activated sludge (RAS) forming the mixed liquor. The recycling of the settled sludge makes the mean cell residence time to be higher than the hydraulic retention time (Sterritt and Lester, 1988), helping to maintain a large number of

microorganisms able to effectively oxidize the organic matter in a relatively short period of time.

- Clarifier used for the sedimentation of sludge flocs produced in the aerobic tank. A part of the settled sludge is recycled while the excess is removed.

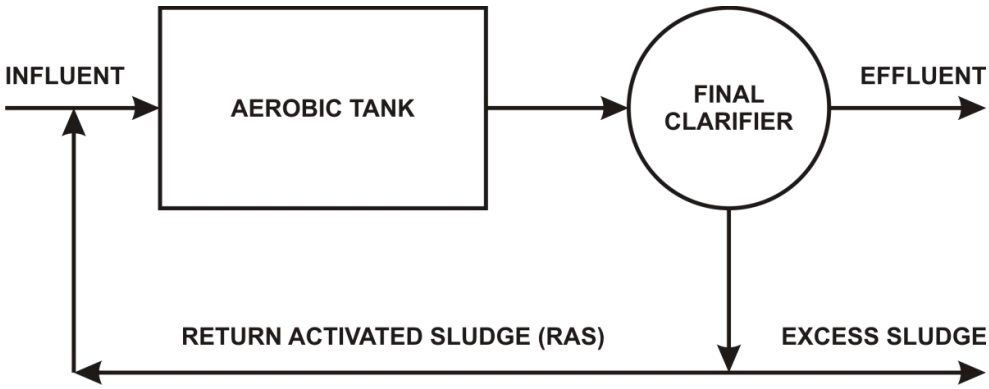

Fig.II.3.1. Conventional activated sludge system

Main biological reactions which take place in the aerobic tank are the removal of the organic carbon, nitrogen and phosphorus. In wastewater treatment processes the aerobes requirements of carbon, nitrogen and phosphorus are usually expressed as ratio (C:N:P) which has an optimum of (100:5:1) for complete biological oxidation of organics. When the nitrogen concentration exceeds the above mentioned ratio, additional treatment stages must be applied (*e.g.* denitrification). Similarly, the high phosphorus content in influent must be treated in separate stages. The lack of nutrients is occasionally supplemented with inorganic compounds (mainly when phosphorus is deficient), but often is more convenient to treat the influent in anaerobic systems.

The main biological reaction which occurs through aerobic growth of heterotrophs is the removal of soluble organic carbon (Fig.II.3.2) which becomes either additional biomass or CO_2 in soluble and gaseous form.

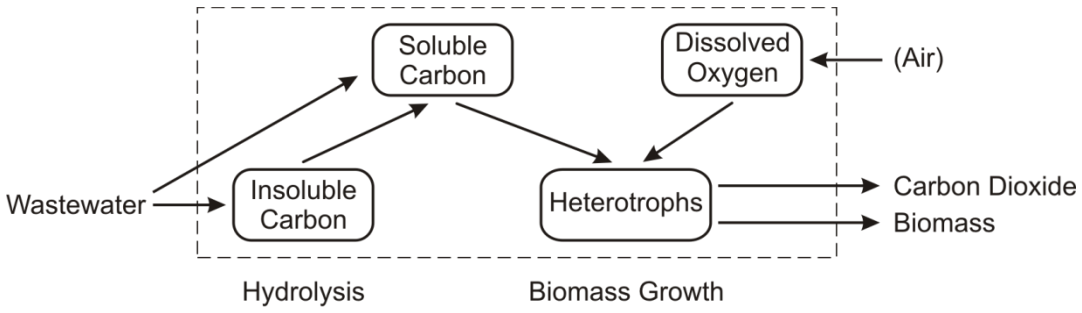

Fig.II.3.2. Main reactions on organic carbon removal

Aerobes necessitate free dissolved oxygen for the decomposition of organic substances present in wastewater influents. In addition the insoluble organic carbon must be first transformed into soluble organic carbon through hydrolysis which is a biocatalyzed enzymatic reaction.

Consequently, the aerobic processes are fast and efficient from a biochemical point of view in comparison with other types of reactions, generating simple and highly oxidized by-products such as carbon dioxide and water.

II.3.2.2. Aerobic Tank Modeling

As mentioned above, the growth of heterotrophic microorganisms which populates the aerobic tank requires free dissolved oxygen. However, their growth is due to the soluble substrate (from wastewater) used as carbon and energy sources. Thus, they are not only oxygen-limited but also restricted by the availability of adequate supplies of organic carbon, nutrients such as nitrogen and phosphorus, trace elements and growth factors. The biomass increase is considered fundamental while the other processes can be coupled through the system stoichiometry.

The simplest model which is able to describe the main state variables (biomass, substrate and oxygen) of a conventional activated sludge process is presented in Table II.3.1.

Table II.3.1. Process kinetics and stoichiometry for heterotrophic microbial growth in an aerobic tank

Component → i / j Process ↓	1 X_B	2 S_S	3 S_O	Process Rate, ρ_j [g·L^{-1}·h^{-1}]
1 Growth	1	$-\frac{1}{Y}$	$-\frac{1-Y}{Y}$	$\mu_{max}\left(\frac{S_S}{K_S+S_S}\right)\left(\frac{S_O}{K_O+S_S}\right)X_B$
2 Decay	-1	-1	-1	$\mu_s X_B$
Observed Conversion Rates [g·L^{-1}·h^{-1}]	$r_i = \sum_j r_{ij} = \sum_j \nu_{ij}\rho_j$			Kinetic Parameters: Maximum specific growth rate: μ_{max} Half-velocity constant: K_S Specific decay rate: μ_s
Stoichiometric Parameters: True growth yield: Y	Biomass [g·L^{-1}]	Substrate [g·L^{-1}]	Dissolved Oxygen [g·L^{-1}]	

In accordance with the IWA nomenclature (Grau *et al.*, 1982), denoted with X are the insoluble components and with S the soluble ones while their subscripts are related to individual components (B – biomass, S – substrate and O – dissolved oxygen).

S_S refers to the carbonaceous substrate usually expressed as COD value (mg $O_2 \cdot L^{-1}$) while the macronutrients are not modeled, being considered non-limiting factors. In what regards the conventional aerobic processes, they can be modeled through simple stoichiometric equations, but are often neglected because a (C:N:P) ratio of app. (100:5:1) assures a good removal capacity. However, if macronutrients exceed the optimal ratio the conventional aerobic treatment technique becomes incompatible with the influent quality requirements.

The growth of biomass is expressed through a double Monod-Herbert model (Herbert, 1958) while its decay is of first order with respect to biomass concentration. The reaction rates which results from table II.3.1. can be written as follows:

$$r_{X_B} = \mu_{max}\left(\frac{S_S}{K_S+S_S}\right)\left(\frac{S_O}{K_O+S_S}\right)X_B - \mu_s X_B \quad \text{(II.3.4)}$$

$$r_{S_S} = -\frac{1}{Y} r_{X_B} \quad \text{(II.3.5)}$$

$$r_{S_O} = -\frac{1-Y}{Y} r_{X_B} \quad \text{(II.3.6)}$$

The growth of heterotrophs results, by any means, from the consumption of carbonaceous substrate whose complete mineralization occurs only in the presence of free dissolved oxygen. Therefore, the second Monod in Eq.II.3.4 is chosen more for mathematical reasoning than accordance to any fundamental rate laws. The S_O Monod expression has the role of a mathematically continuous switching function which turns the process rate equation on and off, thus a small K_O value denotes that the switching function in near unity for moderate DO concentrations but decreases to zero as DO concentration approaches zero.

The rates of substrate removal and dissolved oxygen consumption are, as described by Eq.II.3.5 and Eq.II.3.6, depending on the rate of microbial growth.

Given that the dissolved oxygen level is maintained in the aerobic tank by means of air bubbled into the reactor, a phase transfer must be considered:

$$N_{O_2} = (K_L a)_{O_2}\left(S_{O,sat} - S_O\right) \quad \text{(II.3.7)}$$

where $(K_L a)_{O_2}$ is the overall volumetric mass transfer coefficient and $S_{O,sat}$ is the saturation concentration of dissolved oxygen in water.

The oxygen transfer rate can be expressed as a function of the air flow rate:

$$(K_L a)_{O_2} = \theta W \qquad \text{(II.3.8)}$$

where θ is a diffusion coefficient related to the oxygen transfer rate and thus to the efficiency of the air ejectors and W is the aeration rate.

II.3.2.3. Empirical Clarifier Modeling

The flocs formed in the aerobic tank are allowed to settle in a separate tank (or the same tank if SBR are used) thus clarifying the treated water which exits the plant. The MLSS flow which enters into the clarifier splits in two (Fig.II.3.3), a stream flows upwards exiting the clarifier through the top (overflow) and another stream flows downwards being withdrawn at the bottom (underflow). Overlapped on these flows is the settling of the biomass flocs under the influence of gravity which results in a gradient of concentration (reduced concentration in overflow and increased in underflow). This concentration gradient with height and time creates a distributed parameter system whose modeling is complex.

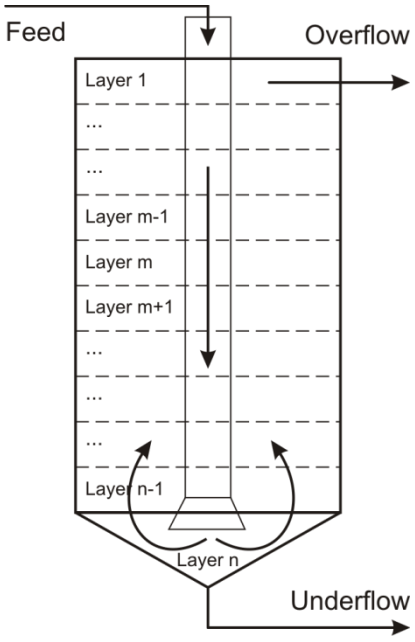

Fig.II.3.3. Multi-layer model

The difficulty comes from the fact that the settling velocity of flocs depends on multiple variables such as sludge density, MLSS dry mass, clarifier geometry, MLSS flow, flocs

dimension, retention time etc. High concentrations of biomass may lead to a compaction phenomenon when high interactions occur between flocs. This phenomenon occurs at the bottom part of the clarifier.

However, the compaction phenomenon is not well understood. On the contrary, low concentration of flocs may lead to less efficient settling, the sludge occupying a higher volume distributed all over the clarifier volume. Consequently, the sludge settling behavior is hard to be predicted on strict physical laws and therefore empirical models can give satisfactory responses.

The modeling approach presented in Fig.II.3.3 is a multi-layer model applied to a vertical clarifier. The clarifier is divided in *n* slices (typically 10 to 100 depending on the required accuracy for predicting the sludge blanket level). Each slice is considered here as being homogeneous in terms of concentrations.

Given that the objective of the present section is to derive a simple and reliable model intended to be used for control purposes, only the *n* slice which corresponds to the bottom of the clarifier will be modeled. The aim is thus to predict the biomass concentration which is recycled between the clarifier and aerobic tank and which influences the overall growth of heterotrophs, the substrate removal and the oxygen requirement.

A simple inventory on the *n* slice can be done by balancing the biomass transported through the feeding flow rate (F_f), the recycled sludge flow rate (F_r) and the excess sludge flow rate (F_e) (Fig.II.3.4.).

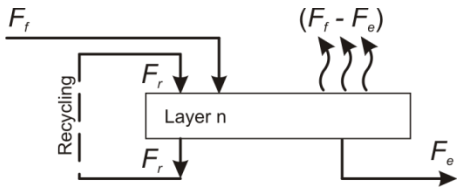

Fig.II.3.4. Mass balance on sludge compartment (layer n)

It must be noted that the aerobic tank works at constant volume and thus the influent feeding flow rate is equal with the output MLSS flow rate and hence with the MLSS flow rate which enters the clarifier.

A simple balance equation can thus be written for the *n* slice (Fig.II.3.4):

$$\frac{dX_{\mathrm{R}}}{dt} = \frac{F_f}{V_s} X_{\mathrm{B}} + \frac{F_r}{V_s} X_{\mathrm{B}} - \frac{F_e}{V_s} X_{\mathrm{R}} - \frac{F_r}{V_s} X_{\mathrm{R}} - \eta \frac{(F_f - F_e)}{V_s} X_{\mathrm{R}} \qquad \text{(II.3.9)}$$

where X_{R} is the concentration of the recycled biomass, V_s is the n slice volume and η is a subunitary parameter which accounts the fraction of biomass which migrates in the n-1 slice along with the upward stream.

II.3.3. Mass-Balance Model

Regrouping the conversion terms which describe the kinetics of biomass, the conversion yields of substrate and of dissolved oxygen along with the transport terms the following mass balance equations can be written:

$$\frac{dX_{\mathrm{B}}}{dt} = r_{X_{\mathrm{B}}}(t) - D(t)(1+r)X_{\mathrm{B}}(t) + rD(t)X_{\mathrm{R}}(t) \tag{II.3.10}$$

$$\frac{dS_{\mathrm{S}}}{dt} = -r_{S_{\mathrm{S}}}(t) - D(t)(1+r)S_{\mathrm{S}}(t) + D(t)S_{\mathrm{S,in}} \tag{II.3.11}$$

$$\frac{dS_{\mathrm{O}}}{dt} = -r_{S_{\mathrm{O}}}(t) + N_{O_2}(t) - D(t)(1+r)S_{\mathrm{O}}(t) + D(t)S_{\mathrm{O,in}} \tag{II.3.12}$$

$$\frac{dX_{\mathrm{R}}}{dt} = D_s(t)(1+r)X_{\mathrm{B}}(t) - D_s(t)(\beta+r)X_{\mathrm{R}}(t) - \eta D_s(t)(1-\beta)X_{\mathrm{R}}(t) \tag{II.3.13}$$

with:

$$D = \frac{F_f}{V} \tag{II.3.14}$$

$$D_s = \frac{F_f}{V_s} = D\frac{V}{V_s} \tag{II.3.15}$$

$$r = \frac{F_r}{F_f} \tag{II.3.16}$$

$$\beta = \frac{F_e}{F_f} \tag{II.3.17}$$

The volumetric rates of biomass growth (r_{X_B}), substrate consumption (r_{S_S}) and oxygen consumption (r_{S_O}) are given by equations (II.3.4), (II.3.5) and (II.3.6) while the volumetric mass transfer for oxygen (N_{O_2}) is determined through equations (II.3.7) and (II.3.8).

II.3.4. Parameters Identification

The identification of model parameters was realized on experimental data obtained from the wastewater treatment pilot plant operated without sludge recycling. The identification experiment unfolded for app. 240 hours on a synthetic wastewater whose composition was presented in section II.2.1. The wastewater treatment pilot plant was operated in open loop by maintaining during the first 165 hours the dilution at 0.02 h^{-1} while pending last hours it was increased to 0.03 h^{-1}. On each dilution plateau several aeration steps were imposed in order to observe the dissolved oxygen dynamics. The dissolved oxygen concentration was measured online along with the turbidity whose value was correlated offline with the dry mass values measured daily. The dry mass was found to be linearly dependent on the turbidity signal, their correlation being determined through linear regression ($R^2 = 0.9$). However, the correlation is available only locally, wider ranges of biomass concentration being necessary to determine a global correlation. Nevertheless, the turbidity value is known to be influenced by the flocs dimension and by the bubbles of gasses in MLSS requiring recalibration if the operating point is changed. The substrate was measured offline in order to monitor the plant. The parameter vector to be identified is:

$$\tau = [\mu_{max}\ K_S\ \mu_s\ \theta]^T \tag{II.3.18}$$

For parameter identification a one-dimensional search method was used. The identification was done on the basis of an Euclidian-distance criterion, given by Eq. (II.3.19), which was minimized with respect to the components of the vector τ.

$$I = \sum_{k=1}^{N} \left[\left(X_B[k] - \hat{X}_B[k] + \right)^2 + \left(S_O[k] - \hat{S}_O[k] \right)^2 \right] \tag{II.3.19}$$

The minimization of the criterion I was done by using a one-dimensional search method on the directions given by the components of the parameter vector τ.

The initial point in the parameter space from where the search procedure begun was the following:

$$\tau_0 = \left[\mu_{max,0}\ K_{S,0}\ \mu_{s,0}\ \alpha_0\right]^T \quad \text{(II.3.11)}$$

where: $\mu_{max,0}$ = 0.16 h^{-1}, $K_{S,0}$ = 0.02 $g \cdot L^{-1}$, $\mu_{s,0}$ = 0.016 h^{-1} and α_0 = 0.018.

The identification procedure was repeated for different clusters of data and the average values obtained were: μ_{max} = 0.11 h^{-1}, K_S = 0.18 $g \cdot L^{-1}$, μ_s = 0.02 h^{-1} and θ = 0.0033.

Certain parameters such as Y and K_O were not identified, therefore standard values were considered. The substrate yield does not vary much (*i.e.* 0.6 – 0.7) for different types of wastewaters and was chosen to be 0.67. K_O, on the other hand, does not have a strict physical significance and must be small enough to turn the Monod switching function on and off. A typical value of 0.2 $mg \cdot L^{-1}$ was chosen for K_O.

Table II.3.2 lists the model parameters used for further simulations and for the design of control algorithms.

Table II.3.2. Aerobic growth model parameters

Group	*Parameter*	*Value*	*Typical values* (Henze *et al.*, 2000)	*Unit*
Kinetic parameters	μ_{max}	0.11	0.12 ÷ 0.55	h^{-1}
	μ_s	0.02	0.002 ÷ 0.07	h^{-1}
	K_S	0.18	0.01 ÷ 0.18	$g \cdot L^{-1}$
	K_O	0.20	0.01 ÷ 0.5	$mg \cdot L^{-1}$
Stoichiometric parameters	Y	0.67	0.46 ÷ 0.69	-
Transfer parameters	α	0.0033		
	$S_{O,sat}$	8.00		$mg \cdot L^{-1}$
	r	1.00		-
	β	0.20		-
Plant geometry	V	35.00		L
	V_S	6.00		L
Settling parameters	η	0.80		-

The operation protocol used for the identification experiment consisted in the open loop operation of the wastewater treatment pilot plant without recycling, therefore only the dynamics of three state variables (*i.e.* X_B, S_S and S_O) can be considered fully validated. η, the subunitary parameter pertaining to the sludge settling dynamics, was chosen empirically based on offline dry mass measurements realized on MLSS sampled from the recycling line.

The obtained experimental values, which will be presented in the following sections, narrow the accuracy of X_R dynamics only at small concentrations of biomass.

II.3.5. Model Validation

In order to validate the afore-described model the data obtained during the identification experiment were compared with the model response. The model was integrated with real input values (*i.e.* D and W) acquired from the wastewater treatment pilot plant. Thus, D was maintained constant at 0.02 h^{-1} during the first 165 hours and 0.03 h^{-1} for the rest, while W variation is depicted in Fig.II.3.5.

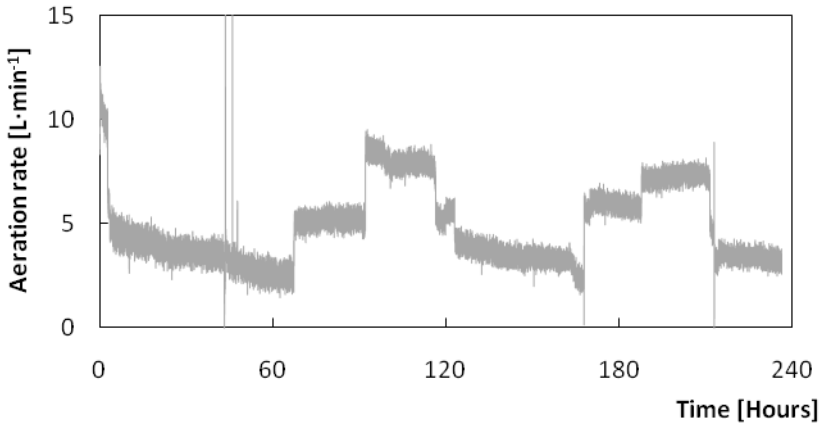

Fig.II.3.5. Aeration rate experimental values

The dry mass points (Fig.II.3.6) appear to be well correlated with the turbidity signal. At the same time the fitting between the biomass online measurements and the model predicted values is satisfactory. The carbonaceous substrate (measured through COD method) also presents a satisfactory fitting with the model predicted values (Fig.II.3.7 – error bars of 0.02 $g \cdot L^{-1}$). In order to obtain accurate COD values, not influenced by the sludge settling capacity, the samples from the aerobic tank were centrifuged and the clarified liquid analyzed. If effective output COD is aimed then the residual biomass in the upper layer of the settler must be modeled and converted into equivalent COD values. The efficiency of the substrate removal is indirectly influenced by the dissolved oxygen dynamics as it can be observed in Fig.II.3.7. However, the main mechanism of substrate removal remains the aerobic growth of heterotrophs. Noting that the initial concentration of the carbonaceous substrate ($S_{S,in}$) is 0.8 $g \cdot L^{-1}$ the difference between the lowest substrate removal efficiency (associated with a DO

concentration of 0 mg·L^{-1}) and the highest performance (correlated with DO > 4 mg·L^{-1}) is of maximum 10%. The aerobic growth of heterotrophs can continue at satisfying levels even at null DO concentrations with the condition of continuously bubbling small volumes of air into the aerobic tank and the oxido-reduction potential (ORP) to be close to zero. At negative ORP values the organics mineralization is incomplete hence the output COD will be increased. Thus, the DO contribution over the overall substrate removal efficiency has an influence of maximum 10% and it is important to discern between highest performance associated with high aeration costs and slight lower performance correlated with rationalized expenses with aeration.

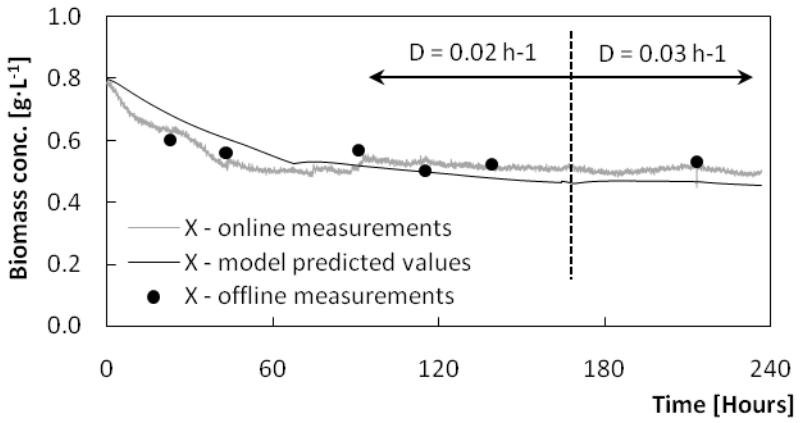

Fig.II.3.6. Biomass dynamics: online values (gray line), offline values (dots) and model predicted values (black line)

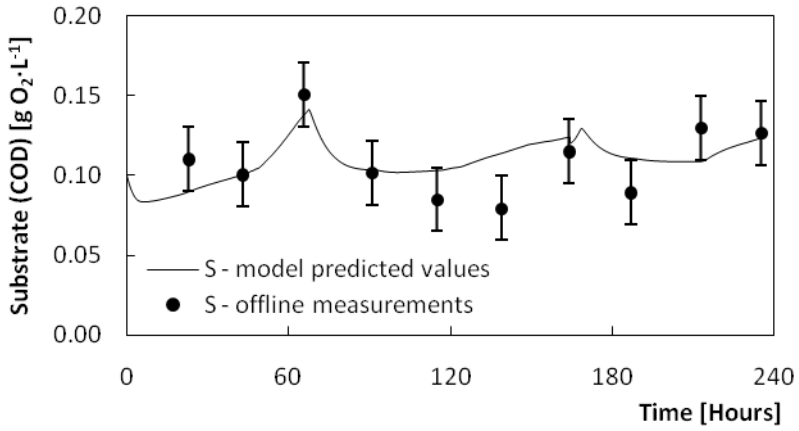

Fig.II.3.7. Substrate dynamics: offline values (dots) and model predicted values (black line)

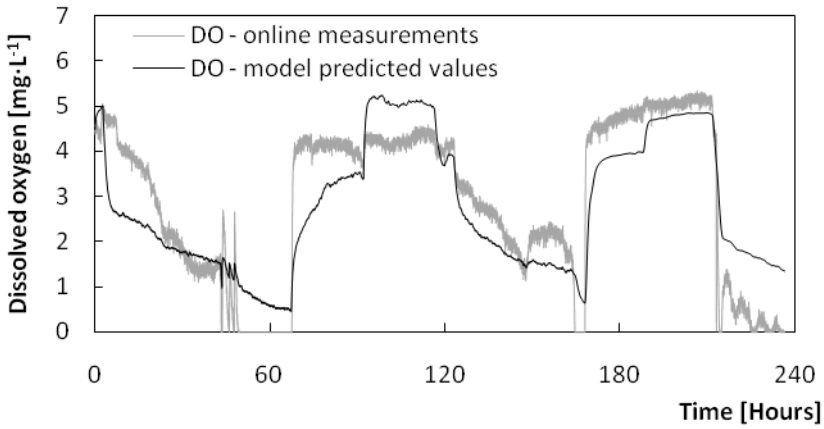

Fig.II.3.8. Oxygen dynamics: online (gray line) and model predicted values (black line)

Fig.II.3.8 presents the comparison between the online DO measurements and its values predicted by the model. As it can be seen the model is not able to accurately predict the DO dynamics, but registers the same tendency. The loss of accuracy in predicting the DO can appear from other processes which are not modeled (*e.g.* a fraction of dead biomass can convert to substrate) therefore, for research purposes, more complex models such as ASM family may be used. However, the proposed model is proper for control purposes considering that a feedback mechanism can eliminate the slight mismatch.

Conclusions regarding the WWTP modeling

A simple nonlinear dynamic model was proposed for the aerobic tank describing three fundamental state variables of the system, the sludge, substrate and the dissolved oxygen concentrations. The model parameters were identified on experimental data from the aerobic wastewater treatment pilot during an experiment operated in open loop. The model fitted well to the experimental data on various operating points. In addition, a simple and reliable model was proposed for the vertical clarifier in order to appreciate the concentration of the recycled biomass.

II.4. CONTROL STRATEGIES FOR AEROBIC WASTEWATER TREATMENT PROCESSES

***Abstract*:** The present chapter targets the design of control algorithms able to globally stabilize the aerobic wastewater treatment processes. The chapter introduces the basic control strategies of the aerobic WWTPs, detailed from a systemic viewpoint. The nonlinear dynamic model validated in the previous chapter results in a non-square system with two inputs (*i.e.* D and W) and three outputs (*i.e.* X_B, S_S and S_O). An NRG analysis was performed around eight steady state points in order to select the significant control channels and to square the system. A nonlinear multivariable control strategy based on the feedback linearizing theory was discussed for two square systems $D, W \rightarrow S_S, S_O$ and $D, W \rightarrow \mathrm{F/M}, S_O$. The RGA analysis was resumed for each system analyzing the interferences hence the possibility of using decentralized SISO controllers. The synthesized controllers were validated in simulation. In addition, considering the parametric uncertainties, the lack of specific sensors for substrates and the significant interferences, a linear monovariable control strategy based on the quantitative feedback theory was proposed for the dissolved oxygen concentration.

II.4.1. Basic Control Strategies for Aerobic WWTPs

II.4.1.1. Chemostatic Control of WWTPs

The chemostatic control of WWTPs is commonly applied in open loop by imposing a constant known influent flow rate and monitoring the system to achieve the desired steady-state operation point. Loop closing has undoubtedly certain advantages such as the global stabilization of the system and the convenience of working at desired setpoints determined in accordance with $S_{S,in}$. Another advantage might be the fact that X_B can be measured in some cases if a turbidity probe is available.

The chemostatic control or WWTPs is similar with the PBR approach (section I.4.2) except that in the present case the biomass accumulation, even though it is a fundamental process, does not represent an end per se. In addition, a part of the settled sludge is recycled in order to maintain a proper sludge concentration in the aerobic tank. The biomass control does not necessarily assure a proper substrate removal in cases such as variable $S_{S,in}$ concentration or eventual transitory phases. Thus, the biomass control may be implemented only when $S_{S,in}$

concentration is known and must be conjoined with a reliable dissolved oxygen controller. In addition, the input variable must be strictly bounded at convenient values in order to prevent high dilution rates to alter the effluent quality.

II.4.1.2. Auxostatic Control of WWTPs

An auxostat is a closed loop system in which the input variable is the dilution rate, employed to control an output variable else than the biomass (*e.g.* various substrates, products, dissolved gases, pH etc). The turbidostat (closed loop chemostat) is actually an auxostat but it is somehow introduced in a distinct category due to its popularity.

II.4.1.2.1. *Auxostatic Substrate Control*

The auxostatic control of the substrate involves the manipulation of the dilution aiming the control of the substrate concentration (*i.e.* COD concentration) inside the aerobic tank. This type of control can satisfy the main goal of wastewater treatment process, which is a low S_S concentration in the effluent.

The advantage of using an auxostatic control of the substrate is obvious, achieving a stable desired S_S concentration in WWTP's effluent regardless of the biomass concentration or of eventual $S_{S,in}$ variations. The disadvantage comes from the fact that the COD analyzers are very expensive and require high amounts of reagents. Specific sensors which measure online the COD values are also expensive (*e.g.* submersible spectrometers) and are a research in progress. Due to the nature of the process the substrate auxostatic control must be also associated with a reliable dissolved oxygen controller.

II.4.1.2.2. *Auxostatic F/M Ratio Control*

Food to microorganism ratio (F/M) can be simply expressed as the ratio between the amount of incoming food and the quantity of biomass present in the aerobic tank (Eq.II.4.1):

$$\frac{dF/M}{dt} = \frac{DS_{S,in}}{X_B} - F/M \qquad \text{(II.4.1)}$$

F/M is often calculated by the WWTP's operators in order to monitor the facility and to push the substrate removal efficiency up to its maximum. The controller assumes the dilution manipulation for the control of F/M ratio around a prescribed value.

This type of control may result in improved substrate removal efficiencies because the $S_{S,in}$ variations are accounted and related to the concentration of biomass present in the aerobic tank. The output variable of the system, F/M, can be calculated from online biomass measurements acquired through a turbidity probe and from offline $S_{S,in}$ determinations furnished periodically to the controller. In comparison with the classical chemostatic control, the F/M-auxostat may lead to safer results in what regards the substrate concentration in the effluent. As mentioned for each previous control strategies the F/M-auxostat must be also associated with a dissolved oxygen controller due to the nature of the bioprocess.

II.4.1.3. Dissolved Oxygen Control in WWTPs

Dissolved oxygen control is fundamental for any aerobic process and even more for the aerobic wastewater treatment process whose effluents are subjected to strict quality requirements. The dissolved oxygen, measured with common electrochemical or optical sensors, is manipulated through the control of the aeration rate.

As it was mentioned earlier a proper DO control can increase the substrate removal efficiency with up to 10%. In many cases the DO-stat is the single controller used for WWTPs, other variables being controlled in open loop. Thus, the DO-stat is of primal concern for any aerobic wastewater treatment process.

II.4.2. State-Space Representation of the Aerobic Wastewater Treatment Model

In the same spirit as approached for photobioreactors the aerobic wastewater treatment model will be rewritten in space-state form (Eq.II.4.2) according to the general nonlinear model (Eq.I.4.1). Most wastewater treatment plants are operated in continuous mode and therefore D is accounted as an input with significant influence over the system. The objective of a wastewater treatment plant is to achieve a good substrate removal efficiency and hence a low substrate concentration in the effluent, thus an inherent output is S_S. The disadvantage in many cases is that the substrate concentration is immeasurable due to the lack of specific sensors narrowing the control design to state estimators. S_S consumption is however the

effect of a fundamental process which is the biomass growth. The dilution also influences X_B dynamics fact based on which it was selected as controllable output remaining to analyze further how much the D control can manipulate each of the two outputs around characteristic operating points. On the other hand the complete mineralization of the substrate occurs at a positive S_O concentration which is manipulated by controlling the aeration rate. Another set of input – output variables must thus be considered: $W \; - S_O$.

$$\begin{cases} \dot{x} = \begin{bmatrix} \dot{X}_B \\ \dot{S}_S \\ \dot{S}_O \\ \dot{X}_R \end{bmatrix} = \begin{bmatrix} r_{X_B} \\ -r_{S_S} \\ -r_{S_O} \\ 0 \end{bmatrix} + \begin{bmatrix} -(1+r)X_B + rX_R \\ -(1+r)S_S + S_{S,in} \\ -(1+r)S_O + S_{O,in} \\ \frac{V}{V_s}\left((1+r)X_B - (\beta+r)X_R - \eta(1-\beta)X_R\right) \end{bmatrix} D + \begin{bmatrix} 0 \\ 0 \\ \alpha\left(S_{O,sat} - S_O\right) \\ 0 \end{bmatrix} W \\ y_1 = X_B \\ y_2 = S_S \\ y_3 = S_O \end{cases} \quad \text{(II.4.1)}$$

associated with a suite of algebraic equations: II.3.4 – II.3.8.

In addition, the F/M ratio expression (Eq.II.4.1) can be associated to the aerobic treatment model. Nevertheless, its variation is mainly given by the activated sludge dynamics and can be thus expressed as an algebraic equation.

II.4.3. WWTP's Main Steady-State Operating Points

The main operating points gravitates around the requirements of the European directive 91/271/CEE of May, 21st, 1991 which limits the concentration of substrate in the effluents at 0.125 g·L^{-1}, and around $S_{S,in}$ concentration. In this regard two main operating points were identified, for low and high $S_{S,in}$ concentration. The DO is also an important variable which strongly influences the bioprocess and therefore each operating point identified on substrate basis is discussed for 1, 2, 3 and 4 mg·L^{-1} DO. Thus, the eight steady-state points which will be used for further control design purposes are:

- $\boldsymbol{S_{S,in}}$ **= 0.8 g·L^{-1}**, X_B = 0.4403 g·L^{-1}, S_S = 0.1 g·L^{-1}, X_R = 0.4786 g·L^{-1} with
  - $\boldsymbol{S_O}$ **= 1 mg·L^{-1}**, D = 0.0140 h^{-1}, W = 1.9932 L·min^{-1} and F/M = 0.0253;
  - $\boldsymbol{S_O}$ **= 2 mg·L^{-1}**, D = 0.0172 h^{-1}, W = 2.8975 L·min^{-1} and F/M = 0.0313;
  - $\boldsymbol{S_O}$ **= 3 mg·L^{-1}**, D = 0.0184 h^{-1}, W = 3.7612 L·min^{-1} and F/M = 0.0335;
  - $\boldsymbol{S_O}$ **= 4 mg·L^{-1}**, D = 0.0191 h^{-1}, W = 4.9129 L·min^{-1} and F/M = 0.0347;

- $\boldsymbol{S_{S,in}}$ **= 3.0 g·L^{-1}**, X_B = 2.0545 g·L^{-1}, S_S = 0.1 g·L^{-1}, X_R = 2.2331 g·L^{-1} with
  - $\boldsymbol{S_O}$ **= 1 mg·L^{-1}**, D = 0.0140 h^{-1}, W = 9.3010 L·min^{-1} and F/M = 0.0204;
  - $\boldsymbol{S_O}$ **= 2 mg·L^{-1}**, D = 0.0172 h^{-1}, W = 13.4140 L·min^{-1} and F/M = 0.0251;
  - $\boldsymbol{S_O}$ **= 3 mg·L^{-1}**, D = 0.0184 h^{-1}, W = 17.2769 L·min^{-1} and F/M = 0.0269;
  - $\boldsymbol{S_O}$ **= 4 mg·L^{-1}**, D = 0.0191 h^{-1}, W = 22.3945 L·min^{-1} and F/M = 0.0278;

These steady-state operating points will be used further to obtain linear tangent models for interpreting the interferences which might appear when a multivariable control is aimed.

II.4.4. Nonlinear Multivariable Control of WWTPs

According to the space-state representation of the nonlinear model (Eq.II.4.2) the bioprocess is a non-square system with two inputs (*i.e.* D and W) and three outputs (*i.e.* X_B, S_S and S_O). Whereas W manipulation is known to lead to S_O control, D manipulation can lead to the control of both X_B and S_S. In order to square the system by eliminating the output which is poorly controlled around the steady-state operating points identified in the previous section, an NRG analysis must be realized on the non-square system (Eq.II.4.3):

$$\begin{bmatrix} X_B \\ S_S \\ S_O \end{bmatrix} = \begin{bmatrix} H_{i,D-X_B} & H_{i,W-X_B} \\ H_{i,D-S_S} & H_{i,W-S_S} \\ H_{i,D-S_O} & H_{i,W-S_O} \end{bmatrix} \begin{bmatrix} D \\ W \end{bmatrix} \tag{II.4.3}$$

The approach is similar with the one used for photobioreactors (section I.4.2.5) where the basic theory for NRG and RGA can be found. The transfer functions, obtained for the first operating point presented in the previous section, are:

$$H_{1,D-X_B}(s) = \frac{4.02\cdot10^{-1}\cdot s^3+7.17\cdot10^{-1}\cdot s^2+1.17\cdot10^{-1}\cdot s+2.72\cdot10^{-3}}{s^4+1.94\cdot s^3+4.14\cdot10^{-1}\cdot s^2+2.08\cdot10^{-2}\cdot s+1.76\cdot10^{-4}} \tag{II.4.4}$$

$$H_{1,D-S_S}(s) = \frac{6.00\cdot10^{-1}\cdot s^3+1.07\cdot s^2+1.73\cdot10^{-1}\cdot s+1.85\cdot10^{-3}}{s^4+1.94\cdot s^3+4.14\cdot10^{-1}\cdot s^2+2.08\cdot10^{-2}\cdot s+1.76\cdot10^{-4}} \tag{II.4.5}$$

$$H_{1,D-S_O}(s) = \frac{9.90\cdot10^{-14}\cdot s^3+2.49\cdot10\cdot s^2+4.43\cdot s+4.20\cdot10^{-2}}{s^4+1.94\cdot s^3+4.14\cdot10^{-1}\cdot s^2+2.08\cdot10^{-2}\cdot s+1.76\cdot10^{-4}} \tag{II.4.6}$$

$$H_{1,W-X_B}(s) = \frac{3.33\cdot10^{-3}\cdot s^2+5.94\cdot10^{-4}\cdot s+1.40\cdot10^{-5}}{s^4+1.94\cdot s^3+4.14\cdot10^{-1}\cdot s^2+2.08\cdot10^{-2}\cdot s+1.76\cdot10^{-4}} \tag{II.4.7}$$

$$H_{1,W-S_S}(s) = \frac{-10^{-15}\cdot s^3 - 4.97\cdot 10^{-3}\cdot s^2 - 8.86\cdot 10^{-4}\cdot s - 9.55\cdot 10^{-6}}{s^4 + 1.94\cdot s^3 + 4.14\cdot 10^{-1}\cdot s^2 + 2.08\cdot 10^{-2}\cdot s + 1.76\cdot 10^{-4}} \quad \text{(II.4.8)}$$

$$H_{1,W-S_O}(s) = \frac{1.39\cdot s^3 + 4.60\cdot 10^{-1}\cdot s^2 + 4.06\cdot 10^{-2}\cdot s + 3.68\cdot 10^{-4}}{s^4 + 1.94\cdot s^3 + 4.14\cdot 10^{-1}\cdot s^2 + 2.08\cdot 10^{-2}\cdot s + 1.76\cdot 10^{-4}} \quad \text{(II.4.9)}$$

The transfer function matrix at steady-state for the linear model (II.4.4 – II.4.9) will thus be:

$$H_1(0) = \begin{bmatrix} 2.72\cdot 10^{-3}/1.76\cdot 10^{-4} & 1.40\cdot 10^{-5}/1.76\cdot 10^{-4} \\ 1.85\cdot 10^{-3}/1.76\cdot 10^{-4} & -9.55\cdot 10^{-6}/1.76\cdot 10^{-4} \\ 4.20\cdot 10^{-2}/1.76\cdot 10^{-4} & 3.68\cdot 10^{-4}/1.76\cdot 10^{-4} \end{bmatrix} \quad \text{(II.4.10)}$$

Considering that the system is not independent of output scaling the diagonal inverse matrix, filled with the steady-state values used for linearization of the nonlinear model, was employed:

$$S_{1,y}^{-1} = \begin{bmatrix} 1/0.4403 & 0 & 0 \\ 0 & 1/0.1000 & 0 \\ 0 & 0 & 1 \end{bmatrix} \quad \text{(II.4.11)}$$

It must be noted that the other operating points gave similar results and therefore their transfer functions were not displayed. The results obtained through the linearization of the nonlinear model around the eight steady-state operating points are the following:

$$\Lambda_1^{0.8} = \begin{bmatrix} 0.0236 & -0.0047 \\ 0.6237 & 0.3690 \\ 0.3527 & 0.6357 \end{bmatrix}; \Lambda_2^{0.8} = \begin{bmatrix} 0.0488 & -0.0106 \\ 0.7507 & 0.2163 \\ 0.2005 & 0.7943 \end{bmatrix}; \Lambda_3^{0.8} = \begin{bmatrix} 0.0710 & -0.0080 \\ 0.8256 & 0.1145 \\ 0.1034 & 0.8935 \end{bmatrix}; \Lambda_4^{0.8} = \begin{bmatrix} 0.0844 & -0.0048 \\ 0.8622 & 0.0601 \\ 0.0534 & 0.9447 \end{bmatrix};$$

$$\Lambda_1^{3.0} = \begin{bmatrix} 0.0007 & -0.0002 \\ 0.5831 & 0.4168 \\ 0.4162 & 0.5834 \end{bmatrix}; \Lambda_2^{3.0} = \begin{bmatrix} 0.0019 & -0.0005 \\ 0.7338 & 0.2651 \\ 0.2643 & 0.7355 \end{bmatrix}; \Lambda_3^{3.0} = \begin{bmatrix} 0.0031 & -0.0004 \\ 0.8491 & 0.1484 \\ 0.1478 & 0.8520 \end{bmatrix}; \Lambda_4^{3.0} = \begin{bmatrix} 0.0040 & -0.0003 \\ 0.9163 & 0.0801 \\ 0.0797 & 0.9202 \end{bmatrix} \quad \text{(II.4.12)}$$

where the subscripts represent the S_O concentration and the superscripts $S_{S,in}$ concentration. Summing each row of each NRG matrix (II.4.12) it can be observed that the first row takes the smallest value which indicates that X_B will be poorly controlled through D in the given configuration. Apparently, D has increased influence over X_B and negligible effect over S_S at

higher values, case which was encountered in section I.4.2.5.4 regarding PBRs when the substrate was the total inorganic nitrogen. Thus, the system can be squared by neglecting $D \rightarrow X_{\mathrm{B}}$ interactions.

II.4.4.1. Nonlinear Multivariable Substrate and DO Control

The objective of such strategy is to control simultaneously in closed loop both measurable or estimable outputs, S_{S} and S_{O}, by manipulating D and W. This control strategy was discussed by Nejjari *et al.*, (1999) for a similar model and validated in simulation. The squared system (II.4.13) will thus consist of two inputs $u = [u_1\ u_2] = [D\ W]$, four states $x^T = [x_1\ x_2\ x_3\ x_4] = [X_{\mathrm{B}}\ S_{\mathrm{S}}\ S_{\mathrm{O}}\ X_{\mathrm{R}}]$ and two outputs $y = [y_1\ y_2] = [S_{\mathrm{S}}\ S_{\mathrm{O}}]$.

II.4.4.1.1. *S- and DO-stat RGA Analysis*

In order to deliberate if the system allows the implementation of decentralized SISO controllers or requires centralized MIMO controllers, the degree of interaction between I/O signals (*i.e.* $D \rightarrow S_{\mathrm{S}}$ and $W \rightarrow S_{\mathrm{O}}$) must be quantified through a RGA analysis. A similar analysis can be found in Barbu, (2009) for a resembling case. The RGA procedure is thus reiterated for the square system (II.4.13).

$$\begin{bmatrix} S_{\mathrm{S}} \\ S_{\mathrm{O}} \end{bmatrix} = \begin{bmatrix} H_{i,D-S_{\mathrm{S}}} & H_{i,W-S_{\mathrm{S}}} \\ H_{i,D-S_{\mathrm{O}}} & H_{i,W-S_{\mathrm{O}}} \end{bmatrix} \begin{bmatrix} D \\ W \end{bmatrix} \tag{II.4.13}$$

The transfer function matrix at steady-state obtained for the linear model given by the II.4.5, II.4.6, II.4.8 and II.4.9 which corresponds to the first operating point is:

$$H_1(0) = \begin{bmatrix} 1.85 \cdot 10^{-3}/1.76 \cdot 10^{-4} & -9.55 \cdot 10^{-6}/1.76 \cdot 10^{-4} \\ 4.20 \cdot 10^{-2}/1.76 \cdot 10^{-4} & 3.68 \cdot 10^{-4}/1.76 \cdot 10^{-4} \end{bmatrix} \tag{II.4.14}$$

The square systems are independent of output and input scaling and hence the RGAs obtained through the linearization of the nonlinear model around the eight steady-state operating points are the following:

$$\Lambda_1^{0.8} = \begin{bmatrix} 0.6298 & 0.3702 \\ 0.3702 & 0.6298 \end{bmatrix};\ \Lambda_2^{0.8} = \begin{bmatrix} 0.7778 & 0.2222 \\ 0.2222 & 0.7778 \end{bmatrix};\ \Lambda_3^{0.8} = \begin{bmatrix} 0.8795 & 0.1205 \\ 0.1205 & 0.8795 \end{bmatrix};\ \Lambda_4^{0.8} = \begin{bmatrix} 0.9358 & 0.0642 \\ 0.0642 & 0.9358 \end{bmatrix}$$

$$\Lambda_1^{3.0} = \begin{bmatrix} 0.5832 & 0.4168 \\ 0.4168 & 0.5832 \end{bmatrix}; \Lambda_2^{3.0} = \begin{bmatrix} 0.7347 & 0.2653 \\ 0.2653 & 0.7347 \end{bmatrix}; \Lambda_3^{3.0} = \begin{bmatrix} 0.8512 & 0.1488 \\ 0.1488 & 0.8512 \end{bmatrix}; \Lambda_4^{3.0} = \begin{bmatrix} 0.9197 & 0.0803 \\ 0.0803 & 0.9197 \end{bmatrix} \quad \text{(II.4.15)}$$

The matrices maintain their diagonal dominance for all steady-state operating points which denotes that the control channels were well chosen. The interferences (anti-diagonal) are however significant for low S_O concentrations and register a slight increase with the increase of $S_{S,in}$ concentration. Considering that many aerobic WWTPs are working at S_O concentrations ranging from 1 mg·L^{-1} to maximum 3 mg·L^{-1}, for reasons of costs, the nonlinear multivariable control is recommended to be done through centralized MIMO controllers in order to assure accurate tracking of setpoints.

In order to obtain the RGAs, the dynamic model (Eq.II.4.2) was reconstructed in Simulink® and linearized in Matlab® by using the `linmod` function.

II.4.4.1.2. *S- and DO- Feedback Linearizing Control*

The feedback linearizing control technique which was presented in section I.4.2.6 can be also used for the present case deriving the following I/O model:

$$\begin{bmatrix} \dot{S}_S \\ \dot{S}_O \end{bmatrix} = \begin{bmatrix} -r_{S_S} \\ -r_{S_O} \end{bmatrix} + \begin{bmatrix} -(1+r)S_S + S_{S,in} & 0 \\ -(1+r)S_O + S_{O,in} & \alpha(S_{O,sat} - S_O) \end{bmatrix} \begin{bmatrix} D \\ W \end{bmatrix} \quad \text{(II.4.16)}$$

The characteristic matrix of the system is nonsingular because $(-(1+r)S_S + S_{S,in})$ and $\alpha(S_{O,sat} - S_O)$ are always different than zero. The objective of the control algorithm is to keep S_S and S_O closely around the prescribed values $y^* = [y_1^* \; y_2^*] = [S_S^* \; S_O^*]$ by actuating D and W. The relative degree for both state variables, S_S and S_O, is equal to one since the inputs (*i.e.* D and W) appear explicitly after the first derivation (Eq.II.3.11 and II.3.12). The control algorithms which result through FLC technique (section I.4.2.6) are:

$$u = \begin{bmatrix} u_1 = D = \frac{\varphi_{S_S} er_{S_S} + r_{S_S}}{-(1+r)S_S + S_{S,in}} \\ u_2 = W = \frac{(1+r)S_O - S_{O,in}}{\alpha(S_{O,sat} - S_O)} D + \frac{\varphi_{S_O} er_{S_O} + r_{S_O}}{\alpha(S_{O,sat} - S_O)} \end{bmatrix} \quad \text{(II.4.17)}$$

where:

$$er_{S_S} = S_S^* - S_S \quad \text{(II.4.18)}$$

$$er_{S_O} = S_O^* - S_O \quad \text{(II.4.19)}$$

II.4.4.1.3. *Results in Simulation*

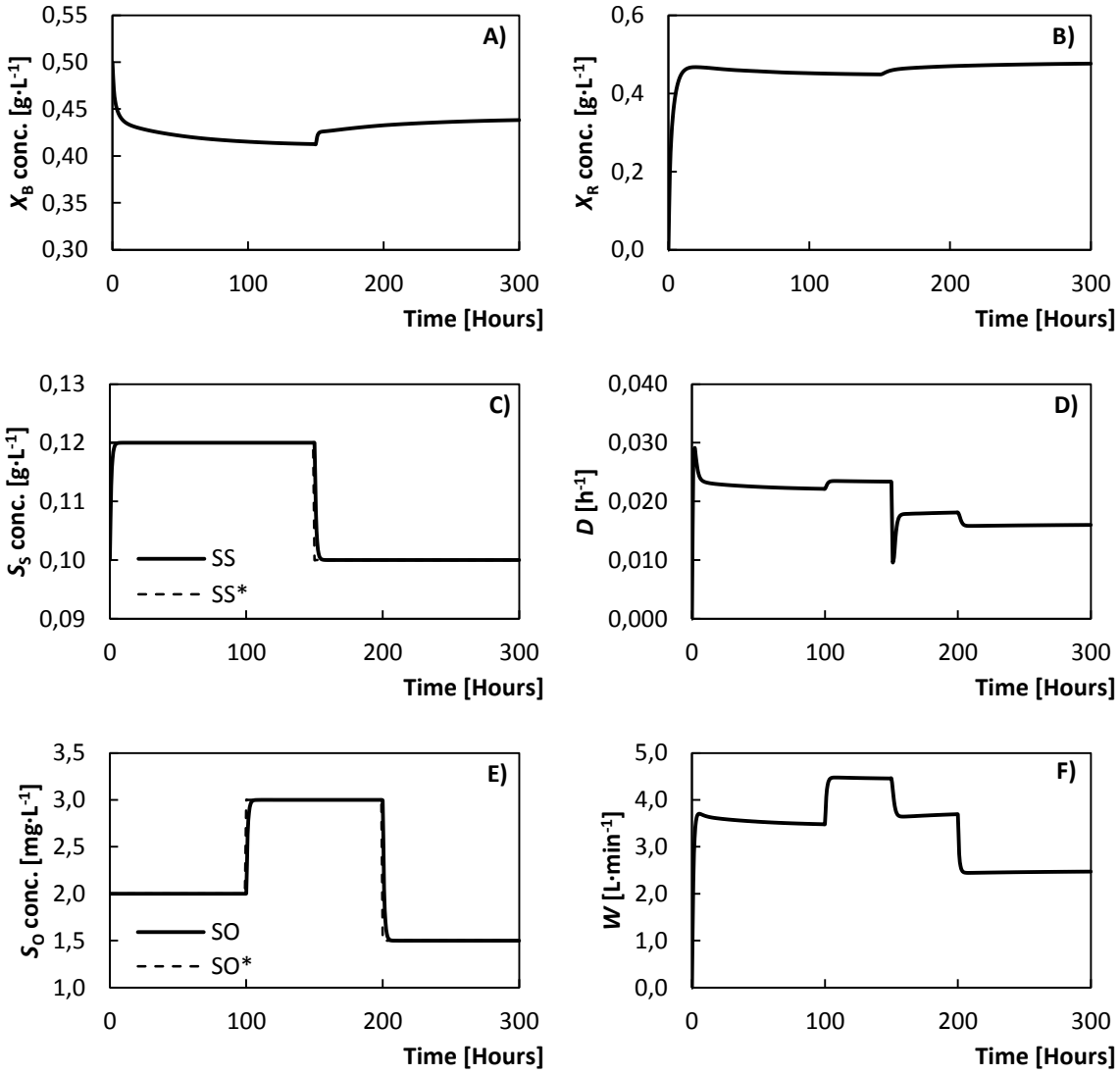

Fig.II.4.1. S- and DO-stat control in aerobic WWTPs (A – Sludge concentration, B – recycled biomass, C – COD concentration, D – dilution rate, E – dissolved oxygen concentration and F – aeration rate)

The control algorithms were validated in simulation (Fig.II.4.1) using for initialization the following values: $X_{B,0}$ = 0.5 g·L^{-1}, $S_{S,0}$ = 0.1 g·L^{-1}, $S_{O,0}$ = 2 mg·L^{-1}, X_R = 0 g·L^{-1} while $S_{S,in}$ = 0.8 g·L^{-1} and $S_{O,in}$ = 2 mg·L^{-1}.

II.4.4.2. Nonlinear Multivariable F/M Ratio and DO Control

The objective of this strategy is to control simultaneously in closed loop both measurable or estimable outputs, $\mathrm{F/M}$ and S_O, by manipulating D and W. The square system (II.4.20) will thus consist of two inputs $u = [u_1\ u_2] = [D\ W]$, five state variables $x^T = [x_1\ x_2\ x_3\ x_4\ x_4] = [X_\mathrm{B}\ S_\mathrm{S}\ S_\mathrm{O}\ X_\mathrm{R}\ \mathrm{F/M}]$ and two outputs $y = [y_1\ y_2] = [\mathrm{F/M}\ S_\mathrm{O}]$. The fifth state variable is practically the F/M ratio described through Eq.II.4.1.

II.4.4.2.1. *F/M- and DO-stat RGA Analysis*

The degree of interaction between I/O signals, $D \rightarrow \mathrm{F/M}$ and $W \rightarrow S_\mathrm{O}$, is quantified through a RGA analysis on the following square system:

$$\begin{bmatrix}\mathrm{F/M}\\ S_\mathrm{O}\end{bmatrix} = \begin{bmatrix}H_{i,D-\mathrm{F/M}} & H_{i,W-\mathrm{F/M}}\\ H_{i,D-S_\mathrm{O}} & H_{i,W-S_\mathrm{O}}\end{bmatrix}\begin{bmatrix}D\\ W\end{bmatrix} \tag{II.4.20}$$

The transfer functions which correspond to the first operating point are:

$$H_{1,D-\mathrm{F/M}}(s) = \frac{1.82\cdot s^4+3.54\cdot s^3+7.93\cdot 10^{-1}\cdot s^2+4.46\cdot 10^{-2}\cdot s+4.77\cdot 10^{-4}}{s^5+2.94\cdot s^4+2.35\cdot s^3+4.34\cdot 10^{-1}\cdot s^2+2.10\cdot 10^{-2}\cdot s+1.76\cdot 10^{-4}} \tag{II.4.21}$$

$$H_{1,D-S_\mathrm{O}}(s) = \frac{9.90\cdot 10^{-14}\cdot s^4+2.49\cdot 10\cdot s^3+2.93\cdot 10\cdot s^2+4.47\cdot s+4.20\cdot 10^{-2}}{s^5+2.94\cdot s^4+2.35\cdot s^3+4.34\cdot 10^{-1}\cdot s^2+2.10\cdot 10^{-2}\cdot s+1.76\cdot 10^{-4}} \tag{II.4.22}$$

$$H_{1,W-\mathrm{F/M}}(s) = \frac{10^{-15}\cdot s^4+10^{-15}\cdot s^3-1.92\cdot 10^{-4}\cdot s^2-3.43\cdot 10^{-5}\cdot s-8.09\cdot 10^{-7}}{s^5+2.94\cdot s^4+2.35\cdot s^3+4.34\cdot 10^{-1}\cdot s^2+2.10\cdot 10^{-2}\cdot s+1.76\cdot 10^{-4}} \tag{II.4.23}$$

$$H_{1,W-S_\mathrm{O}}(s) = \frac{1.39\cdot s^4+1.85\cdot s^3+5.01\cdot s^2+4.10\cdot 10^{-2}\cdot s+3.68\cdot 10^{-4}}{s^5+2.94\cdot s^4+2.35\cdot s^3+4.34\cdot 10^{-1}\cdot s^2+2.10\cdot 10^{-2}\cdot s+1.76\cdot 10^{-4}} \tag{II.4.24}$$

From the linear model (II.4.21 – II.4.24) the following transfer function matrix is obtained:

$$H_1(0) = \begin{bmatrix}4.77\cdot 10^{-4}/1.76\cdot 10^{-4} & -8.09\cdot 10^{-7}/1.76\cdot 10^{-4}\\ 4.20\cdot 10^{-2}/1.76\cdot 10^{-4} & 3.68\cdot 10^{-4}/1.76\cdot 10^{-4}\end{bmatrix} \tag{II.4.25}$$

The results obtained for the other operating points were not presented here, but it must be mentioned that similar responses were attained. The RGAs obtained through the linearization of the nonlinear model around the eight steady-state operating points are the following:

$$\Lambda_1^{0.8} = \begin{bmatrix} 0.8379 & 0.1621 \\ 0.1621 & 0.8379 \end{bmatrix}; \Lambda_2^{0.8} = \begin{bmatrix} 0.9353 & 0.0647 \\ 0.0647 & 0.9353 \end{bmatrix}; \Lambda_3^{0.8} = \begin{bmatrix} 0.9714 & 0.0286 \\ 0.0286 & 0.9714 \end{bmatrix}; \Lambda_4^{0.8} = \begin{bmatrix} 0.9861 & 0.0139 \\ 0.0139 & 0.9861 \end{bmatrix}$$

$$\Lambda_1^{3.0} = \begin{bmatrix} 0.9138 & 0.0862 \\ 0.0862 & 0.9138 \end{bmatrix}; \Lambda_2^{3.0} = \begin{bmatrix} 0.9750 & 0.0250 \\ 0.0250 & 0.9750 \end{bmatrix}; \Lambda_3^{3.0} = \begin{bmatrix} 0.9900 & 0.0100 \\ 0.0100 & 0.9900 \end{bmatrix}; \Lambda_4^{3.0} = \begin{bmatrix} 0.9953 & 0.0047 \\ 0.0047 & 0.9953 \end{bmatrix} \quad \text{(II.4.26)}$$

The diagonal dominance of the matrices is observed for all steady-state operating points, denoting a proper selection of the control channels (*i.e.* $D \rightarrow \mathrm{F/M}$ and $W \rightarrow S_{\mathrm{O}}$). For this particular case the interferences (anti-diagonal) are negligible regardless of the $S_{\mathrm{S,in}}$ and S_{O} concentrations. Consequently, the multivariable F/M- and DO-stat control can be performed through decentralized SISO controllers.

II.4.4.2.2. *F/M- and DO- Feedback Linearizing Control*

The same FLC technique is used to synthesize the control algorithms. Due to the fact that decoupled SISO controllers can be used, the W expression remains the one from Eq.II.4.17 while the dilution rate is expressed through:

$$D = \frac{X_{\mathrm{B}}\left(\varphi_{\mathrm{F/M}} er_{\mathrm{F/M}} - \mathrm{F/M}\right)}{S_{\mathrm{S,in}}} \quad \text{(II.4.27)}$$

where:

$$er_{\mathrm{F/M}} = \mathrm{F/M}^{*} - \mathrm{F/M} \quad \text{(II.4.28)}$$

II.4.4.2.3. *Results in Simulation*

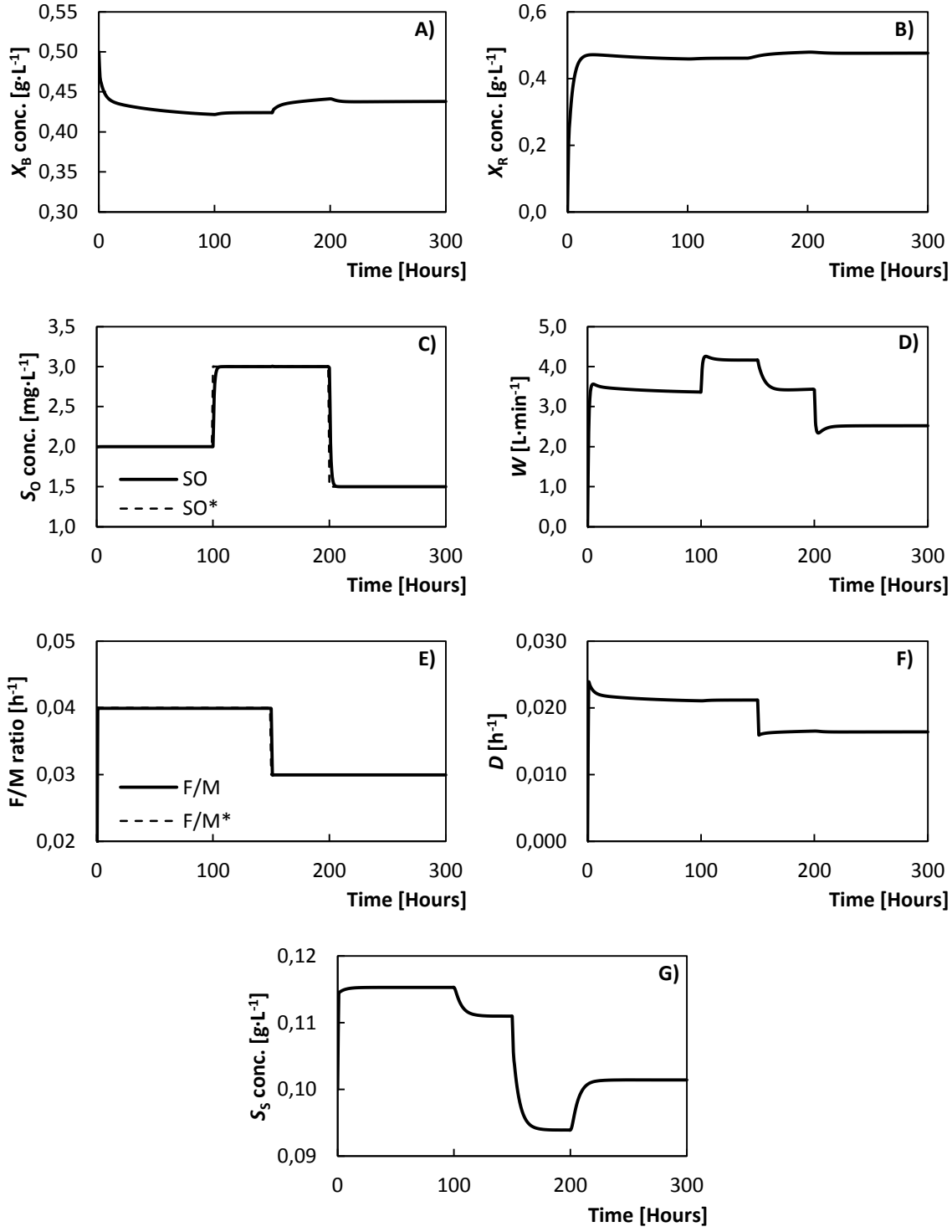

Fig.II.4.2. F/M- and DO-stat control in aerobic WWTPs (A – Sludge concentration, B – recycled biomass, C – dissolved oxygen concentration, D – aeration rate, E – F/M ratio, F – dilution rate and G – COD concentration)

The control algorithms were validated in simulation (Fig.II.4.2) using for initialization the following values: $X_{B,0}$ = 0.5 g·L^{-1}, $S_{S,0}$ = 0.1 g·L^{-1}, $S_{O,0}$ = 2 mg·L^{-1}, X_R = 0 g·L^{-1}, F/M = 0 h^{-1} while $S_{S,in}$ = 0.8 g·L^{-1} and $S_{O,in}$ = 2 mg·L^{-1}.

II.4.5. Linear Monovariable Control of WWTPs

The mass balance model presented in section II.3.3 is able to describe with satisfactory precision the main state variables (*i.e.* sludge concentration, carbonaceous substrate, dissolved oxygen and recycled sludge) of any conventional aerobic wastewater treatment process with the condition to identify for each case a new set of parameters. Unlike the axenic cultures of microalgae whose parameters confer a certain degree of confidence owing to the nature of the process, the activated sludge, which comprises dozens of species of microorganisms with different growth rates, leads almost every time to uncertainties regarding the parameters of the model. The uncertainties are not given only by the activated sludge dynamics but also by the influent whose concentration and/or composition of organic compounds vary during a day, both for municipal and industrial plants. The volume and the composition of wastewaters also depend of rainfall which washes the urban and industrial platforms and which is collected through the sewage network. All these aspects must be considered in order to synthesize reliable control algorithms able to globally stabilize the aerobic wastewater treatment process.

Another widespread problem is the lack of reliable sensors for the online measurement of the main state variables (especially of the substrate) which limits the control of WWTPs to open loop systems.

The multivariable control algorithm (for S_S and S_O) proposed in section II.4.4.1 can be implemented on the wastewater treatment pilot plant only in the presence of a substrate sensor or a substrate observer. Because the wastewater treatment pilot is provided only with a dissolved oxygen sensor and because the model was considered not precise enough (for several operating points or types of wastewater), the control problematics was reduced to a linear feedback control of the dissolved oxygen (which is a fundamental state variable of the process) while the substrate remained to be controlled in open loop.

Nevertheless, as highlighted through matrices II.4.15, the interferences caused by $D \rightarrow S_S$ channel are significant and therefore the DO controller must be robust enough to reject any possible disturbance.

II.4.5.1. Robust Control of Monovariable Processes Using QFT method

Under these circumstances a linear robust control method, QFT – Quantitative Feedback Theory, is proposed in the following lines for the feedback control of the dissolved oxygen. The QFT is a linear method proposed by Horowitz (1973) which is frequently applied to processes described through models with variable parameters.

The QFT method is using the Nichols frequency characteristics and attempts to provide a robust design over a specified area of the process with parametric uncertainties. In order to apply this method to the aerobic wastewater treatment process which is strongly nonlinear the plant model must be linearized around several operating points. The result is a linear model with variable parameters, which describes the process behavior for any operating point. To include the influence of parametric uncertainties which affect the nonlinear process the variation limits of the parameters on the linear model can be extended. The robust controller using the QFT technique is therefore designed for the linear model thus obtained.

The output, $y(t)$, of the closed loop system must be bounded as presented in Fig.II.4.3 which displays the response to a step signal for both limits (upper and lower) in the time domain. The QFT method ensures the operation of a linear system with variable parameters within the imposed domain of evolution.

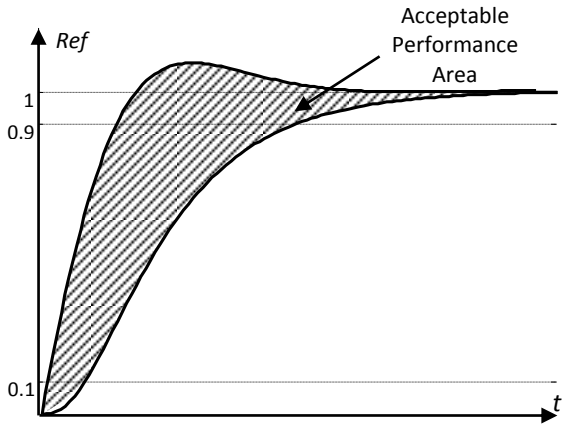

Fig.II.4.3. Upper and lower bounds of the system output

The process is described through a variable parameter transfer function:

$$P(s) = \frac{Ka}{s(s+a)} \qquad \text{(II.4.29)}$$

where the parameters K and a vary according to the operating conditions – $K \in [K_{min}, K_{max}]$ and $a \in [a_{min}, a_{max}]$.

The design control scheme of the system is presented in Fig.II.4.4:

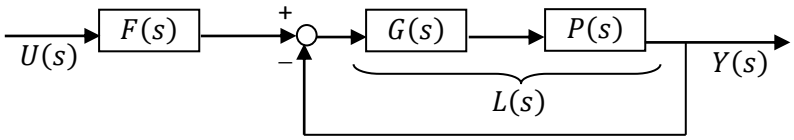

Fig.II.4.4. Linear compensated system

The QFT method lies in the synthesis of a compensator $G(s)$ and a prefilter $F(s)$ for the behavior of the closed loop system to be bounded by the limits imposed to the system. Details regarding the quantitative feedback theory can be found in Houpis and Rasmussen, (1999) and Barbu and Caraman, (2011).

II.4.5.2. QFT Control of Dissolved Oxygen Concentration

II.4.5.2.1. *Identification of the Dissolved Oxygen Control Loop*

The results regarding the synthesis a of the QFT controller for the dissolved oxygen in a WWTP are already published in Barbu *et al.*, (2010). The identification of the DO control loop was realized on a few experiments with wastewater from dairy and beer industry, being observed that its evolution corresponds to the evolution of a first order system. In order to model the DO as a function of W a first order transfer function with variable parameters was considered:

$$H(s) = \frac{K}{Ts+1} \tag{II.4.30}$$

where, the gain factor $K \in [0.8\ 1.4]$ and the time constant of the first order element $T \in [1700\ 2500]$. The ranges result from the identification experiments performed on data from various experiments on dairy, beer and synthetic wastewaters.

II.4.5.2.2. *Design of the Dissolved Oxygen Control Structure*

The bounds imposed to the closed loop system which gives the accepted performance area were determined by taking into account the variation limits of the linear model (Eq.II.4.30) and therefore the two tracking model are:

$$H_{rs}(s) = \frac{10(s+0.1)}{(s+0.007 \pm j0.007)} \quad \text{(II.4.31)}$$

$$H_{ri}(s) = \frac{1}{(300s+1)(310s+1)(30s+1)} \quad \text{(II.4.32)}$$

The steps in the design methodology of QFT (Barbu and Caraman, 2011) for a setpoint tracking problem were accomplished by starting from the linear model with variable parameters (Eq.II.4.30) and from the two tracking models (Eq.4.31 and Eq.4.32). Using the QFT toolbox from MATLAB, the following characteristics were determined: the stability contour, the robust tracking bounds, the overlapping of the stability contours and tracking bounds and, finally, the optimal tracking bounds that will be used in the design of the controller $G(s)$.

The transfer functions of the controller $G(s)$ and of the prefilter $F(s)$, obtained through the QFT toolbox, are the following:

$$G(s) = \frac{0.22143(s+0.00039)}{s(s+0.01217)} \quad \text{(II.4.33)}$$

$$F(s) = \frac{0.0068}{s+0.0068} \quad \text{(II.4.34)}$$

The controller transfer function $G(s)$ also includes an integral component and since the input variable (*i.e.* W) saturates at 25 L·min^{-1} (a characteristic of the air compressor), the implementation of an anti-wind-up structure was required. This structure can prevent the saturation of the control variable (unacceptable values for the integrator) improving the dynamic regime of the controller. A detailed discussion regarding the Black-Nichols characteristics, the overlapping of the stability contours and tracking bounds and simulations using four extreme transfer functions which correspond to the extreme values of the parameters in Eq.II.4.30 can be found in Barbu *et al.*, (2010).

II.5. PRACTICAL IMPLEMENTATION

The lack of specific sensors for the online measurement of the substrate narrowed the control problematics to the monovariable DO-control. The QFT robust controller (section II.4.5.2) was implemented on the wastewater treatment pilot and validated in an experiment with synthetic wastewater. The experiment was unfolded throughout app. 380 hours, the first 220 hours being assigned to the operation of the pilot without recycling while during the last hours the sludge recycling was switched on.

The DO concentration was maintained throughout the whole experiment at 2 $mg \cdot L^{-1}$ as it can be observed in Fig.II.5.1. The robust QFT controller efficiency at other setpoints and on other types of wastewaters was published in Barbu *et al.*, (2010).

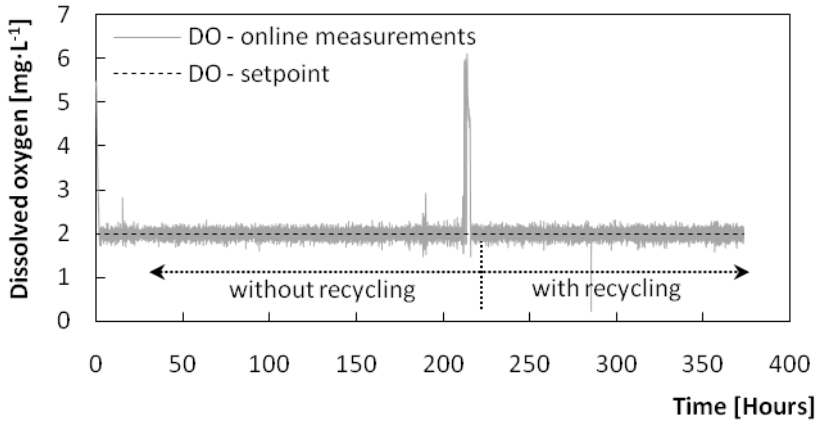

Fig.II.5.1. Robust DO control on various operating points

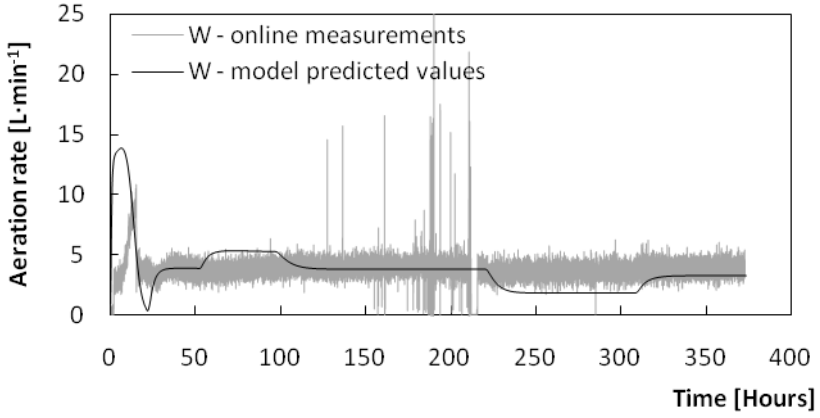

Fig.II.5.2. Time evolution or the aeration rate required to maintain the DO at 2 $mg \cdot L^{-1}$

The DO controller led to a precision of ± 0.08 σ regardless of the operating point. The noise

registered around the 215th hour of operation is due to a technical failure. The incident however highlights the ability of the DO controller to precisely track its setpoint.

Fig.II.5.2 displays the aeration rate required to maintain the DO concentration at 2 mg·L^{-1}. As mentioned in the previous section the control variable saturates at 25 L·min^{-1} and results that the controller is able to rationalize the air consumption and hence the electrical costs. The experimental data acquired from the pilot are compared with the response of the aerobic wastewater treatment model presenting a satisfactory fitting. Thus, the model can be used to predict the electrical consumption with air for any concentration of organics in the wastewater.

In what regards the substrate, the WWTP was operated in open loop at various dilution rates in order to demonstrate the effectiveness of the DO controller to reject any disturbances given by the significant interferences of the $D \rightarrow S_S$ control channel.

The aerobic tank was provided with a turbidity sensor whose signal was correlated with offline dry mass measurements through linear regression. The correlation (0.005*Turbidity + 0.4496) is made on a limited range of biomass concentrations, but the good matching makes the turbidity signal a good candidate for online sludge concentration measurements aiming in perspective the control of the F/M Ratio. The turbidity signal (converted into dry mass units) was compared with the response of the aerobic wastewater treatment model and displayed in Fig.II.5.3.

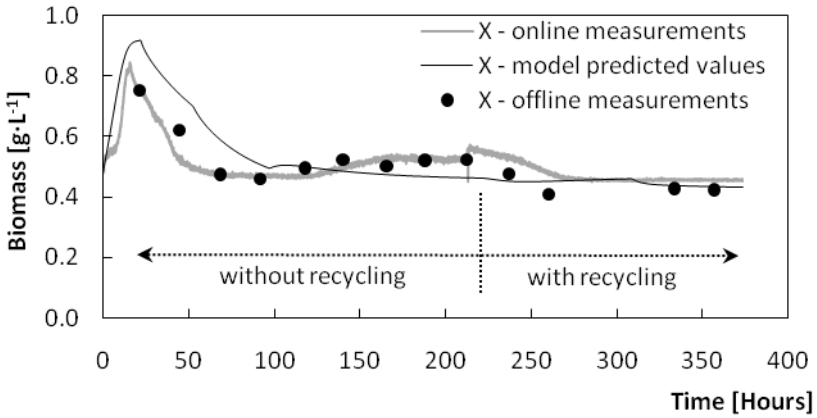

Fig.II.5.3. Time evolution of sludge concentration

The model is able to predict the general tendency of the sludge concentration but the mismatch is significant around certain operating points. However, the parametric uncertainties were questioned and led to the decision of designing a reliable robust controller

for the concentration of dissolved oxygen.

Fig.II.5.4 presents the dilution rate used during the experimentation. It must be mentioned that during the first 24 hours after inoculation, the pilot was operated in discontinuous mode in order to let the sludge to accumulate and to help the sludge flocs to form.

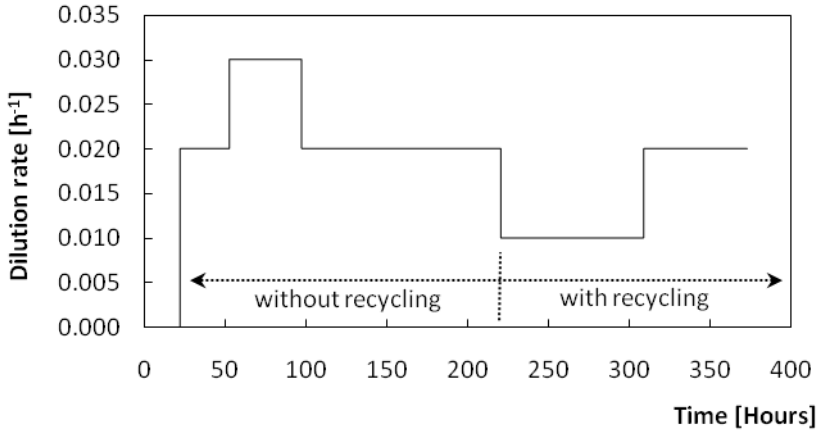

Fig.II.5.4. The variation of dilution rate in open loop

The evolution of COD concentration (offline measurements) in the aerobic tank is presented in Fig.II.5.5 along with the response of the aerobic wastewater treatment model.

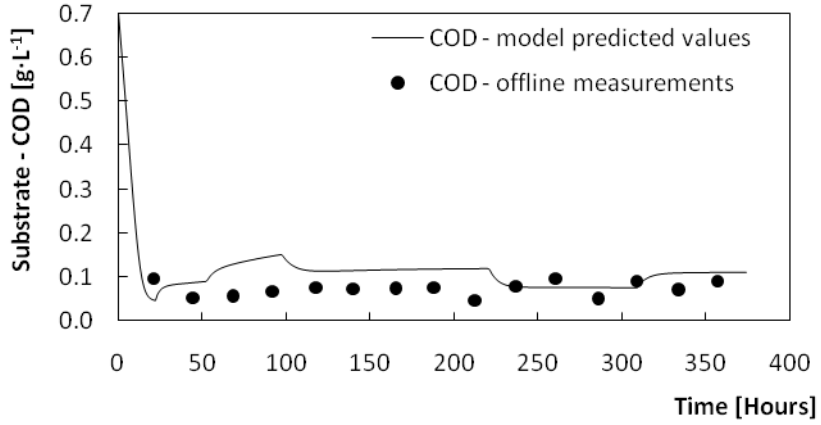

Fig.II.5.5. COD variation at various operation points

During the second part of the experiment three samples from the recycling line were analyzed and compared with the response of the aerobic wastewater treatment model. Fig.II.5.6 depicts the satisfactory fitting between the offline measurements regarding the recycled sludge concentration and the model response. Thus, the empirical model proposed in section II.3.2.3,

can represent a good tool for predicting the recycled sludge concentration.

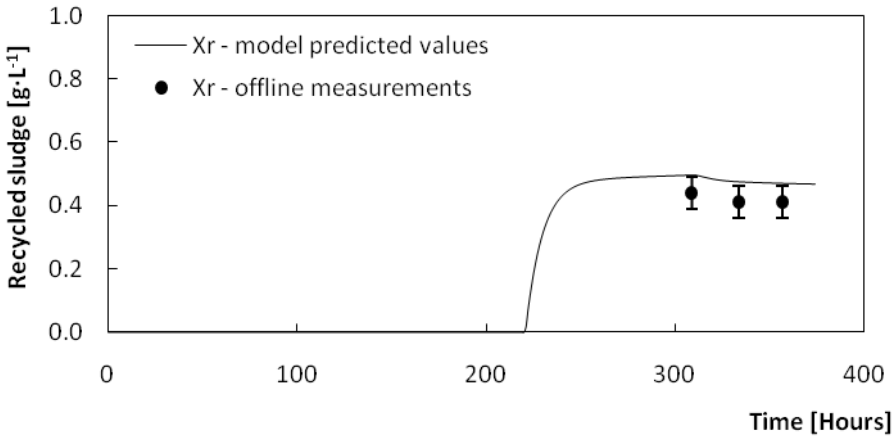

Fig.II.5.6. Recycled sludge concentration (error bars of 0.05 $g \cdot L^{-1}$)

Even though there are certain mismatches between experimental values and model response, it remains a valuable tool for control purposes since they can be easily minimized through specific feedback mechanisms.

Conclusions regarding the control of WWTP

The nonlinear multivariable control of substrate and dissolved oxygen was discussed and the necessity of using a centralized MIMO controller was determined through a RGA analysis. A feedback linearizing controller was proposed and validated in simulation. In addition, a feedback linearizing control algorithm was proposed and validated in simulation for the nonlinear multivariable control of F/M ration and dissolved oxygen. Due to the lack of specific sensors for online substrate measurements and to the parametric uncertainties a robust linear controller was proposed for the dissolved oxygen by using the quantitative feedback theory. The robust controller was implemented on the pilot plant presenting excellent results for various operating points.

PART III

PERSPECTIVES OF COUPLING BETWEEN AN AEROBIC WASTEWATER TREATMENT PLANT AND A PHOTOBIOREACTOR: CASE STUDY

III.1. MODELING OF THE COUPLING BETWEEN WWTP AND PBR

***Abstract*:** The coupling between the photobioreactor presented in the first part of this thesis and the aerobic wastewater treatment plant presented in the second part will be studied in simulation in the following sections from a modeling and control point of view. The coupling aims only the exchange of gases considering that the effluent of the wastewater treatment plant was depleted of nutrients during the aerobic stage. However, the nutrients consumption (*i.e.* nitrogen and phosphorus) can be expressed for both reactors through simple stoichiometric equations such as Eq.I.3.12 and Eq.I.5.2.

The modeling of the coupling between the WWTP and the PBR derives practically from the association of their individual models which were already developed in the first parts of this thesis. Despite the antagonism between the two processes (*i.e.* aerobic respiration and photosynthesis) the common modeling approach of the two pilots ease the modeling of the coupling itself. In this case, the connection between the two models lies in the exchange of gases, the O_2 produced trough photosynthesis represents a substrate for the aerobic bacteria while the CO_2 derived from the respiration of aerobes become a substrate for photoautotrophs. The mass balance of the two gases was described in detail for PBR while for the WWTP only the O_2 was modeled. The CO_2 is of no particular interest for the aerobic treatment process and therefore was poorly modeled. The CO_2 produced through aerobic respiration dissolves in water establishing a series of equilibria (Eq.I.3.2). Thus, the TIC dissolved in the aerobic tank can be expressed through the following equation:

$$r_{S_{\mathrm{TIC}}} = \frac{1-Y}{Y}\frac{r_{X_{\mathrm{B}}}}{M_x} \tag{III.3.1}$$

where $r_{S_{\mathrm{TIC}}}$ is the TIC production rate. $(1-Y)/Y$ comes from the parity between CO_2 produced and O_2 consumed to mineralize the organics. In terms of mass balance the TIC dynamics will be given by:

$$\frac{dS_{\mathrm{TIC}}}{dt} = r_{S_{\mathrm{TIC}}}(t) + N_{\mathrm{CO_2}}(t) - D(t)(1+r)S_{\mathrm{TIC}}(t) + D(t)S_{\mathrm{TIC,in}} \tag{III.3.2}$$

$N_{\mathrm{CO_2}}$ is the volumetric mass transfer rate for carbon dioxide and was defined in the first part of the thesis (Eq.I.3.15). For simplification $S^*_{\mathrm{CO_2}}$ (the saturation constant for CO_2) can be

considered as being equal with 0.03 mol·L^{-1}. In addition, S_{CO_2}, the actual concentration of dissolved carbon dioxide, will be approximated with 5% of TIC at a pH of 7.5 while the rest of 95% will be converted to HCO_3^- and CO_3^{2-}. The model can be written, if required, more detailed adding the output molar fractions ant the equilibria of the ternary solute system (*i.e.* $NH_3 - CO_2 - H_2O$) presented in the first part for PBRs. The influent was assumed to be deficient in inorganic carbon, thus $S_{TIC,in}$ = 0.

The output volumetric rate of CO_2 ($g_{out}^{CO_2}$) results from a basic mass balance equation:

$$\frac{dg_{out}^{CO_2}}{dt} = g_{in}^{CO_2}(t) - g_{out}^{CO_2}(t) - VN_{CO_2}(t) \quad \text{(III.3.3)}$$

where $g_{in}^{CO_2}$ is the input volumetric rate of CO_2. The volumetric rates ($g_{in|out}^{i}$) have the same meaning as the variables described for PHB denoted with $G_{in|out}^{i}$. A similar mass balance equation can be written for output O_2, but the air composition must be taken into account.

The WWTP model was validated in simulation targeting in perspective its validation with experimental data. The numerical simulations presented in Fig.III.1.1 correspond to the case when S_S = 0.1 g·L^{-1} and S_O = 2 mg·L^{-1} pending 500 hours. The initial values of the state variables were set to X_B = 0.4 g·L^{-1}, S_S = 0.1 g·L^{-1}, S_O = 2 mg·L^{-1}, X_R = 0 g·L^{-1}, S_{TIC} = 0 g·L^{-1}, $g_{out}^{CO_2}$ = 0 mol·h^{-1} and $g_{out}^{O_2}$ = 0 mol·h^{-1}. Each line correspond to a different concentration of substrate in the feed (i.e. from 1 g·L^{-1} to 4 g·L^{-1}).

As it can be observed in Fig.III.1.1 – B the dilution at steady state for a wide range of $S_{S,in}$ stabilizes at ~0.17 h^{-1}. By multiplying D with V and $g_{out}^{CO_2}$ it can be stated that for each gram of COD removed ~0.006 moles of CO_2 are produced.

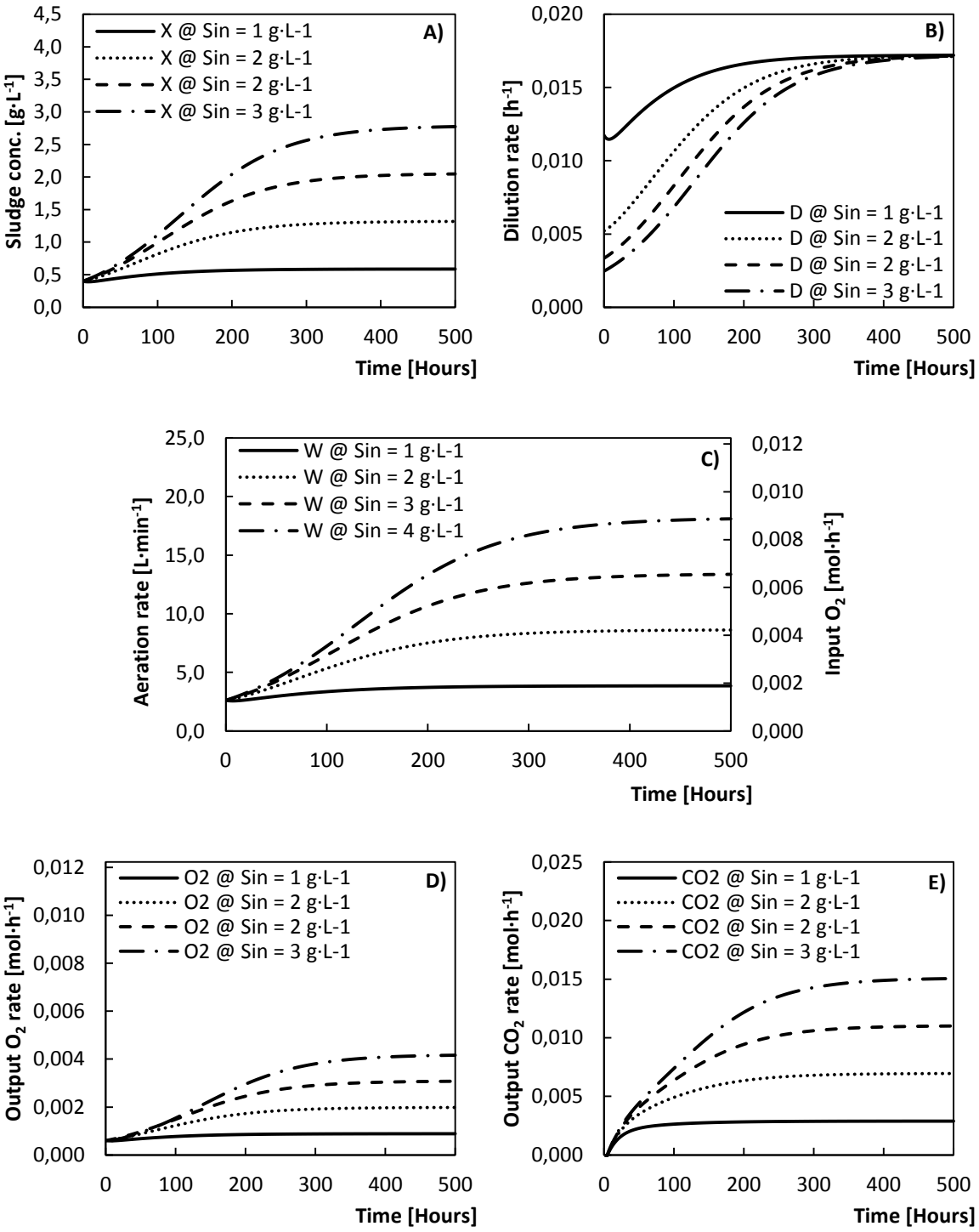

Fig.III.1.1. The dynamics of certain WWTP variables to maintain S_S = 0.1 g·L^{-1} and S_O = 2 mg·L^{-1} (A – Sludge concentration, B – dilution rate, C – aeration rate, D – output O_2 volumetric rate and E – output CO_2 volumetric rate)

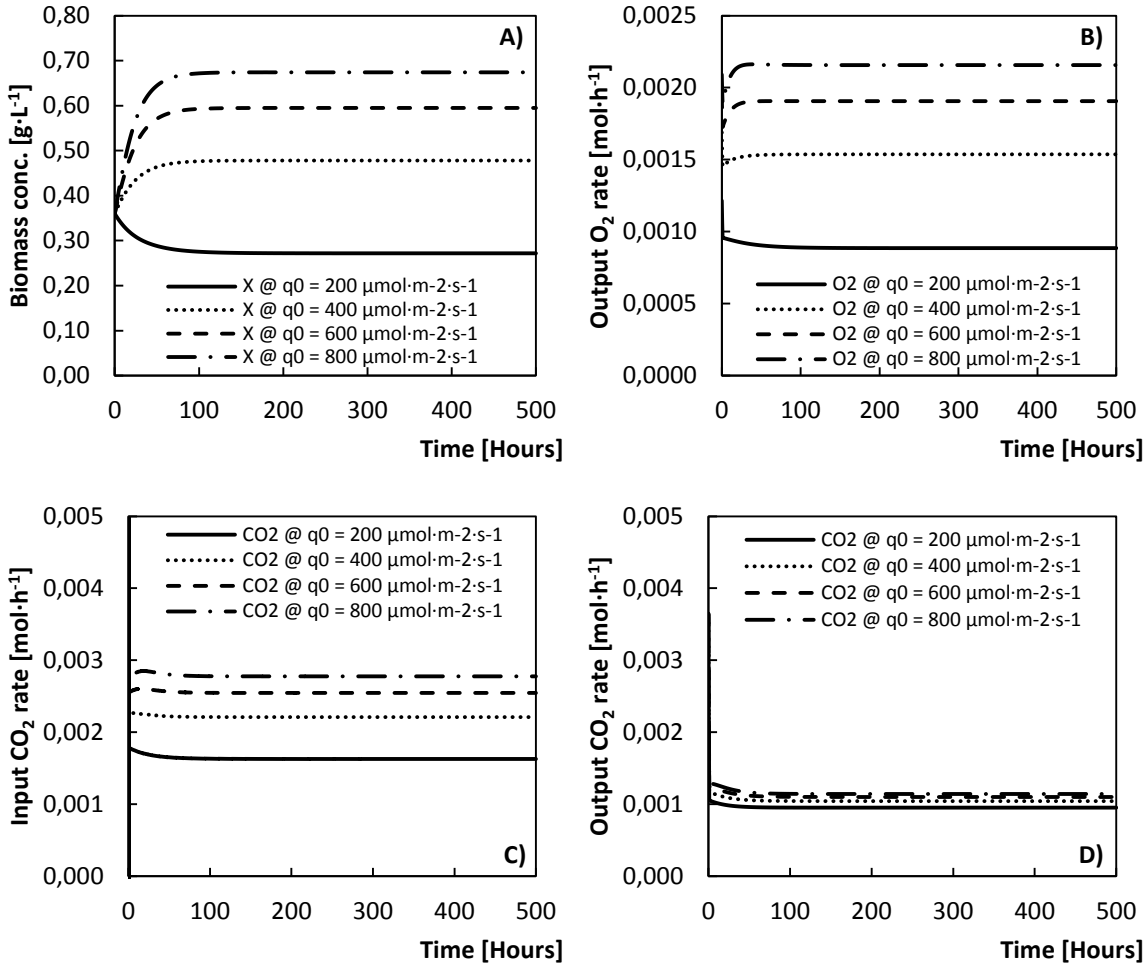

Fig.III.1.2. The dynamics of certain PBR variables to maintain pH to 7.5 at D = 0.05 h^{-1} (A – biomass concentration, B – output O_2 volumetric rate, C –input CO_2 volumetric rate, D – output CO_2 volumetric rate)

For better comparison between the two pilots a simulation of the PBR model is presented in Fig.III.1.2. The simulation was made for a PBR operated in continuous mode (D = 0.05 h^{-1}) with a pH maintained at 7.5. Also, four light intensities were used for better understanding the coupling.

Comparing the two figures it can be concluded that the CO_2 produced by the WWTP can easily cover the PBR requirements in any combination. The O_2 produced from photosynthesis can cover minimum 10% of WWTP requirements, but it can be can go up to 100% if it is scaled up or if the COD load is low.

III.2. CONTROL STRATEGIES FOR THE COUPLING BETWEEN WWTP AND PBR

The control of the coupling can be realized through decentralized SISO controllers. The interactions between the pilots can be viewed as measurable disturbances based on which feed-forward controllers may be designed. For a more precise control the feed-forward controllers can be integrated in reliable feedback controllers. It must be considered that the gases bubbled into the reactors are not dissolving completely and volumes of up to 50% may leave the reactor. The recycling of gases can minimize the losses but, at the same time, it can lead to supersaturation of the reactors. For example the oxygen produced through photosynthesis can become toxic above certain concentration. In addition, the nitrogen from air or from flue gases increases the volume of gas and may interfere with the overall capacity of dissolution of carbon dioxide and oxygen because it increases the bubble velocity through liquid. A solution can be the use of buffering tanks in which the gas is dissolved, the nitrogen lives the tank and the liquid enriched in CO_2 or O_2 can be used as a control variable for the auxostatic control.

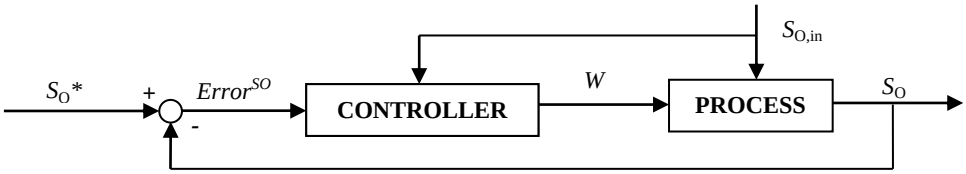

Fig.III.3.3. Combined feed-forward – feedback controller for the dissolved oxygen control

The interferences *D* as input variable with the control of oxygen trough aeration rate might increase and therefore $S_{O,in}$ can be considered a measurable disturbance.

In the same manner the pH controller can consider high concentrations of carbon dioxide which come with the feeding flow.

Other strategies of control were already presented in the first parts of this thesis and can be also applied for the coupling between the two devices.

In perspective a Γ-auxostat in envisaged, that is the manipulation of Γ through the control of dilution. This type of controller would be proper for solar photobioreactor where the light is not a control variable, but a measurable disturbance. To this end a reliable model needs to be developed in order to link Γ with *D*.

Conclusions regarding the coupling

The coupling between WWTPs and PBRs can represent reliable solution to eliminate costly tertiary stages. The use of PHBs is convenient because the biomass can be used to obtain added value compounds.

The coupling between and aerobic WWTP and a PBR represents certainly a solution for reducing the aeration costs, bio-mitigating CO_2 and obtaining microalgal biomass at the same time.

GENERAL CONCLUSIONS

First of all the thesis proposes a global model for the photoautotrophic growth of *Chlamydomonas reinhardtii*, which associates a radiative, a biologic and a thermodynamic model. The proposed model presents an excellent capacity of predicting the dynamics of six state variables which are fundamental for the photoautotrophic growth process (four characteristic to the liquid phase – X, TIN, TIC and $O_{2,aq}$ and two other specific to the gaseous phase – O_2 and CO_2 output molar fractions) and eleven internal variables mainly associated with the ternary solute $NH_3 - CO_2 - H_2O$ system and the pH. The global photoautotrophic growth model was validated with good results on data obtained from two experiments piloted in discontinuous mode at constant light intensities (*i.e.* 110 and 300 $\mu mol \cdot m^{-2} \cdot s^{-1}$). Three inputs (*i.e.* D, $G_{in}^{CO_2}$ and q_0) that were identified to have a significant influence over the system can be designated as control variable.

The nonlinear multivariable control of biomass and pH was developed through feedback linearizing techniques. The global photoautotrophic growth model, which is too complex to be used for control purposes, was reduced. A dynamic nonlinear equation for the concentration of hydrogen ions (negative antilogarithm of pH) was obtained and, associated with the reduced model that led to a proper I/O model derived for control purposes. Through an RGA analysis there were identified the conditions in which decentralized SISO controllers or centralized MIMO controllers are to be used. Because the pH control algorithm requires certain variables which are immeasurable, the global photoautotrophic growth model was integrated in real time in order to furnish them. The nonlinear control algorithm for biomass and pH were validated with excellent results on an experiment piloted both on discontinuous and continuous mode at constant light intensity of 300 $\mu mol \cdot m^{-2} \cdot s^{-1}$.

In addition, the nonlinear multivariable control of the specific light uptake and pH was approached based on the same feedback linearizing control technique. The nonlinear algorithm was validated with excellent results on the experimental bench, proving at the same time the ability of the pH controller to track the prescribed value in conditions of variable incident light intensities.

A nonlinear control algorithm was also discussed for the lighted volume fraction but validated only in simulation.

In what regards the wastewater treatment processes a simple nonlinear dynamic model was proposed for the aerobic tank describing three fundamental state variables of the system, the

sludge, substrate and the dissolved oxygen concentrations. The model parameters were identified on experimental data from the aerobic wastewater treatment pilot during an experiment operated in open loop. The model fitted well the experimental data on various operating points. The nonlinear multivariable control of substrate and dissolved oxygen was discussed and the necessity of using a centralized MIMO controller was determined through a RGA analysis. A feedback linearizing controller was proposed and validated in simulation. In addition, a feedback linearizing control algorithm was proposed and validated in simulation for the nonlinear multivariable control of F/M ratio and dissolved oxygen. Due to the lack of specific sensors for online substrate measurements and to the parametric uncertainties a robust linear controller was proposed for the dissolved oxygen by using the quantitative feedback theory. The robust controller was implemented on the pilot plant presenting excellent results for various operating points.

The perspectives of coupling between the two antagonistic processes were analyzed in various structures. A case study was presented for the coupling between a closed photobioreactor and an aerobic wastewater treatment plant with emphasis on the gases transfer between the plants.

PERSPECTIVES

The researches undertaken in the present thesis motivate a series of new directions of research that match the interests of each laboratory (GEPEA, France and Wastewater Laboratory, Romania), such as:

- The modeling of photobioreactors must be extended for the production of biofuels (biodiesel and biohydrogen) that take place during nitrogen or sulfur deprivation;
- Given that the many important variables cannot be measured online the efforts will be directed to the development of reliable observers which can be valuable tools for the control of both bioprocesses;
- The practical implementation of lighted volume fraction controller which was presented in the first part of this thesis and validated in simulation. The controller will target both the biomass production and the biohydrogen production by determining the most proper setpoint for each case;

- Another challenging research which is a work in progress, is the manipulation of the dissolved oxygen concentration inside a photobioreactor through the incident light control targeting the installation of hypoxic regime which promote the biohydrogen production;
- Based on the developed state observers, the nonlinear controllers for substrate and F/M ratio in the wastewater treatment plants, which were validated in simulation in the second part of this thesis, can be implemented and validated with experimental data;
- The studies regarding the coupling between the two processes, whose perspectives were presented in the third part of this thesis, will be carried further, accentuating the feasibility of photobioreactors to substitute certain treatment stages such as denitrification.

CONTRIBUTIONS

The thesis brings forth in an original manner the control of two biological processes of environmental interest that are the microalgae production in photobioreactor and the biological wastewater treatment and therefore it announces a series of contributions that can be listed as follows:

- A global model for the photoautotrophic growth of *Chlamydomonas reinhardtii* formed through the association of three models (radiative, biologic and thermodynamic) was developed. The global model delineates the main variables which lead to the precise prediction of the culture pH. It is one of the few models for photobioreactors which incorporates the thermodynamic properties of the ternary solute $NH_3 - CO_2 - H_2O$ system and the dynamics of the gases. The developed model represents a reliable computational package which can be applied to other types of photobioreactors with minor changes and can serve for various purposes such as research, design, monitoring and control;
- A reduced model for control purposes was also proposed and it is the first model which proposes a dynamic nonlinear equation for the concentration of hydrogen ions (negative antilogarithm of pH) as a complex function of X, TIN and TIC. The c_{H^+} nonlinear equation is an explicit function of input CO_2 and dilution rate and represents a reliable I/O model for control purposes;
- The nonlinear multivariable control approach is new for photobioreactors and most of all it is the first time when the pH control is treated as a nonlinear problem;

- The nonlinear multivariable control of X and pH led to excellent results on various operating points and especially the pH controller registered the best efficiency which was ever reported for this type of application;
- The lumostatic nonlinear control of the photobioreactor was approached for the first time in closed loop. The nonlinear multivariable control of the specific light uptake rate and pH presented excellent results and confirmed the effectiveness of the pH controller in cultures with variable light intensities. Thus, the proposed nonlinear pH controller is able to globally stabilize the system regardless of the operating point or culturing conditions.
- A simple and reliable model was derived for the aerobic wastewater treatment pilot by associating a classical model for the aerobic tank with an empirical model for the clarifier which is practically an improved version of a published model;
- In the anticipation of reliable sensors or estimators for the substrate concentration two nonlinear multivariable control algorithms were proposed and validated in simulation;
- A reliable robust controller for the dissolved oxygen concentration in the aerobic tank, based on the quantitative feedback linearizing technique, was developed and proved to be effective on various operating points and different types of wastewaters.

DISSEMINATION

A part of the results obtained through the researches attempted within this thesis were disseminated through the publication of 10 papers, out of which 3 papers have the thesis author as first author. Three papers were published in ISI journals, two in B+ journals and five others were presented at national and international conferences. Here follows a chronological list of the papers mentioned above:

- ***ISI Journals***
    1. Mihaela PALELA, **George IFRIM**, Marian BARBU, Gabriela BAHRIM, Sergiu CARAMAN. Strategies for the Aerobic Biological Treatment of the Dairy Wastewaters in Controlled Conditions. *Environmental Engineering and Management Journal*. 2010; 9(3):399-405;
    2. Sergiu CARAMAN, Marian BARBU, Tudor IONESCU, **George IFRIM**, Victor CRISTEA, Emil CEANGA. The analysis of the dynamic properties of the wastewater treatment process in a recirculating aquaculture system. *Romanian Biotechnological Letters*. 2010; 15(4):5457-5466;

3. Marian BARBU, Sergiu CARAMAN, **George IFRIM**, Gabriela BAHRIM, Emil CEANGA. State observers for food industry wastewater processes. *Journal of Environmental Protection and Ecology*. 2011; 12(2):678-687;

- ***B+ Journals***

1. Mihaela PALELA, **George IFRIM**, Gabriela BAHRIM. Microbiological and biochemical characterization of dairy and brewery wastewater microbiota. *The Annals of the University "Dunarea de Jos" of Galati. Fascicle VI Food Technology*. 2008; 2(31) 23-30;
2. **George IFRIM**, Marian Barbu, Mariana Titica, Lionel Boillereaux, Sergiu Caraman. Control of the microalgae photosynthetic growth in a torus photobioreactor. *Annals of the University of Craiova – series: Automation, Computers, Electronics and Mechatronics*. 2010; 7(34):32-38;

- ***Conferences***

1. Mihaela PALELA, **George IFRIM**, Marian BARBU, Gabriela BAHRIM, Sergiu CARAMAN. The metabolic activity evaluation of a specialised inoculum used for aerobic biological treatment of a simulated dairy-processing wastewater. International Workshop, BENA, Jan.16-17, 2009, Galati, Romania;
2. Marian BARBU, Sergiu CARAMAN, **George IFRIM**, Gabriela BAHRIM, Emil CEANGA. State observers for food industry wastewater processes, In: Aeternitas Publishing House (Ed.) Book of abstracts of International UAB-BENA Conference „Management and Sustainable Protection of Environment", May.6-7, 2009, Alba Iulia, Romania, ISBN 978-973-1890-30-2, p. 206;
3. Marian BARBU, Tudor IONESCU, **George IFRIM**, Sergiu CARAMAN, Victor CRISTEA, Emil CEANGA. Results regarding the Water Quality Control in Recirculating Aquaculture Systems, International Conference of Fishery and Aquaculture (BENA 2010), May.26-28, 2010, Galati, Romania;
4. Marian BARBU, **George IFRIM**, Sergiu CARAMAN, Gabriela BAHRIM. QFT Control of Dissolved Oxygen Concentration in a Wastewater Treatment Pilot Plant. In proceedings of 11th International Symposium on Computer Applications in Biotechnology (CAB 2010), Jul.7-9, 2010, Leuven, Belgia;
5. **George IFRIM,** Marian BARBU, Mariana TITICA, Lionel BOILLEREAUX, Sergiu CARAMAN. Control of the microalgae photosynthetic growth in a torus photobioreactor. In proceedings of 14th International Conference on System Theory (SINTES 14), Oct.17-19, 2010, Sinaia, Romania;

6. **George IFRIM,** Tudor IONESCU, Daniela CARP, Marian BARBU, Sergiu CARAMAN, Emil CEANGA. Interdisciplinary training in scientific research on bioprocess control. Case study: control of recirculating aquaculture systems. 1st Workshop on Education and research, Apr.20, 2011, Bucharest, Romania, Ed. Matrix ROM, pp:2-15, ISSN 2248-0811;
7. **George IFRIM**, Marina TITICA, Guillaume COGNE, Lionel BOILLEREAUX, Sergiu CARAMAN, Jack LEGRAND, Nonlinear Multivariable Control of *Chlamydomonas reinhardtii* Photosynthetic Growth in a Torus Photobioreactor, XIIIeme Congres de la Societe Francais de Genie des Procedes (SFGP 2011), Nov.29 – Dec.1, 2011, Lille, France.

A.1. APPENDIX 1

A.1.1. Biotechnological Applications of Microalgae

The microalgae stirred up the interest of scientists and industrialists due to their simple growth requirements which make them potentially attractive for a wide range of applications. The microalgae can be metabolically redesigned as cell factories finding applicability in the biotechnological production of therapeutic and industrial metabolites such as long chain polyunsaturated fatty acids (Wen and Chen, 2001), pigments (Sloth *et al.*, 2006; Zhu and Jiang, 2008), polycarbohydrates (Pulz and Gross, 2004), vitamins (Durmaz, 2007) or various biological active compounds. The researches on microalgae were abundant during last decades even though many of them did not found commercial applicability. Other than being commercialized as such, for human and animal food, as fertilizers or in cosmetic usage, the microalgae are actually employed in the production of certain added value compounds. Important products obtained from algae were reviewed by Radmer and Parker (1994), Radmer (1996) and Spolaore *et al.*, (2006).

A.1.1.1. Pigments

The carotenoids are the most used pigments in applications such as natural food colorants, cosmetics and as feed additives for poultry, livestock, fish and crustaceans. They are tetraterpenoid organic pigments that are naturally occurring in the chloroplasts of photosynthetic microorganisms serving at the absorption of light energy which is channeled to chlorophyll which, in its turn, is protected from photodamage. Certain species such as *Dunaliella*, *Haematococcus*, *Chlorella* and *Euglena* are employed to produce β-carotene, astaxanthin and canthaxanthin (Walker *et al.*, 2005).

β-carotene is also known as pro-vitamin A and is a lipophilic high-value compound. It was reported also to have antioxidant and anticarcinogenic properties. The main source of microalgal β-carotene is *Dunaliella salina* which is able to accumulate it up to a concentration of 10% of its dry weight under stress conditions such as high light intensity, high salinity and nutrient deficiency (Zhu and Jiang, 2008).

The astaxanthin is mainly used in the salmon feed industry. It can be produced by *Haematococcus pluvialis* and it was reported to act as an anti-inflammatory in instances of arthritis, muscle pain and carpal tunnel syndrome.

Other photosynthetic accessory pigments produced by microalgae and which have commercial applicability are the phycobiliproteins (*i.e.* phycoerythrin and phycocyanin which are red and blue). They are mainly used as natural pigments in food, cosmetics, or pharmaceuticals, particularly as substitutes of synthetic dyes. The classical producer of phycocyanin is the cyanobacterium *Arthrospira platensis* (*Spirulina*), but Sloth *et al.*, (2006) reported its production at *Galdieria sulphuraria*. A good candidate in the production of the red pigment phycoerythrin was reported by Bermejo Román *et al.*, (2002) as being *Porphyridium cruentum*.

A.1.1.2. Fatty Acids

Various species of microalgae are rich sources of long chain polyunsaturated fatty acids (LCPUFA), particularly eicosapentaenoic acid – EPA, docosahexaenoic acid – DHA (also known as omega-3 fatty acids) and arachidonic acid – AA (referred as omega-6 fatty acid) which are valuable nutritional supplements for humans and animals (Khozin-Goldberg *et al.*, 2011).

The enzymes required for synthesizing the polyunsaturated fatty acids with more than 18 carbons are lacking from plants and animals, therefore they are forced to get them from their food. Conventional sources of PUFA are the fish and fish oil which have the disadvantage of presenting typical smell, unpleasant taste and poor oxidative stability. The PUFAs existent in fish are practically originating from the microalgae consumed in the oceanic environment, thus they can obviously represent potential sources of PUFAs.

Efficient candidates for PUFAs production are microalgal species such as: *Porphyridium purpureum*, *Phaeodactylum tricornutum*, *Isochrysis galbana*, *Nannochloropsis* sp. and *Nitzschia laevis* (Jiang *et al.*, 1997).

A.1.1.3. Polysaccharides

The interest for microalgal polysaccharides is continuously increasing due to their applications in food, cosmetic and pharmaceutical industries, competing with other natural polysaccharides obtained from macroalgae. Their solubility in water provides them attractive

rheological properties for food industry applications such as food coating, emulsifying and gelling agents, flocculants and hydrating agents.
Certain species of microalgae such as *Porphyridium cruentum*, *Porphyridium purpureum* and *Arthrospira platensis* are able to biosynthesize exopolysaccharides which are able to retain water preventing desiccation (Rebolloso Fuentes *et al.*, 1999; Pulz and Gross, 2004).

A.1.1.4. Potentially Attractive Biotechnological Applications

Brányiková *et al.*, (2010) reported that the freshwater microalga *Chlorella vulgaris* can be employed as a highly productive source of starch which may substitute the starch-rich terrestrial plants used for bioethanol production. The concentration of starch reached up to 40% of the dry mass at 330 $\mu mol \cdot m^{-2} \cdot s^{-1}$ in nutrient limited conditions.
Another innovative application reported by Hempel *et al.*, (2011) regards the production of bioplastic (Poly-3-hydroxybutyrate – PHB) at the diatom *Phaeodactylum tricornutum* by introducing the bacterial PHB pathway into the cytosolic compartment. The levels of PHB reached up to 10.6% of algal dry weight revealing the great potential of this low-cost and environmentally friendly expression system.
Rosenbaum *et al.*, (2004) employed living cells of the green alga *Chlamydomonas reinhardtii* to directly generate electricity from microalgal photosynthetic activity.

A.2. APPENDIX 2

A.2.1. Environmental Applications of Microalgae

The microalgae can be also involved in environmental applications such as greenhouse gas bio-mitigation (Wand *et al.*, 2008), wastewater treatment processes (Mallick, 2002; Chaiklahan *et al.*, 2010) and biosorption of heavy metals (Doshi *et al.*, 2008). The biomass thus obtained can be employed in the production of biofuels (Chisti, 2007; Brennan and Owende, 2010; Singh *et al.*, 2011). Lately, increased attention was conferred to the hydrogen production potential of microalgae (Chen *et al.*, 2006; Skjånes *et al.*, 2008).

A.2.1.1. CO_2 Bio-mitigation

Carbon dioxide gas is known to have an increased capacity to absorb the solar radiation leading to global warming. This phenomenon is known as the greenhouse effect and is potentiated through the combustion of fossil fuels (coal, oil, gas) and through various industrial and domestic activities. In this context, the use of microalgae to fix the CO_2 (*e.g.* from power plants) minimizing thus the amount of carbon released into the atmosphere appears to be an excellent idea.

The advantages in using microalgae to bio-mitigate the CO_2 are their high growth rate, their capacity of tolerating other gases (only a limited number of microalgae) such as NO_x and/or SO_x (Matsumoto *et al.*, 1995) and their capability to convert the carbon into valuable products.

Certain limitations also exist such as variations on the CO_2 concentration in the flue gases and the temperature of gases which may harm the culture of algae therefore, in many cases, they need to be cooled prior to injection into the growth medium.

The CO_2 bio-mitigation in not a standalone process, but targeting in most cases the production of biomass for biofuels, wastewaters treatment, etc. Wand *et al.*, (2008); Brennan and Owende, (2010) reviewed the main technologies for obtaining biofuels from microalgae and listed the potential of biological carbon capture for a series of microalgae species.

A.2.1.2. Biofuels Production

The production of biofuels is probably the most disputed subject when it comes to microalgae potential. In the context of increasing energy demand worldwide the exploitation of unconventional energetic vectors seems to be an attractive idea which led to numerous researches (Chisti, 2007; Brennan and Owende, 2010; Greenwell *et al.*, 2010; Nigam and Singh, 2011).

Certain advantages encourage the usage of microalgae to be employed in the biofuels production:

- The microalgae can be cultivated continuously regardless of season, thus, in comparison with the oilseed crops they present a significantly higher productivity;
- They require less water that the terrestrial crops even though they grow in aqueous medium;
- The culturing can be done on non-potable water and non-arable lands minimizing thus the environmental impact;
- The growth rate of many microalgal species is very high;
- The microalgae are able to accumulate up to 50% oil content from their dry mass;
- As a result of photosynthesis they improve the air quality by absorbing carbon dioxide and producing oxygen;
- They have simple growth requirements which may assure low production costs, such as sunlight, CO_2 and nutrients (nitrogen and phosphorus) which can be provided from wastewaters. Therefore, aside from biofuels production they can be employed in wastewater treatment;
- The microalgae are also able to produce valuable substances such as proteins and residual biomass after oil extraction which can be used as organic fertilizer or can be fermented to produce ethanol or methane;
- They can be metabolically redesigned in order to enhance the production of lipids by limiting certain nutrients;
- Also through the limitation of nutrients the microalgae are able to produce biohydrogen.

There are also certain challenges which are not yet completely solved such as development of reliable culturing techniques, evaporation reduction in open pounds, CO_2 diffusion in atmosphere, high cost of harvesting and extraction, scale-up, etc.

There are few known technologies of converting the microalgal biomass into energy carriers (liquid or gaseous fuels), some of them already used for other types of biomass. The conversion technologies can be divided in thermochemical and biochemical conversion.
The thermochemical conversion can be realized through gasification, thermochemical liquefaction, pyrolysis and direct combustion.
The biochemical conversion includes the anaerobic digestion, alcoholic fermentation and biohydrogen production.

A.2.1.3. Wastewater Treatment

The researches on microalgal culturing also evaluated the use of microalgae in wastewater treatment. They can be used directly, by mixing microalgal cells with waste effluents and thus employing their capacity to consume certain organic compounds, nutrients and heavy metals, or indirectly by associating a wastewater treatment plant (aerobic or anaerobic) with a photobioreactor. However, this subject was discussed in detail earlier.

A.3. APPENDIX 3

A.3.1. Microalgal Culturing Systems

Considering the huge potential of microalgae and their numerous aforementioned applications the microalgal culturing techniques outline specific methods and tools which must be enhanced and well understood in order to reach maximum productivities in feasible facilities. Although the microalgae have been harvested from their natural environments for thousands of years, serving for human consumption, their exploitation on technological basis is no older than 50 years. At the beginning the microalgae were cultivated in open ponds in Eastern Europe, Israel and Japan, mainly for their direct consumption as healthy food. Since then specialized culturing systems were developed and the cultivation purposes were extended.

A.3.1.1. Photobioreactors: Definition and Classification

A bioreactor is defined as "A vessel in which a biological reaction or change takes place, usually a fermentation or a biotransformation, including tank bioreactors, immobilized cell bioreactors, hollow fiber and membrane bioreactors and digesters" (Bains, 1998). The bioreactors are provided with a variety of attached devices used to control the bioreactions. Based on the homogeneity of the bioreactor's content, they can be classified in:

- Stirred tank reactors (STR) where the reacting medium is homogenous and the growth of microorganisms and substrates consumption are described through ordinary differential equations;
- Reactors with a partial concentration gradient, such as fixed beds, fluidized beds, air lifts, etc, where the system has distributed parameters and is described through partial derivative equations.

In this regard, a photobioreactor is a bioreactor that contains a light source which provides photonic energy to the photosynthetic organisms. Usually, a photobioreactor refers to closed systems that have no direct exchange of gases and contaminants with the environment. However, an open pound could be also seen as an open photobioreactor.

According to the nature of the light source, the photobioreactors can be classified as:

- Solar photobioreactors – are used generally for the mass production of microalgae. They benefit of a free source of energy, but have the disadvantage of being productive only during the day and are sensible to the atmospheric conditions;
- Photobioreactors with artificial light – are utilized for small scale production of microalgae. This type of photobioreactors depend on an artificial light source which can be precisely controlled and furnish constant photonic energy regardless of the atmospheric conditions or the day/night cycle.

The photobioreactors provided with artificial light sources can be classified in their turn in:

- Photobioreactors with external artificial light;
- Photobioreactors with internal artificial light.

Based on their geometry certain classes of photobioreactors can be identified, such as:

- Flat-plate photobioreactors;
- Tubular photobioreactors;
- Column photobioreactors.

Each geometry presented above supports certain variations by taking into account the position of the photobioreactor, thus they can be: horizontal, vertical or inclined.

A.3.1.2. Photobioreactor Design

Since the first open pounds were installed for mass production of microalgae a variety of closed photobioreactors from laboratory to industrial scale were designed. The closed photobioreactors stirred up the interest due to certain advantages such as better control of the cultivation conditions, higher biomass productivities and lower contamination risk. Various designs were tested such as bubble column, airlift column, stirred-tank, helical tubular, conical torus and others, but only few were scaled up for the mass cultivation. Principal types of photobioreactors along with certain specific characteristics were reviewed by Ugwu *et al.*, (2008) and Eriksen, (2008). Briefly, the most used designs of photobioreactor are presented in the following lines.

A.3.1.2.1. *Open Pounds*

There are used for mass cultivation of microalgae and can be classified into natural waters (lakes, lagoons, pounds) and artificial pounds. Currently, the production of algae for commercial purposes is carried out in open pound systems (Borowitzka, 1999; Radmann *et*

al., 2007; Masojídek and Torzillo, 2008). The open ponds are easy to be constructed and operated in comparison with the closed systems, being encountered in various constructive shapes such as tanks, circular ponds and raceway ponds (*e.g.* Fig.A.3.1). The major disadvantages of the open ponds are the low availability of light inside the culture, high volumes of CO_2 gas diffused into the atmosphere, the large surface needed and the losses through evaporation. Being open there is also a high risk of contamination, thus the most suitable applications are the extremophile photosynthetic organisms. The homogenization of the culture is hard to be realized in these types of systems due to their large surface leading to low transfer rates and hence to small biomass productivity.

Fig.A.3.1. Open pounds: a) www.algaeforbiofuels.com, b) www.me-newswire.net

A.3.1.2.2. *Flat-plate Photobioreactors*

The flat-plate photobioreactors are characterized by a thin layer of photosynthetic microorganisms (hence small light path) and a large illumination surface (Sierra *et al.*, 2008) (*e.g.* Fig.A.3.2). These types of photobioreactors which are also suitable for mass cultivation of microalgae are used both indoor and outdoor, thus lighted by solar or artificial light. Their construction is relatively cheap and allows to be easily cleaned, but at scale-up they may require many compartments and support materials. The researches on these types of reactors reported high photosynthetic efficiencies (Hu *et al.*, 1988).

Fig.A.3.2. Flat-plate photobioreactors a) www.nanovoltaix.com, b) www.genengnews.com

A.3.1.2.3. *Tubular Photobioreactors*

The tubular photobioreactors are widely used outdoor for the mass cultivation of microalgae (Molina Grima *et al.*, 1994). They can be constructed from glass or plastic while the culture aeration and mixing is realized through air-pumps of airlift mechanisms. Constructively they can be horizontal/serpentine, vertical or inclined (*e.g.* Fig.A.3.3). The large illumination surface area is an advantage which promises good biomass productivities. The main disadvantage of the tubular photobioreactors is the mass transfer which creates dissolved oxygen (DO) and carbon dioxide gradients on the length of the tube (Molina *et al.*, 2001).

Fig.A.3.3. Tubular photobioreactor a) http://brae.calpoly.edu, b) http://www.algatech.com

The accumulation of DO is often met in tubular photobioreactors and was reported in some cases to have a toxic effect. The scale-up of tubular photobioreactors impose the increasing of

the diameter of tubes which also increases the light path resulting in light shading effect (not enough light for cell growth). In order to minimize this effect a good mixing system must be conceived.

A.3.1.2.4. *Column Photobioreactors*

The column photobioreactors (usually vertical, but sometimes inclined) are compact, low-cost and easy to be operated. They are sometimes provided with mixing mechanism (usually the small laboratory reactors) but more encountered are the bubble columns which are aerated from below (*e.g.* Fig.A.3.4). In comparison with other constructive types, the column photobioreactors present the most efficient mixing, the highest mass transfer and offers the best controllable growth conditions (Ranjbar *et al.*, 2008). At scale-up they present the same limitation as the tubular photobioreactor, but the multiplication of the columns can minimize the issue.

Fig.A.3.4. Column photobioreactors a) www.nanovoltaix.com, b) http://www.pittstate.edu

A.3.3.2.5. *Internally-illuminated Photobioreactors*

Certain types of photobioreactors (mainly the column photobioreactors) can be illuminated internally with fluorescent lamps or optical fiber (Ogbonna *et al.*, 1996, 1999; Suh and Lee, 2001). Despite the fact that they can be expensive some of their advantages are still attractive. For example they can work both with artificial and natural light because there is no external lighting device to obscure the sunlight and during the night the internal dispositive can be

used. Another attractive advantage is that there are no dark zones, the light path being small resulting in increased biomass productivity and sustained production.

A.3.1.3. Operating Modes

There were identified three modes of operating the photobioreactors with respect to the liquid phase exchanges (*i.e.* the manner in with the substrate is feed to the reactor): discontinuous mode, semi-continuous mode and continuous mode. In addition, a combination between various operating modes is known as sequencing batch reactor.

A.3.1.3.1. *Discontinuous Mode (Batch Mode)*

In discontinuous mode operation all the requisite nutrients for the photosynthetic growth of microalgae (except the gaseous CO_2) are introduced at start-up, usually before the inoculation of the photobioreactor with algal cells (Fig.A.3.5). During the batch no other nutrient in liquid phase is supplied and nothing is removed, the reaction taking place at constant volume. However, this is only partially true because almost every time, in order to monitor the culture, small volumes are sampled periodically resulting that the reactor's volume register a constant slight decrease. This mode of operation has certain attractive advantages from an industrial point of view, such as: ease in implementation and operation, and decreased risk of contamination.

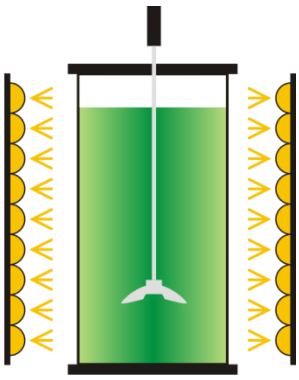

Fig.A.3.5. Photobioreactor operated in discontinuous mode

The discontinuous mode is convenient in studies of the microalgae in various stages of the growth and in studies regarding the gas dynamics, considering that the reactor can be properly sealed. This mode of operation has also certain disadvantages such as inhibition

given by the high concentration of initial supply, delays given by washing, sterilizing and inoculating the reactor and by lag or accelerated growth phases which can take up to two days. Oftentimes the batch mode does not provide the maximum growth rates of microorganisms, the process being lengthened.

A.3.1.3.2. *Semi-continuous Mode (Fed-batch Mode)*

Unlike discontinuous mode, in semi-continuous mode the nutrients are supplied when required by the microalgae culture (Fig.A.3.6). Often the feeding is scheduled according to a previously known growth dynamics (open loop), but in certain cases, when the photobioreactor is provided with specific sensors able to measure various state or internal variables, the feed can be calculated online according to the biomass, substrate or products concentrations from a precise moment in development (closed loop). The substrates' feeding is stopped when the vessel volume reaches its maximum level. In contrast with the batch mode the inhibition problem given by the high initial concentration of substrates is eliminated through the scheduled feed with culture medium and the installation must be provided with a feeding pump.

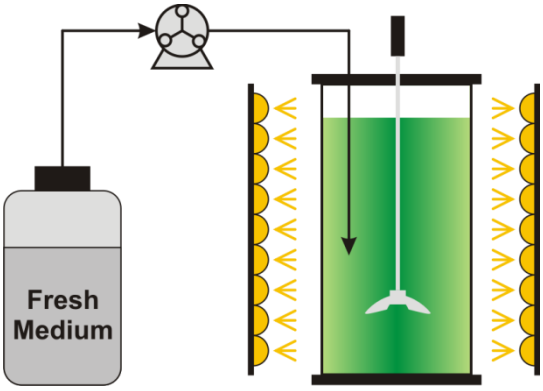

Fig.A.3.6. Photobioreactor operated in semi-continuous mode

In comparison with the batch regime, the photobioreactor functions at higher growth rates close to their maximum values. The semi-continuous mode is recommended when high concentrations of substrate inhibit the growth or when certain metabolites are secreted only in specific environmental conditions (*e.g.* intracellular accumulation or the secondary metabolites production under stress conditions).

A.3.1.3.3. *Continuous Mode (Chemostat)*

The continuous mode is the most attractive manner, in terms of biomass productivity, to operate a photobioreactor. It consist in feeding continuously the reactor with precisely calculated volumes of fresh medium, and hence evacuating in the same time portions of biomass equivalent with the dilution *D* imposed which results in a constant working volume (Fig.A.3.7). The dilution represents the ratio between the substrate feeding flow rate Q and the working volume of the photobioreactor V_l. The photobioreactors operated continuously reach a steady state while preserving the culture in a continuous exponential growth phase and are able to avoid any inhibition phenomenon as a result of the dilution effect.

The photobioreactors can be operated in open loop by imposing a constant feeding flow. The open loop chemostats are used when there is no available online measurement (or estimator) for the biomass concentration. The closed loop chemostats (also referred in literature as turbidostats) are even more efficient by preserving the biomass concentration at a prescribed value while manipulating the dilution, based on a feedback mechanism. They require an online estimated or measured value of biomass concentration, a feeding pump and an evacuation pump.

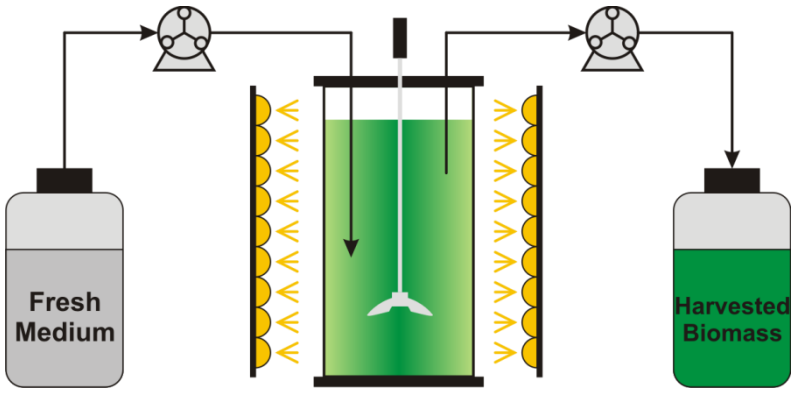

Fig.A.3.7. Photobioreactor operated in continuous mode

A.3.1.3.4. *Sequencing Batch Reactors (SBR)*

The SBR consist in a single tank where more operations take place in sequences (Fig.A.3.8). This type of system is usually used in the wastewater treatment technology where the tank is filled with wastewater and maintained in batch mode under continuous mixing for a few days. After the wastewater is treated the stirrer is stopped and the activated sludge is allowed

to settle. The excess sludge and the treated water are evacuated separately and the process can start again by refilling the tank with wastewater. A part of the activated sludge is however preserved in the tank serving as inoculum for the next step.

A derivation of SBR is the sequencing fed-batch reactor SFBR which differ from the first one only in the manner in which the first filling stage is realized.

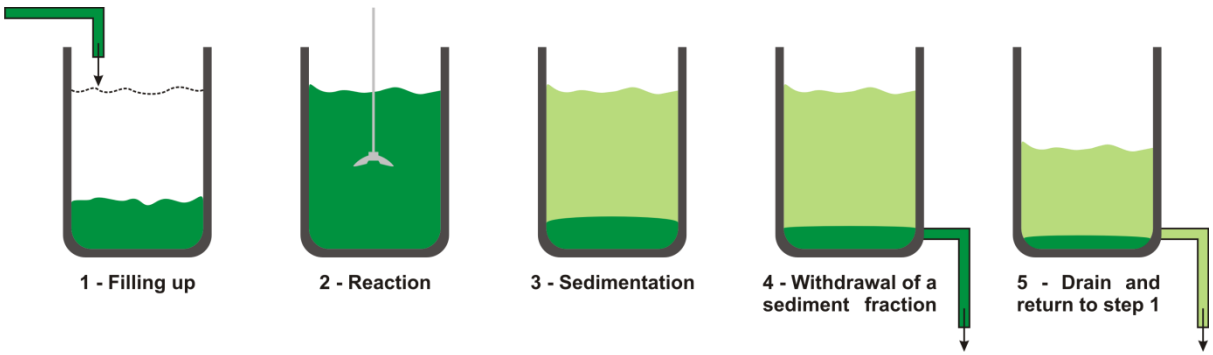

Fig.A.3.8. SBR – sequencing batch reactor – time sequence of various stages

Considering the numerous researches regarding the wastewater treatment with microalgae this operating mode was applied in practice by Tarlan *et al.*, (2002) on pulp and paper industry wastewaters reporting yields of up to 85% chemical oxygen demand COD removal. The SBR is not usually used in microalgal culturing techniques due to the fact that the sedimentation of microalgae is not an efficient process.

A.4. APPENDIX 4

A.4.1. The General Process of Photosynthesis

In brief, the global process of photosynthesis is a light driven chemical process that converts the carbon dioxide into organic compounds (especially sugars), being generally described through equation (A.4.1).

$$n\mathrm{CO_2} + n\mathrm{H_2O} + \text{light} \xrightarrow{\text{Chlorophyll } a} (\mathrm{CH_2O})_n + n\mathrm{O_2} \quad \text{(A.4.1)}$$

Photosynthesis takes place in plants, macroalgae and microalgae (including photosynthetic bacteria). The conversion of light energy into chemical energy is associated with the chlorophyll *a*, a green pigment specific to all photosynthetic organisms, which participates to one of the most thermodynamically demanding reactions in biology – the water photolysis:

$$2\mathrm{H_2O} \rightarrow 4\mathrm{e^-} + 4\mathrm{H^+} + \mathrm{O_2} \quad \text{(A.4.2)}$$

The chlorophyll *a* absorbs energy from violet-blue and orange-red wavelength and reflects the green wavelengths.

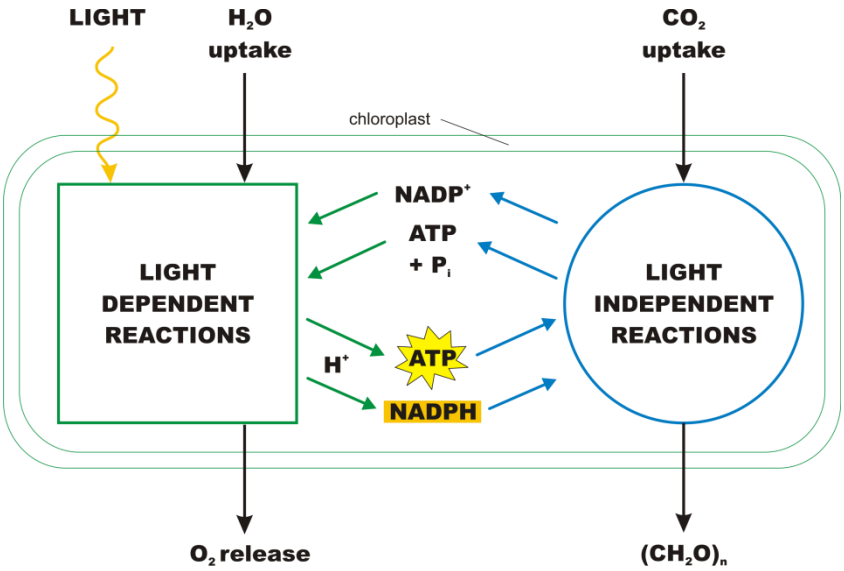

Fig.A.4.1. General process of photosynthesis

If the available energy has not the proper wavelength the photosynthetic organisms synthesize accessory pigments such as chlorophylls *b*, *c*, *d*, *e*, xanthophylls and carotenoids, which channel the energy to chlorophyll *a*. The photosynthesis takes place in specialized organelles named chloroplasts at eukaryotes, while at bacteria it takes place in the plasma membrane.

The photosynthesis includes two major groups of reactions: light dependent and light independent reactions (Fig.A.4.1).

A.4.1.1. Light Dependent Reactions

The light dependent reactions take place in the thylakoid membranes of chloroplasts and involve the capture of light energy and its conversion into NADPH and ATP, which are the assimilatory power required for the reduction of CO_2 into carbohydrates during the light independent phase.

The light dependent reactions are the absorption and transfer of photon energy, the trapping of photonic energy and the generation of chemical potential. The photosynthetic reaction centers which contain chlorophylls consist mainly of highly organized energy transforming units such as enzymes for electron transport and ATP synthesis. The energy transforming units, named photosystem I (PSI) and II (PSII) are two large protein complexes surrounded by light harvesting complexes (LHCs). Specific chlorophyll molecules (P_{700} and P_{680} – P stands for pigment and 700/680 for the wavelength of maximum absorption), excited by the absorbed photons, are initiating the translocation of electrons across the thylakoid membrane through organic and inorganic redox couples which form the electron transfer chains (ETCs). ETCs are consisting in plastoquinones, cytochromes and ferredoxin. The electron translocation process leads to the reduction of $NADP^+$ to NADPH and to a transmembrane difference in the electrical potential and H^+ concentration, the latter leading to the synthesis of ATP by means of an ATP-synthase.

PSI and PSII complexes contain an internal antenna-domain which incorporates the light harvesting chlorophylls and accessory pigments. The chlorophylls perform most of the light harvesting, while accessory pigments protect them against excess light energy and channel the absorbed energy.

PSII is fundamental to photosynthesis because it catalyzes the photo-induced oxidation of water, thus it is able to split water and to use the resulted electrons and protons to derive photosynthesis. The excited chlorophyll cations from PSII (P_{680}^+) are reduced by a redox

active tyrosine, which is reduced in its turn by a Mn ion. Two molecules of water are oxidized when $(Mn)_4$ accumulates four electrons, producing one molecule of O_2 and four protons (Eq.A.4.2).

The electron transport system consists in plastoquinone, cytochrome *b_6f* complex, plastocyanin and ferredoxin which are able to sustain successive cycles of oxidation and reduction transporting electrons from PSII to PSI. The success of electron transport chain is due to the sequential arrangement of all components of PSII and PSI as it can be seen in "schema Z" of photosynthesis presented in Fig.A.4.2.

The transport of electrons through the chain is initiated by the charge separation between P_{680} and pheophytin (first electron carrier – chlorophyll *a* without Mg^{2+} ion) which creates the redox couple $P_{680}^{+}/Pheo^{-}$. The electrons are transferred further to plastoquinone.

Plastoquinone refers to a class of lipid-soluble benzoquinone derivatives which are able to carry both electrons and protons (e^- and H^+) from PSII to cytochrome *b_6f* complex. Their forms are quinone A (Q_A) and quinone B (Q_B); the latter also exists in reduced form when accepts two electrons and two protons – plastoquinol (Q_BH_2).

The plastoquinone are involved in a sequence of reactions known as the Q-cycle. When Q_B is reduced to Q_BH_2, besides the two electrons received from Q_A, it takes two protons from the stroma of chloroplasts (aqueous fluid within the chloroplast) and release them into the thylakoid lumen of chloroplasts (the empty space inside of thylakoid) where the ATP synthesis takes place. The protons are released here because the cytochrome *b_6f* complex is able to receive only electrons. Q_BH_2 is oxidized to Q_B by cytochrome *b_6f* complex, thus being able to transfer additional protons into the lumen for ATP production contributing with free energy to the electrochemical proton potential.

The electrons received by cytochrome *b_6f* complex (plastoquinol – plastocyanin reductase, an enzyme found in the thylakoid membrane of chloroplasts) are transferred to PSI via plastocyanin (copper-containing protein).

In order to continue transport the electron is again excited through the absorption of a photon by PSI which reaches a high redox potential. The electrons are further transported through a chlorophyll *a* (A_0), a quinine acceptor (A_1), a bound Fe-S cluster and ultimately used by ferredoxin to reduce $NADP^+$ to NADPH. Ferredoxin is the strongest soluble reductant found in cells being able to transfer electrons to enzymes involved in other metabolic pathways, such as nitrite reductase, glutamate synthase or thioredoxin reductase.

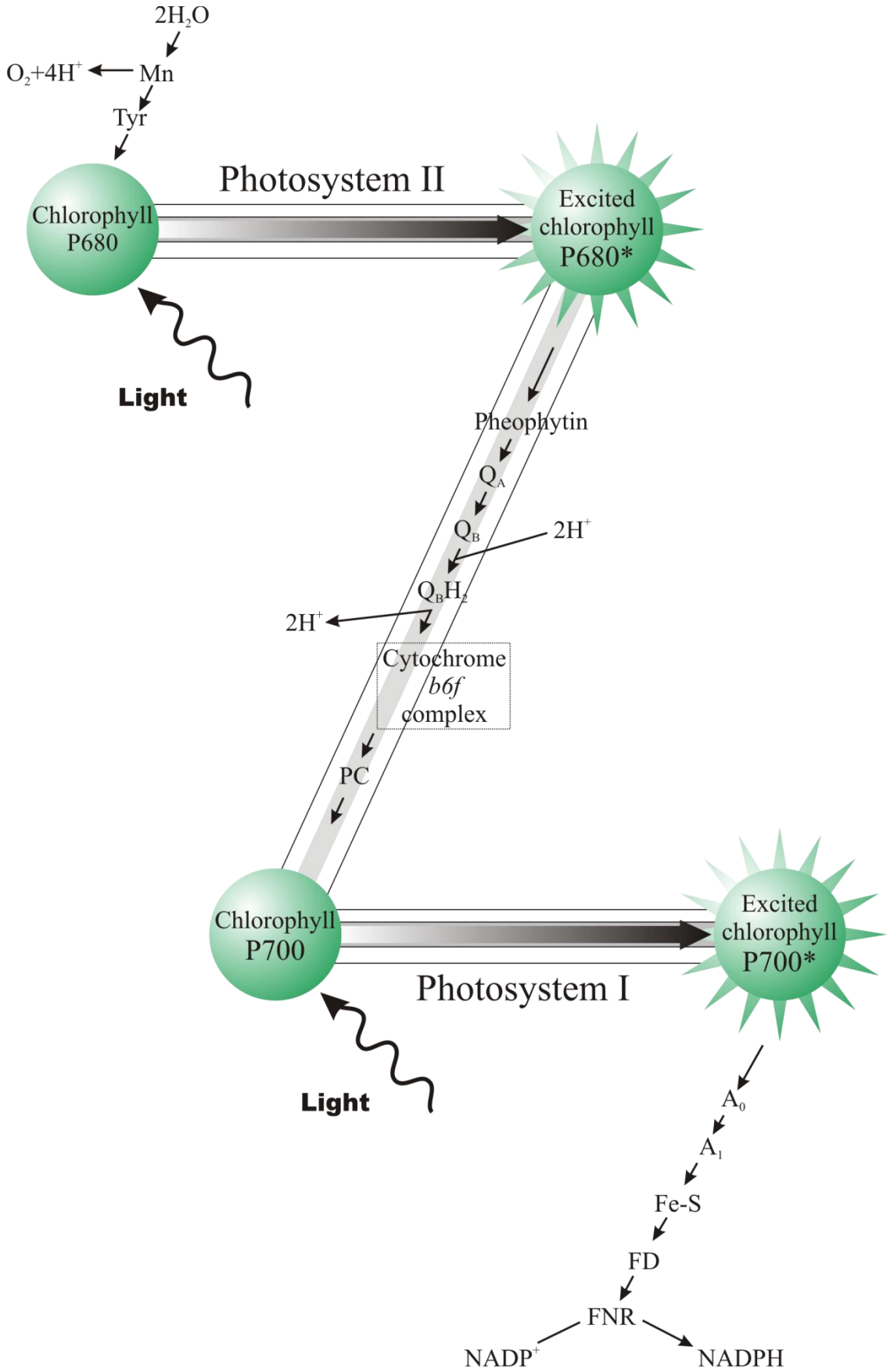

Fig.A.4.2. Schema Z of photosynthetic electron transport, from (Barsanti and Gualtieri, 2006)

The overall reaction of ATP and NADPH production can be expressed as:

$$4\mathrm{NADP^+} + 2\mathrm{H_2O} + 4\mathrm{ADP} + 4\mathrm{P_i} \xrightarrow{8\ \text{photons and}\ 4e^-} 4\mathrm{NADPH} + 4\mathrm{ATP} + \mathrm{O_2} \quad \text{(A.4.3)}$$

The relation involves that for each H_2O molecule split under the influence of light $\frac{1}{2}O_2$ molecule is produced and the protons and electrons released lead to the simultaneous production of two molecules of NADPH and two of ATP.

A.4.1.2. Light Independent Reactions

The light independent reactions consist in the fixation of CO_2 by using the assimilatory power of NADPH and APT formed during the light dependent reactions. The reactions take place in the stroma of chloroplasts at eukaryotes and in cytoplasm at prokaryotes. The light independent reactions are carried out simultaneously with the light dependent reactions and not necessarily in the dark. The group of light independent reactions is also known as Calvin Benson Bassham cycle (CBB cycle) presented in Fig.A.4.3 and takes place in three phases:

- Carboxylation – fixation of CO_2 into a stable organic intermediate with 5 carbons (ribulose-bisphosphate – RuBP). The reaction is catalyzed by RuBisCO (ribulose-1,5-bisphosphate carboxylase/oxygenase) enzyme. The 6 carbon product splits into two 3-phosphoglycerate (3-PG).
- Reduction – the formed intermediate is reduced to carbohydrate in two steps: 3-PG phosphorylation by ATP to form 1,3-biphosphoglycerate (1,3-BPG) which is further reduced to glyceraldehyde-3-phosphate (G3P) by NADPH.
- Regeneration – RuBP is regenerated through a series of reactions which involves the conversion of triose phosphate to ribulose 5-phosphate (Ru5P) which is further phosphorylated to obtain RuBP.

To produce a molecule of glucose six CBB cycles are needed and the overall consumption of ATP and NADPH can be written as:

$$6\mathrm{CO_2} + 18\mathrm{ATP} + 12\mathrm{NADPH} + 12\mathrm{H_2O} \rightarrow \mathrm{C_6H_{12}O_6} + 18\mathrm{ADP} + 18\mathrm{P_i} + 12\mathrm{NADP^+} + 6\mathrm{H^+} \quad \text{(A.4.4)}$$

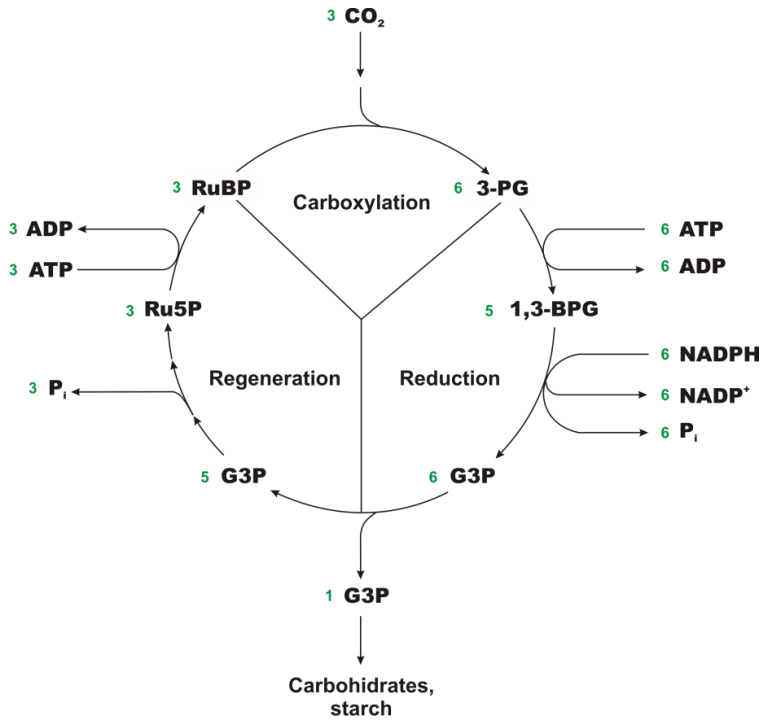

Fig.A.4.3. The Calvin Benson Bassham cycle

A.4.2. Photorespiration

Also known as the mitochondrial respiration, the photorespiration inhibits photosynthesis involving the uptake of O_2 and the release of CO_2. During photorespiration RuBisCO combines with oxygen instead of carbon dioxide and is associated with the burning of cellular fuel to obtain energy in the form of ATP. In other words, photorespiration is a light dependent uptake of oxygen in chloroplasts. The process can be interpreted as a competition between O_2 and CO_2 and is more intense when the O_2 level is elevated sometimes being associated with a certain toxicity of O_2 which decreases the photosynthetic efficiency. In what regards the process modeling a term related to photorespiration must be considered.

A.5. APPENDIX 5

A.5.1. Other Kinetic Equations

Many other algebraic relations were developed in order to serve various applications but their use remains minimal in comparison with Monod and Andrews-Haldane models.

Product Inhibition Kinetics – describes the inhibition given by a specific product *P* which accumulates in the medium.

$$\mu = \mu_0 \frac{S}{K_s + S + \frac{P}{K_I}} \quad \text{(A.5.1)}$$

Modified Monod Form – shows the influence of the initial concentration of substrate

$$\mu = \mu_{max} \frac{S}{K_s S_0 + S} \quad \text{(A.5.2)}$$

Teissier Model – relates μ to *S* exponentially

$$\mu = \mu_{max} \left(1 - e^{-\frac{S}{K_s}}\right) \quad \text{(A.5.3)}$$

Contois Model – expresses the saturation constant as being proportional to the biomass concentration. It is usually used for high concentrations of biomass.

$$\mu = \mu_{max} \frac{S}{K_s X + S} \quad \text{(A.5.4)}$$

Droop Model

$$\mu = \mu_{max} \left(1 - \frac{K_Q}{Q}\right) \quad \text{(A.5.5)}$$

Multiple-Substrate Monod Kinetics – in certain cases more than one substrate may influence the growth.

$$\mu = \mu_{max}\left(\frac{S_1}{K_{S1}+S_1}\right)\left(\frac{S_2}{K_{S2}+S_2}\right) \quad \text{(A.5.6)}$$

The Monod equation written for the second substrate can be only a mathematically continuous switching function with no physical significance which has the purpose to decrease μ when S_2 is close to 0.

NOMENCLATURE

a_i	activity of component *i*
a_w	water activity
A	optical surface of photobioreactor
b, b_λ	backward scattering fraction (for a specific wavelength λ) (-)
$B(x)$	characteristic matrix of the system
c_i, c_i'	mass and molar concentration of i^{th} species (mg or $g \cdot L^{-1}$; $mol \cdot L^{-1}$); c_i is sometimes deliberately used to express the molar concentration of i^{th} species in order to simplify the notation, however those cases are explicitly mentioned
$c_{i,0}$, $c_{i,0}'$	concentration of i^{th} species in the feed (mg or $g \cdot L^{-1}$; $mol \cdot L^{-1}$)
$c_{i,\mathrm{aq}}'$	molar concentration of dissolved species *i* ($mol \cdot L^{-1}$)
$c_{i,\mathrm{gas}}'$	molar concentration of gaseous component *i* ($mol \cdot L^{-1}$)
$c_{i,\mathrm{sat}}'$	molar concentration of component *i* at saturation ($mol \cdot L^{-1}$)
$c_{\mathrm{TIC},i}$	concentration of TIC in the feed ($mol \cdot L^{-1}$)
$c_{\mathrm{TIN},i}$	concentration of TIN in the feed ($mol \cdot L^{-1}$)
ct	constant associated with chemical species with low influence in the electroneutrality relation such as Na^+ and Cl^- ($mol \cdot L^{-1}$)
C_p	specific heat
D	dilution (h^{-1})
d_i	relative degree of a nonlinear system
er_i	error between i^{th} output variable and its setpoint
E_a, $E_{a\lambda}$	mass absorption coefficient (for a specific wavelength λ) ($m^2 \cdot kg^{-1}$)
E_s, $E_{s\lambda}$	mass scattering coefficient (for a specific wavelength λ) ($m^2 \cdot kg^{-1}$)
$f(x)$	*n*-dimensional vector of nonlinear functions
F	volumetric flow rate ($L \cdot h^{-1}$)
F_e	excess sludge flow ($L \cdot h^{-1}$)
F_f	feeding flow with wastewater ($L \cdot h^{-1}$)
F_r	recycled sludge flow ($L \cdot h^{-1}$)
$\mathrm{F/M}$	food to microorganisms ratio
$g(x)$	(*m* x *n*)-dimensional matrix of nonlinear functions
$G_{in\|out}$	input/output flow rate of gas mixtures ($mol \cdot h^{-1}$)

$G^i_{in\|out}$	input/output flow rate of i^{th} gaseous species (mol·h^{-1})
$G_{m\|v}$	mass or volumetric flow rate of the gas
$h(x)$	n-dimensional vector of nonlinear functions
H_i	Henry's constant for i^{th} gaseous species (Pa·m^3·mol^{-1})
$H_{i,u-y}$	transfer function of the system in i^{th} operation point
h_{ij}	elements of transfer function
I, I_λ	irradiance (for a specific wavelength λ) (μmol·m^{-2}·s^{-1})
I_c	compensation point (μmol·m^{-2}·s^{-1})
J	molar specific rate of reaction (mol·L^{-1}·h^{-1})
k	attenuation coefficient
K	equilibrium constant (–)
K_I	irradiance half-saturation constant (μmol·m^{-2}·s^{-1})
K_{II}	irradiance inhibition constant (μmol·m^{-2}·s^{-1})
K_J	substrate inhibition constant (mg·L^{-1})
K_O	half-saturation constant for dissolved oxygen (mg·L^{-1})
K_Q	minimum intracellular quota (mg·L^{-1} or g·L^{-1})
K_S	half-saturation constant for substrate (mg·L^{-1})
K_{TIC}	TIC half-saturation constant (mol·L^{-1})
$(K_L a)_i$	overall volumetric mass transfer coefficient for i^{th} gaseous species (h^{-1})
L	photobioreactor depth (m)
$L_f h, L_g h$	Lie derivatives of h with respect to f and g
M_i	molar mass of component i
M_x	C-mole mass (kg·C-mole^{-1})
N_i	volumetric mass transfer rate of i^{th} gaseous species (mol·L^{-1}·h^{-1})
P	pressure (Pa)
q_e	specific light uptake rate
q_0	incident light intensity (μmol·m^{-2}·s^{-1})
q_z	intensity of light at depth z (μmol·m^{-2}·s^{-1})
q_λ^+, q_λ^-	incident light intensity at wavelength λ – the signs + and – denotes the direction of propagation
Q	intracellular quota – Droop model (mg·L^{-1} or g·L^{-1})
Q_P	photosynthetic quotient (–)

P_i	product i (mg·L^{-1} or g·L^{-1})
R	universal gas constant (J·mol^{-1}·K^{-1})
r	ratio between Q_r and Q_f (-)
r_i, r_i'	mass or molar conversion rate of component i (mg or g·L^{-1}·h^{-1}; mol·L^{-1}·h^{-1})
$r_{\mathrm{O_2}}$	volumetruc $\mathrm{O_2}$ production rate (mol $\mathrm{O_2}$·L^{-1}·h^{-1})
r_s	external substrate consumption rate – Droop model (mg or g·L^{-1}·h^{-1})
r_{S_O}	volumetric $\mathrm{O_2}$ consumption rate (mg·L^{-1}·h^{-1})
r_{S_S}	volumetric COD consumption rate (mg·L^{-1}·h^{-1})
r_{TIC}	TIC consumption rate (mol TIC·L^{-1}·h^{-1})
r_{TIN}	TIN consumption rate (mol TIN·L^{-1}·h^{-1})
r_{X_B}	volumetric growth rate of sludge (g·L^{-1}·h^{-1})
r_x	global volumetric growth rate (g X·L^{-1}·h^{-1})
r_{x_p}	volumetric growth rate due to photosynthesis (g X·L^{-1}·h^{-1})
r_{x_s}	volumetric decrease rate due to respiration
s	Laplace operator
S_0	initial concentration of substrate (mg·L^{-1} or g·L^{-1})
S_i	substrate i (mg·L^{-1} or g·L^{-1})
S_S	substrate concentration (COD concentration) (g·L^{-1})
S_O	dissolved oxygen concentration in the aerobic tank (mg·L^{-1})
$S_{\mathrm{O,sat}}$	saturation concentration of dissolved oxygen in water (mg·L^{-1})
$S_{i,y}^{-1}$	output scaling matrix for i^{th} operating point
t	time (h)
T	temperature (K)
u	$u \in \mathbb{R}^m$ is the input vector
$V_{g\|l}$	gas/liquid volume (m^3)
V_s	n^{th} slice volume in a clarifier (m^3)
W	aeration rate (L·min^{-1})
x	$x \in \mathbb{R}^n$ is the state vector
X	biomass concentration (mg·L^{-1} or g·L^{-1})
X_B	activated sludge concentration (g·L^{-1})
y	$y \in \mathbb{R}^m$ is the output vector
$y_{in\|out}^{i}$	input/output molar fraction of i^{th} gaseous species (*e.g.* $\mathrm{CO_2}$, $\mathrm{O_2}$ or $\mathrm{N_2}$) (–)

y_i^{lm}	logarithmic mean between input and output molar fraction of i^{th} gaseous species (*e.g.* $\mathrm{CO_2}$ or $\mathrm{O_2}$) (–)
Y	growth yield of activated sludge (-)
$Y_{i/j}$	yield of convertion of substrate *i* into product *j*
z	culture depth (m)
$\times$	denotes element-by-element multiplication (Schur product)
$\langle \ \rangle$	denotes a spatial averaging
$\dot{.}$	accent which denotes a derivative

Superscripts

T	denotes a transposed matrix
-1	denotes the inverse of a matrix
†	denotes the Moore-Penrose pseudo inverse of a matrix
$*$	denotes a prescribed value

Greek letters

α	linear scattering modulus
β	ratio between Q_e and Q_f (-)
γ_i	activity coefficient of i^{th} chemical species (*e.g.* $\mathrm{CO_2}$, $\mathrm{HCO_3^-}$, $\mathrm{CO_3^{2-}}$, $\mathrm{NH_3}$, $\mathrm{NH_4^+}$, $\mathrm{NH_2COO^-}$, $\mathrm{OH^-}$ or $\mathrm{H^+}$) (–)
Γ	lighted volume fraction
δ	two-flux extinction coefficient ($\mathrm{m^{-1}}$)
ε	group of constants (*i.e.* $\varepsilon = K_1\gamma_{\mathrm{CO_2}}a_w/\gamma_{\mathrm{HCO_3^-}}$)
η	parameter of the clarifier model
θ	coefficient related with the diffusion of air into the tank
λ_{ij}	elements of the relative gain array
Λ	relative gain array
μ	general notation of the specific growth rate ($\mathrm{h^{-1}}$)
μ_{max}	maximum specific growth rate ($\mathrm{h^{-1}}$)
μ_0	related to $\mu_{max} - \mu_0 = \mu_{max}\left(1 + 2\sqrt{K_S/K_I}\right)$ ($\mathrm{h^{-1}}$)

μ_I, μ_p	specific growth rate due to photosynthesis (h^{-1})
μ_s	respiration kinetic rate (h^{-1})
ν_i	stoichiometric coefficients (ν_{S_i} – consumption yields of S_i; ν_{P_i} – production yields of P_i) (-)
ρ	gas density
υ	new input vector
φ_i	the poles of the system which impose the error dynamics (*e.g.* for X or H^+) (h^{-1})
σ	standard deviation
Φ	φ_i diagonal matrix
ω	frequency ($rad \cdot sec^{-1}$)
ω_{cf}	cutting frequency ($rad \cdot sec^{-1}$)

Chemical species

Ca	calcium
$CaC\ell_2$	calcium chloride
CH_4	methane
$C\ell$	chlorine
Co	cobalt
CO_2	carbon dioxide gas
$CO_{2,aq}$	dissolved carbon dioxide
CO_3^{2-}	carbonate ion
Cu	copper
Fe	iron
H^+	hydrogen ion
HCO_3^-	bicarbonate ion
H_2CO_3	carbonic acid
H_2O	water
HPO_4^{2-}	phosphate ion
H_2S	hydrogen sulfide
K	potassium
KH_2PO_4	monopotassium phosphate

K_2HPO_4	dipotassium phosphate
Mg	magnesium
$MgSO_4$	magnesium sulfate
Mn	manganese
Mo	molybdenum
N_2	nitrogen gas
Na	sodium
$NaC\ell$	sodium chloride
$NaHCO_3$	sodium bicarbonate
NH_3	ammonia
NH_4^+	ammonium ion
$NH_4C\ell$	ammonium chloride
NH_2COO^-	carbamate ion
Ni	nickel
NO_x	nitrogen oxides
NO_3^-	nitrate ion
O_2	oxygen gas
$O_{2,aq}$	dissolved oxygen
OH^-	hydroxyl ion
Se	selenium
SO_x	sulfur oxides
SO_4^{2-}	sulfate ion
Zn	zinc

Abbreviations

AA	Arachidonic Acid
ANAMMOX	Anaerobic Oxidation of Ammonium
AMO	Anaerobic Methane Oxidation
ATP	Adenosine Triphosphate
DHA	Docosahexaenoic Acid
DM	Dry Matter
DO	Dissolved Oxygen

EPA	Eicosapentaenoic Acid
ETC	Electron Transfer Chain
FLC	Feedback Linearizing Control
I/O	Input – Output
LCPUFA	Long Chain Polyunsaturated Fatty Acids
LHC	Light Harvesting Complex
MGM	Minimum Growth Medium
MIMO	Multiple Input Multiple Output
MLSS	Mixed Liquor Suspended Solids
NADP+	Nicotinamide Adenine Dinucleotide Phosphate
NADPH	Reduced form of NADP+
NRG	Non-square Relative Gain Array
PAR	Photosynthetic Active Radiation
PBR	Photobioreactor
PSI	Photosystem I
PSII	Photosystem II
PUFA	Polyunsaturated Fatty Acids
RGA	Relative Gain Array
SBR	Sequencing Batch Reactor
SFBR	Sequencing Feed-Batch Reactor
SISO	Single Input Single Output
STR	Stirred Tank Reactors
TIC	Total Inorganic Carbon
TIN	Total Inorganic Nitrogen
WWTP	Wastewater Treatment Plant

REFERENCES

Acién Fernández FG, Fernández Sevilla JM, Sánchez Pérez JA, Molina Grima E, Chisti Y. Airlift-driven external-loop tubular photobioreactors for outdoor production of microalgae: assessment of design and performance. *Chemical Engineering Science*. 2001; 56(8):2721-2732.

Alex J, Beteau JF, Copp JB, Hellinga C, Jeppsson U, Marsili-Libelli S, Pons MN, Spanjers H, Vanhooren H. Benchmark for evaluating control strategies in wastewater treatment plants, ECC'99 (European Control Conference), Karlsruhe, Germany, Sept. 1999.

Alex J, Benedetti L, Copp J, Gernaey KV, Jeppsson U, Nopens I, Pons MN, Rieger L, Rosen C, Steyer JP, Vanrolleghem P, Winkler S. Benchmark Simulation Model. 1 (BSM1). Report by the IWA Taskgroup on Benchmarking of Control Strategies for WWTPs. 2008.

Anderson R. Algal Culturing Techniques. Elsevier Academic Press, San Diego, California, USA. 2005.

Andrews J. A mathematical model for the continuous culture of microorganisms utilizing inhibitory substrates. *Biotechnology and Bioengineering*. 1968; 10:707-723.

Armstrong WP. Watermelon Snow. *Environment Southwest*. 1987; 517:20-23.

Bains W. Biotechnology from A to Z. 2nd ed. Oxford: Oxford University Press, 1998.

Bannister TT. Quantitative description of steady state, nutrient–saturated algal growth, including adaptation. Limnology and Oceanography. 1979; 24(1):76–96.

Barbu M, Barbu G, Ceanga E. The Multi-model Control of the Wastewater Treatement Process with Activated Sludge, Proceedings of 12th Mediterranean Conference on Control and Automation - MED'04, 2004, Kusadasi, Turkey.

Barbu M. Conducerea automata a proceselor biotehnologice. Galati University Press. Galati, Romania. 2009.

Barbu M, Ifrim G, Caraman S, Bahrim G. QFT Control of Dissolved Oxygen Concentration in a Wastewater Treatment Pilot Plant. In Proceedings of 11th IFAC Symposium on Computer Applications in Biotechnology. 2010. Leuven, Belgium.

Barbu M and Caraman S. QFT Robust Control of Wastewater Treatment Processes, In Bartoszewicz A (ed.). Robust Control, Theory and Applications. InTech. 2011; 577-602.

Barsanti L and Gualtieri P. Algae. Anatomy, Biochemystry and Biotechnology. CRC Press Taylor & Francis Group, Boca Raton, Florida, USA. 2006.

Baquerisse D, Utilisation de la simulation dynamique des procédés pour la conduit et le contrôle commande des bioréacteurs. Thèse Doctorale, Ecole Centrale Paris, France, 1999.

Bastain G and Dochain D, On-line Estimation and Adaptive Control of Bioreactors. 1990. Elsevier, Amsterdam, NL.

Becerra-Celis G, Tebbani S, Joannis-Cassan C, Isambert A, Boucher P. Estimation of Microalgal Photobioreactor Production Based on Total Inorganic Carbon in the Medium. In Proceedings of 17th IFAC World Congress. 2008a. COEX, South Korea.

Becerra-Celis G, Hafidi G, Tebbani S, Dumur D, Isambert A. Nonlinear predictive control for continuous microalgae cultivation process in a photobioreactor. In Proceedings of 10th Conference on Control, Automation, Robotics and Vision. 2008b. Hanoi, Vietnam.

Becker W, Microalgae in Human and Animal Nutrition. In Richmond A (ed.). Handbook of microalgal culture. Blackwell, Oxford, UK. 2004; 312-351.

Belia E, Amerlinck Y, Benedetti L, Johnson B, Sin G, Vanrolleghem PA, Gernaey KV, Gillot S, Neumann MB, Rieger L, Shaw A, Villez K. Wastewater treatment modelling: dealing with uncertainties. *Water Science & Technology*. 2009; 60(8):1929-1941.

Belkin S and Boussiba S. Resistance of *Spirulina platensis* to Ammonia at High pH Values. *Plant and Cell Physiology*. 1991; 32(7):953-958.

Benson BC and Rusch KA. Investigation of the light dynamics and their impact on algal growth rate in a hydraulically integrated serial turbidostat algal reactor (HISTAR). Aquacultural Engineering. 2006; 35(2):122-134.

Benson BC, Gutierrez-Wing M, Rusch KA. Optimization of the lighting system for a Hydraulically Integrated Serial Turbidostat Algal Reactor (HISTAR): Economic implications. *Aquacultural Engineering*. 2009; 40(1):45-53.

Berenguel M, Rodríguez F, Acién FG, García JL. Model predictive control of pH in tubular photobioreactors. *Journal of Process Control*. 2004; 14(4):377-387.

Bermejo Román R, Alvárez-Pez JM, Acién Fernández FG, Molina Grima E. Recovery of pure B-phycoerythrin from the microalga *Porphyridium cruentum*. *Journal of Biotechnology*. 2002; 93(1):73-85.

Bernard O. Hurdles and challenges for modelling and control of microalgae for CO_2 mitigation and biofuel production. *Journal of Process Control*. 2011; 21(10):1378-1389.

Bitton G. Wastewater Microbiology. Third Edition. John Wiley & Sons, Inc., Hoboken, New Jersey; 2005.

Borowitzka MA. Commercial production of microalgae: ponds, tanks, tubes and fermenters. *Journal of Biotechnology*. 1999; 70(1-3):313-321.

Brányiková I, Maršálková B, Doucha J, Brányik T, Bišová K, Zachleder V, Vítová M. Microalgae-novel highly efficient starch producers. *Biotechnology and Bioengineering*. 2010; 108(4):766-776.

Brennan L and Owende P. Biofuels from microalgae – A review of technologies for production, processing, and extractions of biofuels and co-products. *Renewable and Sustainable Energy Reviews*. 2010; 14(2):557-577.

Bristol E. On a new measure of interaction for multivariable process control. *IEEE Transactions on Automatic* Control. 1966; 11(1):133-134.

Brdys MA and Konarczak K. Dissolved Oxygen Control for Activated Sludge Processes, Preprints of the 9th IFAC/IFORS/IMACS/IFIP Symposium Large Scale Systems: Theory & Applications – LSS'2001, Bucharest, Romania, pp.548-553.

Brdys MA and Zhang Y. Robust Hierarchical Optimising Control of Municipal Wastewater Treatment Plants, Preprints of the 9th IFAC/IFORS/IMACS/IFIP Symposium Large Scale Systems: Theory & Applications – LSS'2001, Bucharest, Romania, pp.540-547.

Brown LM. Uptake of carbon dioxide from flue gas by microalgae. *Energy Conversion and Management*. 1996; 37(6–8):1363-1367.

Buehner MR, Young PM, Willson B, Rausen D, Schoonover R, Babbitt G, Bunch S. Microalgae growth modeling and control for a vertical flat panel photobioreactor. In Proceedings of American Control Conference. 2009. St. Louis, MO, USA.

Camacho Rubio F, Acién Fernandez FG, Sánchez Perez JA, García Camacho F, Molina Grima E. Prediction of dissolved oxygen and carbon dioxide concentration profiles in tubular photobioreactors for microalgal culture. *Biotechnology and Bioengineering*. 1999; 62(1):71-86.

Cao Y. Control Structure Selection for Chemical Processes Using Input-Output Controllability Analysis. 1995. PhD thesis, University of Exeter.

Carmichael WW. The Cyanotoxins. In: Callow JA (ed.), Advances in Botanical Research. Academic Press. 1997; 27:211-256.

Chaiklahan R, Chirasuwan N, Siangdung W, Paithoonrangsarid K, Bunnag B. Cultivation of *Spirulina platensis* Using Pig Wastewater in a Semi-Continuous Process. *Journal of Microbiology and Biotechnology*. 2010; 20(3):609-614.

Chang JW and Yu CC. The relative gain for non-square multivariable systems. *Chemical Engineering Science*. 1990; 45(5):1309-1323.

Chau PC. Process Control. A First Course With Matlab. Cambridge University Press, New York, USA. 2002.

Chen CY, Lee CM, Chang JS. Hydrogen production by indigenous photosynthetic bacterium *Rhodopseudomonas palustris* WP3–5 using optical fiber-illuminating photobioreactors. *Biochemical Engineering Journal*. 2006; 32(1):33-42.

Chen D and Seborg E. Relative gain array analysis for uncertain process models. *AIChe Journal*. 2002; 48(2):302-310.

Chisti Y. Biodiesel from microalgae. *Biotechnology Advances*. 2007; 25(3):294-306.

Choi SL, Suh IS, Lee CG. Lumostatic operation of bubble column photobioreactors for *Haematococcus pluvialis* cultures using a specific light uptake rate as a control parameter. Enzyme and Microbial Technology. 2003; 33(4):403-409.

Cogne G, Lasseur C, Cornet JF, Dussap CG, Gros JB. Growth monitoring of a photosynthetic micro-organism (Spirulina platensis) by pressure measurement. *Biotechnology Letters*. 2001; 23(16):1309-1314.

Colt J, Watten B, Rust M. Modeling carbon dioxide, pH, and un-ionized ammonia relationships in serial reuse systems. *Aquacultural Engineering*. 2009; 40(1):28-44.

Copp JB (ed.). The COST Simulation Benchmark. In Description and Simulator Manual. Office for Official Publications of the European Communities, Luxembourg. 2002.

Cornet JF, Dussap CG, Gros JB, Binois C, Lasseur C. A simplified monodimensional approach for modeling coupling between radiant light transfer and growth kinetics in photobioreactors. *Chemical Engineering Science*. 1995; 50(9):1489-1500.

Cornet JF, Dussap CG, Gros JB. Kinetics and energetics of photosynthetic micro-organisms in photobioreactors. Application to Spirulina growth. *In* Scheper T (ed.). Bioprocess and Algae Reactor Technology, Apoptosis. Springer, Berlin/Heidelberg. 1998; 59:153-224.

Cornet JF and Dussap CG. A simple and reliable formula for assessment of maximum volumetric productivities in photobioreactors. *Biotechnology Progress*. 2009; 25(2):424-435.

Csőgör Z, Herrenbauer M, Schmidt K, Posten C. Light distribution in a novel photobioreactor – modelling for optimization. *Journal of Applied Phycology*. 2001; 13(4):325-333.

D'Azzo JJ and Houpis CH. Linear Control System Analysis and Design with Matlab. Marcel Dekker, Inc., New York, USA, 2003.

Degerenne B. Production d'hydrogène par *Chlamydomonas reinhardtii* en photobioréacteur : Analyse des conditions de culture et mise en place d'un protocol autotrophe. Thèse de doctorat. Nantes, 2009.

Degrenne B, Pruvost J, Legrand J. Effect of prolonged hypoxia in autotrophic conditions in the hydrogen production by the green microalga *Chlamydomonas reinhardtii* in photobioreactor. *Bioresource Technology*. 2011; 102(2):1035-1043.

Denny MW. Air and water. The biology and physics of life's media. Princeton, NJ: Princeton University Press. 1993.

Derks PWJ and Versteeg GF. Kinetics of absorption of carbon dioxide in aqueous ammonia solutions. *Energy Procedia*. 2009; 1(1):1139-1146.

Deschênes JS, Desbiens A, Perrier M, Kamen A. On Simultaneous Control of Biomass and Metabolite Concentration in Perfusion Bioreactors. In Proceedings of DCDIS Conference. 2005. Guelph, ON, Canada.

Dilek FB, Taplamacioglu HM, Tarlan E. Colour and AOX removal from pulping effluents by algae. *Applied Microbiology and Biotechnology*. 1999; 52(4):585-591.

Dochain D. Automatic Control of Bioprocesses. John Wiley & Sons, Inc. Great Britain, 2008.

Doshi H, Seth C, Ray A, Kothari IL. Bioaccumulation of Heavy Metals by Green Algae. *Current Microbiology*. 2008; 56(3):246-255.

Droop MR. Vitamin B12 and Marine Ecology. IV. The Kinetics of Uptake, Growth and Inhibition in *Monochrysis Lutheri*. *Journal of the Marine Biological Association of the United Kingdom*. 1968; 48(3), 689-733.

Durmaz Y. Vitamin E (α-tocopherol) production by the marine microalgae *Nannochloropsis oculata* (*Eustigmatophyceae*) in nitrogen limitation. *Aquaculture*. 2007; 272(1–4):717-722.

Edwards TJ, Maurer G, Newman J, Prausnitz JM. Vapour-liquid equilibria in multicomponent aqueous solutions of volatile weak electrolytes. *AIChE Journal*. 1978; 24:966-975.

Eriksen NT, Riisgård FK, Gunther WS, Lønsmann Iversen JJ. On-line estimation of O_2 production, CO_2 uptake, and growth kinetics of microalgal cultures in a gas-tight photobioreactor. *Journal of Applied Phycology*. 2007; 19(2):161-174.

Eriksen NT. The technology of microalgal culturing. *Biotechnology Letters*. 2008; 30(9):1525-1536.

Favier-Teodorescu L, Cornet JF, Dussap CG. Modelling continuous culture of *Rhodospirillum rubrum* in photobioreactor under light limited conditions. *Biotechnology Letters*. 2003; 25(4):359-364.

Fernández SI, Peña MJ, Guzman JL, Berenguel M, Acién FG. Modelling and Control Issues of pH in Tubular Photobioreactors. In Proceedings of 11th IFAC Symposium on Computer Applications in Biotechnology. 2010. Leuven, Belgium.

Ford TW. Thermostability of the Photosynthetic System of the Thermoacidophilic Alga *Cyanidium caldarium* in Continuous Culture. *Journal of Experimental Botany*. 1986; 37(11):1698-1707.

Fouchard S, Hemschemeier A, Caruana A, Pruvost J, Legrand J, Happe T, Peltier G, Cournac L. Autotrophic and Mixotrophic Hydrogen Photoproduction in Sulfur-Deprived *Chlamydomonas* Cells. *Applied and Environmental Microbiology*. 2005; 71(10):6199-6205.

Fouchard S, Pruvost J, Degrenne B, Legrand J. Investigation of H_2 production using the green microalga *Chlamydomonas reinhardtii* in a fully controlled photobioreactor fitted with on-line gas analysis. *International Journal of Hydrogen Energy*. 2008; 33(13):3302-3310.

Fouchard S, Pruvost J, Degrenne B, Titica M, Legrand J. Kinetic modeling of light limitation and sulfur deprivation effects in the induction of hydrogen production with *Chlamydomonas reinhardtii*: Part I. Model development and parameter identification. *Biotechnology and Bioengineering*. 2009; 102(1):232-245.

Garbayo I, Forjan E, Salguero A, Cuaresma M, Vega JM, Vilchez C. Enhancement of photorespiration in immobilized *Chlamydomonas reinhardtii* cells. *Biotechnology Letters*. 2005; 27:265-267.

García JL, Berenguel M, Rodríguez F, Fernández JM, Brindley C, Acién FG. Minimization of carbon losses in pilot-scale outdoor photobioreactors by model-based predictive control. *Biotechnology and Bioengineering*. 2003; 84(5):533-543.

García Camacho F, Contreras Gómez A, Acién Fernández FG, Fernández Sevilla J, Molina Grima E. Use of concentric-tube airlift photobioreactors for microalgal outdoor mass cultures. *Enzyme and Microbial Technology*. 1999; 24(3-4):164-172.

Garcia-Sanz M, Eguinoa I, Gil M, Irizar I, Ayesa E.). MIMO Quantitative Robust Control of a Wastewater Treatment Plant for Biological Removal of Nitrogen and Phosphorus, 16th Mediterranean Conference on Control and Automation, Corcega, 2008.

Granum E and Myklestad SM. A photobioreactor with pH control: demonstration by growth of the marine diatom Skeletonema costatum. *Journal of Plankton Research*. 2002; 24(6):557-563.

Grau P, Sutton PM, Henze M, Elmaleh S, Grady CP, Gujer W, Koller J. Recommended Notation for use in the Description of Biological Wastewater Treatment Processes. *Water Research*. 1982; 16:1501-1505.

Gray NF. Water Technology. An Introduction for Environmental Scientists and Engineers. Second Edition. Elsevier, Oxford. 2005.

Greenwell HC, Laurens LML, Shields RJ, Lovitt RW, Flynn KJ. Placing microalgae on the biofuels priority list: a review of the technological challenges. *Journal of the Royal Society Interface*. 2010; 7(46):703-726.

Grossman AR, Harris EE, Hauser C, Lefebvre PA, Martinez D, Rokhsar D, Shrager J, Silflow CD, Stern D, Vallon O, Zhang Z. *Chlamydomonas reinhardtii* at the crossroads of genomics. *Eukaryotic cell*. 2003; 2(6):1137-1150.

Grossman AR, Lohr M, Im CS. *Chlamydomonas reinhardtii* in the Landscape of Pigments. *Annual Review of Genetics*. 2004; 38(1):19-73.

Gutzeit G, Lorch D, Weber A, Engels M, Neis U. Bioflocculent algal–bacterial biomass improves low-cost wastewater treatment. *Water Science and Technology*. 2005; 52(12):9-18.

Haario H, Kalachev L, Laine M. Reduced models of algae growth. *Bulletin of Mathematical Biology*. 2009; 71(7):1626-1648.

Harris EH. The *Chlamydomonas reinhardtii* sourcebook. A comprehensive guide to biology and laboratory use. San Diego, CA, Academic Press. 1989.

Harris EH. The *Chlamydomonas* Sourcebook. Vol.1. Introduction to *Chlamydomonas* and Its Laboratory Use. Second Edition. San Diego, CA, Academic Press. 2009.

Hempel F, Bozarth AS, Lindenkamp N, Klingl A, Zauner S, Linne U, Steinbüchel A, Maier UG. Microalgae as bioreactors for bioplastic production. *Microbial Cell Factories*. 2011; 10:81.

Henson MA and Seborg DE. Nonlinear Process Control. 1997. Prentice Hall, Upper Saddle River, NJ, USA.

Henze M, Grady CPL Jr. Gujer W, Marais GVR, Matsuo T. Activated Sludge Model No.1, IAWPRC Scientific and Technical Report No.1, 1987, IAWQ, Great Britain.

Henze M, Gujer W, Mino T, Matsuo T, Wentzel MC, Marais GVR. Activated Sludge Model No.2, IAWQ Scientific and Technical Report No.3, IAWQ, 1995, Great Britain.

Henze M, Gujer W, Mino T, Matsuo T, Wentzel MC, Marais GVR van Loosdrecht MCM. Activated Sludge Model No.2d. Water Science and Technology. 1999; 39(1):165-182.

Henze M, Gujer W, Mino T, van Loosdrecht M. Activated Sludge Models ASM1, ASM2, ASM2d and ASM3, 2000, IWA Publishing, London, Great Britain.

Herbert D. Some Principles of continuous culture. In: Recent Progress in Microbiology, (ed.) Tunevall G. Almquist and Wiksell, Stockholm. 1958:381-396.

Horowitz IM. Optimum Loop Transfer Function in Single-Loop Minimum Phase Feedback Systems. International Journal of Control. 1973; 22:97-113.

Houpis CH and Rasmussen SJ. Quantitative Feedback Theory Fundamentals and Applications, Marcel Dekker, Inc., New York. 1999.

Hu Q, Kurano N, Kawachi M, Iwasaki I, Miyachi S. Ultrahigh-cell-density culture of a marine green alga *Chlorococcum littorale* in a flat-plate photobioreactor. *Applied Microbiology and Biotechnology*. 1998; 49(6):655-662.

Hutner SH, Provasoli L, Schatz A, Haskins CP. Some approaches to the study of the role of metals in the metabolism of microorganisms. *Proc. Am. Philos*. 1950; 94:152–170.

Ifrim G, Barbu M, Titica M, Boillereaux L, Caraman S. Control of the microalgae photosynthetic growth in a torus photobioreactor. *In* proceedings of 14th International Conference on System Theory (SINTES 14), Oct.17-19, 2010, Sinaia, Romania.

Ingildsen P. Realising Full-Scale Control in Wastewater Treatment Systems Using In Situ Nutrient Sensors, Ph.D. Thesis, Department of Industrial Electrical Engineering and Automation, 2002, Lund University, Sweden.

Janssen M, Kuijpers TC, Veldhoen B, Ternbach MB, Tramper J, Mur LR, Wijffels RH. Specific growth rate of *Chlamydomonas reinhardtii* and *Chlorella sorokiniana* under medium duration light/dark cycles: 13–87 s. *Journal of Biotechnology*. 1999; 70(1-3):323-333.

Jaworski Z, Czernuszewicz M, Gralla L. A comparative study of thermodynamic electrolyte models applied to the Solvay soda system. Chemical and Process Engineering. 2011; 32(2):135-154.

Jeppsson U. Modelling aspects of wastewater treatment processes, Ph.D. thesis, Dept. of Industrial Electrical Eng. and Automation, 1996, Lund University, Sweden.

Jeppsson U and Pons MN. The COST 624 benchmark simulation model – current state and future perspective (Editorial). *Control Engineering Practice*. 2004; 12(3):299-304.

Jiang Y, Chen SF, Liang SZ. Production of polyunsaturated fatty acids (PUFA) by microalgae culture. In: Peng, Z.Y. & Zeng, Q.X. (eds). Developments in Food Science and Technology. 1997:54-62.

Jilvero H, Normann F, Andersson K, Johnsson F. Thermal integration and modelling of the chilled ammonia process. *Energy Procedia*. 2011; 4:1713-1720.

Jiménez C and Niell FX. Growth of *Dunaliella viridis* Teodoresco: effect of salinity, temperature and nitrogen concentration. *Journal of Applied Phycology*. 1991; 3(4):319-327.

Katebi MR, Johnson MA, Wilke J. Control and Instrumentation for Wastewater Treatment Plant. 1999, Springer-Verlag, London.

Khozin-Goldberg I, Iskandarov U, Cohen Z. LC-PUFA from photosynthetic microalgae: occurrence, biosynthesis, and prospects in biotechnology. *Applied Microbiology and Biotechnology*. 2011; 91(4):905-915.

Kinnaert M. Interaction measures and pairing of controlled and manipulated variables for multiple-input multiple-output systems: A survey. *Journal A*. 1995; 36(4):15-23.

Kong QX, Li L, Martinez B, Chen P, Ruan R. Culture of Microalgae *Chlamydomonas reinhardtii* in Wastewater for Biomass Feedstock Production. *Applied Biochemistry and Biotechnology*. 2010; 160(1):9-18.

Kosourov S, Seibert M, Ghirardi ML. Effects of Extracellular pH on the Metabolic Pathways in Sulfur-Deprived, H_2-Producing *Chlamydomonas reinhardtii* Cultures. *Plant and Cell Physiology*. 2003; 44(2):146-155.

Larsson T and Skogestad S. Plantwide control – A review and a new design procedure. *Modelling, Identification and Control*. 2000; 21(4):209-240.

Lee HS, Seo MW, Kim ZH, Lee CG. Determining the best specific light uptake rates for the lumostatic cultures in bubble column photobioreactors. *Enzyme and Microbial Technology*. 2006; 39(3):447-452.

Li J, Xu NS, Su WW. Online estimation of stirred-tank microalgal photobioreactor cultures based on dissolved oxygen measurement. *Biochemical Engineering Journal*. 2003; 14(1):51-65.

Loubière P, Cocaign-Bousquet M, Matos J, Goma G, Lindley ND. Influence of end-products inhibition and nutrients limitations on the growth of *Lactococcus lactis* subsp. *lactis*. *Journal of Applied Microbiology*. 1997; 82(1):95-100.

Mailleret L, Bernard O, Steyer JP. Nonlinear Adaptive Control for Bioreactors with Unknown Kinetics. *Automatica*. 2004; 40(8):1379-1385.

Mailleret L, Gouzé J, Bernard O. Nonlinear control for algae growth models in the chemostat. *Bioprocess and Biosystems Engineering*. 2005; 27(5):319-327.

Mairet F, Titica M, Bernard O, Pruvost J. Coupling Biological and Radiative Models to Describe Microalgal Growth in a Photobioreactor. In Proceedings of *11th IFAC Symposium on Computer Applications in Biotechnology*. 2010. Leuven, Belgium.

Mairet Francis, Bernard O, Lacour T, Sciandra A. Modelling Microalgae Growth in Nitrogen Limited Photobiorector for Estimating Biomass, Carbohydrate and Neutral Lipid Productivities. In Proceedings of the *18th IFAC World Congress*. 2011. Milano, Italy.

Mallick N. Biotechnological potential of immobilized algae for wastewater N, P and metal removal: A review. *Biomedical and Life Sciences*. 2002; 15(4):377-390.

Manesis SA, Sapidis DJ, King RE. Intelligent Control of Wastewater Treatment Plants, Artificial Intelligence in Engineering. 1998; 12(3):275-281.

Martinez Sancho ME, Jimenez Castillo JM, Yousi FE, Influence of phosphorus concentration and temperature on growth and phosphorus uptake by the microalga Scenedesmus obliquus. *Bioresource Technology*. 1999; 67(3):233-240.

Marxen K, Vanselow KH, Lippemeier S, Hintze R, Ruser A, Hansen UP. A photobioreactor system for computer controlled cultivation of microalgae. *Journal of Applied Phycology*. 2005; 17(6):535-549.

Masojídek J and Torzillo G. Mass Cultivation of Freshwater Microalgae, In: Editors-in-Chief: Sven Erik Jorgensen and Brian Fath, Editor(s)-in-Chief, Encyclopedia of Ecology, Academic Press, Oxford; 2008:2226-2235.

Matsumoto H, Shioji N, Hamasaki A, Ikuta Y, Fukuda Y, Sato M, Endo N, Tsukamoto T. Carbon dioxide fixation by microalgae photosynthesis using actual flue gas discharged from a boiler. *Applied Biochemistry and Biotechnology*. 1995; 51-52(1):681-692.

Melis A, Zhang L, Forestier M, Ghirardi ML, Seibert M. Sustained photobiological hydrogen gas upon reversible inactivation of oxygen evolution in the green alga *Chlamydomonas reinhardtii*. *Plant Physiology*. 2000; 122:127-135.

Melis A. Photosynthetic H_2 metabolism in *Chlamydomonas reinhardtii* (unicellular green algae). *Planta*. 2007; 226(5):1075-1086.

Mohr PJ, Taylor BN, Newell DB. CODATA Recommended Values of the Fundamental Physical Constants: 2006. *Reviews of Modern Physics*. 2008; 80:633-730.

Molina Grima E, Sánchez Pérez JA, García Camacho F, García Sánchez JL, Acién Fernández FG, López Alonso D. Outdoor culture of *Isochrysis galbana* ALII-4 in a closed tubular photobioreactor. *Journal of Biotechnology*. 1994; 37(2):159-166.

Molina Grima E, Fernandez Sevilla JM, Sanchez Perez JA, Garcia Camacho F. A study on simultaneous photolimitation and photoinhibition in dense microalgal cultures taking into account incident and averaged irradiances. *Journal of Biotechnoly*. 1996; 45(1):59–69.

Molina Grima E, García Camacho F, Sánchez Pérez JA, Acién Fernández FG, Fernández Sevilla JM. Evaluation of photosynthetic efficiency in microalgal cultures using averaged irradiance. *Enzyme and Microbial Technology*. 1997; 21(5):375-381.

Molina Grima E, Acién Fernández FG, García Camacho F, Chisti Y. Photobioreactors: light regime, mass transfer, and scaleup. *Journal of Biotechnology*. 1999; 70(1-3):231-247.

Molina E, Fernández J, Acién FG, Chisti Y. Tubular photobioreactor design for algal cultures. *Journal of Biotechnol*. 2001; 92(2):113–131.

Monod J. Recherché sur la croissance des cultures bactériennes. Thèse de docteur es sciences naturelles, Herman, Paris. 1942.

Muñoz R, Guieysse B. Algal–bacterial processes for the treatment of hazardous contaminants: A review. *Water Research*. 2006; 40(15):2799-2815.

Nagase HYK, Yoshihara KI, Hirata K, Miyamoto K. Improvement of microalgal NOx removal in bubble column and airlift reactors. *Journal of Fermentation and Bioengineering*. 1998; 86(4):421-423.

Nagase HYK, Eguchi K, Okamoto Y, Murasaki S, Yamashita R, Hirata K, Miyamoto K. Uptake pathway and continuous removal of nitric oxide from flue gas using microalgae. *Biochemical Engineering*. 2001; 7(3):241-246.

Nedbal L, Cervený J, Keren N, Kaplan A. Experimental validation of a nonequilibrium model of CO_2 fluxes between gas, liquid medium, and algae in a flat-panel photobioreactor. *Journal of Industrial Microbiology and Biotechnology*. 2010; 37(12):1319-1326.

Nejjari F, Dahhou B, Benhammou A, Roux G. Non-linear multivariable adaptive control of an activated sludge wastewater treatment process. *International Journal of Adaptive Control and Signal Processing.* 1999; 13(5):347-365.

Nielsen DR, Daugulis AJ, Mclellan PJ. A novel method of simulating oxygen mass transfer in two-phase partitioning bioreactors. *Biotechnology and Bioengineering*. 2003; 83(6):735-742.

Nigam PS and Singh A. Production of liquid biofuels from renewable resources. *Progress in Energy and Combustion Science*. 2011; 37(1):52-68.

Nouals S, Modélisation d'un photobioréacteur pour le pilotage de microalgues. Thèse Doctorale, Ecole Centrale Paris, France, 2000.

Obeid J, Magnin JP, Flaus JM, Adrot O, Willison JC, Zlatev R. Modelling of hydrogen production in batch cultures of the photosynthetic bacterium *Rhodobacter capsulatus*. *International Journal of Hydrogen Energy*. 2009; 34(1):180-185.

Ogata K. Modern Control Engineering. Prentice Hall, Upper Saddle River, New Jersey, USA, 1997.

Ogbonna JC, Yada H, Masui H, Tanaka H. A novel internally illuminated stirred tank photobioreactor for large-scale cultivation of photosynthetic cells. *Journal of Fermentation and Bioengineering*. 1996; 82(1):61-67.

Ogbonna JC, Soejima T, Tanaka H. An integrated solar and artificial light system for internal illumination of photobioreactors. *Journal of Biotechnology*. 1999; 70(1-3):289-297.

Okuyama H, Kogame K, Mizuno M, Kobayashi W, Kanazawa H, Ohtani S, Watanabe K, Kanda H. Extremely psychrophilic microalgae isolated from the Antarctic ocean. Proceedings of *NIPR Symposium on Polar Biology*. 1992; 5:1-8.

Olguín EJ. Phycoremediation: key issues for cost-effective nutrient removal processes. *Biotechnology Advances*. 2003; 22(1-2):81-91.

Olsson G. Control strategies for the activated sludge process, Comprehensive Biotechnology, Editor M. Moo-Young, 1985. Pergamon Press, 1107-1119.

Olsson G and Newell B. Wastewater treatment systems – modelling, diagnosis and control, 1999, IWA Publishing, Great Britain.

Paraskevopoulous PN, Modern Control Engineering. Marcel Dekker, Inc., New York, USA, 2002.

Park W and Moon I. A discrete multi states model for the biological production of hydrogen by phototrophic microalga. *Biochemical Engineering Journal*. 2007; 36(1):19-27.

Pittman JK, Dean AP, Osundeko O. The potential of sustainable algal biofuel production using wastewater resources. *Bioresource Technology*. 2011; 102(1):17-25.

Pitzer KS. Thermodynamics of electrolytes. I. Theoretical basis and general equations. *The Journal of Physical Chemistry*. 1973; 77(2):268-277.

Pottier L, Pruvost J, Deremetz J, Cornet JF, Legrand J, Dussap CG. A fully predictive model for one-dimensional light attenuation by *Chlamydomonas reinhardtii* in a torus photobioreactor. *Biotechnology and Bioengineering*. 2005; 91(5):569-582.

Pruvost J, Legrand J, Legentilhomme P. Numerical investigation of bend and torus flows, part I: effect of swirl motion on flow structure in U-bend. *Chemical Engineering Science*. 2004a; 59(16):3345-3357.

Pruvost J, Legrand J, Legentilhomme P, Rosant JM. Numerical investigation of bend and torus flows - Part II: Flow simulation in torus reactor. *Chemical Engineering Science*. 2004b; 59(16):3359-3370.

Pruvost J, Pottier L, Legrand J, Numerical investigation of hydrodynamic and mixing conditions in a torus photobioreactor. *Chemical Engineering Science*. 2006; 61(14):4476-4489.

Pruvost J, Cornet JF, Legrand J. Hydrodynamics influence on light conversion in photobioreactors: An energetically consistent analysis. *Chemical Engineering Science*. 2008; 63(14):3679-3694.

Pulz O and Gross W. Valuable products from biotechnology of microalgae. *Applied Microbiology and Biotechnology*. 2004; 65(6):635-648.

Radmann EM, Reinehr CO, Costa JAV. Optimization of the repeated batch cultivation of microalga *Spirulina platensis* in open raceway ponds. *Aquaculture*. 2007; 265(1-4):118-126.

Radmer RJ and Parker BC. Commercial applications of algae: opportunities and constraints. *Biomedical and Life Sciences*. 1994; 6(2):93-98.

Radmer RJ. Algal Diversity and Commercial Algal Products. *BioScience*. 1996; 46(4):263-270.

Raj K, Dev Dutt P, Deen Dayal B, Saurabh M, Anis M, Rajesh A, Ashok S, Rakesh Kumar S, Rajendra Prasad T. Extremophiles: Sustainable Resource of Natural Compounds-Extremolytes. In Singh OV and Harvey SP (ed.) Sustainable Biotechnology. Springer, Netherlands. 2010:279-294.

Ranjbar R, Inoue R, Shiraishi H, Katsuda T, Katoh S. High efficiency production of astaxanthin by autotrophic cultivation of *Haematococcus pluvialis* in a bubble column photobioreactor. *Biochemical Engineering Journal*. 2008; 39(3): 575-580.

Rebolloso Fuentes MM, García Sánchez JL, Fernández Sevilla JM, Acién Fernández FG, Sánchez Pérez JA, Molina Grima E. Outdoor continuous culture of *Porphyridium cruentum* in a tubular photobioreactor: quantitative analysis of the daily cyclic variation of culture parameters. *Journal of Biotechnology*. 1999; 70(1-3):271-288.

Reeves DE and Arkun Y. Interaction measures for nonsquare decentralized control structures. *AIChE Journal*. 1989; 35(4):603-613.

Roels JA. Energetics and kinetics in biotechnology. Elsevier Biomedical Press, Amsterdam, 1983.

Rosenbaum M, Schröder U, Scholz F. Utilizing the green alga *Chlamydomonas reinhardtii* for microbial electricity generation: a living solar cell. *Chemistry and Materials Science*. 2005; 68(6):753-756.

Roustan M. Transferts gaz-liquide dans les procédés de traitement des eaux et des effluents gazeux. Tec et Doc, Paris, 2003.

Rubio FC, Fernandez FG, Perez JA, Camacho FG, Grima EM. Prediction of dissolved oxygen and carbon dioxide concentration profiles in tubular photobioreactors for microalgal culture. *Biotechnology and Bioengineering*. 1999; 62(1):71-96.

Sánchez O and Mas J. Measurement of light absorption and determination of the specific rate of light uptake in cultures of phototrophic microorganism. Applied and Environmental Microbiology. 1996; 62(2):620-4.

Sandnes JM, Ringstad T, Wenner D, Heyerdahl PH, Källqvist T, Gislerød HR. Real-time monitoring and automatic density control of large-scale microalgal cultures using near infrared (NIR) optical density sensors. *Journal of Biotechnology*. 2006; 122(2):209-215.

Schumpe A. Gas solubilities in biomedia. *In* Rehm HJ and Reed G (eds.). Biotechnology. Vol.2. VCH Publishers, Weinheim, 1985; 160-170.

Shi J, Podola B, Melkonian M. Removal of nitrogen and phosphorus from wastewater using microalgae immobilized on twin layers: an experimental study. *Journal of Applied Phycology*. 2007; 19(5):417-423.

Sierra E, Acién FG, Fernández JM, García JL, González C, Molina E. Characterization of a flat plate photobioreactor for the production of microalgae. *Chemical Engineering Journal*. 2008; 138(1-3):136-147.

Singh A, Nigam PS, Murphy JD. Mechanism and challenges in commercialisation of algal biofuels. *Bioresource Technology*. 2011; 102(1):26-34.

Skjånes K, Knutsen G, Källqvist T, Lindblad P. H_2 production from marine and freshwater species of green algae during sulfur deprivation and considerations for bioreactor design. *International Journal of Hydrogen Energy*. 2008; 33(2):511-521.

Skogestad S and Postlethwaite I. Multivariable Feedback Control: Analysis and Design. Second Edition. 2001. John Wiley & Sons, Chichester, UK.

Sloth JK, Wiebe MG, Eriksen NT. Accumulation of phycocyanin in heterotrophic and mixotrophic cultures of the acidophilic red alga *Galdieria sulphuraria*. *Enzyme and Microbial Technology*. 2006; 38(1-2):168-175.

Spanjers H, Vanrolleghem PA, Nguyen K, Vanhooren H, Patry GG. Towards a simulation benchmark for evaluating respirometry-based control strategies. *Water Science and Technology*. 1998; 37(12):219-226.

Spijkerman E. Inorganic carbon acquisition by *Chlamydomonas acidophila* across a pH range. *Canadian Journal of Botany*. 2005; 83(7):872-878.

Spolaore P. Optimisation et modélisation de la croissance de microalgues en vue de la validation des performances d'un photobioréacteur pilote. Thèse Doctorale, Ecole Centrale Paris, France, 2005.

Spolaore P, Joannis-Cassan C, Duran E, Isambert A. Commercial applications of microalgae. *Journal of Bioscience and Bioengineering*. 2006; 101(2):87-96.

Steele JH. In: Lapidus, L., Amundson, N.R. (Eds.), Microbial Kinetics and Dynamics in Chemical Reactor Theory. Prentice-Hall, Englewood Cliffs, NJ, 1977:405–483.

Sterritt RM and Lester JN. Heavy metals immobilisation by bacterial extracellular polymers, In: Immobilisation of Ions by Bio-Sorption, (eds.) Eccles H and Hunt S, Ellis Horwood, Chichester, U.K. 1988:121-134.

Suh IS and Lee SB. Cultivation of a cyanobacterium in an internally radiating air-lift photobioreactor. *Journal of Applied Phycology*. 2001; 13(4):381-388.

Takache H, Christophe G, Cornet JF, Pruvost J. Experimental and theoretical assessment of maximum productivities for the micro-algae *Chlamydomonas reinhardtii* in two different geometries of photobioreactors. *Biotechnology Progress*. 2010; 26 (2):431-440.

Tamiya H, Hase E, Shibata K, Mituya A, Iwamura T, Nihei T, Sasa T. Kinetics of growth of *Chlorella*, with special reference to its dependence on quantity of available light and on temperature. In: Burlew JS (Ed.), Algal Culture from Laboratory to Pilot Plant. Carnegie Institution of Washington, Washington DC. 1953:204–232.

Tarlan E, Yetis U, Dilek FB. Algal treatment of pulp and paper industry wastewaters in SBR systems. *Water Science and Technology*. 2002; 45(12):151-158.

Tchobanoglous, G., F.L. Burton, and H.D. Stensel. Meltcalf & Eddy, Inc.'s Wastewater Engineering: Treatment, Disposal, and Reuse, 4th Edition. McGraw-Hill, Inc., New York; 2003.

Ugwu CU, Aoyagi H, Uchiyama H. Photobioreactors for mass cultivation of algae. *Bioresource Technology*. 2008; 99(10):4021-4028.

Waller JB and Waller KV. Defining directionality: Use of directionality measures with respect to scaling. *Industrial & Engineering Chemistry Research*. 1995; 34(4):1244-1252.

Walker TL, Purton S, Becker DK, Collet C. Microalgae as bioreactors. *Plant Cell Reports*. 2005; 24(11):629-641.

Wang B, Li Y, Wu N, Lan CQ. CO_2 bio-mitigation using microalgae. *Applied Microbiology and Biotechnology*. 2008; 79(5):707-718.

Wei Q, Hu Z, Li G, Xiao B, Sun H, Tao M. Removing nitrogen and phosphorus from simulated wastewater using algal biofilm technique. *Earth and Environmental Science*. 2008; 2(4):446-451.

Wen ZY and Chen F. A perfusion–cell bleeding culture strategy for enhancing the productivity of eicosapentaenoic acid by *Nitzschia laevis*. *Applied Microbiology and Biotechnology*. 2001; 57(3):316-322.

Van Liere L and Mur LR. Growth kinetics of *Oscillatoria agardhii* Gomont in continuous culture, limited in its growth by the light energy supply. Journal of General MicrobioIog. 1979; 115(1):153-160.

Van Oorschot JLP. Conversion of light energy in algal cultures. Med van Lund. Wang. 1955; 55:225–277.

Voltolina D, Gómez-Villa H, Correa G. Nitrogen removal and recycling by Scenedesmus obliquus in semicontinuous cultures using artificial wastewater and a simulated light and temperature cycle. *Bioresource Technology*. 2005; 96(3):359-362.

Yagi, S. et al. Fuzzy Control of a Wastewater Treatment Plant for Nutrients Removal, Proceedings of the International Conference on Artificial Intelligence in Engineering & Technology, 2002, Sabah, Malaysia.

Yamaoka T, Satoh K, Katoh S. Photosynthetic activities of a thermophilic blue-green alga. *Plant and Cell Physiology*. 1978; 19(6):943-954.

Zemaitis JF, Clark DM, Rafal M, Scrivner NC. Handbook of aqueous electrolyte thermodynamics. Design Institute for Physical Property Data, American Institute of Chemical Engineers, New York. 1986.

Zhao Z, Wang T, Chen L. Dynamic analysis of a turbidostat model with the feedback control. *Communications in Nonlinear Science and Numerical Simulation*. 2010; 15(4):1028-1035.

Zhu YH and Jiang JG. Continuous cultivation of *Dunaliella salina* in photobioreactor for the production of β-carotene. *European Food Research and Technology*. 2008; 227(3):953-959.